COPY NO. 20

STUDY OF STRUCTURAL ACTIVE COOLING AND HEAT SINK SYSTEMS FOR SPACE SHUTTLE

30 JUNE 1972

MDC E0638

FINAL REPORT

MCDONNELL DOUGLAS ASTRONAUTICS COMPANY - EAST

Saint Louis, Missouri 63166 (314) 232-0232

MCDONNELL DOUGLAS CORPORATION

Table of Contents

FOREWORD

This report contains a summary of work conducted for the Astronautics Laboratory of the Marshall Space Flight Center (MSFC) under Contract NAS8-27708, "Structural Active Cooling and Heat Sink Systems for Space Shuttle". The NASA Contracting Officer Representative for this study was Mr. Farouk Huneidi, and the Program Manager at McDonnell Douglas Astronautics Company was Mr. Robert V. Masek. Major contributions to this report were made by Mr. G. A. Niblock, Principal Investigator for Tasks 1 and 3, Mr. C.C. Miller of Martin Marietta Corporation, Principal Investigator for Task 2 and Mr. J.S. Holmgren, Principal Investigator for Task 4.

Table of Contents (Continued)

Table of Contents (Continued)

List of Pages

Title Page

ii through v

1 through 200

1. INTRODUCTION

This technology investigation was conducted to evaluate the feasibility of a number of Thermal Protection Systems (TPS) concepts which are alternate candidates to the Space Shuttle baseline TPS. Four independent tasks were performed. Task 1 consisted of an in-depth evaluation of active structural cooling of the Space Shuttle orbiter. This analytical task developed a preliminary design of a circulating loop cooling system and comparative weight/cost trades of the active system with baseline passive TPS concepts. In Task 2, heat sink concepts for the booster were studied to identify and postulate solutions for design problems unique to heat sink TPS. In addition, heat sink material combinations which could provide a more efficient design than thick aluminum skin were evaluated. Task 3 consisted of a feasibility demonstration test of a phase change material PCM incorporated into a reusable surface insulation (RSI) thermal protection system for the Shuttle orbiter. The test environment consisted of an orbiter reentry thermal simulation. In Task 4 the feasibility of heat pipes for stagnation region cooling was studied for the booster and the orbiter. Designs were developed for the orbiter leading edge and used in trade studies of leading edge concepts.

At the time this program was initiated, a 2-stage fully reusable Shuttle system was envisioned; therefore, the majority of the tasks were focused on the fully reusable system environments. Subsequently, a number of alternate Shuttle system approaches, with potential for reduced Shuttle system development funding requirements, were proposed. Where practicable, appropriate shifts in emphasis and task scoping were made to reflect these changes.

Tasks 1, 3, and 4 were performed by McDonnell Douglas Astronautics Company-East (MDAC-E) in St. Louis, Missouri with substantial supporting effort in Task 4 from Donald W. Douglas Research Laboratories of McDonnell Douglas at Richland, Washington. The Martin Marietta Company, Denver Division, performed the majority of Task 2 under subcontract.

2. SUMMARY

The four tasks to evaluate the feasibility of a number of thermal protection system concepts which were alternate to Space Shuttle baseline showed:

1. The payoff for structural active cooling of the orbiter is highly dependent on mission constraints and thermal control approaches.
2. No insurmountable thermostructural problems are foreseen for a heat sink booster.
3. Integration of a phase change material (PCM) in the orbiter TPS is feasible and provides a small weight saving.
4. Sodium filled Hastelloy-X heat pipes are capable of reducing orbiter leading edge temperatures from the columbium reuse temperature limit to superalloy allowable temperatures.

Further technology efforts should concentrate on definition of orbiter mission flexibility requirements, evaluation of drop tank insulation concepts, studies of PCM packaging approaches,and feasibility demonstration tests of a heat-pipe-cooled leading edge.

2.1 Task 1: Orbiter Structural Active Cooling - In this study, the feasibility of a circulating cooling loop subsystem to provide active cooling of the orbiter structure was assessed and an optimal subsystem was defined. Two orbiter configurations were studied. Only one of these showed potential weight and cost advantages for an active subsystem; a configuration derived by MDC from the NASA 040A Orbiter concept. The analytical and design effort applied to the other configuration, the MDC Phase B Orbiter, was terminated without optimization of the active subsystem because of the minimal payoff identified. The 040A derived version, designated the Model 101, was studied in depth to define an optimal active subsystem and TPS combination. Weight and cost estimates revealed significant Orbiter weight and program cost reduction potential. The results indicated that the cost reduction could be achieved only if the active subsystem were incorporated into the early design phase so that the accrued weight reduction could impact the entire Space Shuttle system design. No cost reduction would occur if the active cooling system were added after the design freeze of the solid rocket motors (SRM) and expendable orbiter fuel tank. An active subsystem to cool the Orbiter structure could be implemented subsequent to the design freeze to achieve an orbiter weight reduction, but would result in an orbiter and total Space Shuttle program cost increase.

2.2 Task 2: Heat Sink Concepts For The Booster - The prime objectives of this task were to investigate thermostructural design problems which could be significant after any total commitment to heat sink boosters for the Shuttle system, and postulate and evaluate heat sink material combinations other than the thick aluminum skin approach.

Investigations of potential thermal and structural problems common to a number of booster configurations were conducted. The Single Body Canard Configuration (SBC) derived in the Phase B extension by the McDonnell Douglas Team and the modified Saturn S-IC booster proposed by Boeing, in two booster/orbiter mating arrangements (piggyback and tank-end loaded) were considered.

The major analytical efforts were conducted for the piggyback version of the S-IC booster configuration, with a separation velocity of 2.14 km/sec (7000 ft/sec). While these results are typical for a variety of booster configurations and separation velocities, booster heating problems are more severe with the piggyback version than with the tank-end loaded case. Consequently, trends shown by the studies are generally applicable, and problems should be less severe for tank-end loaded versions. The results of this study are applicable, in part, to the large H/O drop tanks currently associated with the shuttle program but no effort was expended to extend these results.

Heat sink concepts other than thickened aluminum structure for thermal protection of the Shuttle booster, (e.g., material substitutions, shingles, shims, overcoats, and undercoats) were evaluated. In addition to the conventional alternative sink method of substituting titanium for aluminum, a nonmetallic overcoat on aluminum structure was found to have potential for considerable weight reduction in low and moderate heating environments.

2.3 Task 3: Phase Change Material (PCM) Applications - Analyses and tests to determine the feasibility of a concept which provides structural cooling with a phase change material (PCM) were performed in this task. The analyses included identification and selection of an appropriate PCM, the structural analysis to define an optimized structural panel, thermal analyses to determine the optimum combination of PCM and insulation, and post test analyses of the feasibility demonstration. A test article was constructed that utilized a honeycomb structure consisting of graphite/epoxy composite face sheets bonded to aluminum honeycomb, with mullite reusable surface insulation (RSI) thermal protection. A total of five test cycles were performed. The test panel survived these tests, but the RSI was damaged in the second cycle due to a facility-related malfunction. Subsequent tests did not appear to aggravate the initial damage. Analysis of the test data indicated that a weight reduction (compared with a passive system) of the TPS was achieved, confirming the analytical prediction. The initial analyses of this system which had been concentrated on a Phase B configuration were extended to include an 040A-type TPS arrangement. In the latter configuration the estimated weight reduction was smaller,but remained significant. The smaller weight reduction stemmed from a packaging weight penalty avoided in the Phase B design by containing the PCM in the structural honeycomb panel. The results indicated that the weight of PCM packaging is significant in establishing both the weight reduction potential and the cost of this type of TPS.

2.4 Task 4: Heat Pipe Application to Leading Edge and Stagnation Points - The feasibility of using heat pipes in the leading edge and stagnation regions of shuttle orbiter and booster to reduce peak temperatures (to values below coated columbium allowables where carbon-carbon was required and to superalloy allowables where columbium was required) was evaluated in this task.

The configuration and environments were based on the Phase B Shuttle Program results obtained by the McDonnell Douglas team. Analysis of the launch and reentry heating environments indicated that there was little advantage to the use of heat pipes on the heat sink booster since reentry temperatures were below the allowables for superalloys. On the orbiter, however, significantly higher reentry temperatures occur and the use of heat pipes to reduce the stagnation temperature by several hundred degrees has the potential for replacing a carbon-carbon design with metallic systems.

A detailed analysis was performed to determine the optimum heat pipe configuration, wick design,and working fluid for the orbiter vehicle. Two temperature levels were considered: 1000°C (1832°F) - compatible with superalloys; and 1300°C (2370°F) - compatible with refractory metals. Based on thermal performance and compatibility, a working fluid of sodium was selected for the lower temperature and calcium (with lithium as an alternate) for the higher temperature application. The analysis of wick requirements showed that a simple screen wick was adequate, primarily because g-load effects facilitate the liquid flow throughout most of the heat pipe. A leading edge was designed which used the heat pipe as an integral part of the structure. For the lower temperature application, the pipe system consisted of an assembly of circular tubes (formed to conform to the leading edge chord) brazed to a thin face sheet. This configuration resulted from weight optimizations of various container/structural designs. Trade studies showed that a heat-pipe-cooled design was slightly heavier than carbon-carbon or columbium designs, but was competitive in terms of total system costs.

3. TASK 1: ORBITER STRUCTURAL ACTIVE COOLING

In this effort the potential for active cooling of the Shuttle orbiter structure was evaluated for two general orbiter configurations. These were the MDC Phase B baseline orbiter and an MDC Model 101 (an 040A derivative) orbiter design. Two TPS arrangements for the Phase B design were analyzed; a metallic shingle configuration and another using a reusable surface insulation (RSI). Little potential for weight improvement was apparent in the Phase B configurations, but a significant weight reduction appeared possible in the Model 101 version. Consequently, system analyses were concentrated on the Model 101 configuration and environments which did exhibit the potential for a significant weight reduction through cooling of the structure with an active subsystem.

The results obtained for the Phase B designs indicated that the baseline TPS was efficient and lightweight. Thus, the potential for weight reduction was small. In the case of the metallic system the weight trade study was between insulation and the active cooling subsystem. Here, the low density insulations available precluded a significant weight reduction; put simply, a reduction in insulation thickness allowed by active cooling could not produce a large TPS weight reduction because the insulation weight was initially small. With the higher density RSI, the insulation weight reduction was constrained by heat transfer limitations. Cooling of the RSI/substructure bond was accomplished by radiation from the substructure to the cooled primary structure. The bondline temperature could not exceed 316°C (600°F), which limited the heat transfer to the cooled structure, and the RSI thickness reduction was constrained to such an extent that the weight reduction was insignificant.

The Model 101 configuration analysis did reveal the potential for a significant weight reduction and was evaluated in greater depth than the Phase B configuration. The active subsystem was defined in greater detail, the most appropriate working fluid was selected, and the system analyzed to determine an optimal combination of cooling passage diameter and spacing. Estimates of the impact of incorporating an active cooling subsystem on total program cost were also prepared to allow an assessment of the value of the weight reduction.

3.1 Phase B Configuration Orbiter - To enable a thorough analysis of active cooling approaches, the Phase B configuration developed by the MDC led team

was initially selected as the baseline for the study. Reference 1 contains a detailed description of this configuration. This was a fully reusable vehicle with internal main propulsion tanks (oxygen and hydrogen) that served as the principal load carrying structure. The configuration and TPS arrangement is illustrated in figure 1. The baseline configuration utilized metallic shingles backed with packaged low-density insulation. The shingles and insulation were supported from the propellant tank structure (aluminum) by a trusswork of columbium and hastelloy struts, with a radiation shield between the tank and TPS structure. An alternate configuration was also considered, in which the metallic TPS was replaced with RSI bonded to honeycomb panels. These panels were supported by a strut trusswork similar to that used with the metallic panels. An illustration of the vehicle general arrangement is included in Figure 2. The applications for active cooling considered in this study were the LO_2(LOX) and LH_2 tanks and the wing lower surface areas. As shown in Figure 2,the tanks were located between BS X390 and BS X1770. Looking at the cross-section,it was apparent that much of the tank periphery would require little cooling because it was away from the high heating experienced on the surface. The lower surface planform area btween these two body stations is approximately 280 m^2 (3000 ft^2) as shown in the plan form view of Figure 2.

The other principal application for active cooling, the wing structure, was constructed of titanium and consequently had a much higher allowable temperature limit (371°C/700°F) than the aluminum tank structure (149°C/300°F). A prior study, Reference 2, indicated a substantial weight penalty if active cooling was used as wing structure TPS. Consequently this phase of the study was confined to the lower fuselage surface in the region of the main propellant tanks which are used as the main structure elements in the MDC design.

3.1.1 Flight Environments - The MDC final baseline environments, based on the boost and entry trajectories shown in Figures 3 and 4,were selected for the thermal analysis. The corresponding heating environment lower surface centerline heating rates are shown in Figure 5,and the off-centerline distribution in Figure 6. Sidebody heating was computed assuming a constant value of $q/q_{REF} = 0.011$, where q_{REF} was the heating rate experienced by a sphere of 1-ft radius.

PHASE B CONFIGURATION

METALLIC TPS SUPPORT ARRANGEMENT

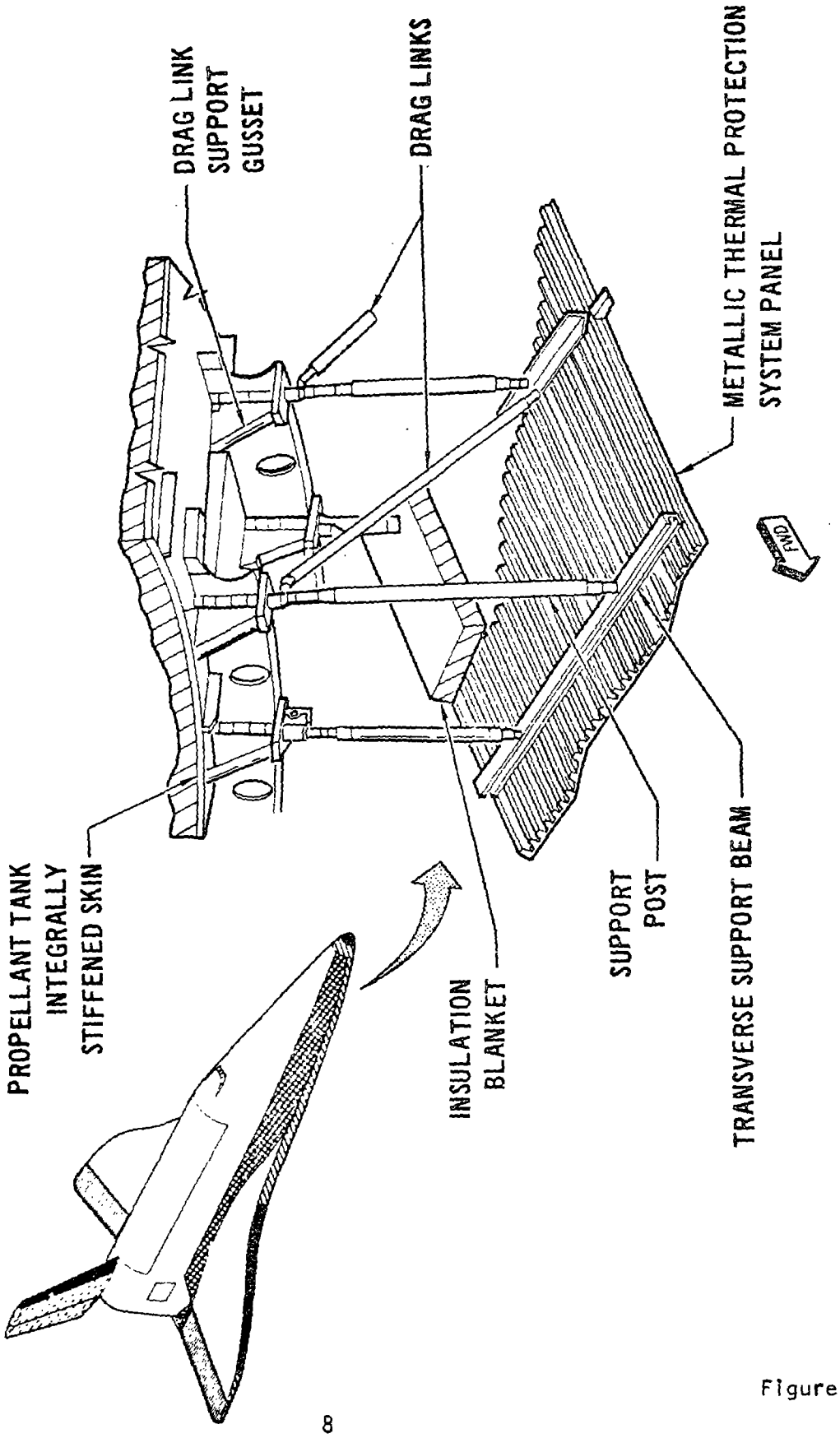

Figure 1

GENERAL ARRANGEMENT - SIAMESE TANK DELTA WING ORBITER

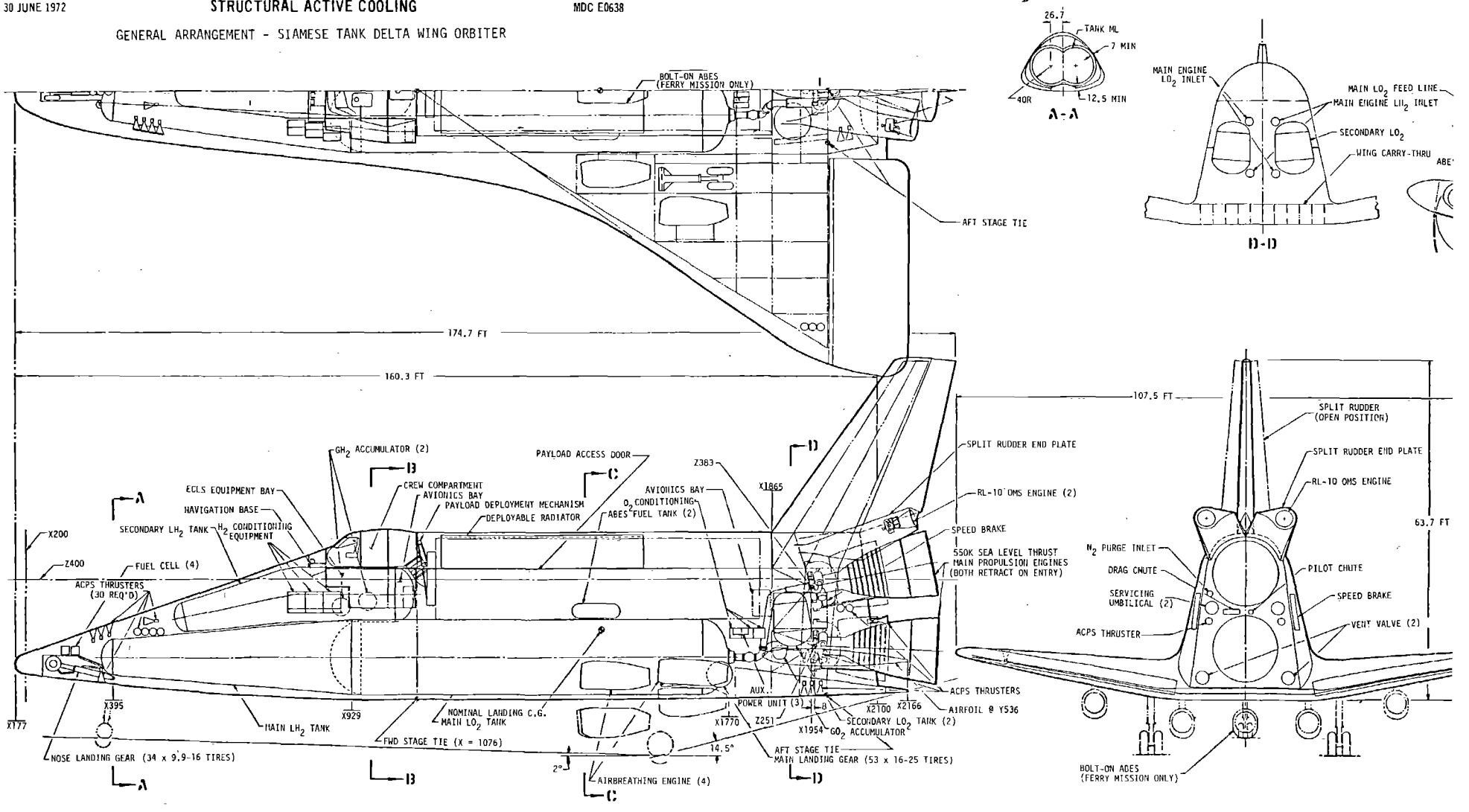

Figure 2

ING ORBITER

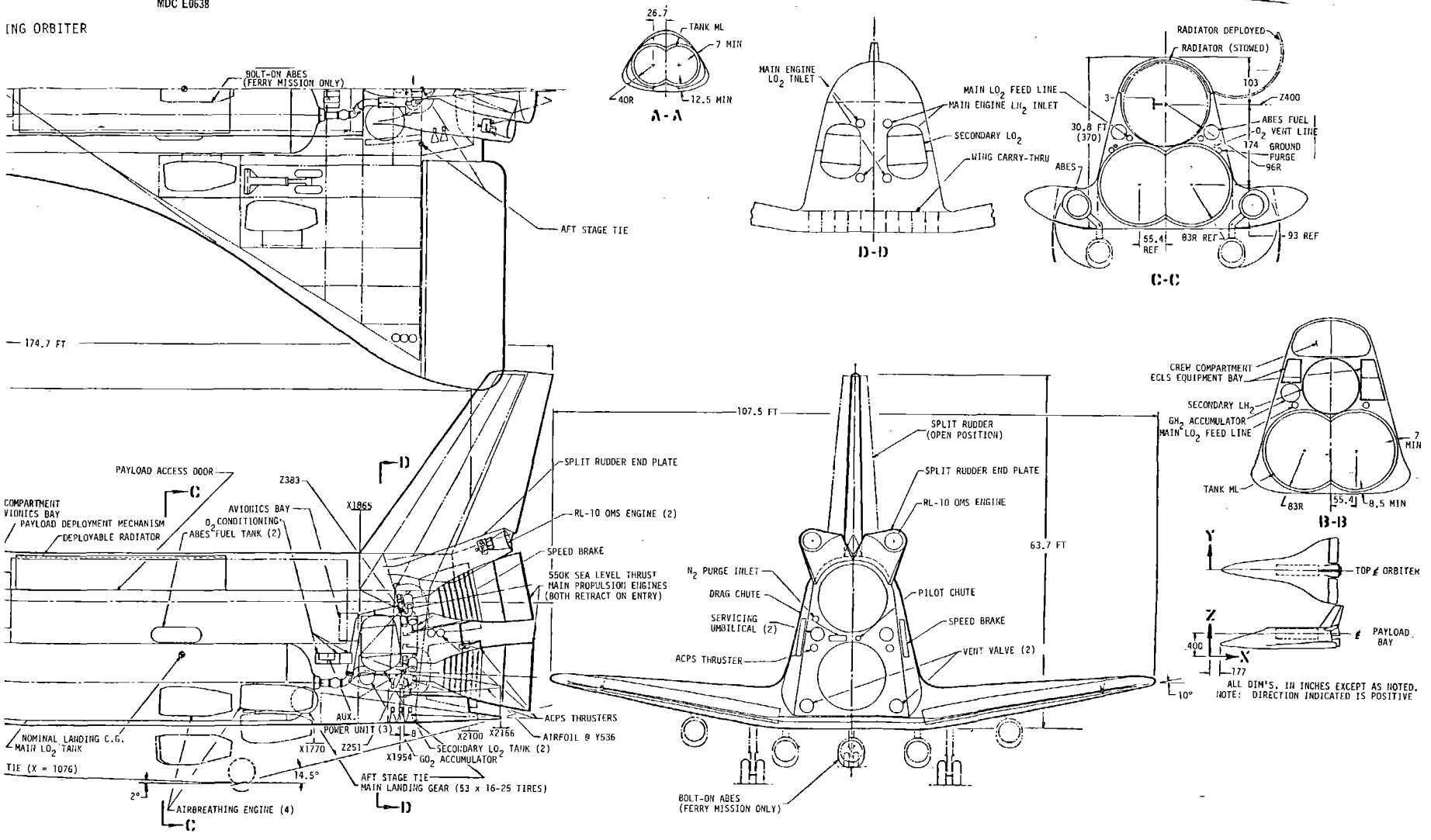

Figure 2

ORBITER AND BOOSTER ASCENT TRAJECTORY

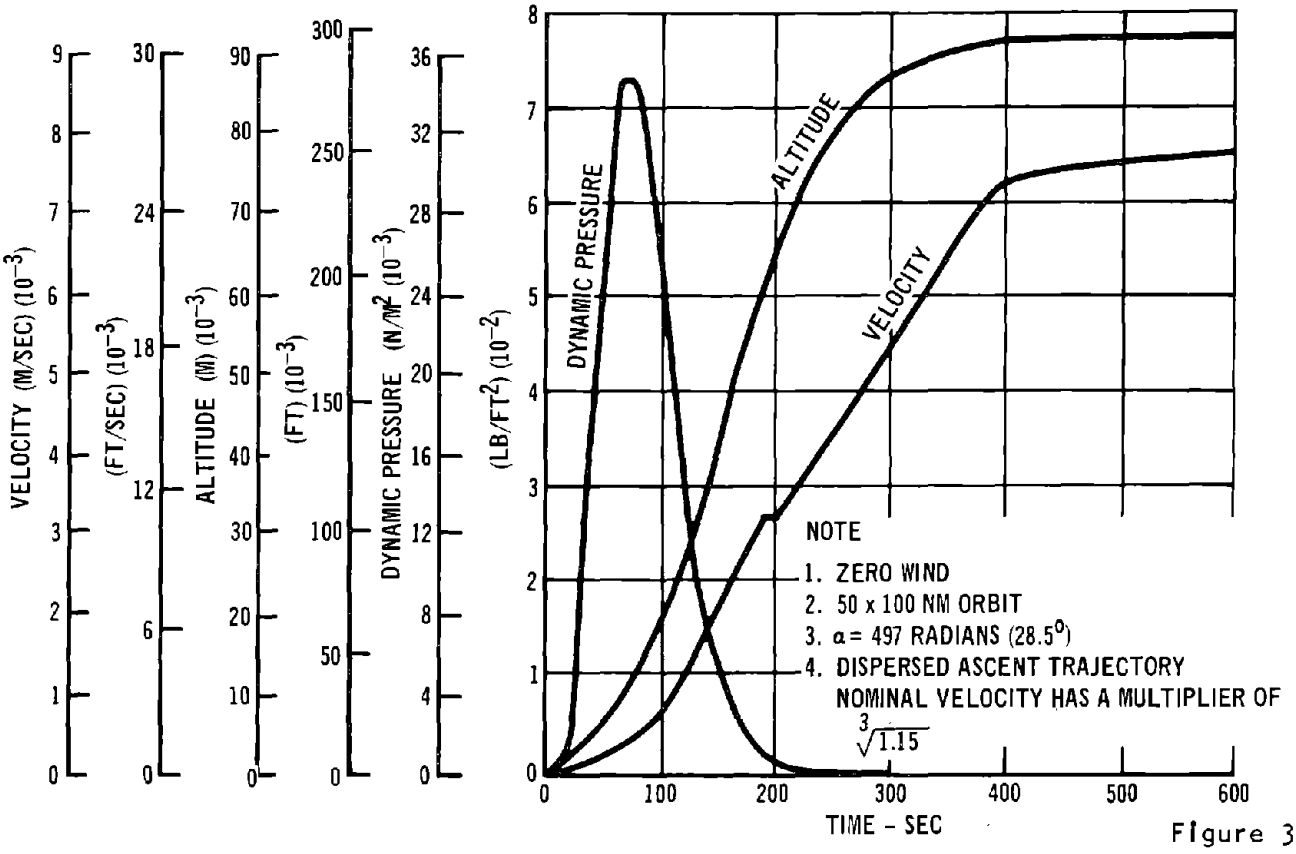

Figure 3

ORBITER ENTRY TRAJECTORY
(From Polar Entry)

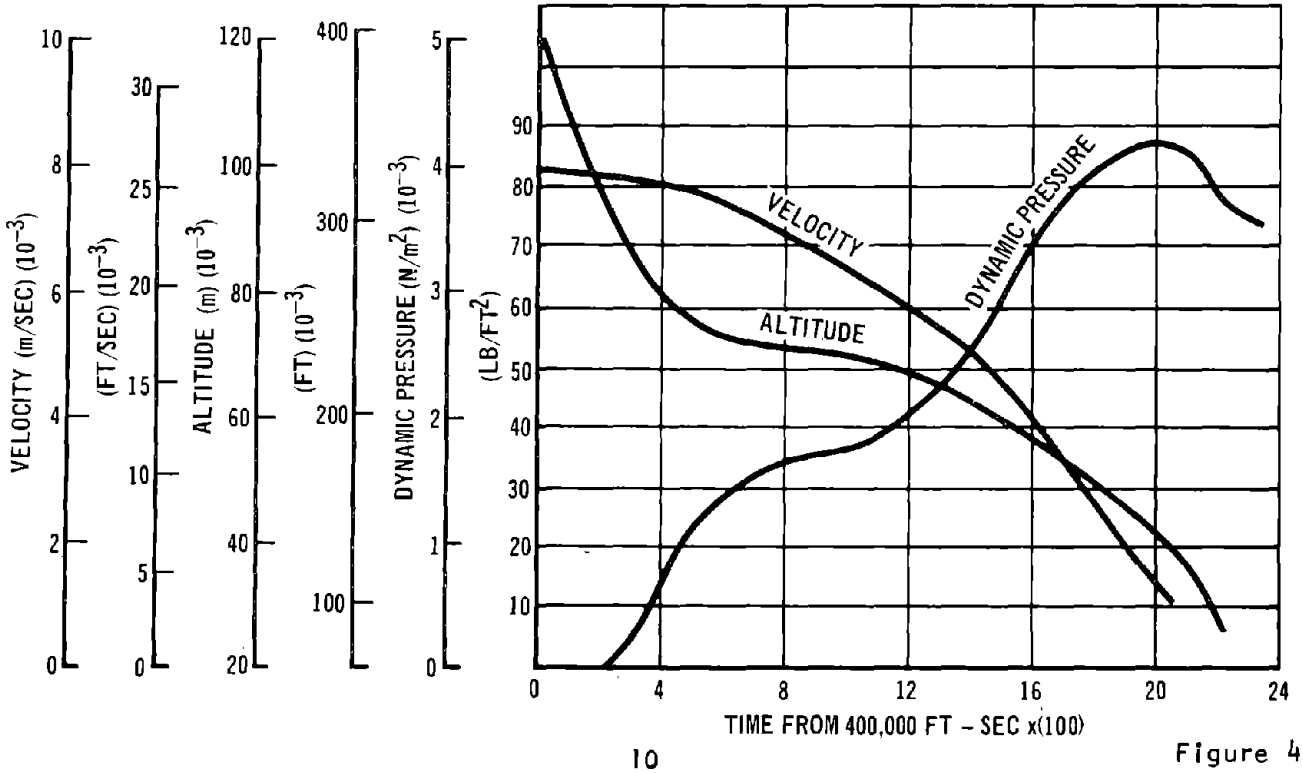

Figure 4

ORBITER BOTTOM CENTERLINE HEAT FLUX

(Phase B Baseline Orbiter)

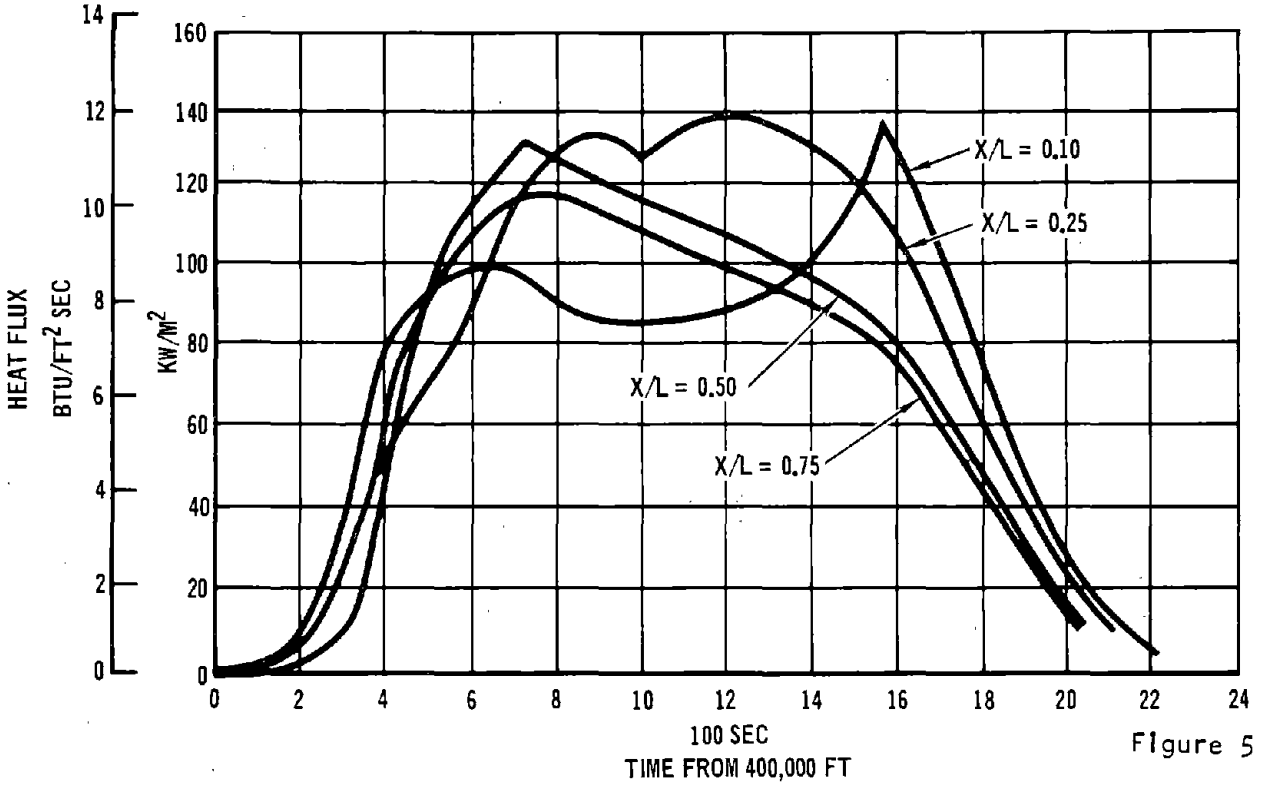

Figure 5

ORBITER OFF-CENTERLINE HEATING DISTRIBUTION

(Final Baseline Design)

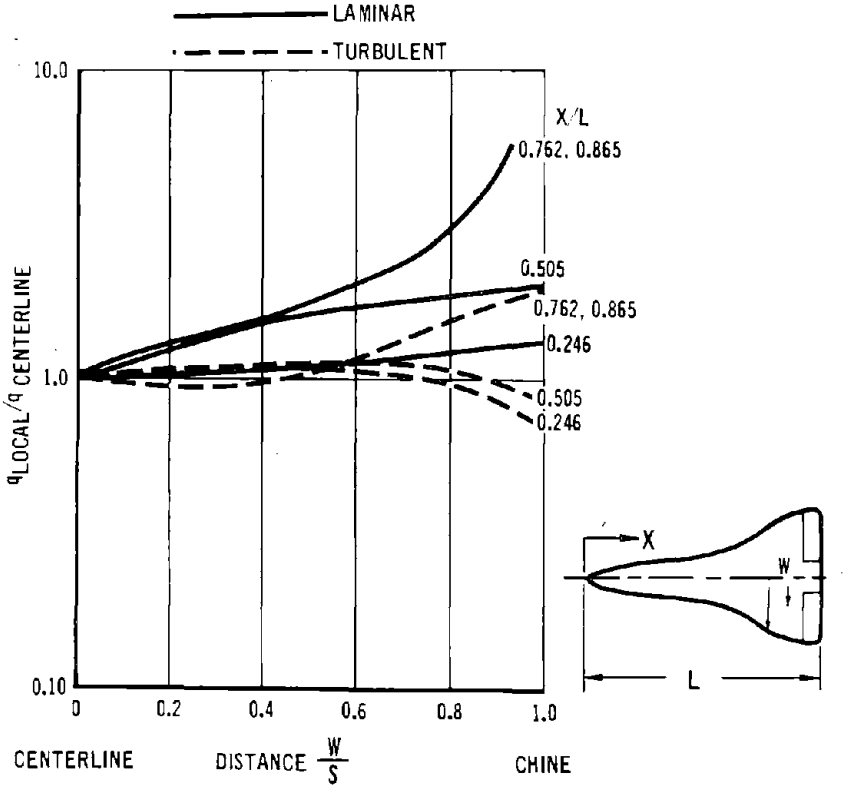

Figure 6

3.1.2 TPS Arrangement Trade Study - A preliminary trade study was conducted to assess alternate TPS arrangements for both the metallic shingle and RSI thermal protection approaches. A one-dimensional thermal analysis was conducted using the bottom centerline heating profile for X/L = 0.5, (given in Figure 5) for both the metallic and RSI systems. This trade study was made based on the structure in the region of the LH_2 tanks, but the concepts were also evaluated for application to other vehicle areas.

Three general arrangements of the metallic shingle system, shown in Figure 7, were analyzed. The insulation thickness was parametrically varied to determine the minimum weight for each configuration. In addition, each cooling arrangement was assessed qualitatively with respect to reliability and fabricability. Figure 7 summarizes the configuration trade study considerations. Active cooling with passages integral with the LH_2 main propellant tank structure yielded the lightest and least complex (probably least expensive) system. Structural integration of this configuration on the LH_2 tank would be relatively straightforward since the internal cryogenic insulation would prevent unacceptably low coolant temperature. This configuration could result in a freezing problem, however, on forward portions of the vehicle at the noninsulated oxygen tank. One coolant fluid (Freon E-1), however, has a pour point of $95^{\circ}K$, and careful integration of the coolant passage with the structure or a stagnation controlled circuit (similar to space radiator designs) could obviate the freezing problem. An alternate configuration with external insulation on the hydrogen tanks was heavier, and the lack of insulation on the oxygen tank posed the same potential freezing problem. The third configuration, with the cooled surface acting as a part of the insulation package, was the heaviest of the three. This weight was caused by greater heat loads and by the penalty associated with replacing a foil insulation package with a much heavier coolant passage assembly.

A similar study was performed for several RSI concepts with cooling applied at the bondline interface, the backface of the supporting honeycomb panel, and the tank wall. These concepts are shown schematically in the Figure 8 trade study summary. The configuration with cooling of the primary propellant tank structure was the lightest of the RSI configurations. Both of the other configurations were slighly heavier and considerably more complex. Prior to the results of the parametric analysis, physical arrangements for these more complex configurations were studied in order to assess their feasibility. The results indicated that even the more complex configurations could be assembled using brazed hardline

STRUCTURAL ACTIVE COOLING

METALLIC SYSTEM PRELIMINARY CONFIGURATION

TRADE STUDY SUMMARY

CONFIGURATION / CONSIDERATIONS	NO. 1 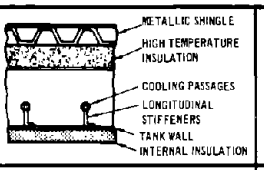	NO. 2 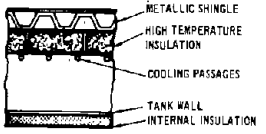	NO. 3 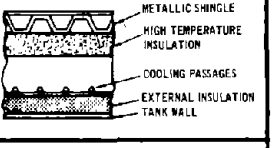
RELATIVE WEIGHT	1.0	1.2	1.1
RELIABILITY	• POTENTIAL FREEZING PROBLEM • MINIMAL LEAKAGE POTENTIAL	• LITTLE POTENTIAL FOR FREEZING • CONNECTORS REQUIRED FOR EACH TPS PANEL (SEVERAL THOUSAND CONNECTORS) • LARGE LEAKAGE POTENTIAL	• POTENTIAL FREEZING PROBLEM • MINIMAL LEAKAGE POTENTIAL • CRYOGENIC INSULATION CONTAINED AND PROTECTED
MANUFACTURING COMPLEXITY	• LEAST COMPLEX FABRICATION AND SYSTEM ASSEMBLY	• MOST COMPLEX FABRICATION AND SYSTEM ASSEMBLY	• COMPLEX FABRICATION, STRAIGHT FORWARD SYSTEM ASSEMBLY
SYSTEM CHECKOUT	• SIMPLE - OCCURS PRIOR TO TPS INSTALLATION	• DIFFICULT - OCCURS AFTER TPS INSTALLATION; POOR ACCESS	• SIMPLE - OCCURS PRIOR TO TPS INSTALLATION

Figure 7

RSI SYSTEM PRELIMINARY CONFIGURATION

TRADE STUDY SUMMARY

CONFIGURATION / CONSIDERATIONS	NO. 1 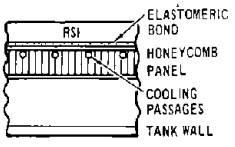	NO. 2 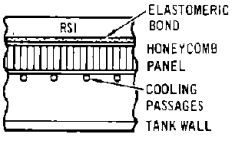	NO. 3 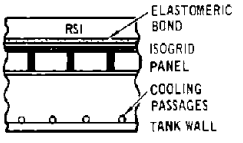
RELATIVE WEIGHT	1.05	1.05	1.0
RELIABILITY	• MINIMAL POTENTIAL FOR FREEZING • CONNECTORS REQUIRED FOR EACH TPS PANEL (SEVERAL THOUSAND CONNECTORS) • LARGE LEAKAGE POTENTIAL	• MINIMAL POTENTIAL FOR FREEZING • CONNECTORS REQUIRED FOR EACH TPS PANEL (SEVERAL THOUSAND CONNECTORS) • LARGE LEAKAGE POTENTIAL	• POTENTIAL FREEZING PROBLEM • MINIMAL LEAKAGE POTENTIAL
MANUFACTURING COMPLEXITY	• MOST COMPLEX FABRICATION AND SYSTEM ASSEMBLY	• COMPLEX FABRICATION AND SYSTEM ASSEMBLY	• LEAST COMPLEX FABRICATION AND SYSTEM ASSEMBLY
SYSTEM CHECKOUT	• DIFFICULT – OCCURS AFTER TPS INSTALLATION; VERY POOR ACCESS	• DIFFICULT – OCCURS AFTER TPS INSTALLATION; POOR ACCESS	• SIMPLE – OCCURS PRIOR TO TPS INSTALLATION

Figure 8

coolant circuit connections. Access for assembly and maintenance could be provided by including small uncooled TPS segments. Bondline surface cooling could be accomplished with the passages brazed to the face sheet, or with passages hydroformed in the face sheet. Additional details of the fabrication and assembly procedures were reported in Reference 3.

3.1.3 Metallic TPS Thermal Model/Analyses - Based on the configuration trade study indications, thermal analyses were conducted for the TPS configuration using cooling of the main propellant tank structure. A comprehensive thermal model (two-dimensional) of the vehicle was constructed for this detailed analysis. The analysis model, shown schematically in Figure 9, consisted of 105 nodes, and represented a cross section of the orbiter at a body station approximating an X/L of 0.5. The heating distribution, shown in Figure 6, was applied to the lower surface and side body heating was based on a constant value of $q/q_{REF} = 0.011$. Three TPS insulation combinations were analyzed to determine insulation requirements and heat loads to the tank structure. The three insulation configurations were: a composite of 96.4kg/m^3 (6 PCF) Dynaflex for temperatures above 978°C (1800°F) with 56 kg/m^3 (3.5 PCF) Microquartz and two Dynaflex configurations of 96.4 kg/m^3 (6.0 PCF) and 192.5 kg/m^3 (12.0 PCF) densities, respectively. The pressure and temperature effects of the entry environments on insulation thermal protection properties were included in the analysis. The analytical procedure also allowed heat storage in the main propellant tank structure until heat removal became necessary for a main propellant tank wall temperature limit of 149.8°C (300°F).

The peak heat load distribution on the main propellant tank structure was calculated for each insulation configuration as a function of insulation thickness. These heat load data have been previously reported in Reference 4. The results showed that an increase in insulation thickness had two effects: (1) reduction of the peripheral areas of the tank wall requiring cooling, and (2) a reduction of the local heat flux and the total heating rate on the tank cross-sections.

Direct comparisons of the three insulation approaches indicated that the lowest density insulation (a Dynaflex/Microquartz composite) yielded the lightest insulation system. In addition, the lowest heat load on the tank resulted for this material combination.

Although Dynaflex was selected to protect the Microquartz insulation from temperatures exceeding 978°C (1800°F), the results of materials analysis at MDAC-E under Contract NAS 8-26115 now indicate that Microquartz is suitable for use (and reuse) up to 1090°F (2000°F). Only the most forward portions of the

TWO-DIMENSIONAL THERMAL MODEL SCHEMATIC

(METALLIC TPS)

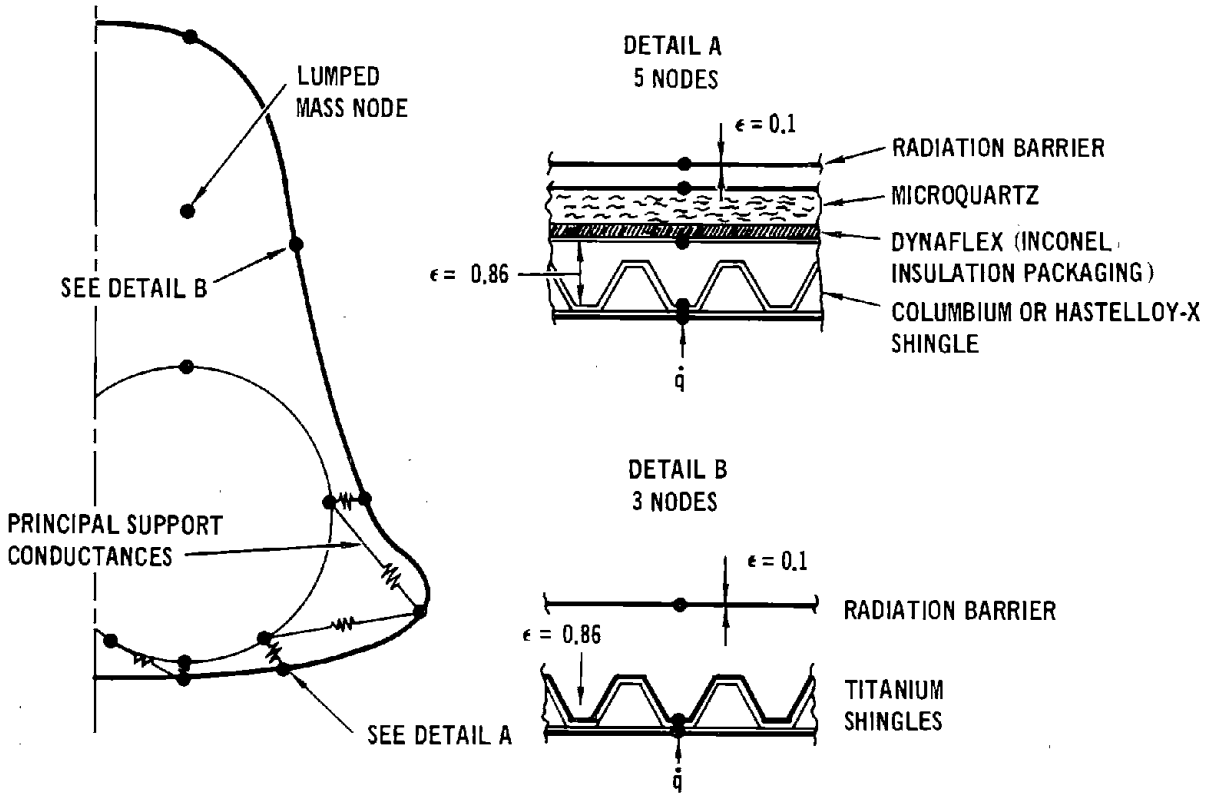

Figure 9

vehicle will expose the insulation to temperatures in excess of 1090°C (2000°F), but in these regions, protection will be required for the Microquartz. The higher density (192.5 kg/m^3 - 12 PCF) Dynaflex which has reuse temperatures up to 1200°C (2200°F), would be used to protect the Microquartz in these limited areas.

The analyses of the Phase B metallic TPS utilizing an active subsystem were completed in sufficient detail to determine that the active subsystem provided little payoff in this Phase B configuration and TPS arrangement. Prior to analysis of several vehicle cross-sections with two-dimensional thermal models, an optimum weight actively cooled system was defined, based on data from the first cross-section analyzed. Optimization studies for a metallic TPS at a body station corresponding to X/L = 0.5 formed the basis for the analysis. The integrated heat load on the orbiter structure (main propellant tanks) was computed in the following manner. It was assumed that the time integrated heat load on the structure was proportional to the time integral of the environmental heating rate. Further, it was assumed that the total heat load at any body station was proportional to the periphery of tank cooled and that the peripheral heating rate distribution on the propellant tank structure remained constant. The axial heat load distributions are shown in Figure 10 as a function of insulation thickness. Integrating these heat loads along the axis of the vehicle yielded the total heat to be absorbed by the structural cooling subsystem. This heat load is depicted as a function of insulation thickness in Figure 11 for an assumed initial temperature of 38°C (100°F). Two radiation shield emittances were assumed, an initial value of 0.1 and another, degraded at end-of-life to a value of 0.5.

Active subsystem component weights were based on these heat loads and the weight estimating relationships described previously in Reference 5. The active system weight included the circulating system tubing and coolant, coolant pumps and motors, coolant reservoirs, heat exchangers, expendable coolant (water), coolant supply tanks, miscellaneous valves and circuitry, and mounting structure. The quantity of expendable coolant (water) was calculated assuming an evaporation efficiency of 98 percent (2 percent carry-over) and evaporation at a temperature of 20°C (68°F). The results of these analyses for the metallic TPS are illustrated in Figure 12. This figure shows that, by considering only the expendable supply portions of the active cooling subsystem, a small weight saving occurs. Inclusion of the weight of the active subsystem components, however, yields a minimum total system weight for the actively cooled TPS which is actually greater than that for the passive TPS. The totals of Figure 12 are included in Figure 13, with a detailed system weight breakdown. It is also shown in this figure that the active cooling system yields a

APPROXIMATE AXIAL HEAT LOAD DISTRIBUTION
(Structure)

NOTE:
- PHASE B ORBITER CONFIGURATION
- HEAT SINK STRUCTURE TO 149.8°C (300°F)
- INITIATE COOLING AT 149.8°C (300°F)
- SINGLE RADIATION SHIELD, EMITTANCE = 0.1
- DYNAFLEX/MICROQUARTZ COMPOSITE INSULATION

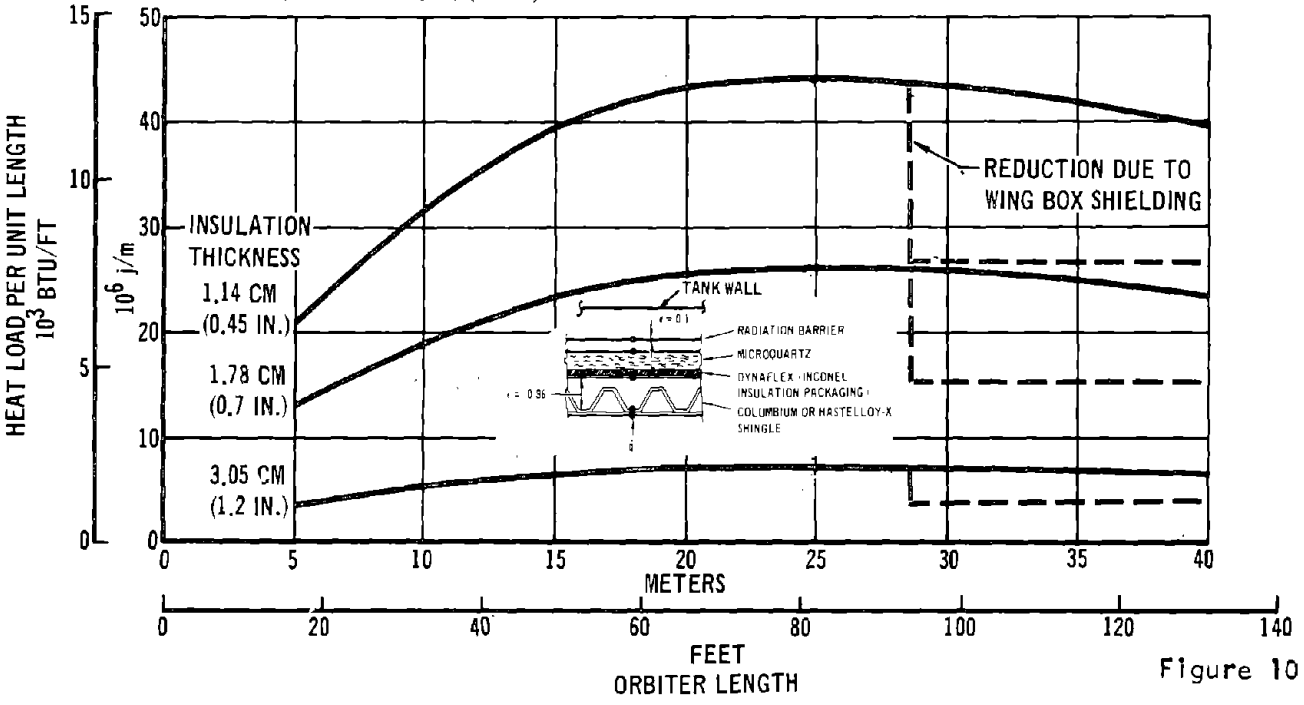

Figure 10

ESTIMATED TOTAL PRIMARY STRUCTURE HEAT LOAD FOR SPACE SHUTTLE ORBITER

NOTE:
- PHASE B ORBITER CONFIGURATION
- HEAT SINK STRUCTURE TO 149.8°C (300°F)
- INITIATE COOLING AT 149.8°C (300°F)
- DYNAFLEX/MICROQUARTZ INSULATION
- SINGLE RADIATION SHIELD

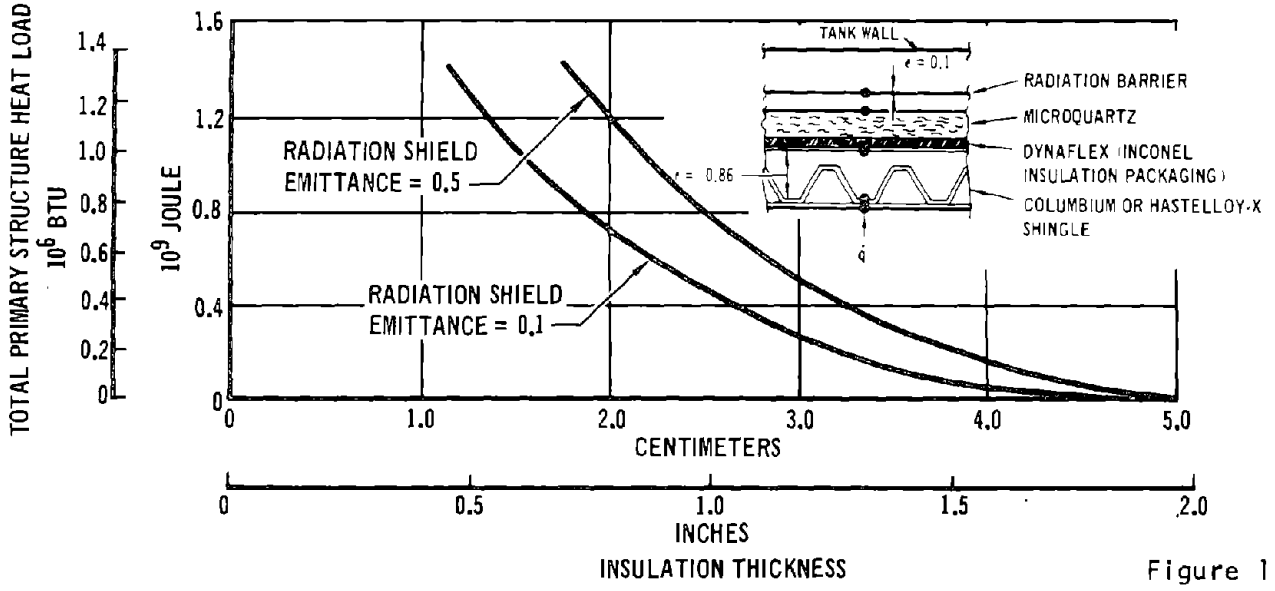

Figure 11

LOWER SURFACE INSULATION/COOLANT TRADE

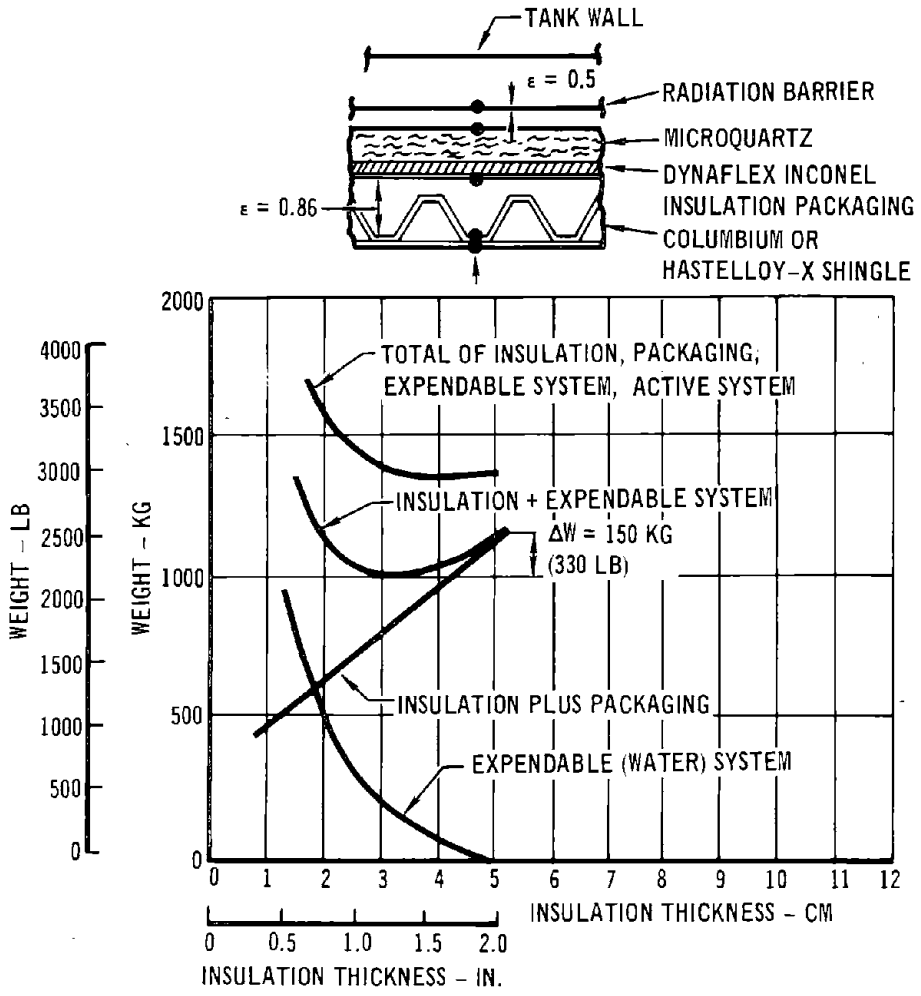

Figure 12

weight increase rather than a weight reduction.

The above result contradicted the results from earlier studies (References 6 and 7) which did indicate a potential for weight reduction with active cooling. Since the trade between active and passive systems depended strongly on the efficiency of the passive system, the effect of system configuration was thought to account for the different result. The MDC design utilized radiation gaps and a radiation shield that functioned effectively as extremely lightweight insulation. If the insulation were not separated from the structure by the the radiation gaps and shield, then additional insulation would be required to protect the primary structure. An analysis of a configuration without the radiation gap and shields was performed and the TPS weight increase was found to be substantial; the insulation thicknesses (and weights) were more than doubled by the change in TPS arrangement. Data from the prior study cited above (Reference 7) agree well with these computed requirements (as shown in Figure 14). These results indicate that the potential weight savings which can be obtained with active cooling are greatly dependent on the efficiency of the passive system it is to replace, and that little payoff (or even weight penalties) may occur for highly efficient TPS arrangements.

METALLIC THERMAL PROTECTION SYSTEM WEIGHTS

COMPONENT	ACTIVE SYSTEM WEIGHT		PASSIVE SYSTEM WEIGHT	
	TOTAL (LB)	UNIT (LB/FT^2)	TOTAL (LB)	UNIT (LB/FT^2)
SHINGLE	4,550	1.19*	4,550	1.19*
TRANSVERSE SUPPORT BEAMS	664	0.21	664	0.21
RETAINER, ATTACHMENTS	568	0.18	664	0.18
SUPPORT STRUTS, FITTINGS	538	0.17	538	0.17
SECONDARY STRUCTURE SUBTOTAL	6,320	1.75	6,320	1.75
STRUCTURAL NON-OPTIMUM FACTOR	632	0.17	632	0.17
SECONDARY STRUCTURE TOTAL	6,952	1.92	6,952	1.92
INSULATION, PACKAGING	1,980	0.63	2,560	0.81
RADIATION SHIELD, SPACER	126	0.04	126	0.04
EXPENDABLE COOLANT, TANKS	316	0.10	0	0.00
CIRCULATING COOLANT SYSTEM	750	0.22	0	0.00
LOAD BEARING INSULATION	190	0.06	190	0.06
INSULATION RETENTION	158	0.05	158	0.05
NON-STRUCTURE SUBTOTAL	3,520	1.10	3,034	0.96
TOTAL	10,472	3.02	9,986	2.88
10% CONTINGENCY	1,047	0.30	999	0.29
TPS TOTAL (COOLED REGION ONLY)	11,519	3.32	10,985	3.17

*TYPICAL NON-COLUMBIUM

Figure 13

COMPARISON OF PASSIVE INSULATION REQUIREMENTS - NO RADIATION GAP

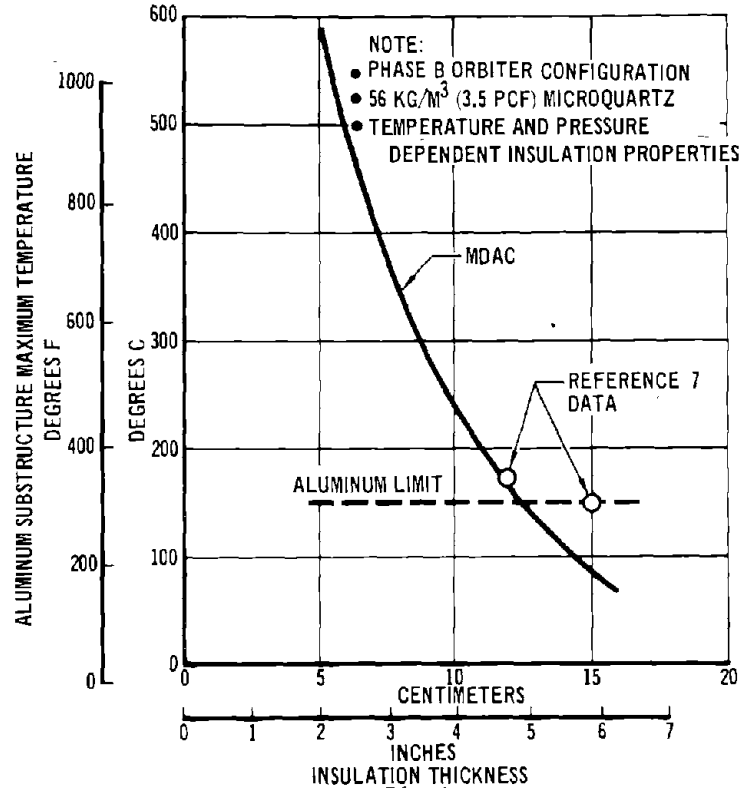

Figure 14

3.1.4 RSI Thermal Protection System Model/Analyses - Based on the results of the configuration trade study, the RSI-protected Phase B configuration was modeled with an active cooling subsystem on the primary structure. The model, shown schematically in Figure 15, represented a cross-section at body station X/L = 0.5 and consisted of a network of 101 nodes. The lower surface and side body heating rates used in the metallic system analyses were also used in analysis of the RSI design. Since cooling was applied to the primary structure, the radiation shield used in the metallic system design was omitted to improve the thermal coupling between the primary structure and the substructure to which the RSI was attached. Omitting the radiation shield improved heat transfer from the RSI to the cooled primary structure, allowing a reduction of the RSI thickness for the same bondline temperature.

Using the model for this configuration, analyses were conducted to determine the minimum RSI thickness that would prevent the bondline temperature from exceeding 316°C (600°F). Since the metallic system analyses had indicated that the configuration with a radiation gap would have a small payoff with an active subsystem,a check of the potential in the RSI configuration was made prior to conducting extensive analysis. For this purpose, the minimum allowable RSI thickness determined by the bondline temperature constraint was used to estimate the minimum actively cooled system unit weight for comparison with a passive system unit weight. The results are tabulated in Figure 16 and show a small weight saving. The weight reduction indicated is less than either the structural nonoptimum, or the contingency allowances. Perhaps more significant, however, is the fact that the unit weight of the minimum weight cooled RSI system is greater than that of either the active or passive metallic TPS. Although adding the active subsystem to a Phase B TPS using RSI exhibits a marginal potential for weight reduction, it can be concluded that the metallic system is superior to that using RSI. For these reasons, more detailed analyses of the RSI design were not conducted.

The analytical results did indicate, however, a potential for active cooling in an RSI configuration if radiation gaps were not present. With RSI bonded directly to the structure better cooling of the bondline could be achieved and a greater insulation thickness reduction could be achieved. In addition, the insulation thickness required for a passive system would be greater because of the lower allowable bondline temperature with an aluminum structure.

RSI TWO-DIMENSIONAL THERMAL MODEL SCHEMATIC

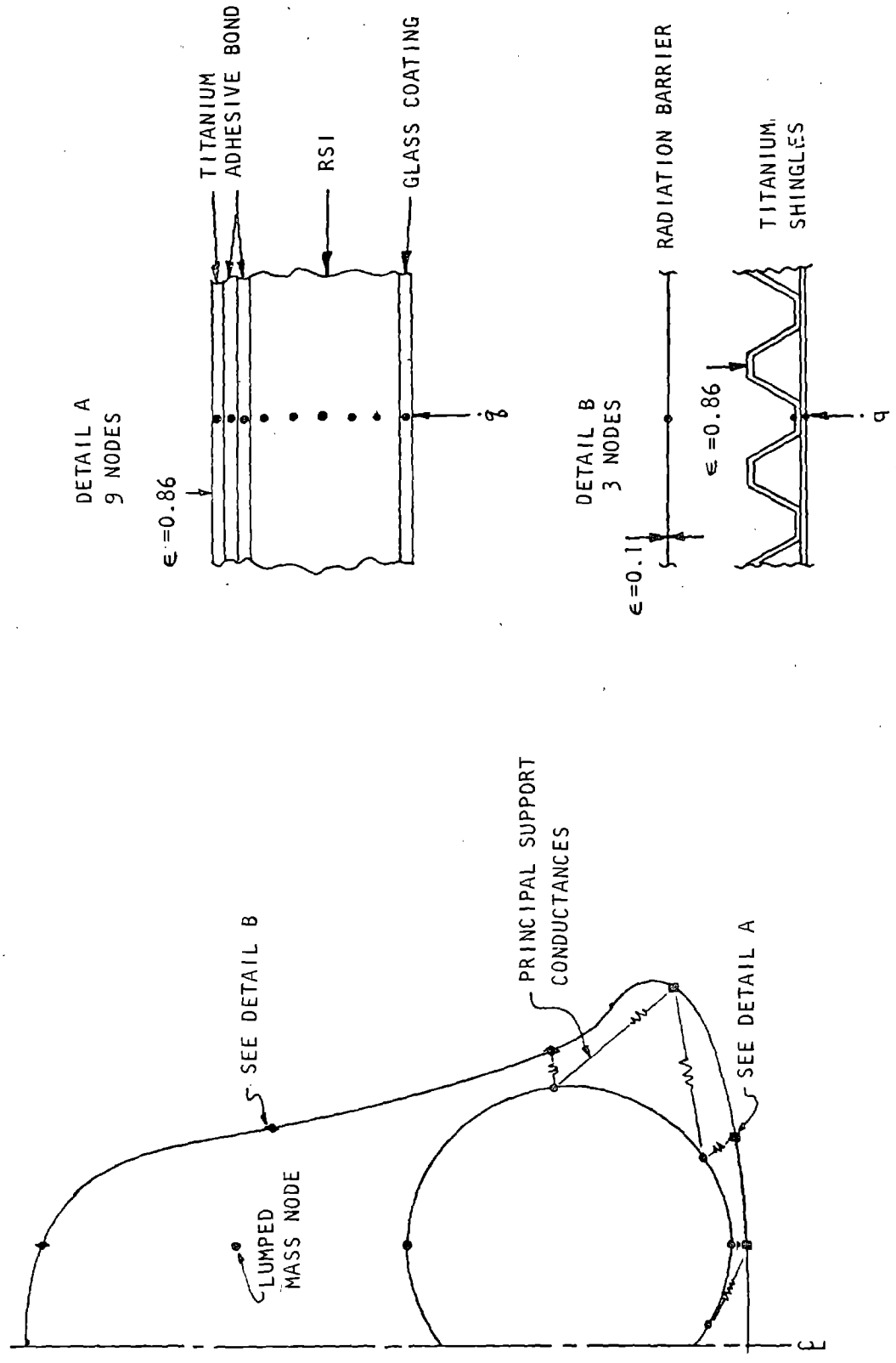

Figure 15

RSI THERMAL PROTECTION SYSTEM WEIGHTS

COMPONENT	ACTIVE SYSTEM UNIT WEIGHT (kg/m^2)	ACTIVE SYSTEM UNIT WEIGHT (LB/FT^2)	PASSIVE SYSTEM UNIT WEIGHT (kg/m^2)	PASSIVE SYSTEM UNIT WEIGHT (LB/FT^2)
PANEL	2.29	0.47	2.29	0.47
TRANSVERSE SUPPORT BEAMS	1.02	0.21	1.02	0.21
RETAINER, ATTACHMENTS	0.88	0.18	0.88	0.18
SUPPORT STRUTS, FITTINGS	0.83	0.17	0.83	0.17
STRUCTURE SUBTOTAL	5.02	1.03	5.02	1.03
STRUCTURAL NON-OPTIMUM FACTOR	0.50	0.10	0.50	0.10
STRUCTURE TOTAL	5.52	1.13	5.52	1.13
RSI	8.39	1.72	9.57	1.96
WATERPROOF COATING	1.32	0.27	1.51	0.31
RSI/PANEL BOND	0.83	0.17	0.83	0.17
EXPENDABLE COOLANTS, TANKS	0.59	0.12	-	-
CIRCULATING COOLANT SYSTEM	0.68	0.14	-	-
RADIATION SHIELD, SPACER	-	-	0.20	0.04
NON-STRUCTURE TOTAL	11.80	2.42	12.10	2.48
TOTAL	17.32	3.55	17.61	3.61
10% CONTINGENCY	1.73	0.35	1.76	0.36
TPS TOTAL	19.03	3.90	19.37	3.97

Figure 16

3.1.5 Structural Integration of Cooling Passages - In parallel with the analytical effort, methods for integrating the cooling passage with the primary structure were investigated. The Phase B design of the main propellant tank was stiffened with integral rings and stringers in a 10.4 by 51-cm(4 by 20-in.) rectangular pattern with the long side acting as a stringer. The pattern would be machined from a large plate and roll formed with rubber blocks in the machined cavities. The integral rings served principally as members for the attachment of deep rings to give the tank structural stability, with the stringers stiffening the shell between the deep rings.

The thermal analysis, discussed previously, revealed that a large portion of the periphery of the tank near the top would require no cooling. The heating intensity varied considerably on the tank, from zero near the top to a maximum near the lower fuselage surface. This suggested that the coolant passage weight penalties could be minimized if the cooling passages were installed oriented along the tank longitudinal axis. This approach could allow the tube spacing to vary with the heat load while retaining a fairly simple installation, e.g., extrusions riveted to the longitudinal stiffeners. With the assumption of a longitudinal orientation the required cooling passage spacing was computed for the three insulation materials studied. The required spacing varied considerably (Figure 17) but at all peripheral locations the spacing was wider with the Microquartz insulation because of its superior performance.

This figure also shows that the Phase B stringer spacing would be adequate for only a small part of the tank, nearest the payload bay. The remainder of the circumference would require a variable spacing with a minimum spacing of about 6.4 cm (2.5 in.). This could be accomplished with a design (Figure 18) for which the stringer spacing and height were varied in order to reduce the weight penalty for attachment of the cooling passages. The cooling passages would consist of aluminum extrusions containing either single or redundant passages riveted to the stringers as shown in Figure 19. The passages are riveted to allow use of high strength aluminum alloys. This approach allows the use of the full coolant passage cross sectional area as structure. The weight penalty is not much greater than the weight increase associated with the coolant contained in the passage and the overlap of the riveted joint. The percentage weight increase varies along the length of the vehicle, but

COOLANT PASSAGE SPACING

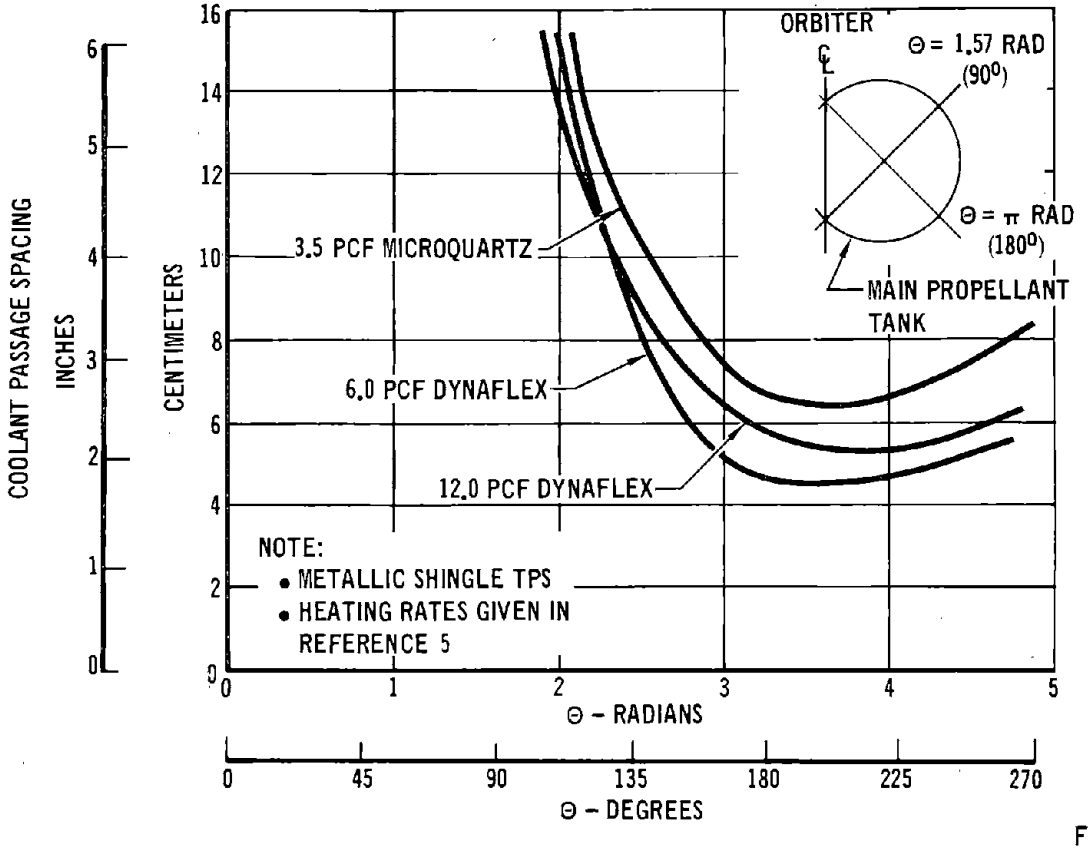

Figure 17

INTEGRATION OF COOLING PASSAGES WITH PRIMARY STRUCTURE

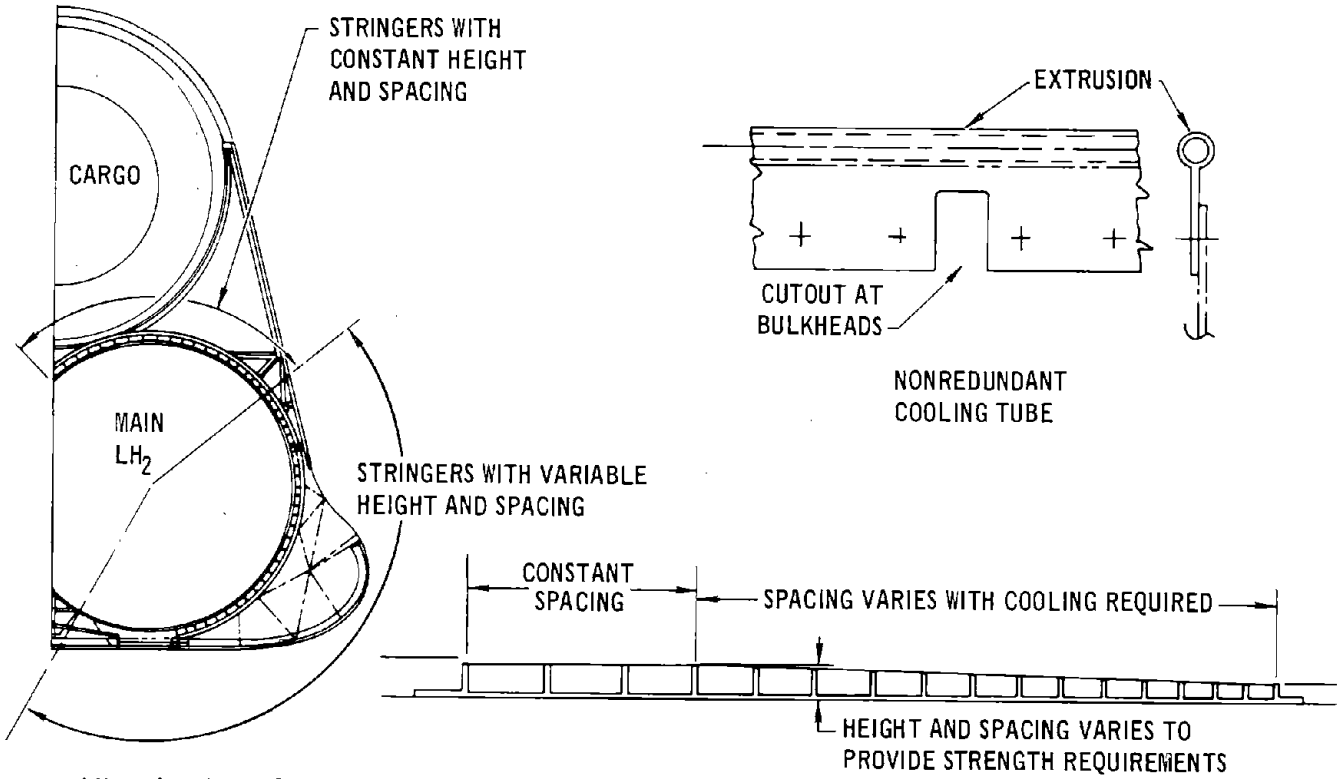

Figure 18

at a typical body station (X/L = 0.5), the weight of the tank structure without cooling is 5.63 kg/m^2 (1.15 lb/ft^2) and with cooling passages is 5.95 kg/m^2 (1.22 lb/ft^2) for a nonredundant system.

APPLICATION OF NON-REDUNDANT COOLING PASSAGES

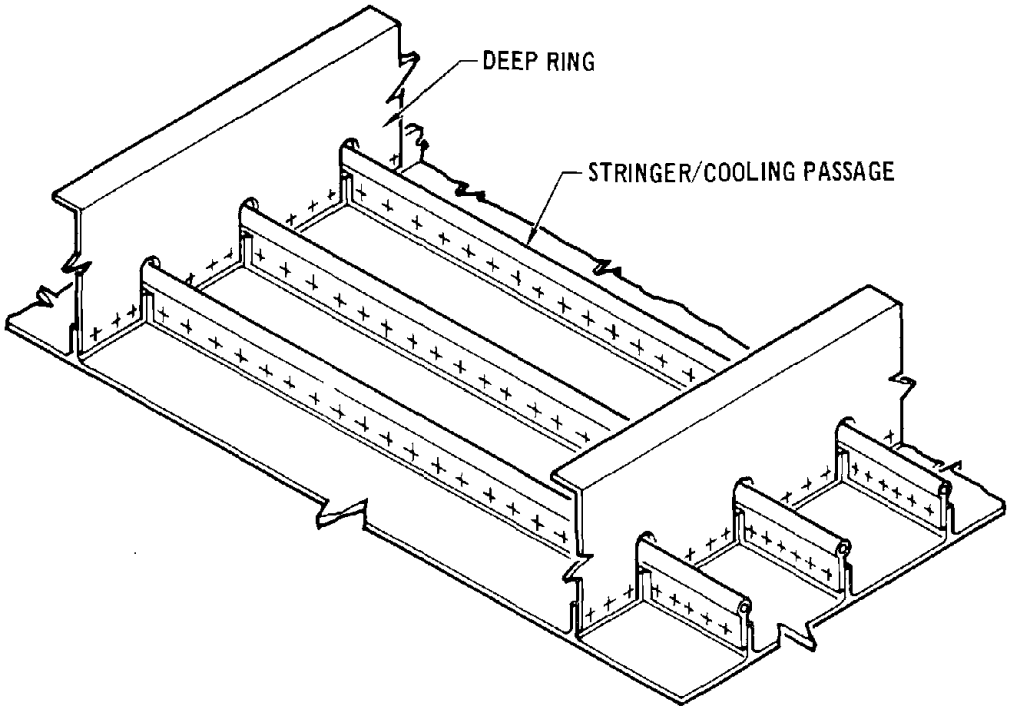

Figure 19

3.2 040A Derivative Configuration - As with the analysis of the Phase B design, an MDC configuration (derived from the NASA 040A concept) served as the basis for study. The specific configuration, shown in Figure 20, was designated the 101. This was a reusable orbiter designed for launch with solid rocket motors and an expendable cryogenic oxygen/hydrogen propellant supply. The design utilized an RSI of hardened, compacted mullite fibers with an organic waterproof coating. The RSI was attached to a silicone foam which was bonded to the orbiter structure (see Figure 20 detail). The silicone foam provided a compliant attachment that isolated the RSI from strain or buckling in the orbiter structure while serving as a thermal insulator. Because of the direct conductive attachment of the RSI, this system was amenable to bond line temperature control by direct cooling of the structural skin. The results obtained in a comprehensive study of this system indicate the potential for a substantial weight reduction and a corresponding, though small, Shuttle Program cost reduction by incorporating an active subsystem to cool the lower fuselage.

3.2.1 Configuration and Environment Description - The 040A derived configuration, designated the 101, was substantially different from the Phase B configurations. The thermal protection system consisted of an RSI directly attached to a structural skin, increasing the likelihood of a sizable thickness reduction. Additionally, the selected RSI has a nominal density of 240 kg/m^3 (15 lb/ft^3), well above the Reference 7 break-even density for active cooling of about 6 lb/ft^3. The 101 version is depicted in Figure 21. The primary fuselage structure was a conventional aircraft type aluminum semimonocoque shell. The wing structure consisted of aluminum truss spars and ribs and skin/stringer covering panels. The wing carry-through structure was integrated with the fuselage with the major wing joint located at the side of the fuselage. Zee stringers were used as skin stiffeners. The zee stiffeners were oriented along the longitudinal axis on the fuselage and spanwise on the wing. Buckling of the stiffened skin was not precluded; skin buckling was accommodated by protecting the RSI from structural loadings with a strain isolation layer of silicone sponge rubber. The arrangement of the zee stiffeners suggested replacement of the zee with a stiffener containing an integral coolant passage. This approach has been used for the Gemini and Airlock (Skylab) radiators produced at MDAC-E which utilized tee-shaped magnesium extrusions with the cooling passage in a bulb at the stem of the tee.

The lower surface regions in which active cooling might be applied are shown in Figure 22 with the net area, exclusive of doors, hatches, etc, which could be affected. The study was concentrated on the lower fuselage surface but also included an evaluation of active cooling of the wing structure.

The 101 configuration environment yielded higher surface temperatures because a "hotter, faster" trajectory was permitted. A peak lower surface temperature of 1260°C (2300°F) was used as a constraint in shaping the trajectory for the 101 configuration while the Phase B trajectory was tailored to an allowable peak temperature of 1090°C (2000°F). The trajectories are compared in Figure 23. The 101 trajectory, although hotter, subjected the vehicle to high heating rates for a shorter period of time. Typical 101 lower surface heating rates, shown in Figure 24, yield higher surface temperatures but the heating duration is shortened sufficiently that the time-integral of the surface heat flux is nearly the same as for the Phase B vehicle. Thus, it appeared that trajectory changes would not preclude the possibility of a weight reduction with an active cooling system.

MODEL 101 ORBITER TPS ARRANGEMENT

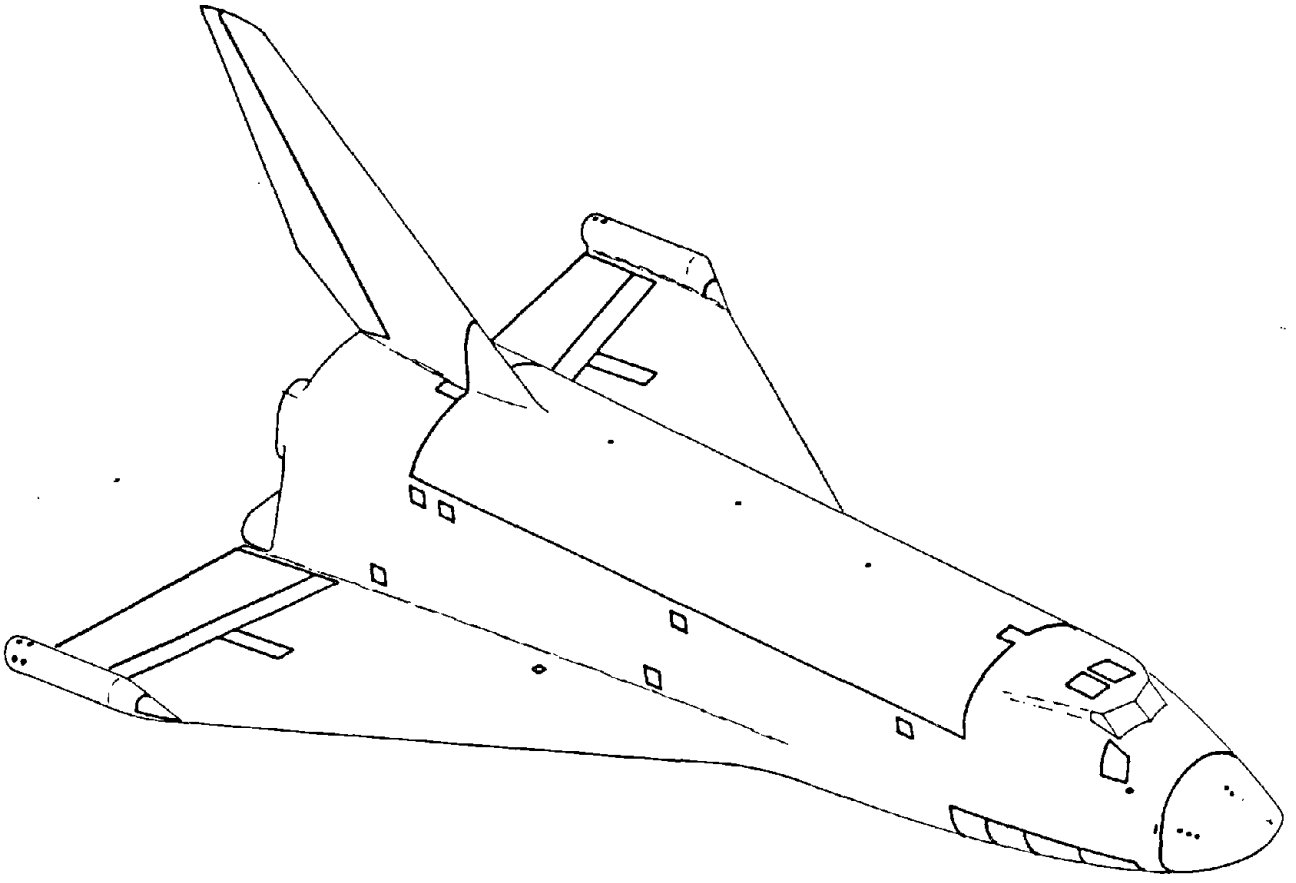

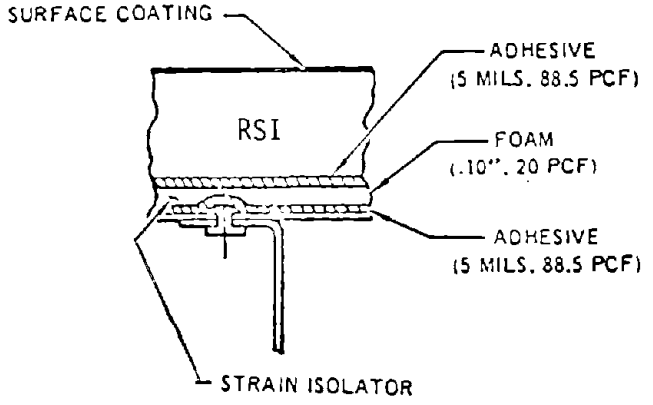

Figure 20

MODEL 101 ORBITER GENERAL ARRANGEMENT

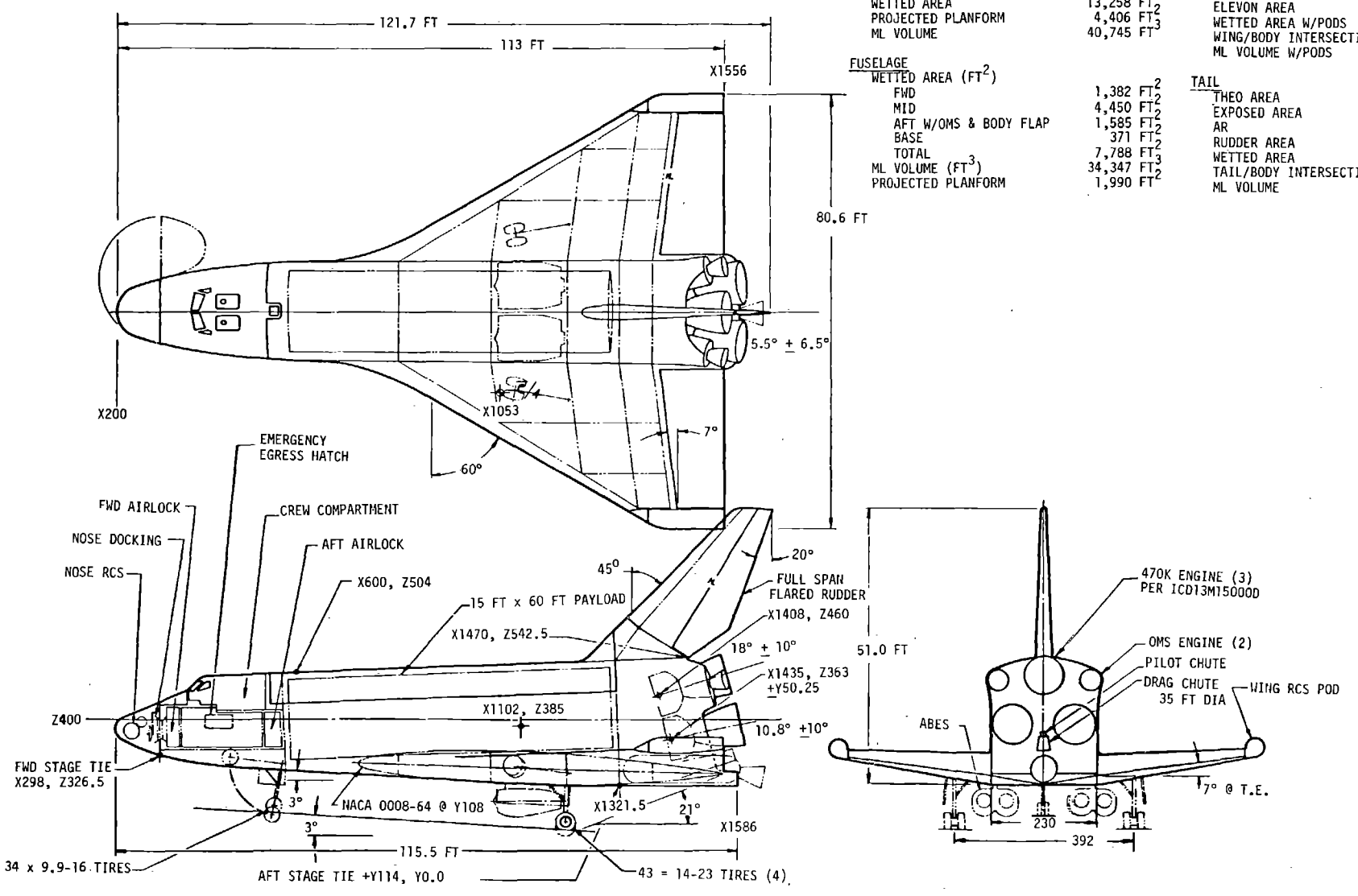

TOTAL VEHICLE		**WING**	
WETTED AREA	13,258 FT^2	THEO AREA	3,800 FT^2
PROJECTED PLANFORM	4,406 FT^2	EXPOSED AREA	2,416 FT^2
ML VOLUME	40,745 FT^3	AR	1.71
FUSELAGE		ELEVON AREA	548 FT^2
WETTED AREA (FT^2)		WETTED AREA W/PODS	5,074 FT^2
FWD	1,382 FT^2	WING/BODY INTERSECTION	462 FT^2
MID	4,450 FT^2	ML VOLUME W/PODS	5,988 FT^3
AFT W/OMS & BODY FLAP	1,585 FT^2	**TAIL**	
BASE	371 FT^2	THEO AREA	450 FT^2
TOTAL	7,788 FT^2	EXPOSED AREA	432 FT^2
ML VOLUME (FT^3)	34,347 FT^3	AR	1.74
PROJECTED PLANFORM	1,990 FT^2	RUDDER AREA	157 FT^2
		WETTED AREA	888 FT^2
		TAIL/BODY INTERSECTION	30 FT^2
		ML VOLUME	410 FT^3

Figure 21

STRUCTURAL ACTIVE COOLING

LOWER SURFACE AREAS

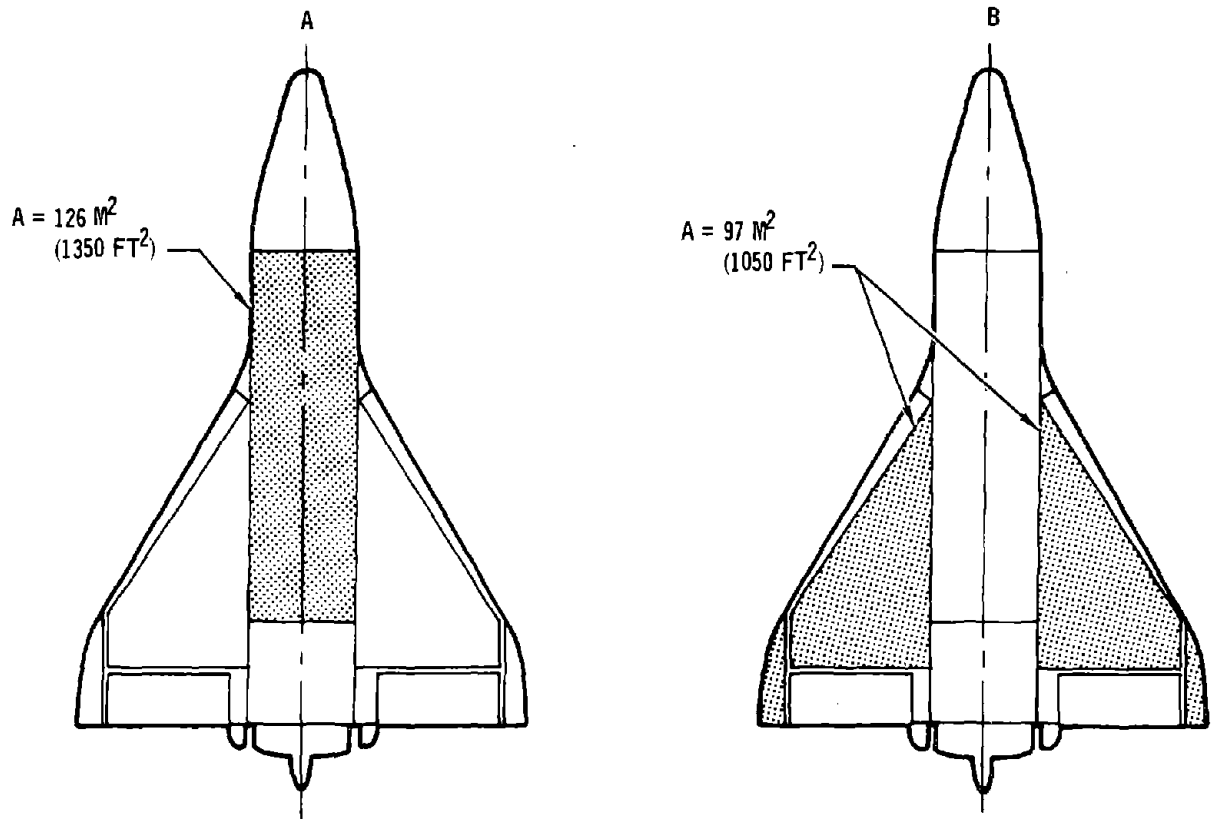

Figure 22

ORBITER ENTRY TRAJECTORY

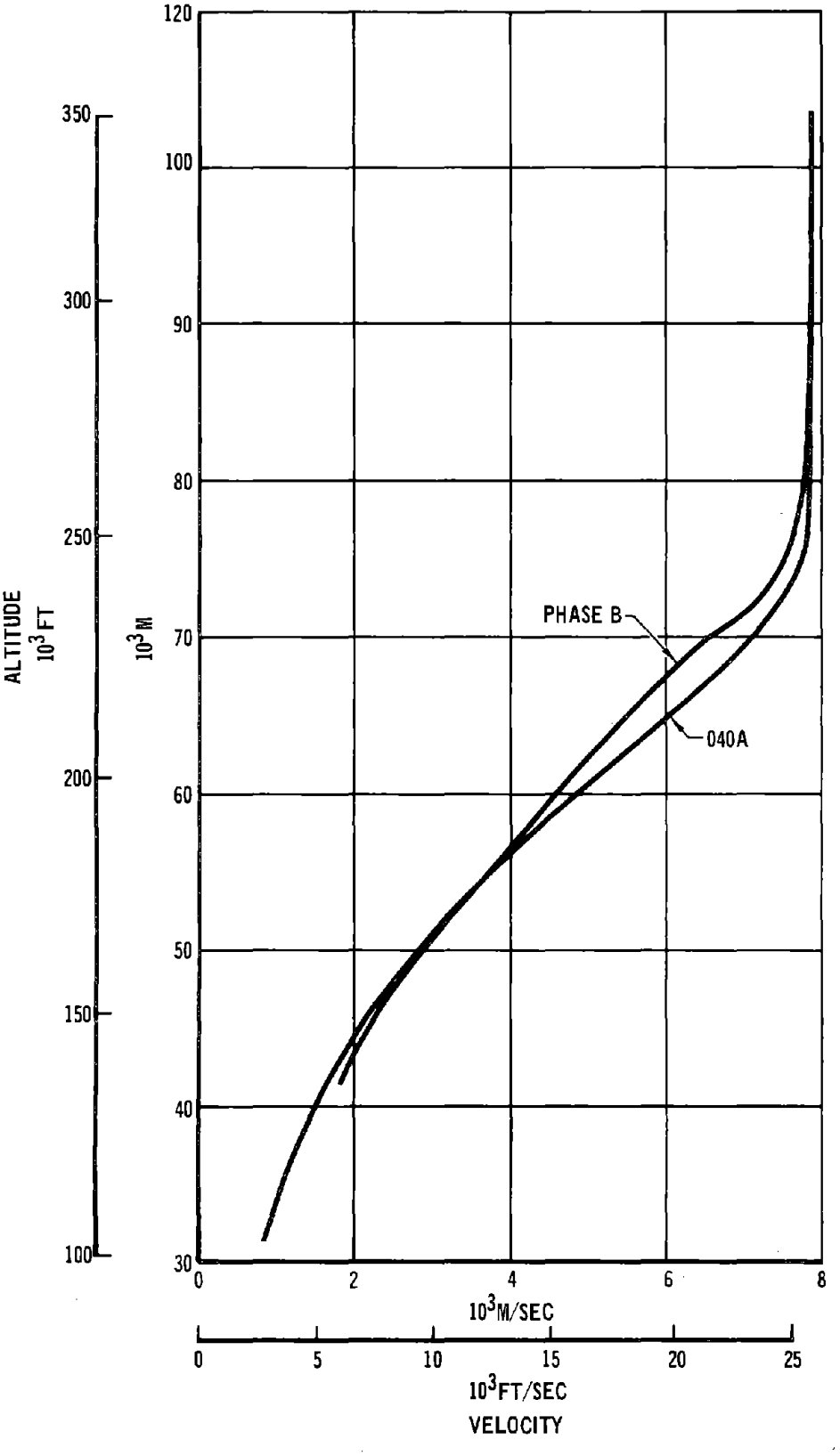

Figure 23

ORBITER BOTTOM CENTERLINE HEAT FLUX

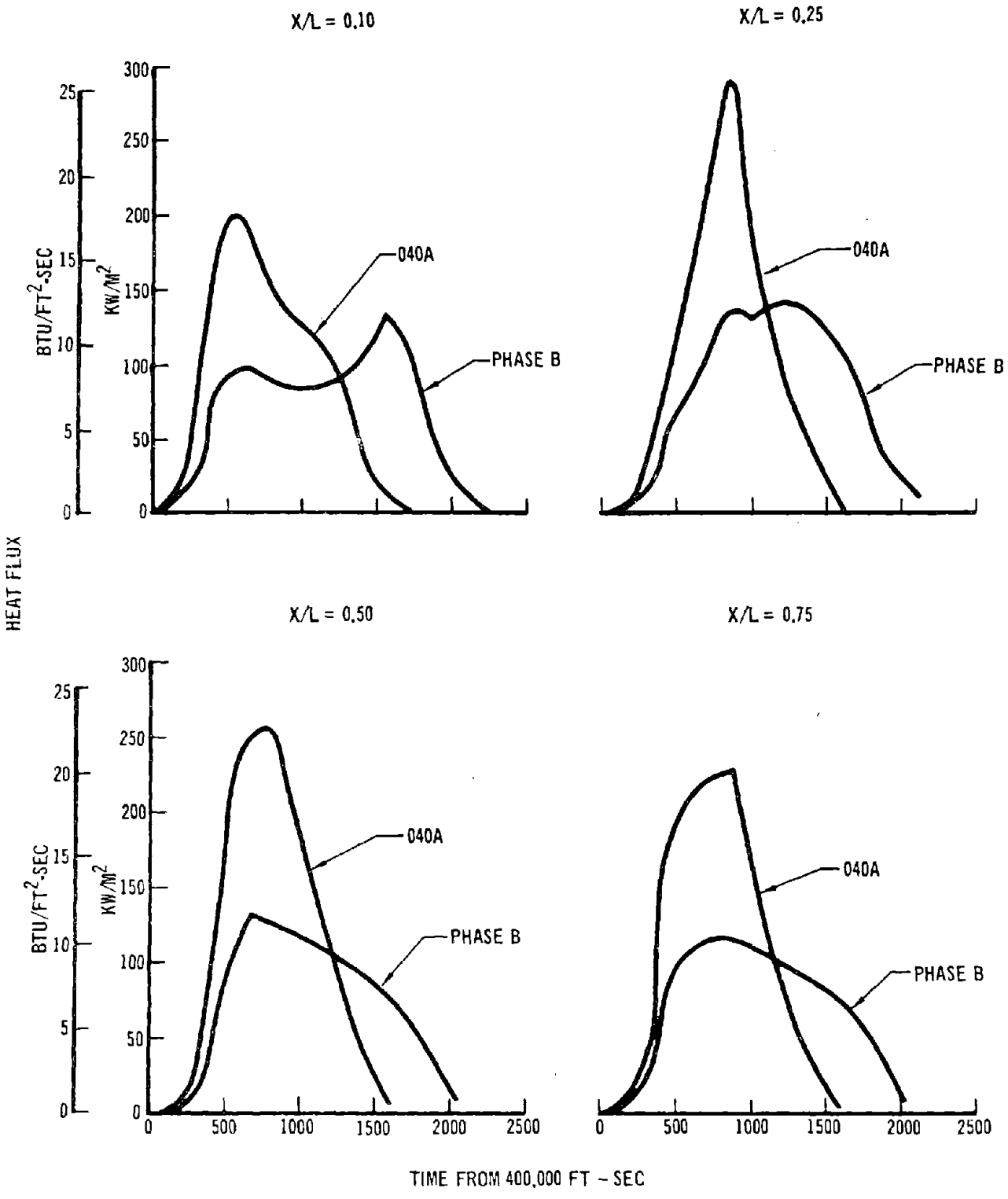

Figure 24

3.2.2 101 Configuration Thermal Model/Analyses - The 101 configuration thermal model was developed to evaluate the locally strong two-dimensional heat transfer in the region between cooling passages, which were integral with skin stiffeners. The model representing the local structure and TPS with the cooling passages is given in Figure 25. Typical dimensions consistent with this illustration were as follows:

skin thickness:	0.81 mm (0.032 in.)
stringer spacing:	10.16 cm (4.0 in.)
stringer height:	3.81 cm (1.5 in.)
stringer thickness:	1.016 mm (0.040 in.)
strain isolation foam thickness:	6.35 cm (0.25 in.)
RSI thickness:	2.54 cm (1.0 in.)

The thermal network consisted of 105 nodes and permitted solution for both local temperatures and active subsystem heating loads, with nodes representing cooling passages held at a constant temperature. The heat loads determined in this fashion were then used as inputs for the fluid circuit analysis. Because the external heat load varies over the orbiter lower surface the analyses were conducted parametrically with variations of the time-integrated external convective heat load, cooling passage spacing, and RSI thickness. In all cases the analyses included transient effects of a heating profile consistent with the entry trajectory shown previously. The TPS thermal analysis was concentrated on a region of the lower surface of the orbiter fuselage,but the results obtained with the parametric analysis are also applicable for the wing lower surface.

Typical results of the study are shown in Figure 26 which illustrates the sensitivity of maximum structure temperature to RSI thickness for a 10.2 cm (4 in.) cooling passage spacing. It was found, Reference [8], that in all cases the RSI thickness reduction was constrained by limits on the aluminum structure temperature rather than the bond. The peak temperature occurred, as expected, at a point midway between cooling passages. Analysis was performed for three passage spacings, 5.08 cm, 10.16 cm, and 20.32 cm (2, 4, and 8 in.).

The cooling rate provided on the selected coolant temperature was calculated simultaneously with the temperatures. This instantaneous rate then was integrated to determine the total cooling required. Results of these computations, normalized to a unit of TPS surface area, are illustrated in Figures 27 and 28 which present

ACTIVE COOLING THERMAL MODEL

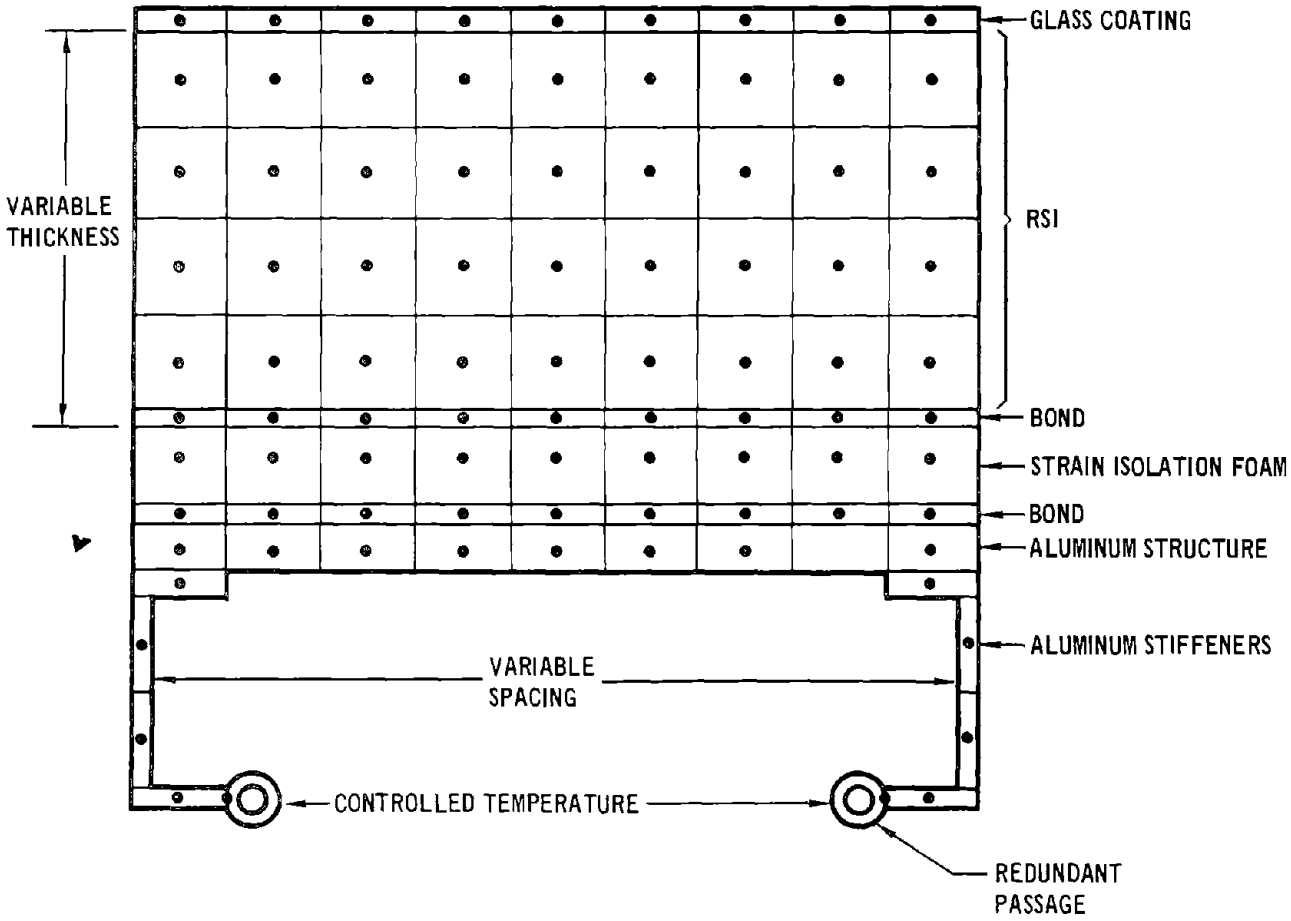

Figure 25.

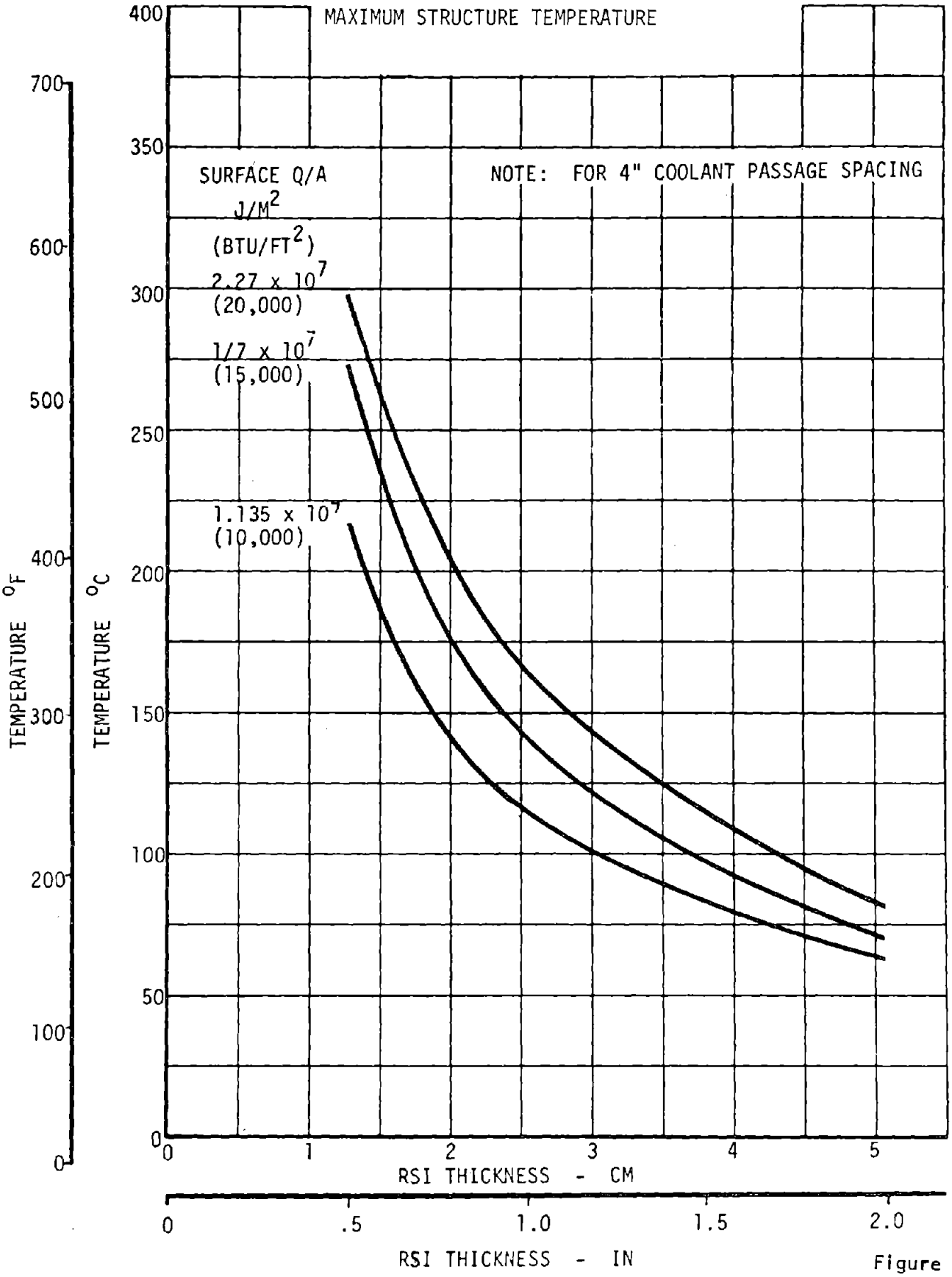
MAXIMUM STRUCTURE TEMPERATURE
NOTE: FOR 4" COOLANT PASSAGE SPACING
SURFACE Q/A
J/M2
(BTU/FT2)
2.27 x 10^7
(20,000)
1.7 x 10^7
(15,000)
1.135 x 10^7
(10,000)
TEMPERATURE °F
TEMPERATURE °C
RSI THICKNESS - CM
RSI THICKNESS - IN

Figure 26

STRUCTURAL COOLING REQUIREMENTS

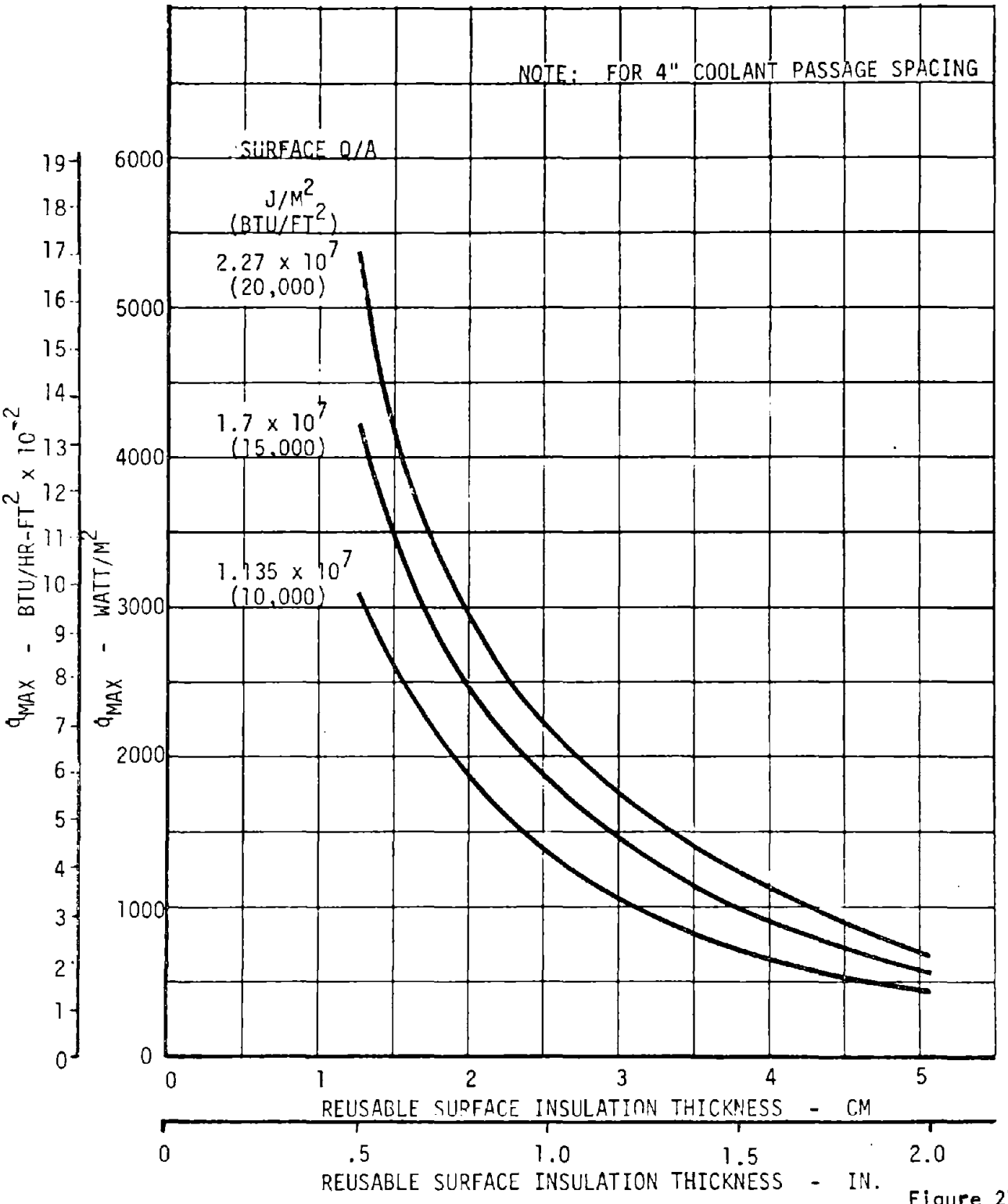

Figure 27

TOTAL HEAT REMOVED FROM STRUCTURE

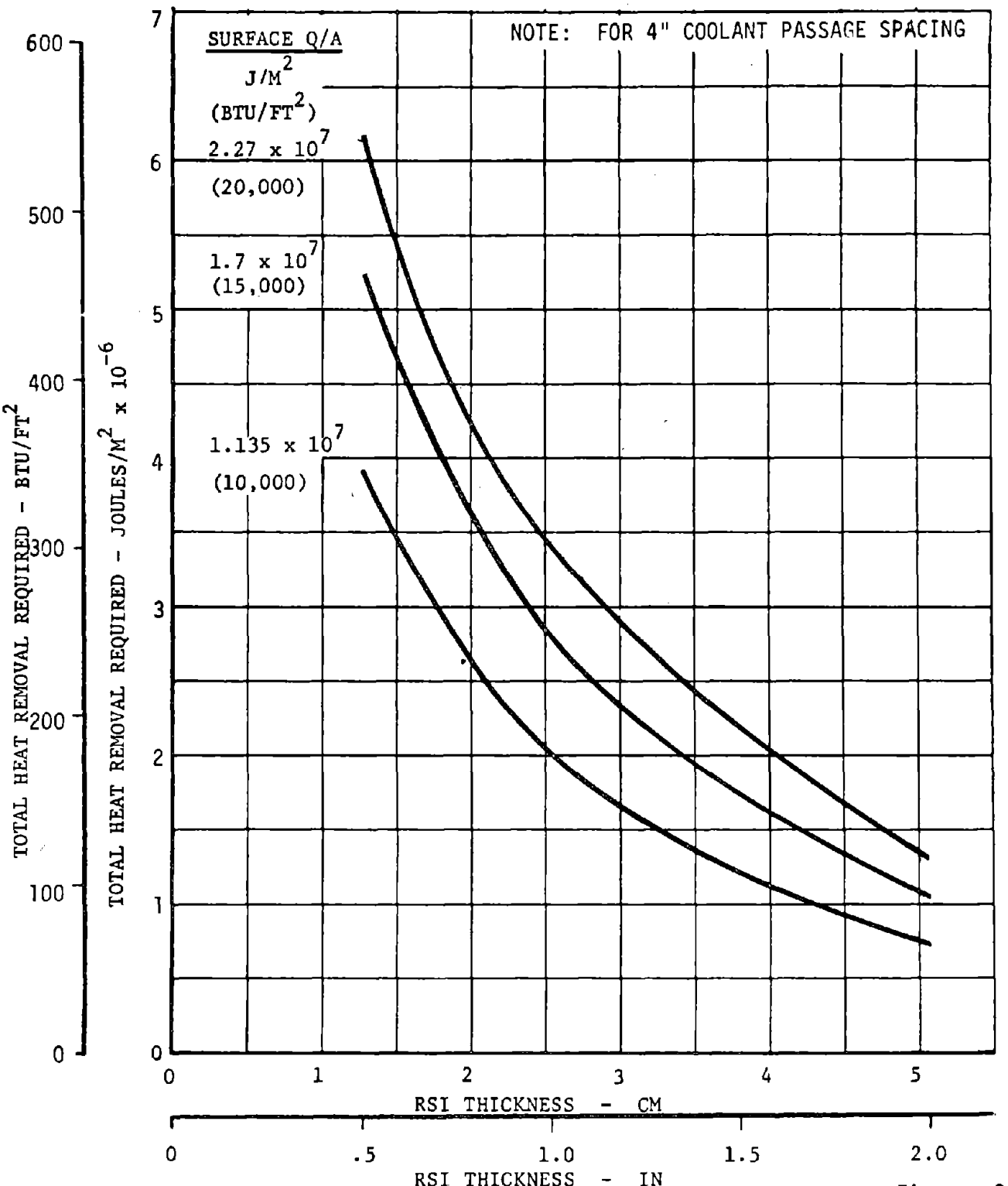

Figure 28

the required cooling rate and total heat removal, respectively. These data then served as inputs in determining the total system requirements for sizing the active cooling system.

In addition to the heat loads data, the weight sensitivity of the passive TPS components (RSI, foam, coating) was available from the parametric thermal analysis. The principal variables were cooling passage spacing and the time-integral of the surface heat flux as illustrated in Figure 29. Note that the passive components are more sensitive to cooling passage spacing than to the surface heat flux integral.

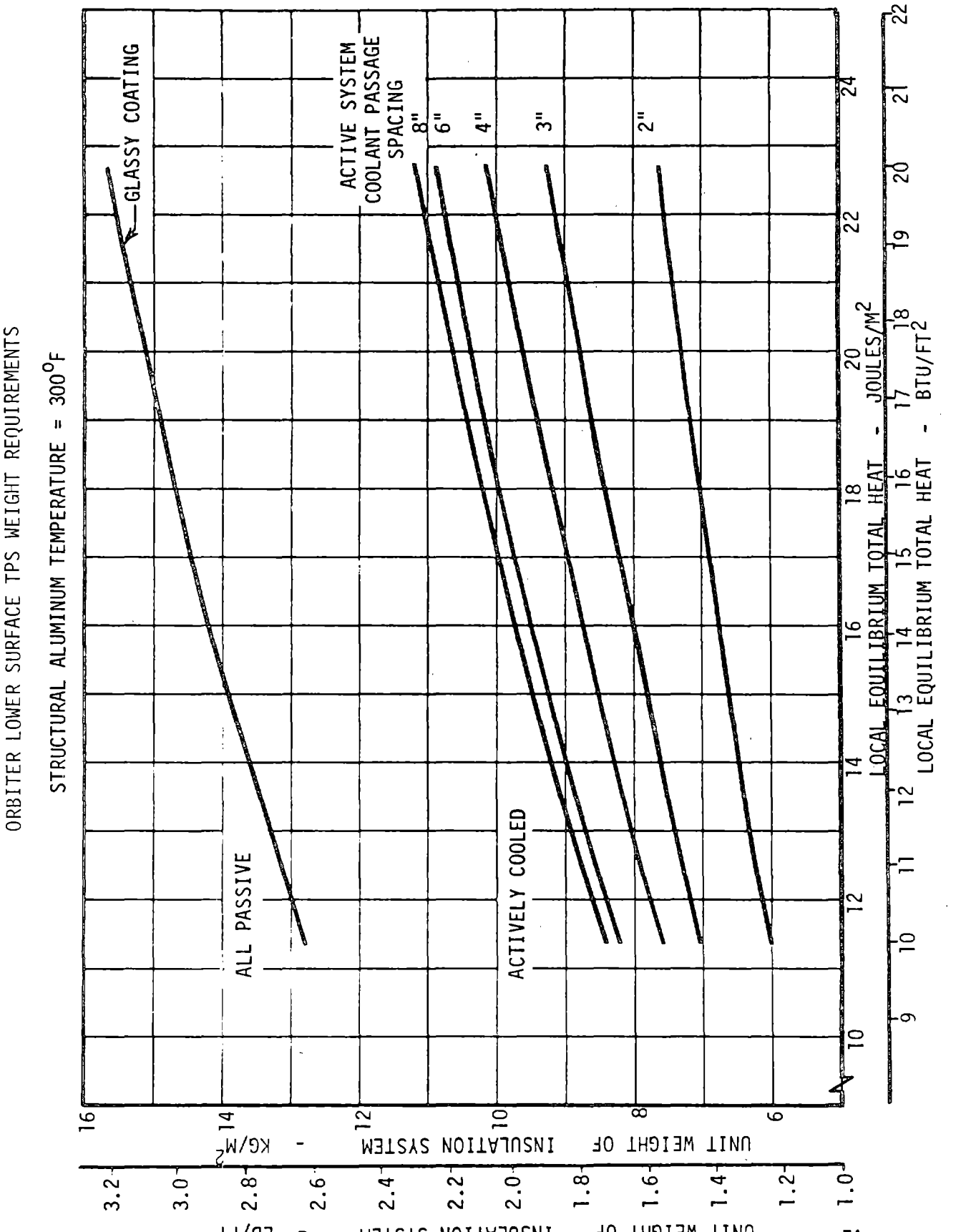
ORBITER LOWER SURFACE TPS WEIGHT REQUIREMENTS
STRUCTURAL ALUMINUM TEMPERATURE = 300°F
GLASSY COATING
ACTIVE SYSTEM COOLANT PASSAGE SPACING
8"
6"
4"
3"
2"
ALL PASSIVE
ACTIVELY COOLED
LOCAL EQUILIBRIUM TOTAL HEAT - JOULES/M2
LOCAL EQUILIBRIUM TOTAL HEAT - BTU/FT2
UNIT WEIGHT OF INSULATION SYSTEM - KG/M2
UNIT WEIGHT OF INSULATION SYSTEM - LB/FT2

Figure 29

3.2.3 Active Subsystem Optimization - The heat transfer data given previously served as the primary study inputs, along with the postulated active subsystem configuration. Several subsystem concepts were examined and two were analyzed in depth. One, a redundant circulating system with a single pump and drive for each circuit, formed the basis for subsystem weight minimization studies. Figure 30 shows the major elements of the active subsystem used in the system evaluations. The second system was nearly identical, the principal difference being the incorporation of redundant coolant pumps in each of the two cooling circuits. This version served as the basis for the estimates of weight and cost for cooling the entire lower surface. It should be noted that only the components in the circulating coolant loop were redundant. The expendables supply contained a 10 percent reserve but was nonredundant.

The coolant passages were arranged on the structure and plumbed to minimize connections and manifolding. The installation of cooling passages integrated with the structure could be accomplished in the same manner as in the Gemini and Airlock radiators. To minimize the number of connectors, extruded stiffeners containing the cooling passages would be used. A tee-shaped stringer as shown in Figure 31 on similar zee-shape extrusion could be used. End connections would be brazed connectors of the type shown in Figure 31. The subsystem uses an expendable coolant for heat dissipation, either water or hydrogen. In the Phase B configuration studies an alternate heat sink -nonexpendable hydrogen (attitude control fuel) was considered, but the total quantity required for attitude control was insufficient to cool the structure. Each pump was driven by a separate hydrazine fueled auxiliary power unit (APU). Both expendable coolant and APU fuel were supplied from prepressurized bladder-type tanks.

System sizing was accomplished with an automated technique using empirical and semiempirical weight relationships. The basis for the sizing approach was a set of correlations of spaceflight equipment weights with either a performance parameter or a parameter which was a function of performance. The computations were performed with a small FORTRAN IV program that was a simplified version of a subroutine of the Preliminary Design Analysis Program (PDAP) reported in Reference 9. The type of weight correlation used is illustrated in Figure 32, which gives correlations for the weight of water storage tanks, equipment mounting weights, hydrogen storage tanks, and the weight of miscellaneous circuitry, lines, and fittings. Each of these was ultimately related, although indirectly, to a performance characteristic. For example, the quantity of expendable cooling water was related to the time-integrated cooling load which, in turn, was a function of the insulation system performance.

ACTIVE STRUCTURAL COOLING SUBSYSTEM SCHEMATIC
(Single Loop Shown)

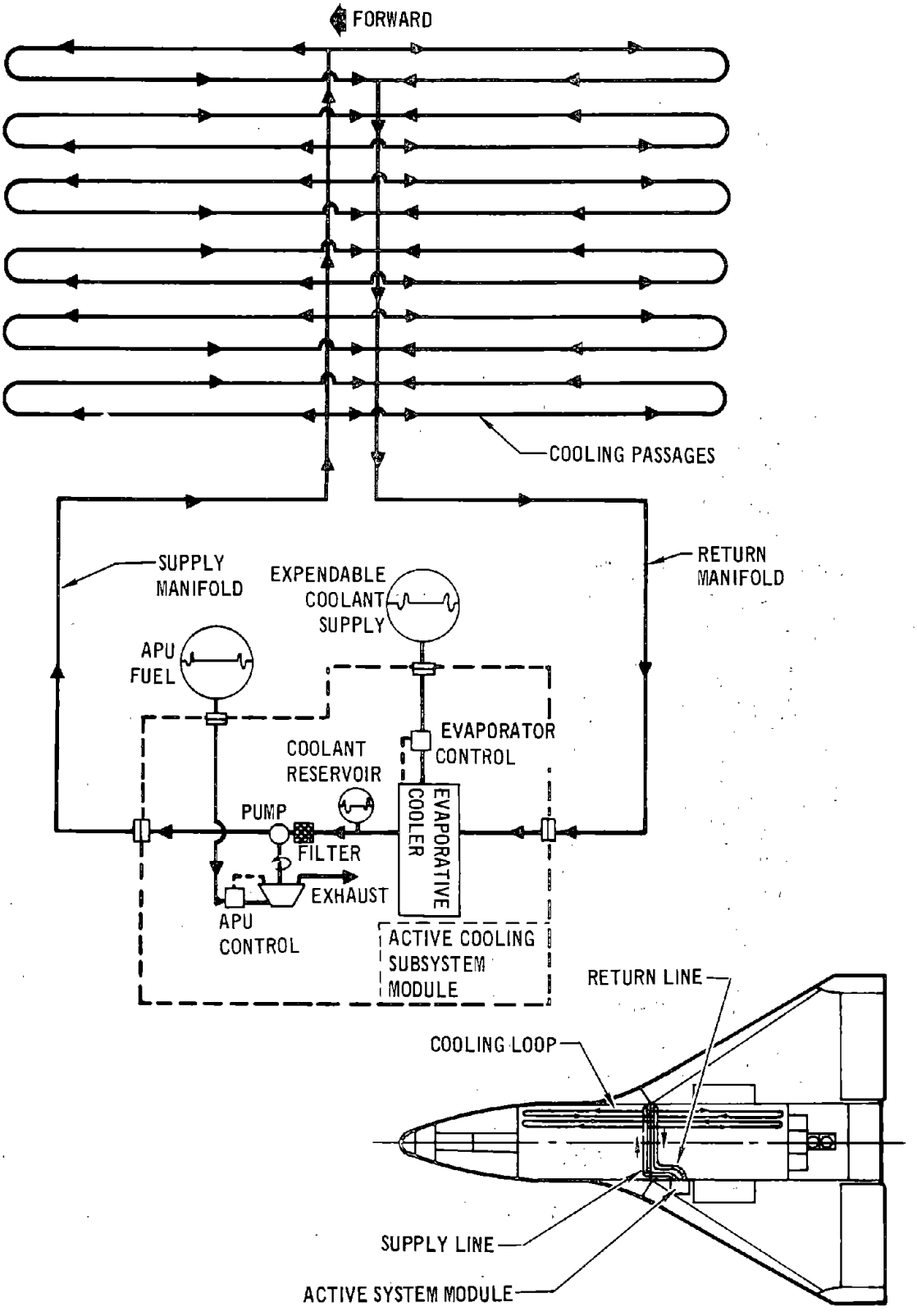

Figure 30

STRUCTURAL INTEGRATION OF COOLING PASSAGE

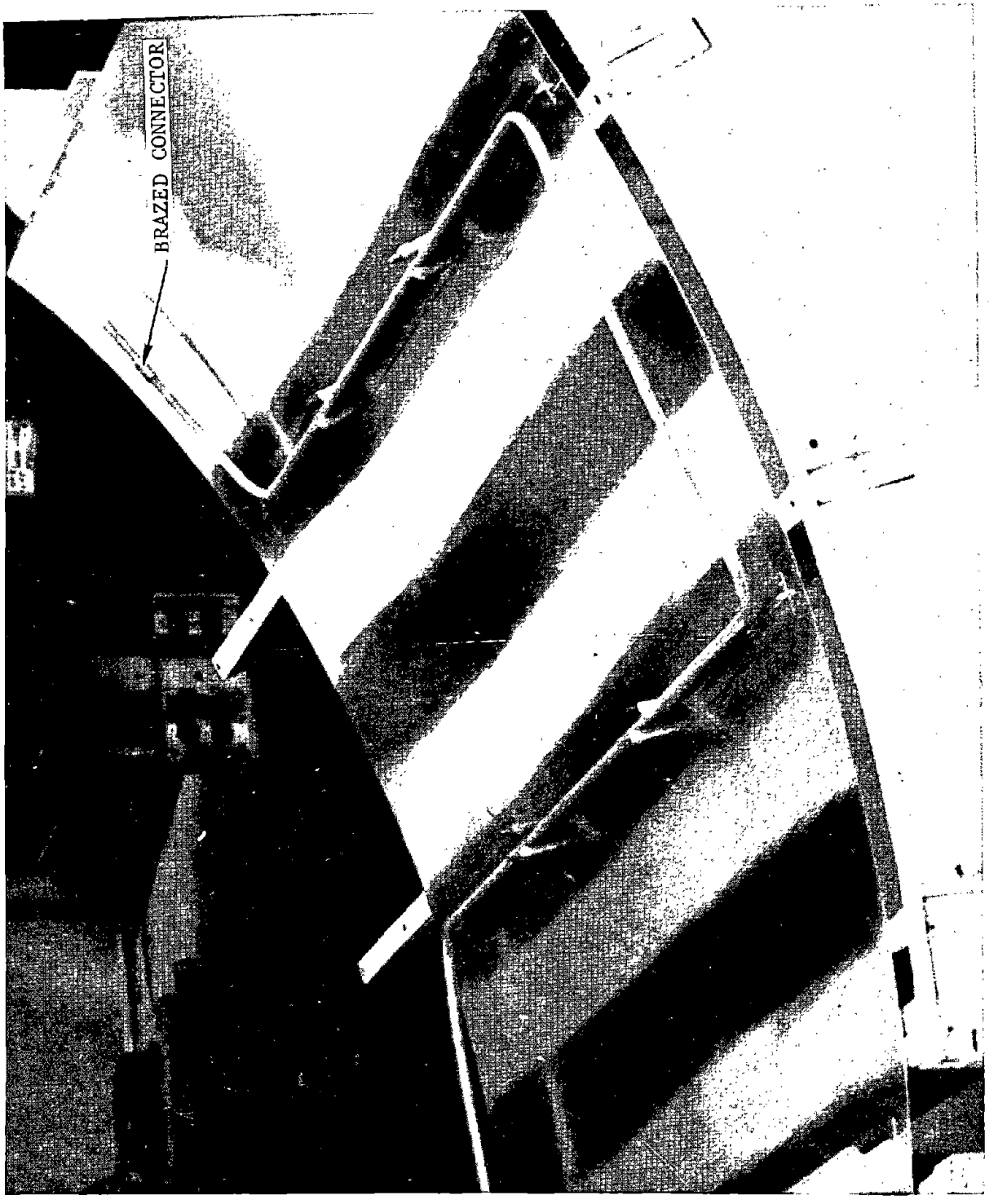

Figure 31

ACTIVE SUBSYSTEM WEIGHT CORRELATIONS

Water Tank Weight Correlation

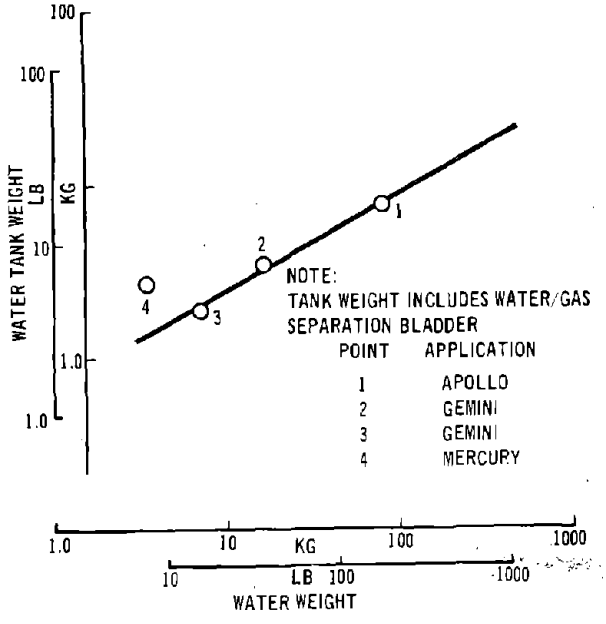

Weight of Miscellaneous Circuitry, Lines and Fittings

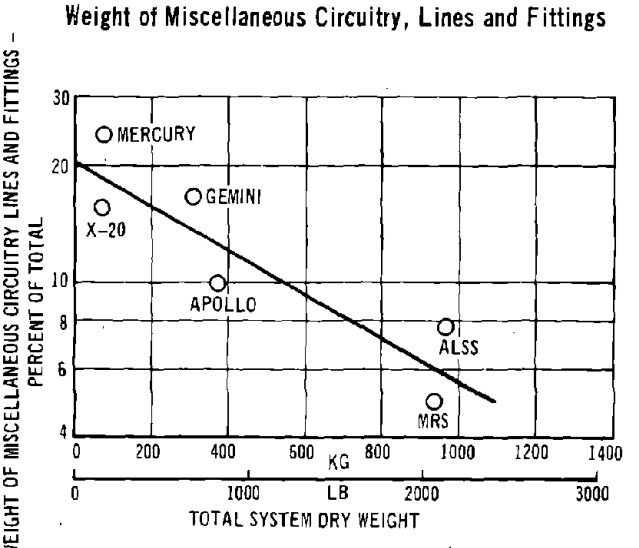

Cryogenic Hydrogen Tankage Weight Supercritical Storage

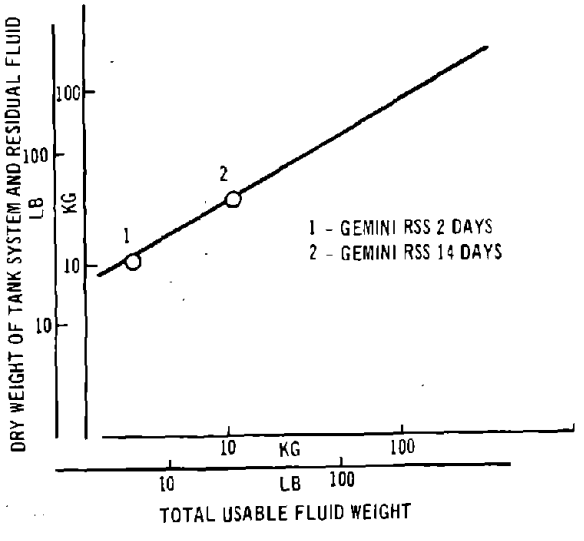

Mounting Structure Weight

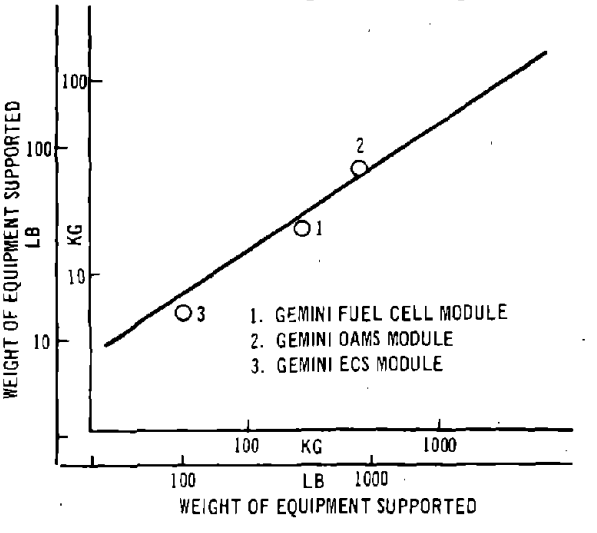

Figure 32

The approach allowed parametric evaluations to quantify certain selections, such as the circulating coolant. Considerable work has been done to simplify coolant fluid selection, e.g., References 10 through 14,but frequently the selection was made on a qualitative basis by ranking fluids in terms of specific pumping power or other criteria. This was useful as a screening technique but by utilizing the quantitative approach, a number of fluids could be evaluated in a manner that determined their effect on the weight of the active system. The results of such a trade study, shown in Figure 33, indicated that the difference in system weight caused by differences in circulating coolant properties were significant. In addition to fluid selection, determination of the optimum cooling passage size was facilitated by this methodology. If the cooling passage was too large, then too much weight was invested in the circulating coolant. If it was too small, then the pumping power and the pumping subsystem weight were excessive. The effect of coolant passage diameter on the weight of the active system was investigated and is shown in Figure 34 for lower fuselage surface.

Combining the effect of cooling passage spacing on the weight of the TPS insulation and the active subsystem allowed determination of the weight of an optimum actively cooled TPS. Figure 35 shows the active subsystem and insulation weights for the optimum tube diameter as a function of tube spacing. Although the total actively cooled TPS weight exhibited a minimum at 10-cm (4 in.) spacing, it was more remarkable for its insensitivity to cooling passage spacing. Consequently, it seemed possible to optimize the structure without consideration of thermal effects. Thus, structural optimization might be conducted as a completely separate problem if the stringer spacing were in the range of 5 to 20 cm (2 to 8 in.).

The actively cooled TPS weight breakdown is tabulated in Figure 36 for the lower fuselage surface, assuming a 10-cm (4 in.) cooling passage spacing. For this condition the addition of active subsystem yields an average unit weight reduction of 2.58 kg/m^2 (0.53 lb/ft^2).

In the analysis discussed previously, the initial entry temperature was assumed to be 37.8°C (100°F). Since the Shuttle orbiter attitude may not be constrained during orbital flight, it was considered possible that the lower surface of the vehicle could be exposed to solar and earth reflected heating for long periods. The "hot" attitudes would tend to remove heat sink capacity from the TPS and substructure by preheating. With an active subsystem the effect of "hot" attitudes on total heat sink

COOLANT SELECTION TRADE STUDY SUMMARY

COOLANT	COLD ORBIT CRITERIA: POUR POINT - -100°C (-150°F)	MAXIMUM TEMPERATURE CRITERIA: VAPOR PRESSURE AT 177°C (350°F) - 6.9 (10^5) N/M² (100 PSIA)	COMPATIBILITY WITH METALS	COMPATIBILITY WITH SEAL MATERIALS	MANNED SPACECRAFT EXPERIENCE	STRUCTURAL ACTIVE COOLING SYSTEM WEIGHT	
						Kg	LB
WATER (REFERENCE ONLY)	NOT ACCEPTABLE	NOT ACCEPTABLE	CORROSION INHIBITOR REQUIRED	ACCEPTABLE WITH MOST ELASTOMERS	SKYLAB ASTRONAUT COOLING CIRCUIT	361	795
ETHYLENE-GLYCOL WATER	NOT ACCEPTABLE	ACCEPTABLE	CORROSION INHIBITOR REQUIRED	ACCEPTABLE WITH MOST ELASTOMERS	APOLLO ECLS	369	811
PROPYLENE-GLYCOL WATER	NOT ACCEPTABLE	ACCEPTABLE	CORROSION INHIBITOR REQUIRED	ACCEPTABLE WITH MOST ELASTOMERS	NONE	367	806
FREON-21	ACCEPTABLE	NOT ACCEPTABLE	DECOMPOSITION ABOVE 300°F	TEFLON ACCEPTABLE	NONE	562	1236
FREON-22	ACCEPTABLE	NOT ACCEPTABLE	DECOMPOSITION ABOVE 300°F	-	NONE	530	1167
FREON-E1	ACCEPTABLE	NOT ACCEPTABLE	-	-	NONE	420	924
FREON-E2	ACCEPTABLE	ACCEPTABLE	-	-	NONE	425	935
FREON-E3	ACCEPTABLE	ACCEPTABLE	DECOMPOSITION ABOVE 300°F	TEFLON ACCEPTABLE	NONE	436	960
FREON-E4	ACCEPTABLE	ACCEPTABLE	-	-	NONE	433	953
FC-75	NOT ACCEPTABLE	ACCEPTABLE	COMPATIBLE WITH MOST METALS	ACCEPTABLE WITH TEFLON, NEOPRENE, KEL-F	NONE	424	932
FC-77	ACCEPTABLE	ACCEPTABLE	COMPATIBLE WITH MOST METALS	ACCEPTABLE WITH TEFLON, NEOPRENE, KEL-F	NONE	420	925
√ COOLANOL 15	ACCEPTABLE	ACCEPTABLE	COMPATIBLE WITH MOST METALS	ACCEPTABLE WITH TEFLON, VITON A, POLYURETHANE, BUTYL	GEMINI, SKYLAB, ECLS	384	846
COOLANOL 25	NOT ACCEPTABLE	ACCEPTABLE	COMPATIBLE WITH MOST METALS	-	NONE	382	840

√ SELECTED COOLANT FOR CIRCULATING SYSTEM

Figure 33

EFFECT OF COOLING PASSAGE SIZE
ON
ACTIVE SUBSYSTEM WEIGHT

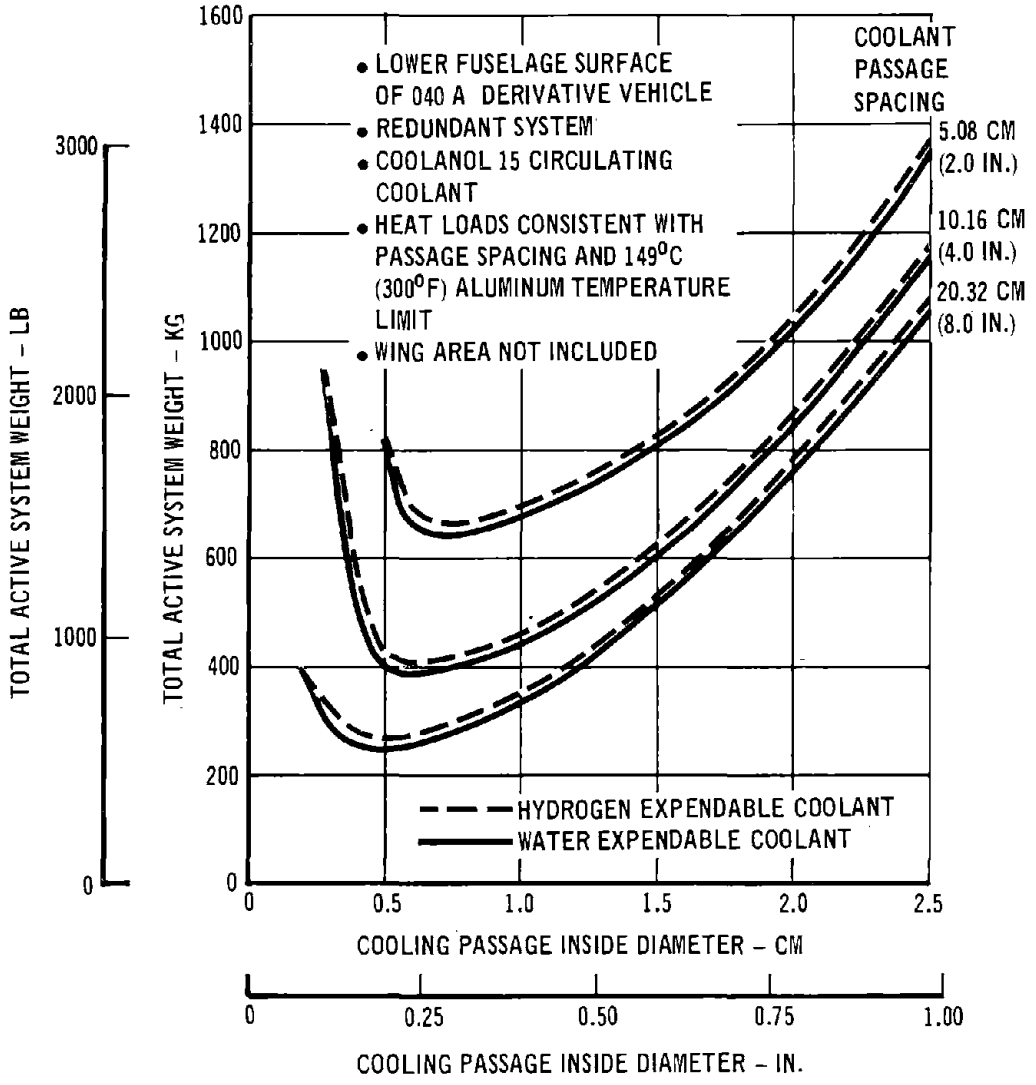

Figure 34

EFFECT OF COOLING PASSAGE SPACING
ON
TOTAL ACTIVE TPS WEIGHT

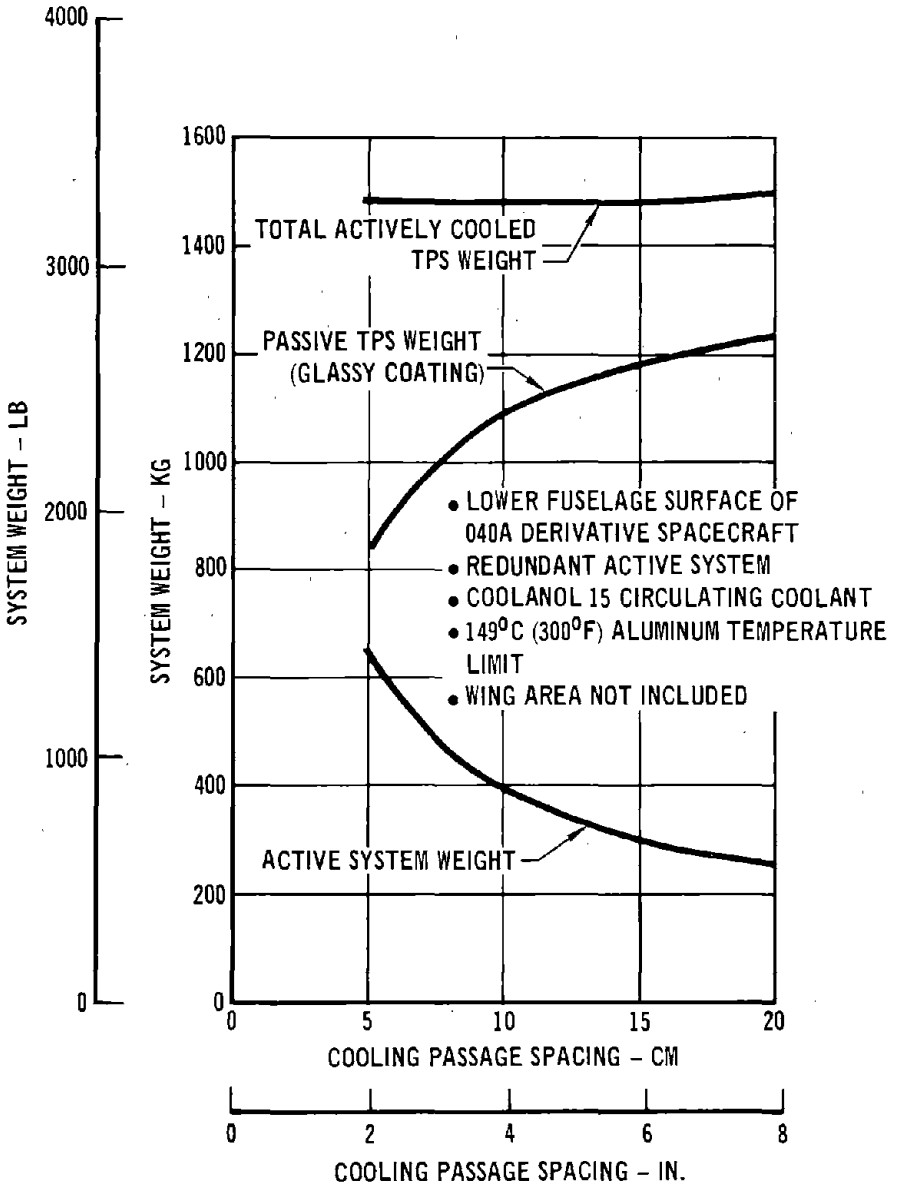

Figure 35

TPS WEIGHT COMPARISON
LOWER FUSELAGE SURFACE

COMPONENT	PASSIVE SYSTEM		ACTIVELY COOLED SYSTEM	
	Kg	LB	Kg	LB
RSI, GLASS COATING, STRAIN ISOLATION FOAM, ADHESIVE	1800	3970	1101	2427
EXPENDABLE WATER (+ 10% RESERVE)			148	326
SUPPLY TANK			11	25
CIRCULATING COOLANT/RESERVOIR			44	96
EVAPORATIVE COOLER			42	92
COOLANT PUMPS			20	45
APU SYSTEM			21	46
CONTROL ELECTRONICS			14	30
SUPPORTING STRUCTURE			53	117
CIRCUITRY, LINES, AND FITTINGS			29	64
ACTIVE SYSTEM SUBTOTAL			382	841
TOTAL TPS WEIGHT	1800	3970	1485	3268

TOTAL AREA COOLED: 126 M^2 (1340 FT^2)

UNIT WEIGHT SAVING ACCOMPLISHED WITH ACTIVE COOLING: 2.59 Kg/M^2 (0.53 LB/FT^2)

Figure 36

capacity would be negligible, as shown in Figure 37, which contrasts the effect of the two system approaches. With typical properties for the surface coating (α_s = 0.72, ϵ = 0.8), normal incident solar heating would result in maximum steady-state skin temperatures approaching 121°C (250°F), increasing the unit weight advantage of active cooling to 8.3 kg/m^2 (1.7 lb/ft^2). A weight saving of this magnitude accrued over the entire 223 m^2 (2400 ft^2) of lower surface which could be cooled would be 1850 kg (4070 lb), a significant fraction of the nominal shuttle payload of 11,950 kg (25,000 lb).

In addition to assessments of system weight for the lower surface of the fuselage, a system weight estimate for the entire lower surface, including the wing, was prepared. This weight estimate (for the entire lower surface) was prepared for two key conditions, level of redundancy and degree of structural integration but in both cases assumed an initial entry temperature of 38°C (100°F). Based on reliability analysis, two levels of system redundancy were considered. The simplest system considered was nonredundant except for the inclusion of redundant coolant pumps. The second redundancy level was a fully redundant active subsystem utilizing two cooling circuits, each with redundant pumps with a nonredundant expendable coolant supply. The degrees of structural integration were essentially bounding values, nonintegral where the cooling passages were considered to be entirely a weight penalty, and fully integrated so that no penalty was incurred by the addition of cooling passages. The results of these analyses are summarized in Figure 38, which gives the weight reductions associated with the above conditions. It should be noted that the effect of a higher design entry temperature than that assumed would be to increase the weight savings shown in the figure. The weight reductions apply to a passive system weight of 3230 kg (7100 lb) for the total lower surface area (223 m^2 - 2400 ft^2) cooled. The active subsystem parameters that characterize the subsystem were:

Circulating Coolant Flowrate:	26,800 kg/hr	(59,000 lb/hr)
System Pressure Drop:	9.3 (10^5) n/m^2	(135 psi)
Coolant Pump Power:	16 kw	(21.5 Hp)
Coolant Temperature Rise	33.4°C	(60°F)

These characteristics were specific for the optimum weight system for which the weight reduction estimates and also detailed cost estimates were prepared.

TPS UNIT WEIGHT SENSITIVITY
TO INITIAL ENTRY TEMPERATURE

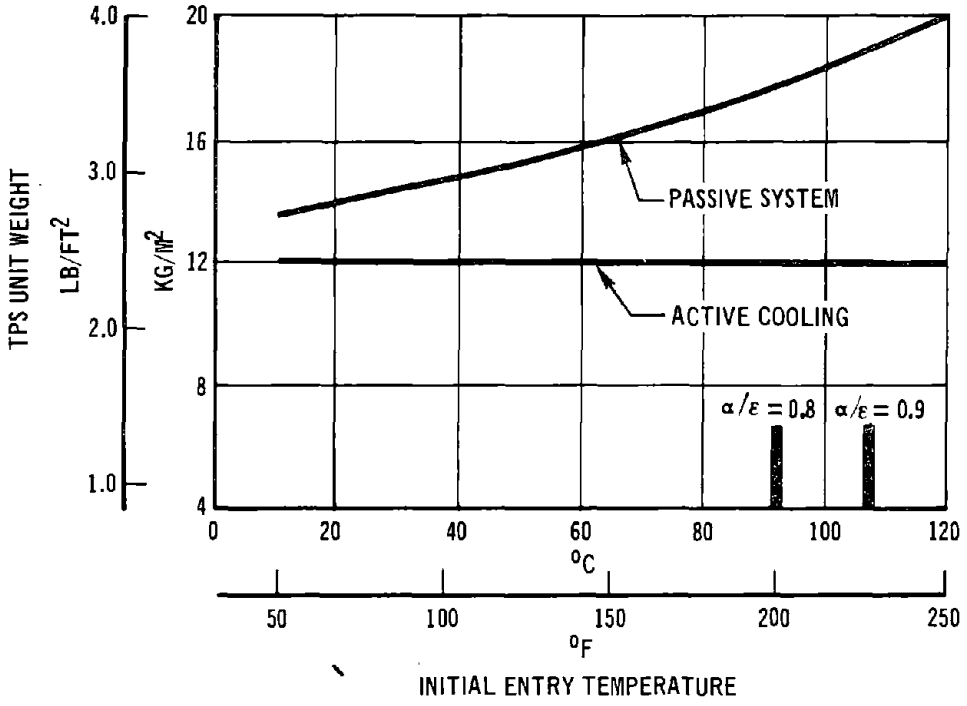

Figure 37

WEIGHT REDUCTION POTENTIAL
FOR ORBITER STRUCTURAL ACTIVE COOLING

	REDUNDANT SYSTEM	NON-REDUNDANT SYSTEM
Cooling Passages Fully Integrated with Structure	ΔW = 581 kg (1280 lb)	ΔW = 697 kg (1534 lb)
Cooling Passages Non-structural	ΔW = 418 kg (920 lb)	ΔW = 615 kg (1354 lb)

Above is for 223 m^2 2400 ft^2 lower surface area cooled, with an initial entry temperature of 38°C (100°F).

Figure 38

3.2.4 Impact of Active Cooling on Shuttle System Cost - The purpose of the active cooling system is to produce a net reduction in the weight of the TPS, or to add to the flexibility of operations so that the value of the orbiter is enhanced. A TPS weight reduction, considered in the context of the total Space Shuttle Program, could allow a substantial cost reduction with no loss of function. Recent estimates by MDC yield a cost/weight sensitivity of about $32,300/kg ($14,700/pound).

The cost benefit from the net weight reduction made possible by active cooling would be offset by the cost of developing and procuring the system components and the costs incurred in integrating the system with the vehicle structure. The weight reductions and the system definitions were used to estimate the total program cost impact of structural active cooling. These results are summarized in Figure 39 and indicate that under some circumstances active cooling may provide a cost saving as well as a weight reduction. The total program cost reduction is in all cases, however, small compared with the orbiter program cost.

The costs for components, the required modifications to the orbiter structure, and added operations were estimated with empirical correlations based on historical data. The saving due to RSI thickness reduction was based on estimated production cost reductions possible with thinner RSI. Generally, thinner RSI tiles have more uniform properties (mechanical and thermal). Consequently, the amount trimmed and the scrap rate should be less for thinner tiles. It should be noted that the RSI thickness (or weight) reduction was based on a 38°C (100°F) design entry temperature and higher design values would indicate greater cost reductions.

The payload cost effect is based on a payload cost sensitivity of $32,300/kg ($14,700 / lb) developed by MDC with the methodology described in Reference 15. The value represents changes in total program cost, including changes in the solid rocket motors, expendable tank, and orbiter that correspond with a change in payload weight. As a first approximation, the program cost change which should result from an orbiter weight change is taken as equal to a corresponding payload weight change.

The expected vehicle refurbishment cost, which is significant only for the nonredundant system, is the statistically expected cost based on the estimated system probability of failure. The expected cost was computed as the product of the probability of failure (445 missions) and the replacement cost for a single vehicle. Failure was taken to be the occurrence of an event in which substantial refurbishment would be required due to overheating of the primary structure, but does not connote a catastrophic event. It was assumed that any failures would be

TOTAL PROGRAM COST IMPACT

ITEM	PROGRAM COST CHANGE[1]	
	REDUNDANT SYSTEM – $MILLION	NON-REDUNDANT SYSTEM – $MILLION
EXPENDABLE COOLANT(WATER) SUPPLY[2]	1.49	1.49
EVAP. COOLERS	2.39	1.20
COOLANT PUMPS AND COOLANT	2.36	1.18
ELECTRONIC CONTROLS	3.00	3.00
APU SYSTEM IMPACT	4.77	2.38
SUPPORT STRUCTURE	2.18	1.09
MISC. VALVES, FILTERS, ETC.	1.38	0.69
ACTIVE SUBSYSTEM TOTAL	17.57	11.03
ADDITION OF COOLING PASSAGES TO ORBITER STRUCTURE	6.70	3.35
ADDITIONAL OPERATIONS COST	1.58	1.58
REDUCTION OF RSI THICKNESS	– 9.00	– 9.00
PAYLOAD EFFECT	– 18.82	– 22.55
EXPECTED LOSS	0.12	31.61
TOTAL NET COST CHANGE	– 1.23	16.02

1. FOR 5 VEHICLES, 445 FLIGHTS, BASED ON INITIAL TEMPERATURE OF 38° C (100°F), STRUCTURALLY INTEGRATED COOLING PASSAGES.
2. USE OF EXPENDABLE HYDROGEN FOR COOLING ADDS $2.5 MILLION
3. ESTIMATED VEHICLE REPLACEMENT COSTS BASED ON ACTIVE SUBSYSTEM RELIABILITY.

Figure 39

of a random nature, and that failures due to a systematic change would be prevented by detection and routine maintenance.

The cost data indicate a potential program cost reduction, permitted by the weight reduction that an active subsystem should provide. It must be noted, though, that the cost of the orbiter itself is increased. The cost savings can only accrue if the active system is implemented prior to booster and tankage design freeze.

It was noted previously (Figure 37) that the total weight reduction attainable with active cooling was dependent on the initial entry temperature. Since the major cost reduction potential was associated with the net orbiter weight reduction, the cost impact showed a similar sensitivity to initial starting temperature. Figure 40 presents these data, which indicate that active and passive system costs would be equal at a relatively low initial entry temperature. If, for operational reasons, the initial temperature of the structure, just prior to entry, was near the structural limit temperature, the potential cost savings would increase.

PROGRAM COST IMPACT OF ACTIVE COOLING

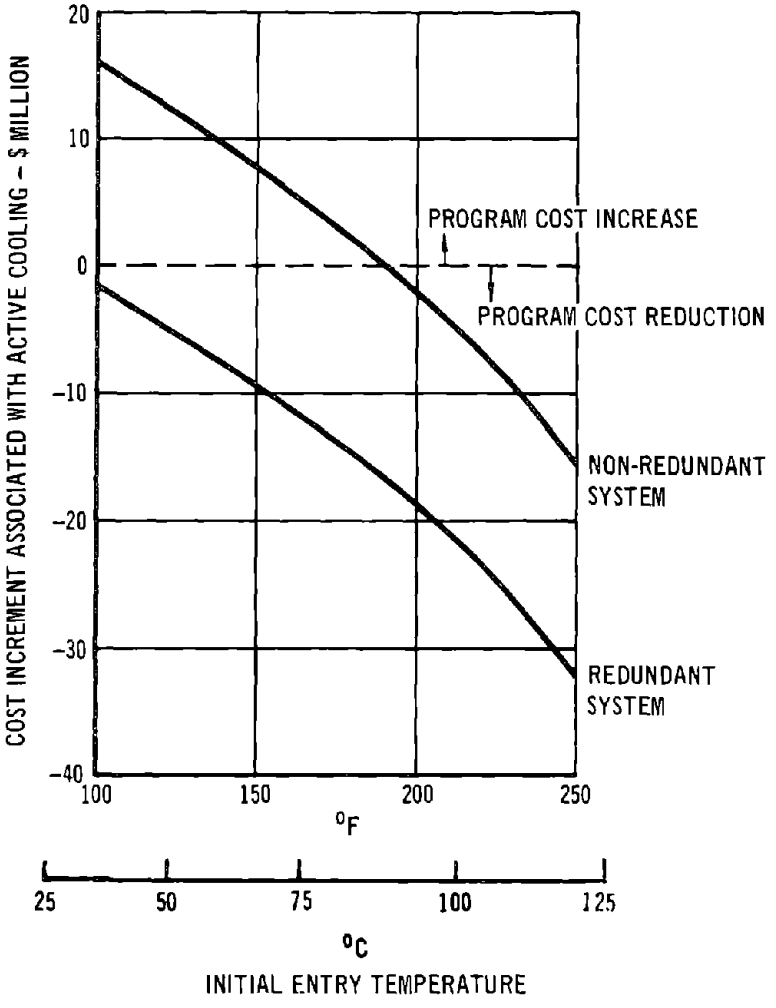

Figure 40

4. TASK 2: HEAT SINK CONCEPTS FOR THE BOOSTER

This task investigated the problems which could occur in heat sink design of a reusable Shuttle booster. Various alternatives to a thickened aluminum skin approach to heat sink design were postulated and evaluated.

4.1 Booster Descriptions - Several booster-orbiter combinations (Figure 41) were postulated in order to provide information of general applicability. After overall loads and heating histories of each were compared, it was decided to concentrate the analytical investigations on the piggyback S-IC configuration since this combination was representative and appeared most likely to be used for the Shuttle. This figure also identifies common and unique problem areas studied in this task. Figure 42 lists the figures which contain loads and heating histories for the two boosters. Since the critical wing heating and load conditions occur during entry, they are independent of the relative position of the orbiter during ascent.

4.1.1 Shuttle Fully Reusable Booster - The fully reusable booster, illutrated in Figure 43, was derived in the Phase B extension studies conducted by the McDonnell Douglas Team. This design had the LOX tank forward and the LH_2 tank aft, with a low canard mounted between the tanks. The separation velocity of later versions of this booster was 2.35 km/sec (7700 ft/sec) as shown in Figure 44. Heating histories at various vehicle locations are presented in Figure 45 while the limit body and wing loading parameters are found in Figures 46 and 47 .

4.1.2 Saturn IC Stage (S-IC) - A winged modification of the Saturn Stage IC, proposed by Boeing, is shown in Figure 48. Using an aft delta wing at the bottom of the body, this booster has LOX forward and RP-1 propellant aft. The trajectory history is presented in Figure 49. Heating environments are described in Figure 50, supplemented by local heating relationships around the body in Figure 51. Body and wing loading envelopes for the modified S-IC are presented in Figures 52, 53, and 54.

4.2 Heat Sink Concepts - A heat sink approach to accommodate aerodynamic heating on a reusable booster during its ascent and entry is logical in view of the relatively low total heating involved, the design simplicity, and the minimum recertification required after each flight. The arguments against this method of thermal protection were the necessity to rely on the structure for protection, the fact that the structure would be continually working near its maximum temperature (each flight) and the small degree of overheating permitted.

HEAT SINK BOOSTERS POTENTIAL PROBLEM AREAS

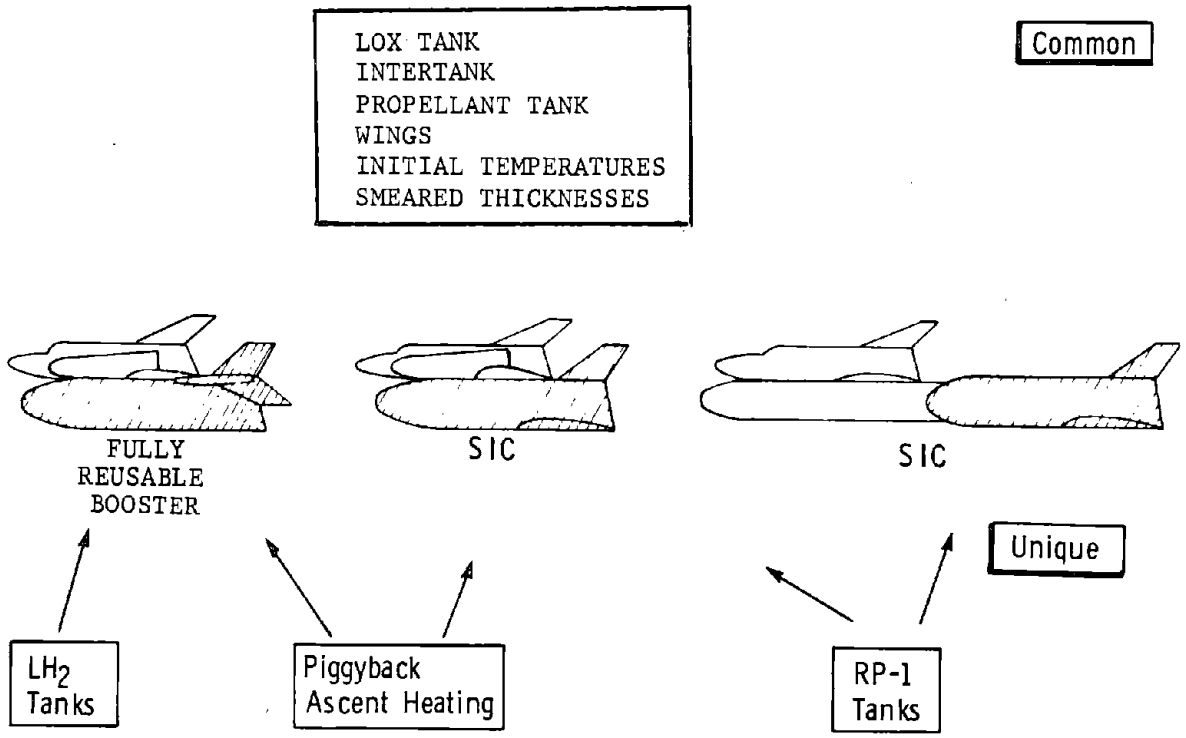

Figure 41

SUMMARY OF BOOSTER ENVIRONMENTS

		FULLY REUSABLE BOOSTER		S-IC	
		END/LOADED	PIGGYBACK	END/LOADED	PIGGYBACK
LOADS	BODY	FIG. 46	FIG. 48	FIG. 54	FIG. 52
	WING		FIG. 47		FIG. 53
HEAT	BODY	FIG. 45	FIG. 45	FIG. 50	FIG. 50
	WING				

Figure 42

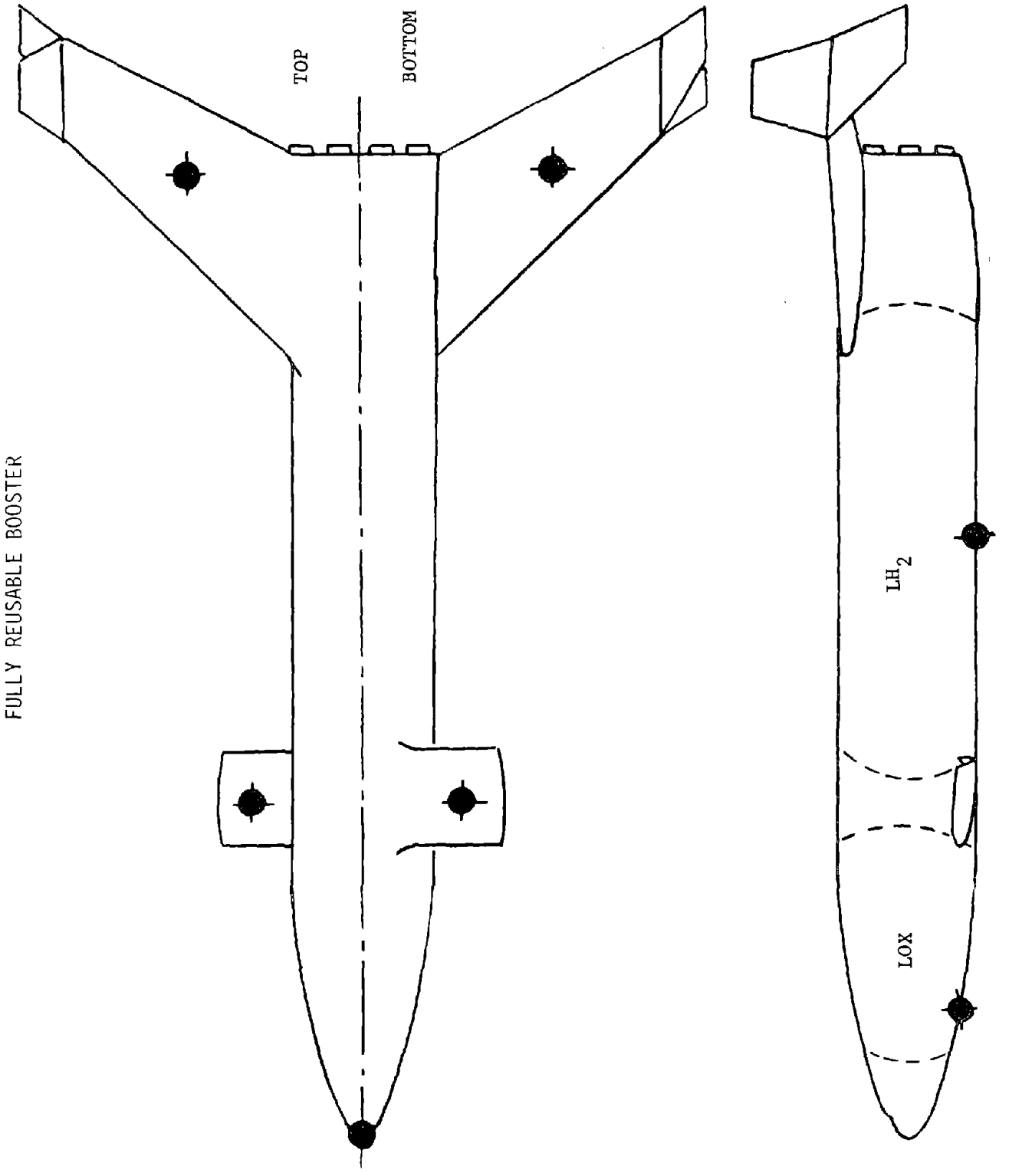

Figure 43

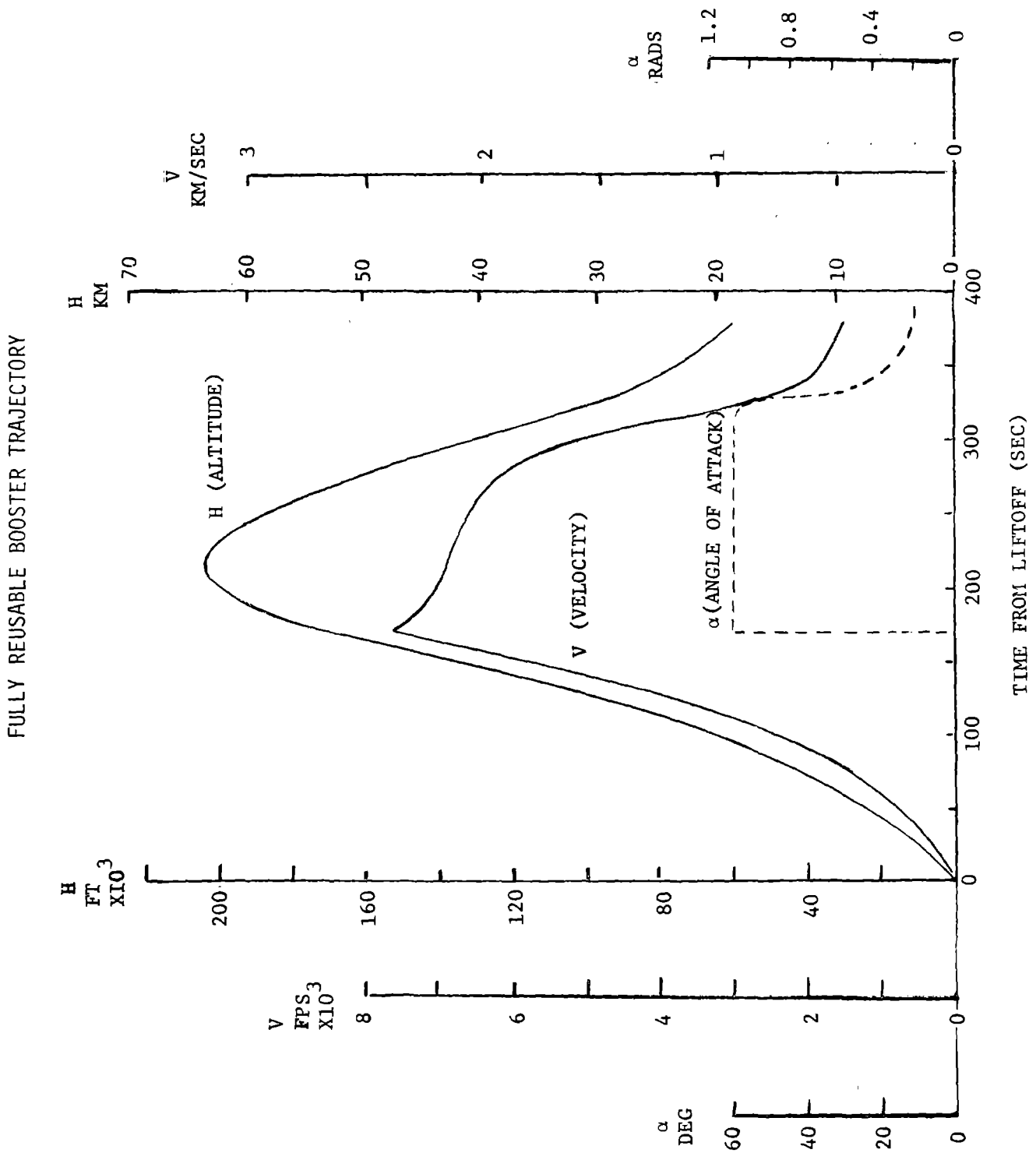
FULLY REUSABLE BOOSTER TRAJECTORY
H (ALTITUDE)
V (VELOCITY)
α (ANGLE OF ATTACK)
TIME FROM LIFTOFF (SEC)
H FT X10^3
V FPS X10^3
α DEG
H KM
V KM/SEC
α RADS

Figure 44

HEATING HISTORIES, FULLY REUSABLE BOOSTER

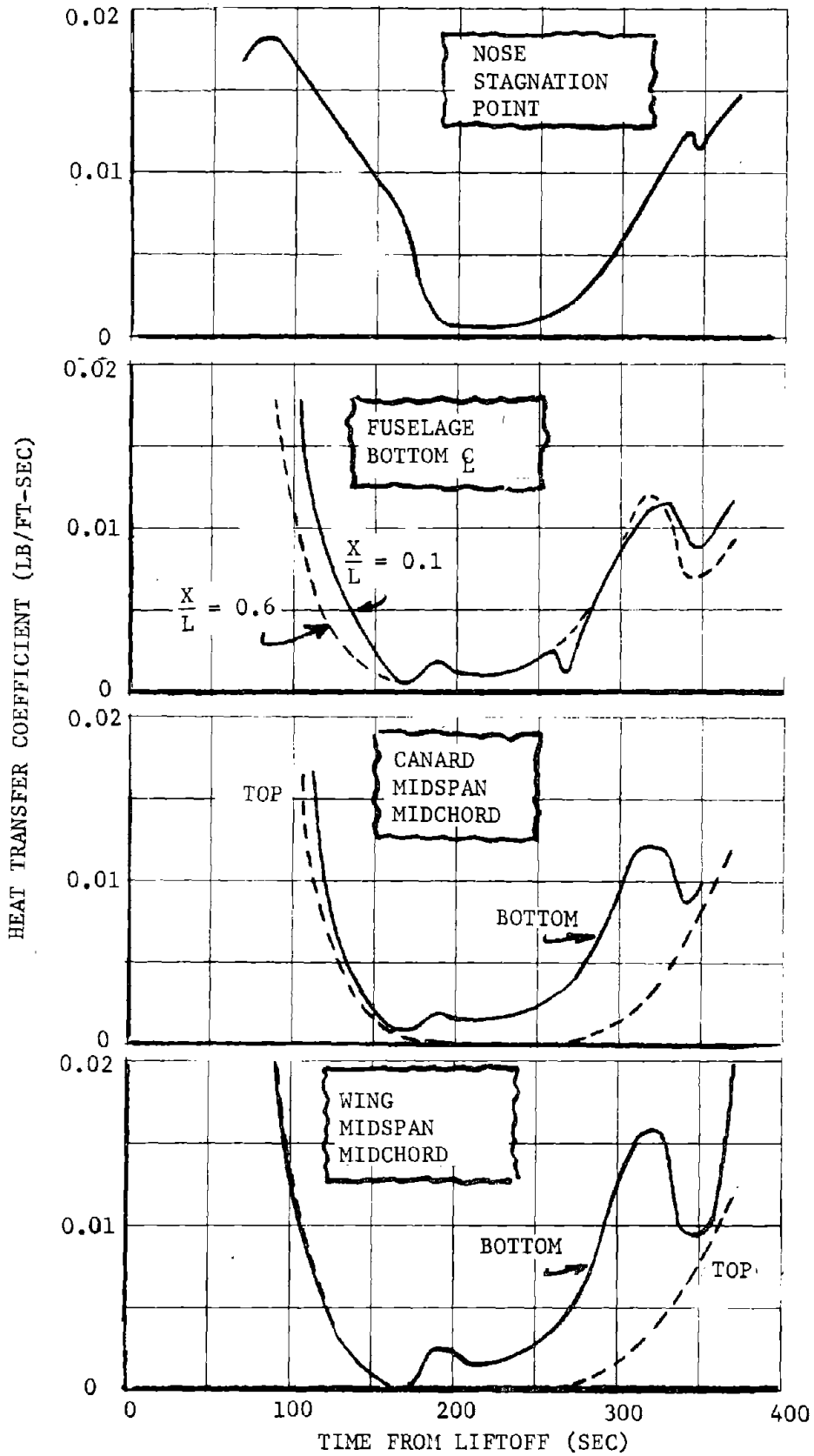

Figure 45

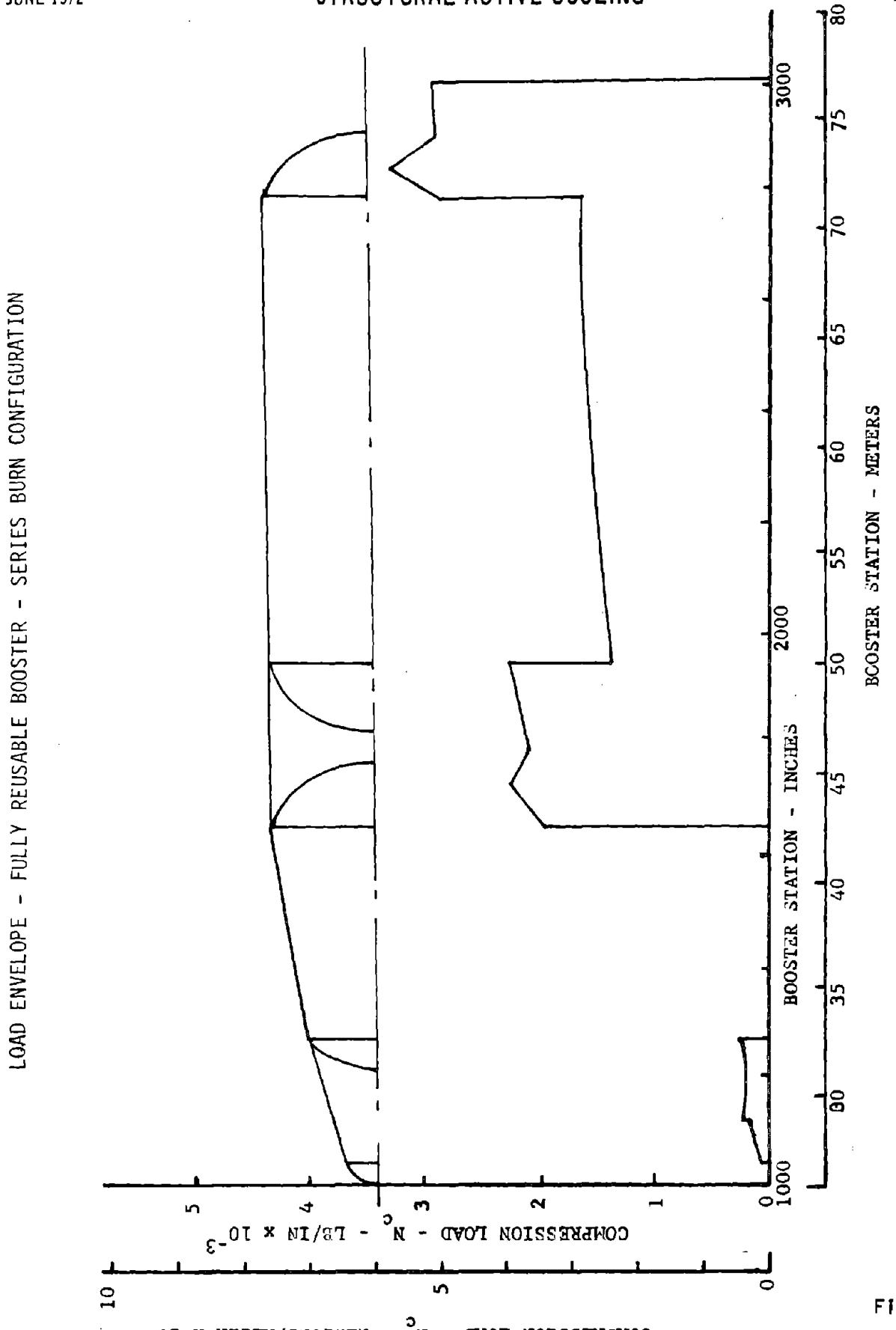
LOAD ENVELOPE - FULLY REUSABLE BOOSTER - SERIES BURN CONFIGURATION
BOOSTER STATION - METERS
BOOSTER STATION - INCHES
COMPRESSION LOAD - N_c - LB/IN x 10^{-3}
COMPRESSION LOAD - N_c - NEWTONS/METER x 10^{-5}

Figure 46

WING BENDING MOMENT
FULLY REUSABLE PIGGYBACK BOOSTER

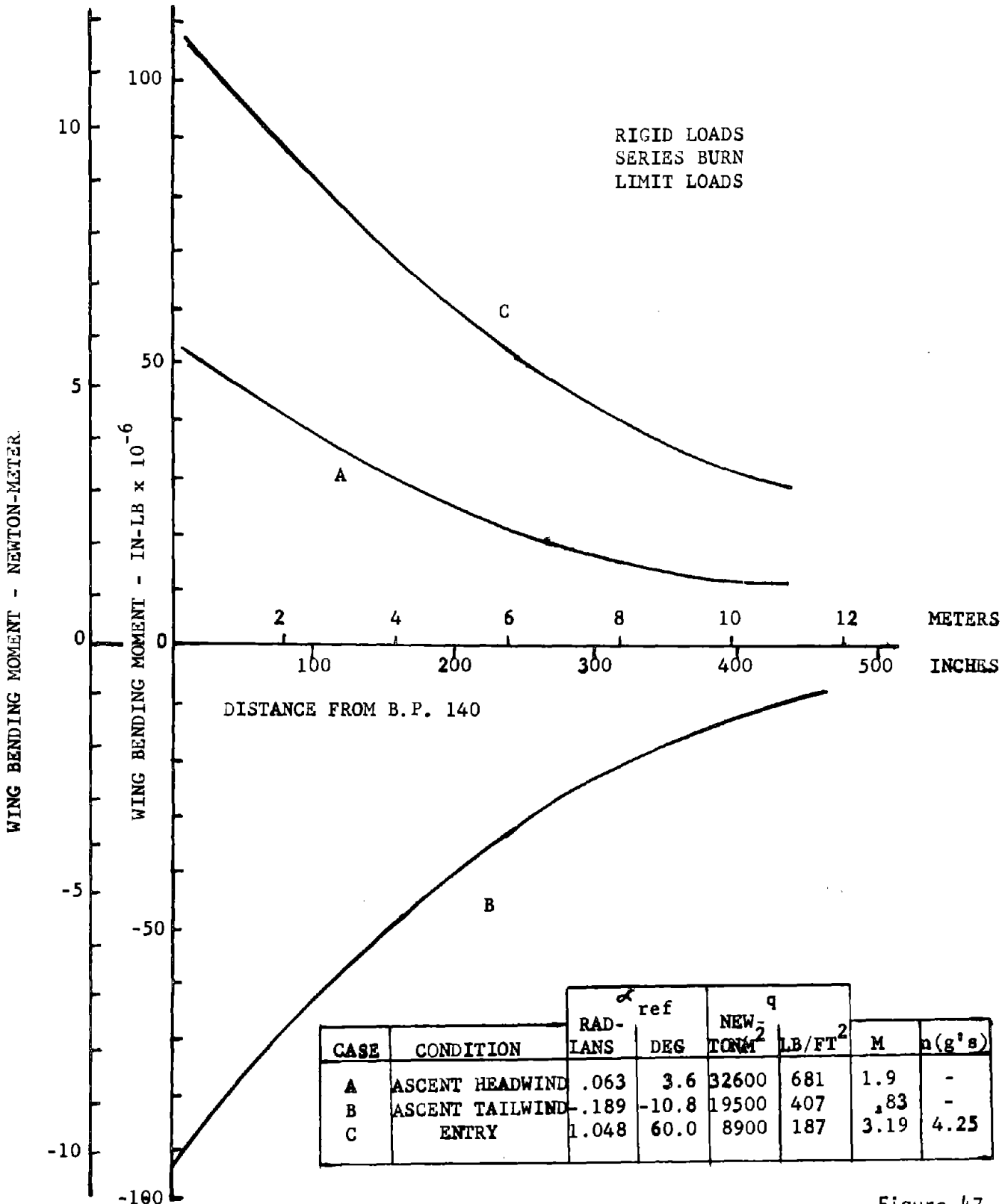

CASE	CONDITION	α_{ref} RADIANS	α_{ref} DEG	q NEWTON/M^2	q LB/FT^2	M	n(g's)
A	ASCENT HEADWIND	.063	3.6	32600	681	1.9	-
B	ASCENT TAILWIND	-.189	-10.8	19500	407	.83	-
C	ENTRY	1.048	60.0	8900	187	3.19	4.25

Figure 47

HEATING HISTORY LOCATIONS
S-IC BOOSTER

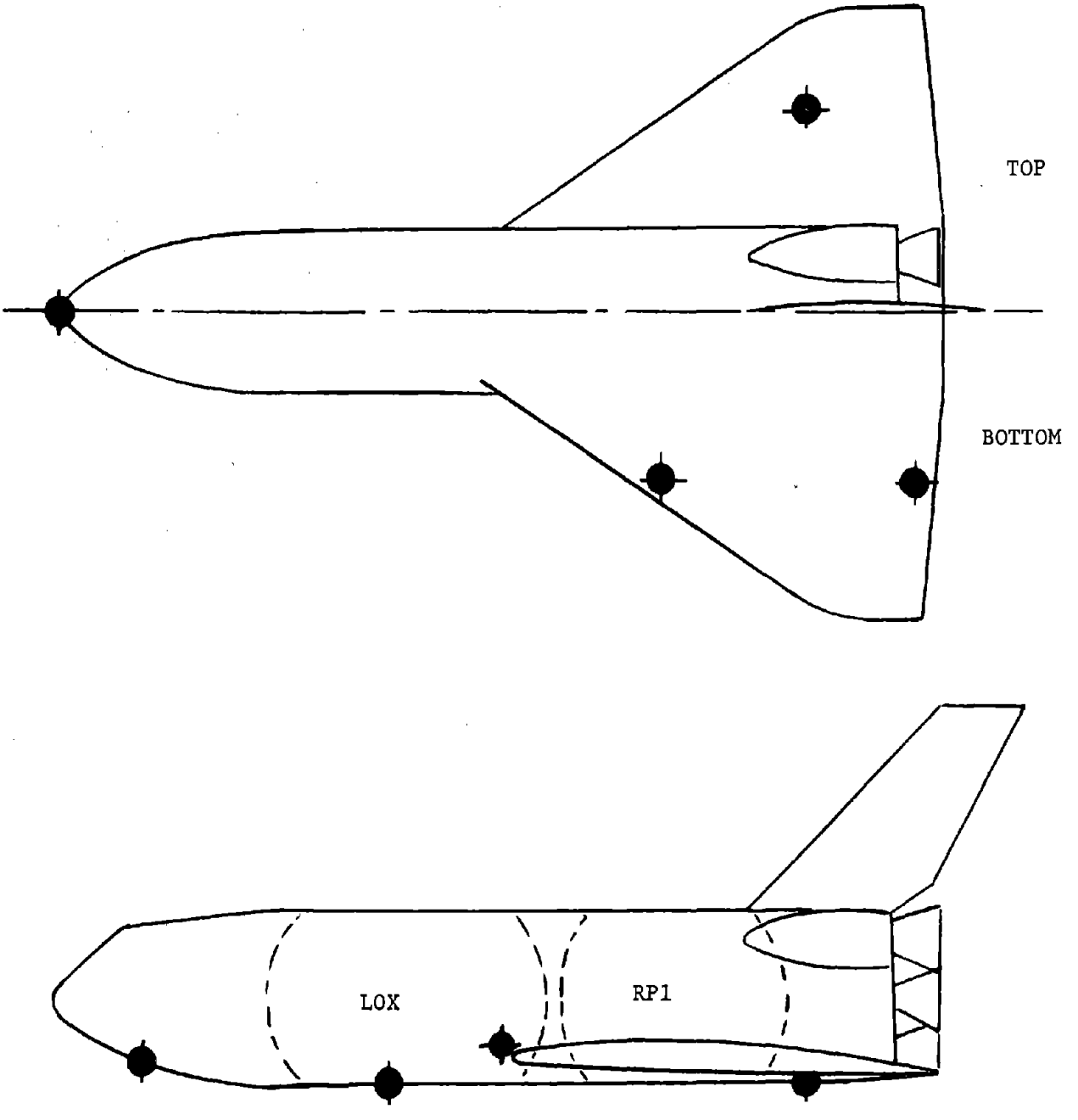

Figure 48

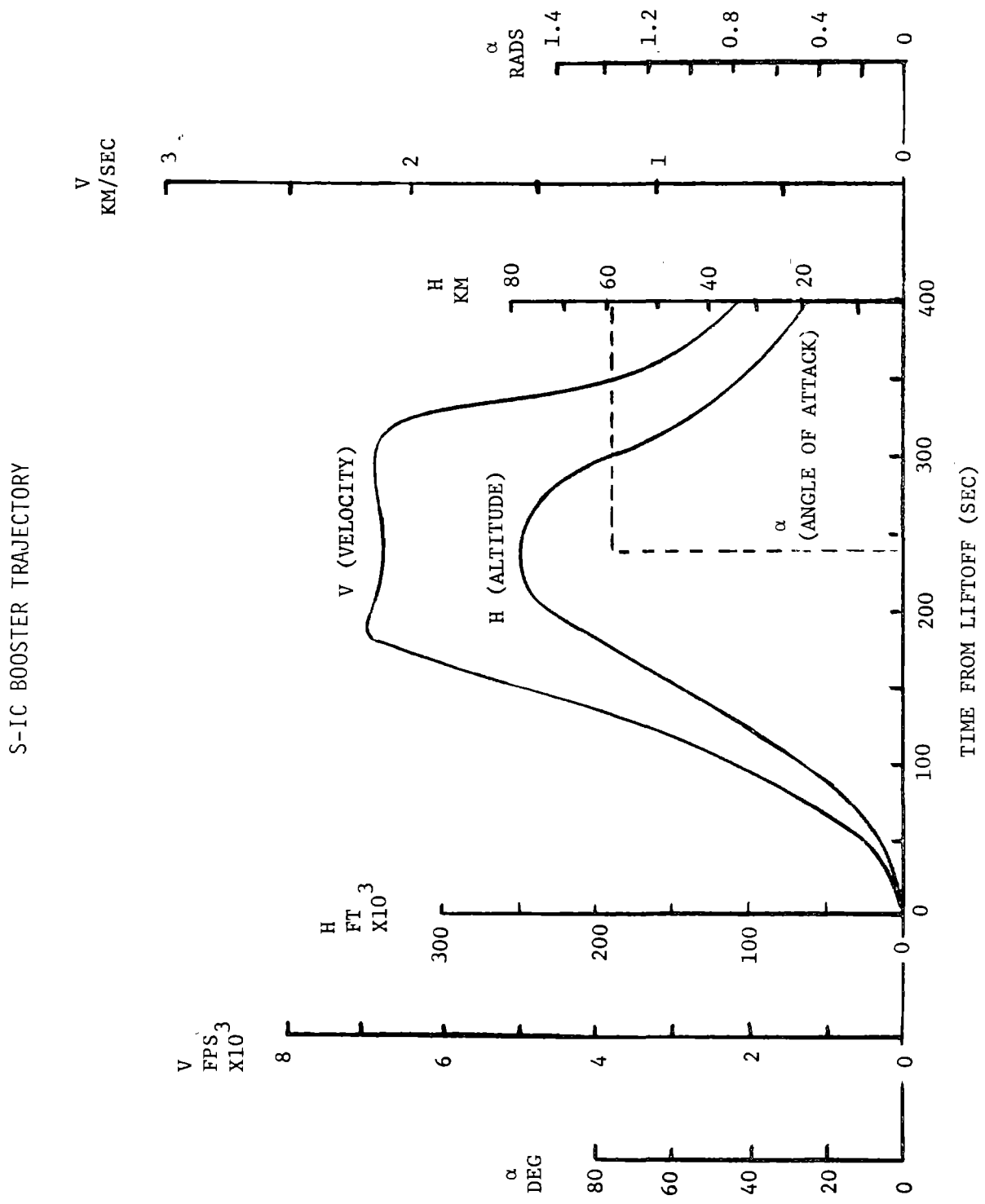
S-IC BOOSTER TRAJECTORY
V (VELOCITY)
H (ALTITUDE)
α (ANGLE OF ATTACK)
TIME FROM LIFTOFF (SEC)
V FPS X10^3
H FT X10^3
α DEG
V KM/SEC
H KM
α RADS

Figure 49

HEATING HISTORIES, S-IC BOOSTER

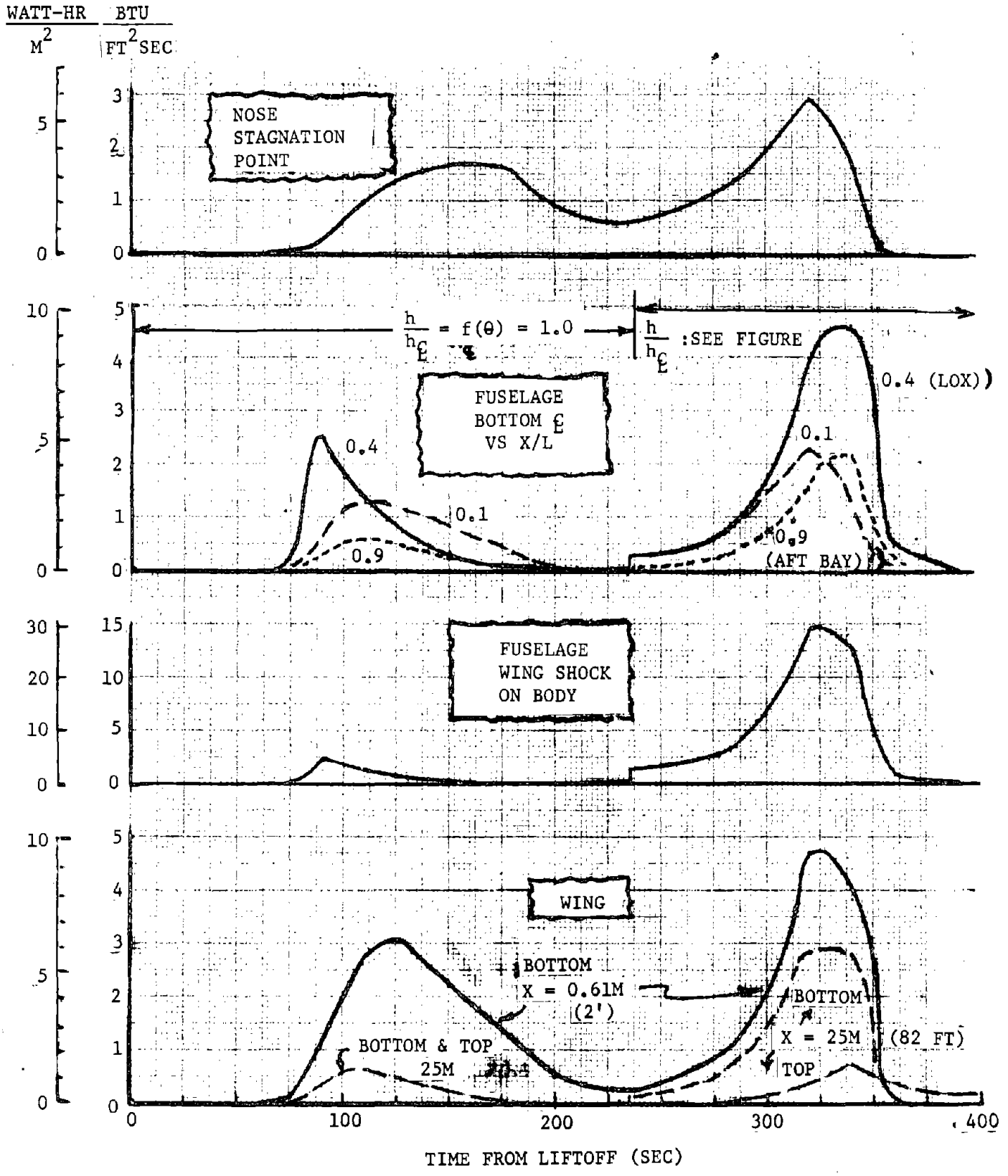

Figure 50

FUSELAGE LOCAL HEATING FACTORS

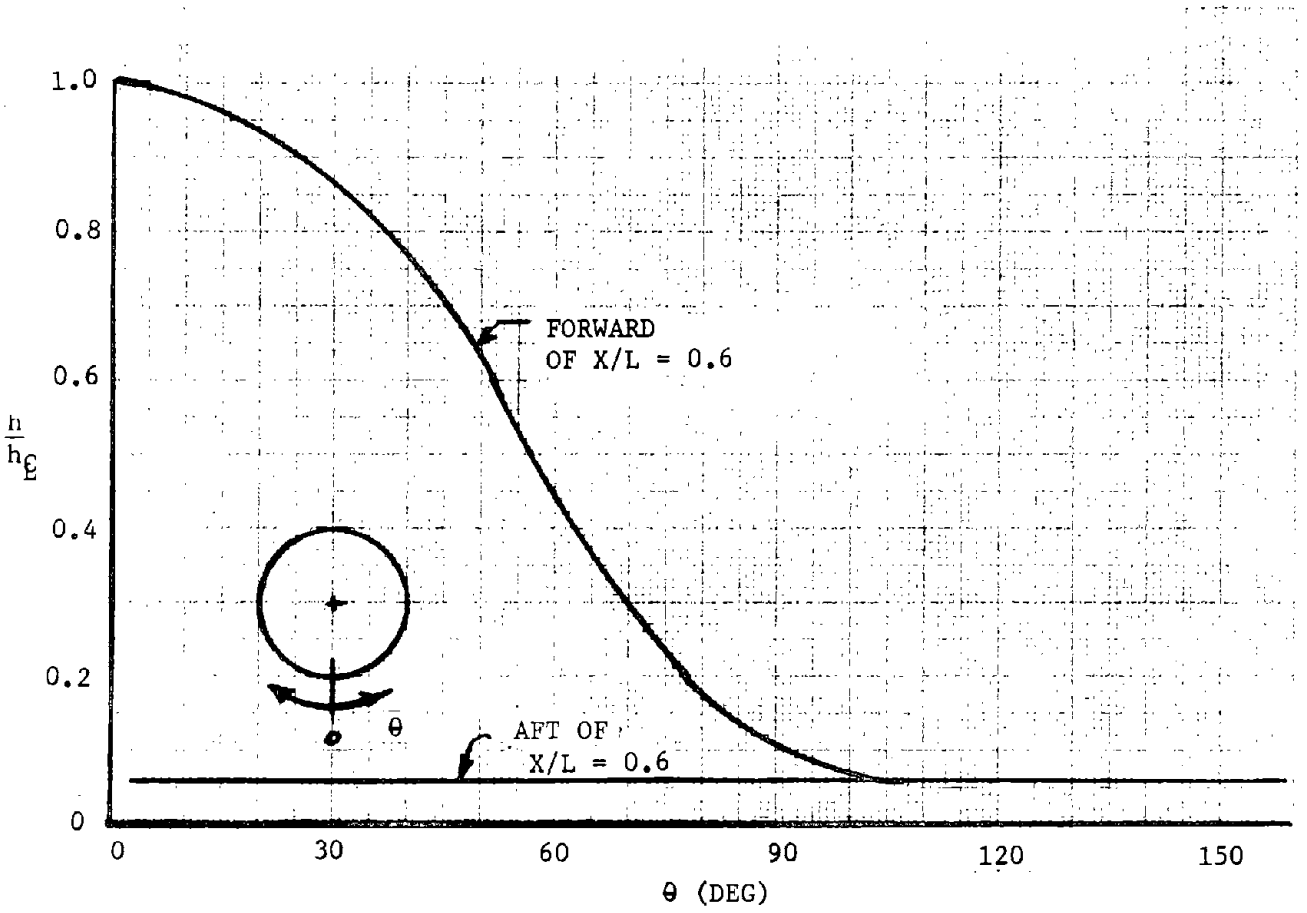

Figure 51

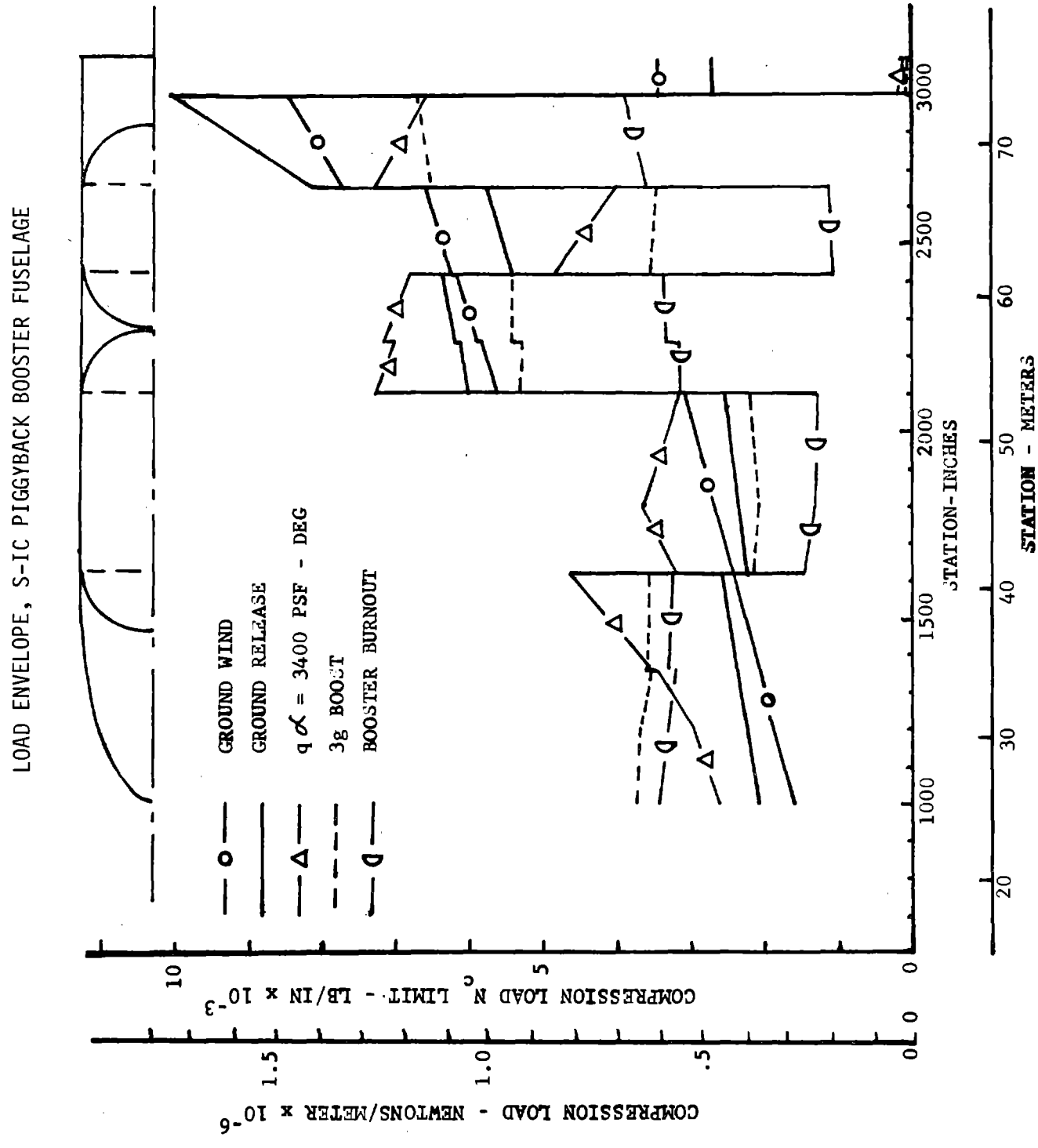
LOAD ENVELOPE, S-IC PIGGYBACK BOOSTER FUSELAGE
GROUND WIND
GROUND RELEASE
q α = 3400 PSF - DEG
3g BOOST
BOOSTER BURNOUT
COMPRESSION LOAD - NEWTONS/METER x 10^-6
COMPRESSION LOAD N_c LIMIT - LB/IN x 10^-3
STATION-INCHES
STATION - METERS

Figure 52

S-IC PIGGYBACK BOOSTER - NET WING STREAM WISE LIMIT BENDING MOMENT

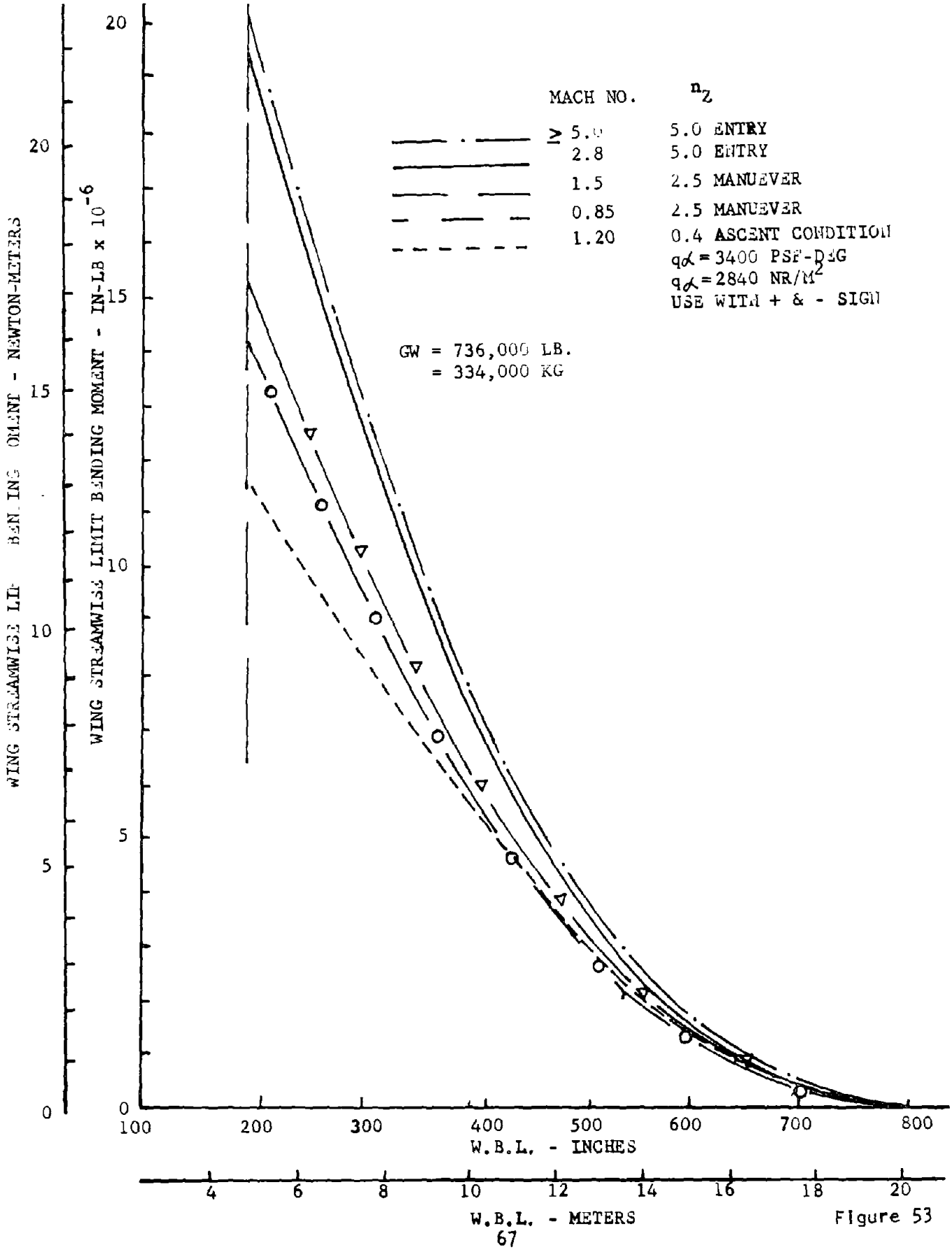

Figure 53

LOAD ENVELOPE - S-IC TANK END LOADED BOOSTER FUSELAGE

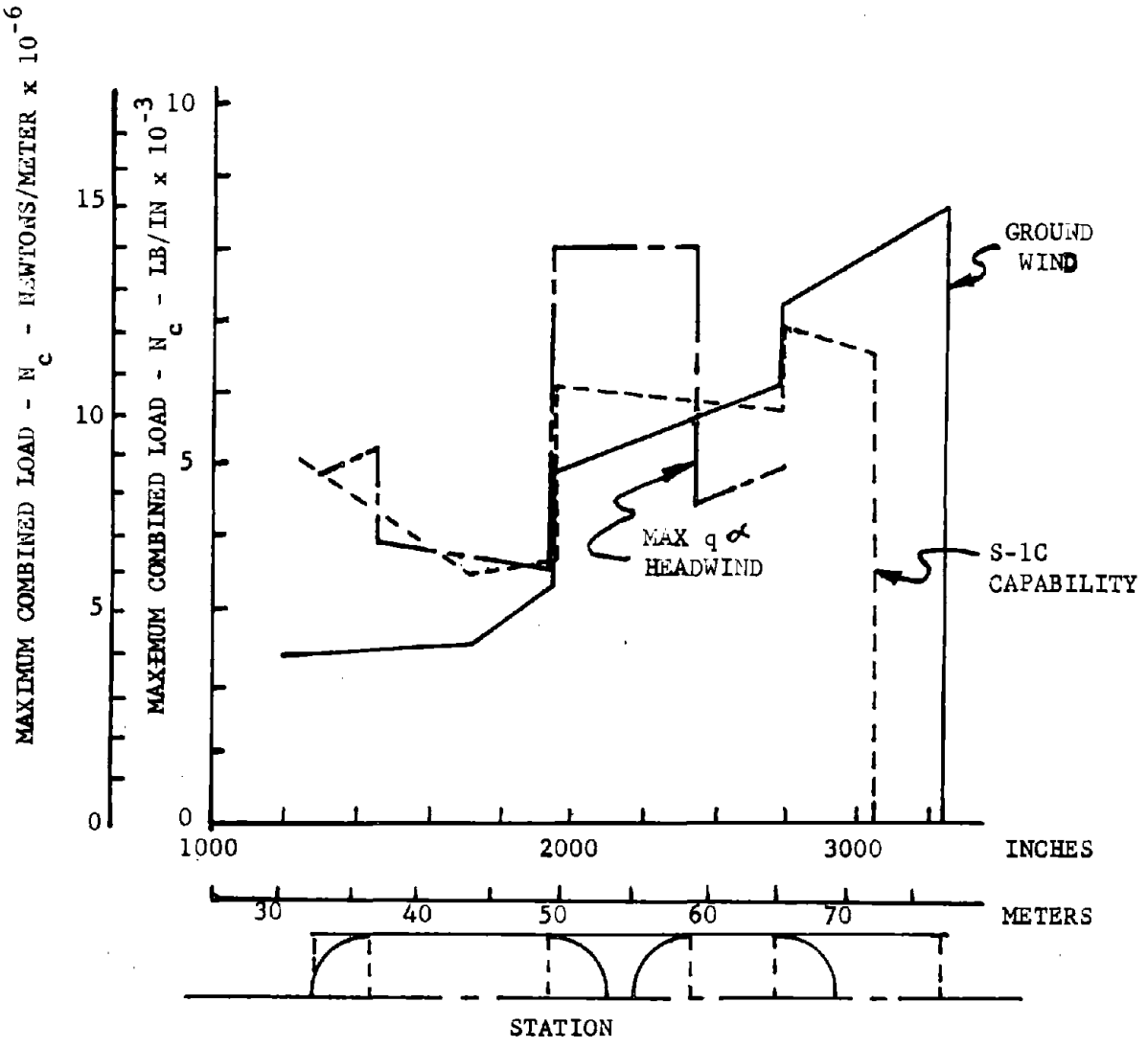

Figure 54

4.2.1 Aluminum - The baseline heat sink concept was an all aluminum vehicle with internal stiffening; the shell and its reinforcements were assumed to carry the overall loads. In this concept, the absorption of the heating encountered during ascent and entry was accomplished by thickening the aluminum structural shell. Where LH_2 propellant was involved, the cryogenic insulation protection was to be internally installed. Since such an approach can be heavy other sink approaches were investigated.

4.2.2 Alternate Methods - The alternate concepts in this study were restricted to those which involved material substitution and/or supplements to aluminum. These alternates were to be self-supporting (after attachment) and were not to be of the contained and/or phase change type. Under these criteria, the concepts shown in Figure 55 emerged and are discussed below and presented in detail in Section 4.4.

ALTERNATE HEAT SINK APPROACHES

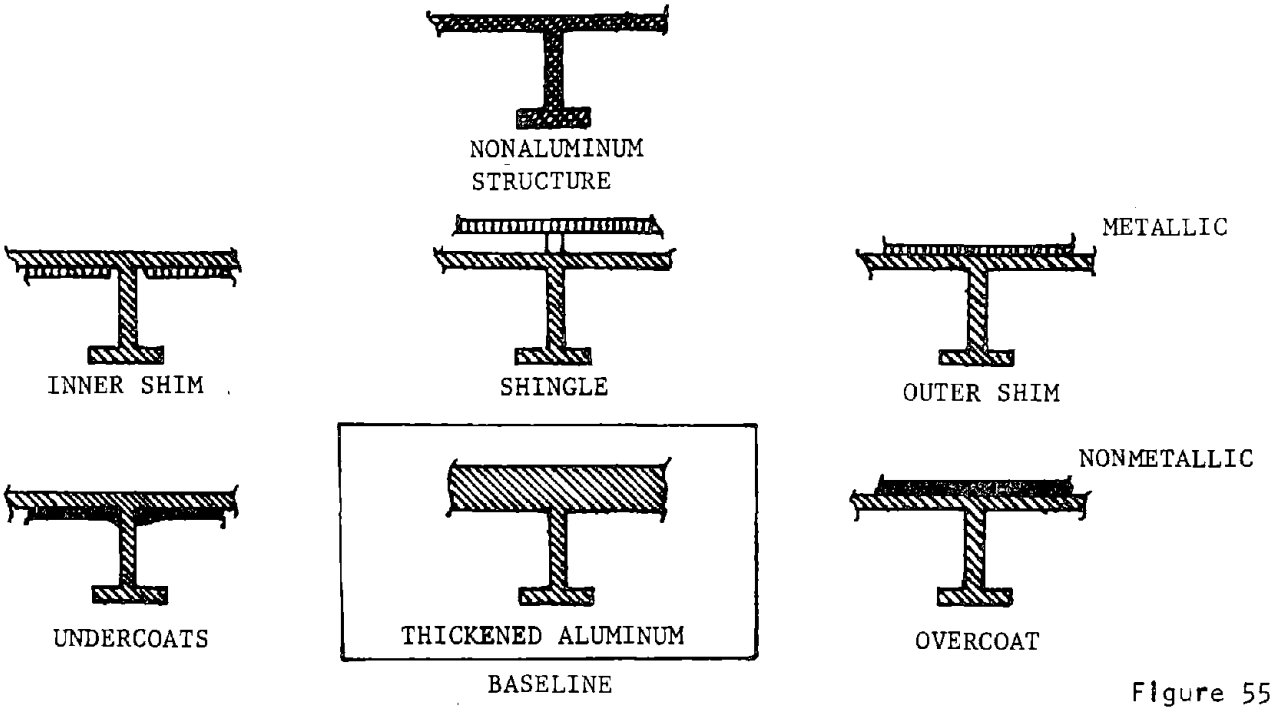

Figure 55

Other Metals - Metals such as titanium and Inconel have greater strength to weight ratios than aluminum, as well as being able to absorb a large change in temperature from the liftoff value to maximum allowed temperature. (Preliminary information on the modified S-IC booster had already indicated the substitution of titanium in high heated nontank regions, namely, in the body

forward of the LOX tank and over the wing bottom.) Beryllium, with its high specific heat, could be closely attached to the internal side of a basic aluminum shell.

Nonmetals - The most promising alternates to thickened aluminum were found to be high thermal capacity nonstructural, nonmetallic materials bonded to the aluminum structure either externally or internally. The external location, with proper sizing of overcoats, gave significantly lower unit weights than the baseline. Internal, undercoating supplements, as in the case of Beryllium, required aluminum temperature limitations.

4.3 Design Requirements - The analytical efforts were concentrated on a piggyback version of the S-IC booster configuration, with a separation velocity of 2.14 km/sec (7000 ft/sec). While results are typical for a variety of booster configurations and separation velocities, heating problems are more severe with the piggyback version than with the tank-end loaded version. Consequently, trends shown by the studies are generally applicable and problems should be less severe with other configurations.

Combined effects of load, heat sink, and thermal influences were considered in the selected problem areas. It was found that over much of the fuselage, where the thickness was fixed by structural and not thermal considerations, there was unused heat capacity, and the separation velocity could be increased without penalty for thermal protection. No insurmountable situations were encountered, although the use of higher temperature structural metals (titanium, etc) in the nontank regions yielded more efficient material use and lower unit weights.

4.3.1 LOX Tank - During ascent, the emptying LOX tank is heated by incident aerodynamic heating, with one part of the tank at LOX temperatures and the other part warmer. The location of LOX during various portions of the mission is shown in Figure 56. It was postulated that the effect of the resulting thermal gradients on tank stress levels could significantly modify the theoretical structural requirements.

A study was conducted to determine the temperature histories of various parts of the liquid oxygen tank, including the effect of changing liquid level. Temperature histories for different smeared thicknesses of aluminum are shown for two different

EFFECT OF LOX DEPLETION - ANTICIPATED PROBLEM AREA

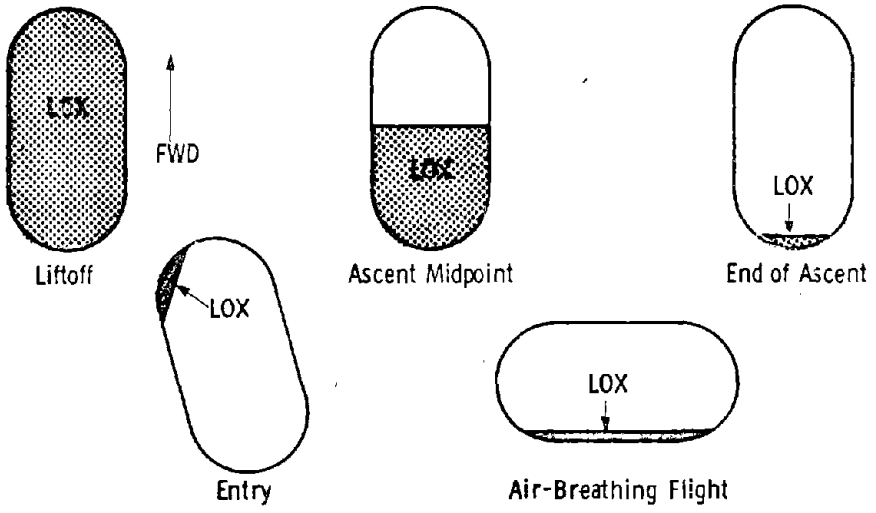

Figure 56

points on the tank in Figures 57 and 58. These curves assume that the LOX is not in contact with the skin. The transient effects of shifting LOX residuals (when analyzing thermal gradients, not sizing) can be superimposed on these as a nearly instantaneous drop in temperature to the LOX temperatures.

The load distribution on the oxidizer tank shown in Figure 59 was used to define structural thickness requirements. The structural and heat sink requirements are compared in Figure 60. It should be noted that the structural thickness requirements shown in the figure do not include the effect of peripheral thermal stresses. This figure shows that the greater portion of the tank is sized by structural rather than by heat sink requirements. The resulting thickness requirements and the maximum temperatures corresponding to those thicknesses are tabulated in Figure 61.

Peripheral thermal stresses occurring in the design because of peripheral temperature distributions were computed at three stations at several different flight times. The stresses at the times at which they are most severe are shown in Figure 62; also included are assumptions on shifting LOX residuals. The location of the maximum thermal stresses indicates that increasing the thickness at the points of higher heating would reduce the stresses. The thermal stresses were reduced to acceptable values with the thickness distribution shown in Figure 63. The weight of the barrel section of the oxidizer tank was estimated from these thicknesses for comparison with a tank sized by requirements only. The weight penalty for the heat sink design was found to be approximately 11 percent.

ASCENT TEMPERATURE HISTORIES ON VARIOUS LOX TANK THICKNESSES

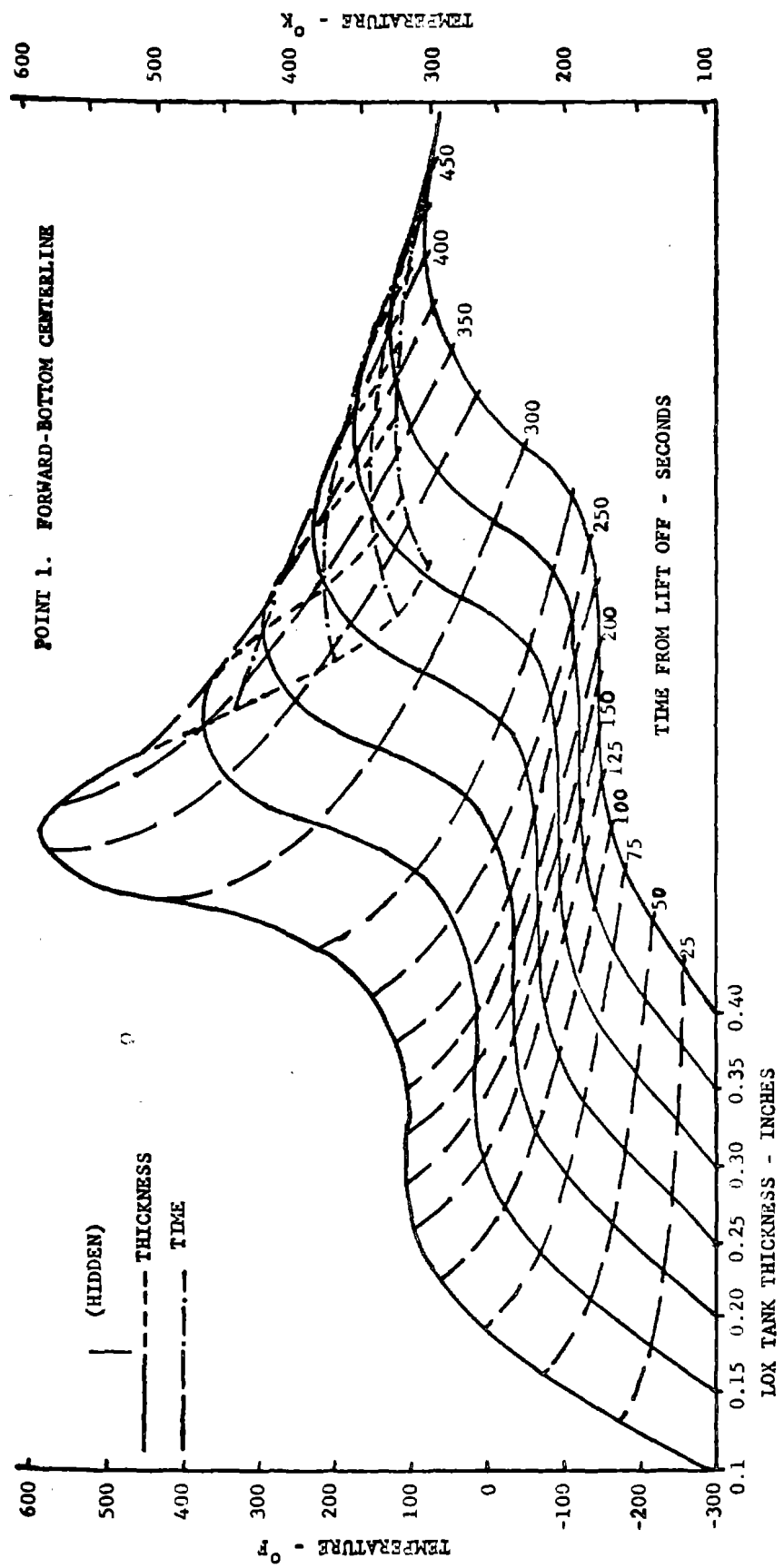

Figure 57

TEMPERATURE HISTORIES FOR VARIOUS LOX TANK THICKNESSES

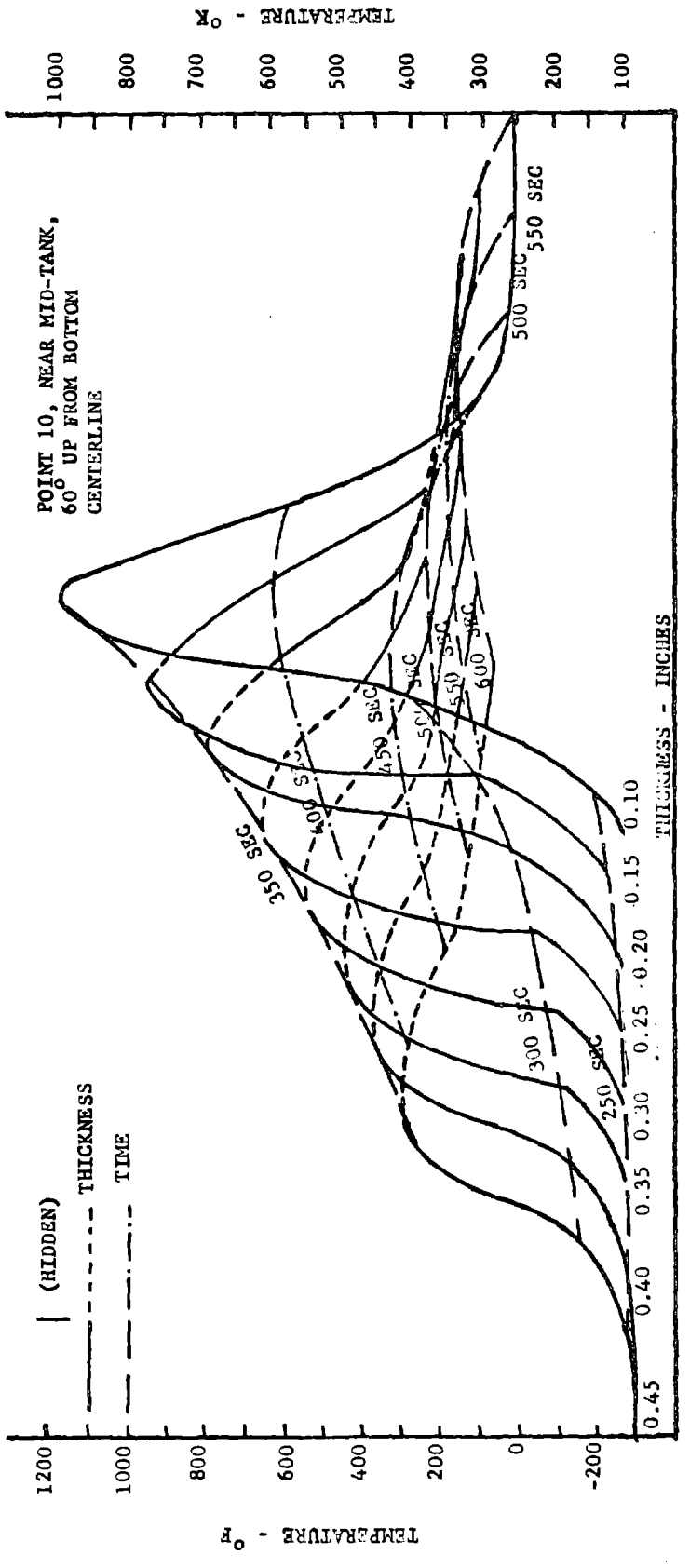

Figure 58

STRUCTURAL ACTIVE COOLING

LOX TANK FLIGHT LOAD STRESSES

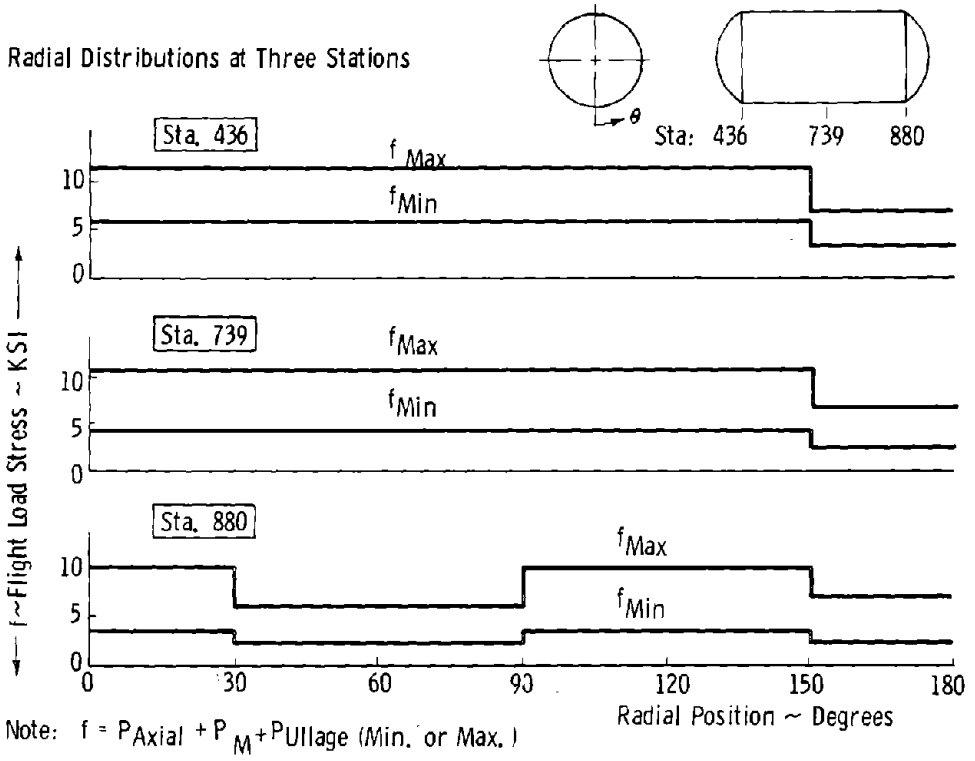

Figure 59

LOX TANK STRUCTURAL AND HEAT SINK THICKNESS REQUIREMENT

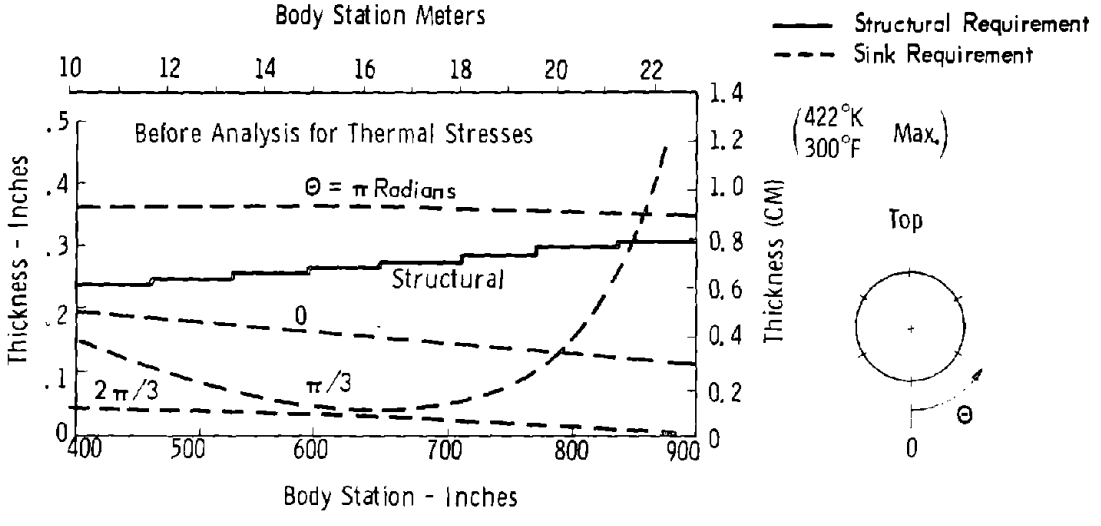

Figure 60

BOOSTER LOX TANK GAGES & MAXIMUM TEMPERATURES

(Prior to Thermal Stress Evaluation)

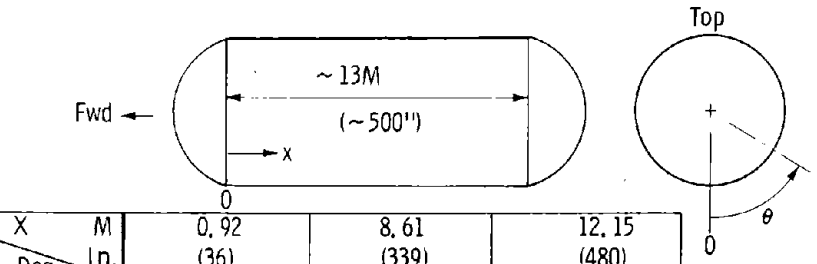

θ RAD	Deg	X M In.	0.92 (36)	8.61 (339)	12.15 (480)		
3.14	(180)		* .90 (.35)	* .91 (.35)	* .89 (.35)	CM/IN	$\bar{\tau}$ Alum
			422 (300)	422 (300)	422 (300)	°K/°F	T_{Max}
2.09	(120)		.62 (.24)	.73 (-28)	.79 (.31)		Typ
			230 (-40)	225 (-50)	220 (-60)		
1.05	(60)		.62 (.24)	.73 (.28)	* 1.30 (.50)		
			325 (130)	240 (-25)	422 (300)		
0	(0)		.62 (.24)	.73 (.28)	.79 (.31)		
			422 (300)	390 (240)	295 (70)		

* Controlled by Heat Sink Limit

Figure 61

LOX TANK THERMAL STRESSES

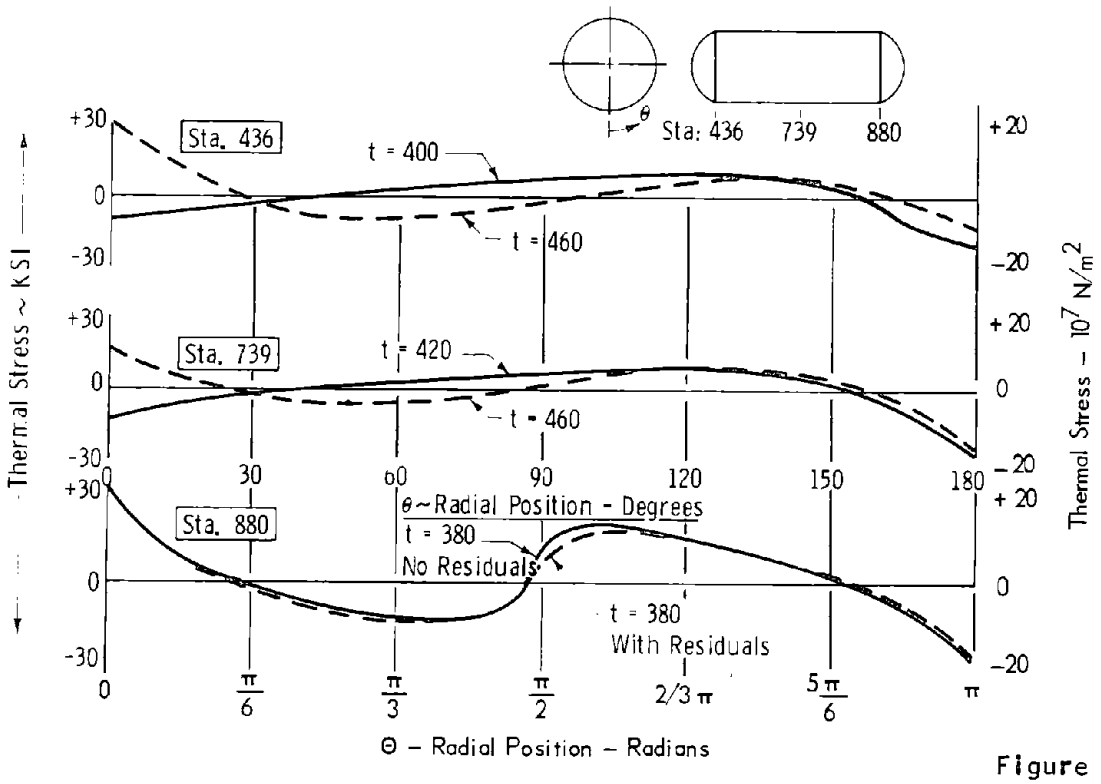

Figure 62

LOX TANK - FINAL THICKNESS REQUIREMENTS

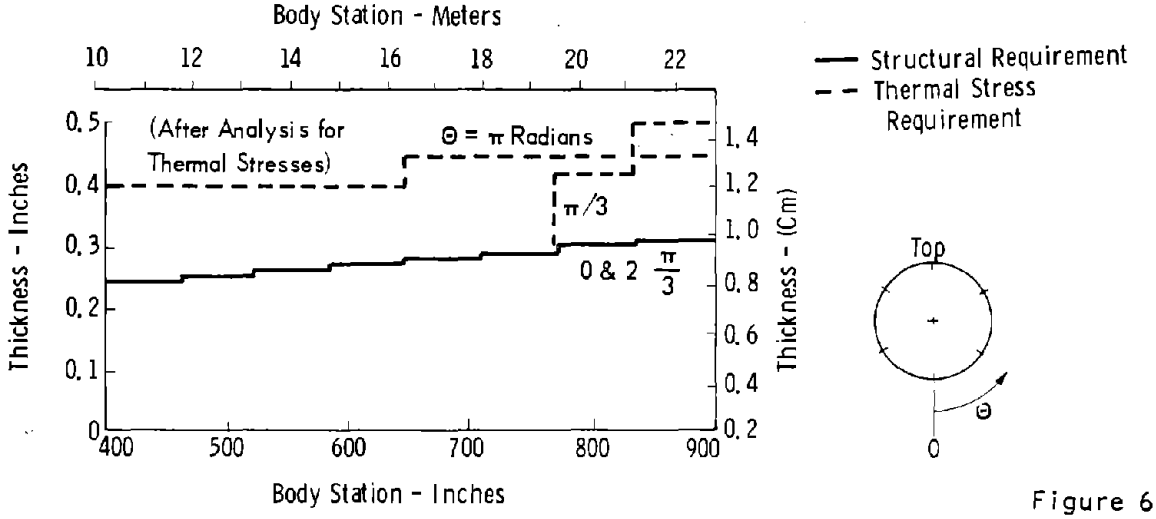

Figure 63

The major contributor to the increase in weight of the oxidizer tank, was the high heating rate encountered during ascent along the top centerline with the piggy-back arrangement. In a tank-end loaded configuration, this increased ascent heating would not occur. Therefore, radial temperature gradients and thermal stresses would be less severe,and the weight penalty for heat sink thermal protection would be less than for the piggyback configuration.

4.3.2 Intertank - The structural and heat sink thickness requirements for the fuselage between tanks are presented in Figure 64. The corresponding thermal stress levels due to axial and peripheral temperature gradients did not require any resizing of the cylinder walls.

4.3.3 Fuel Tanks - A similar study was made of the fuel tank region. It was assumed that no interference heating occurred during boost for this region,and that highest temperatures occurred at the bottom centerline. The required structural thickness was found to be adequate from a heat sink standpoint (Figure 65). Since the temperature differences shown in Figure 66 were great enough to produce unacceptable thermal stresses, these were alleviated by a slight increase in thickness (shown in Figure 67) over the lower part of the tank.

The use of LH_2 as fuel for the booster would not introduce significant differences in the results, since internal insulation would be used to maintain the surface temperature above the liquefaction temperature of air prior to launch. Therefore, the minimum surface temperature would be similar to that of the LOX tank, and the maximum surface temperature would be no higher than that of the RP-1 tank which has been analyzed. Also, the internal insulation would provide additional heat sink capability. Therefore, the penalty for applying the heat-sink concept to a hydrogen-fueled booster should be of the same order as for the LOX/RP-1 fueled booster.

INTERTANK - THICKNESS REQUIREMENTS

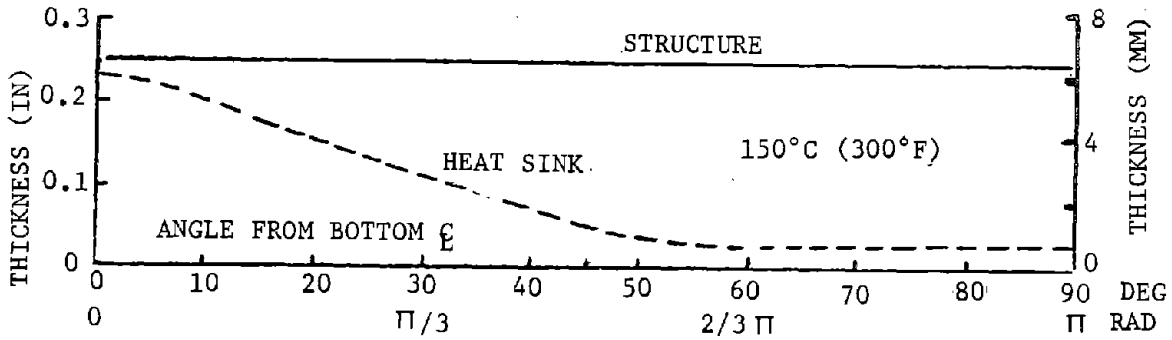

Figure 64

RP-1 TANK - THICKNESS REQUIREMENTS

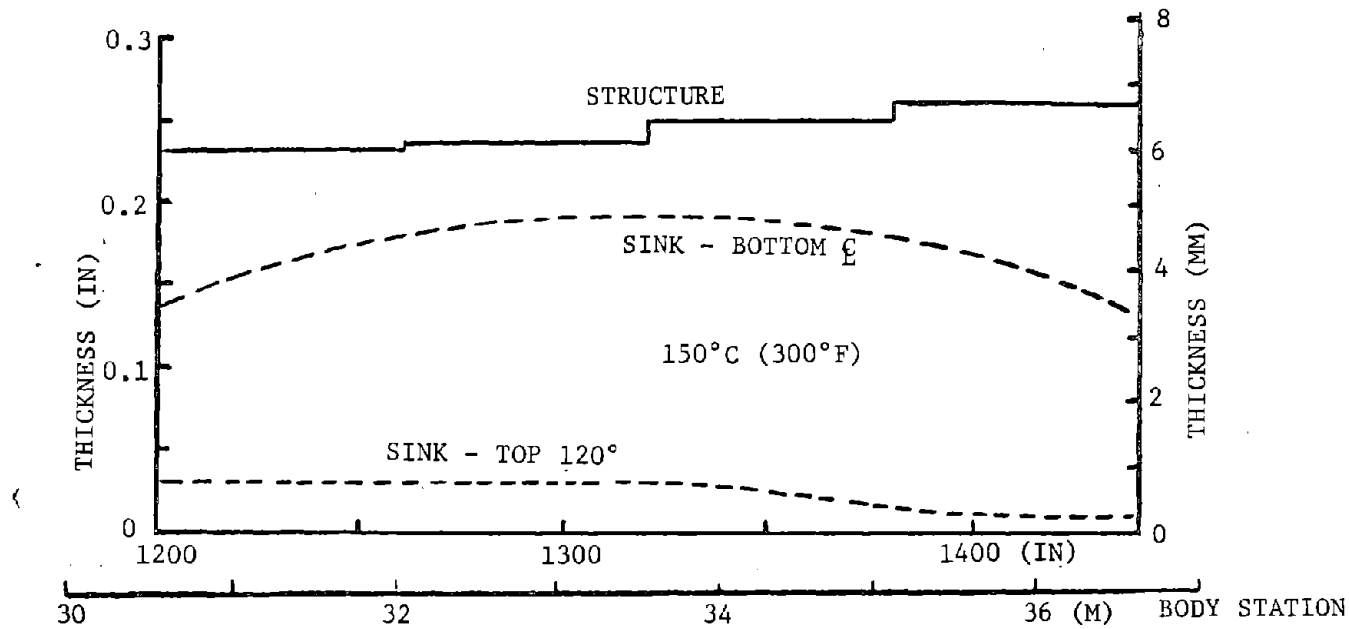

Figure 65

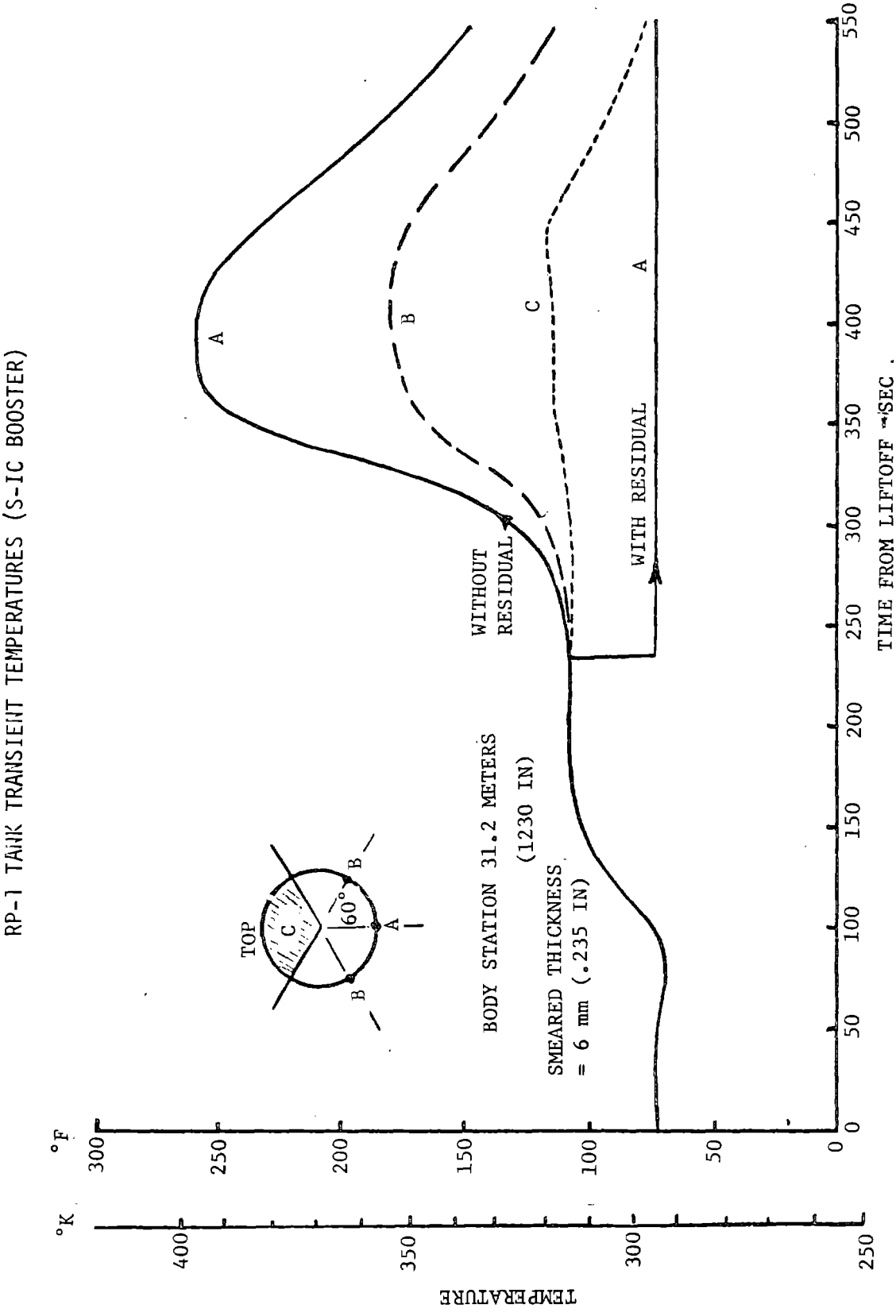
RP-1 TANK TRANSIENT TEMPERATURES (S-IC BOOSTER)
TEMPERATURE
°F
°K
300
250
200
150
100
50
0
400
350
300
250
0
50
100
150
200
250
300
350
400
450
500
550
TIME FROM LIFTOFF - SEC.
A
B
C
A
WITHOUT RESIDUAL
WITH RESIDUAL
BODY STATION 31.2 METERS
(1230 IN)
SMEARED THICKNESS
= 6 mm (.235 IN)
TOP
60°
A
B
B
C

Figure 66

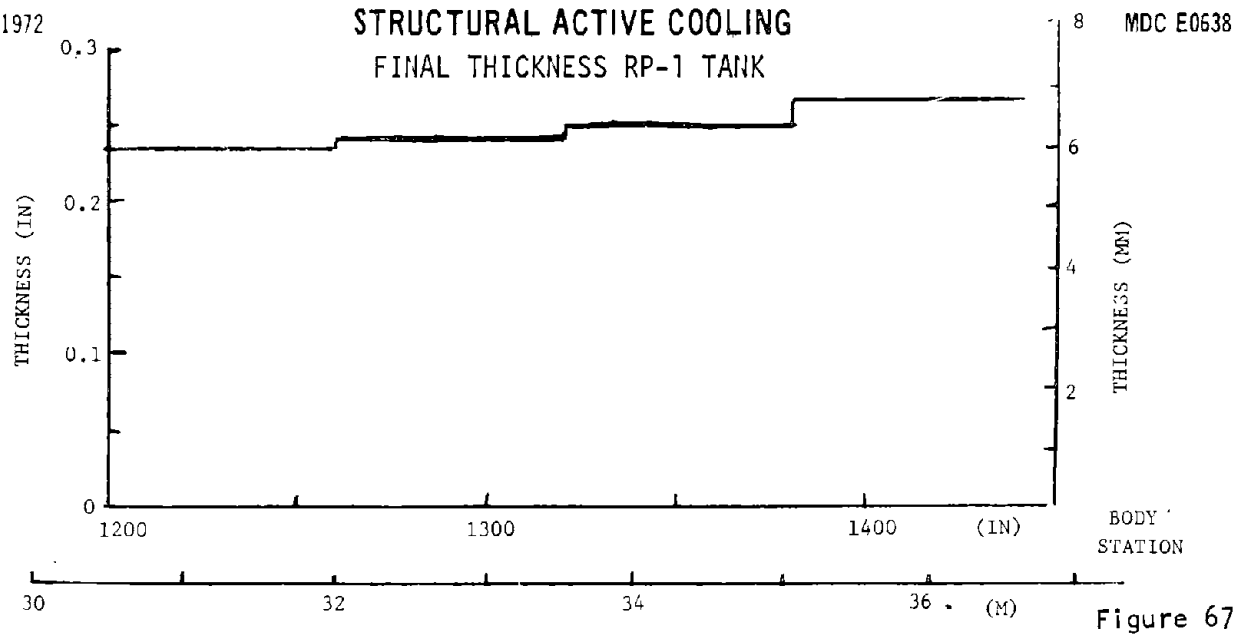

Figure 67

4.3.4 Wing - Three regions of the wing lower surface were analyzed assuming a maximum allowable temperatures of 177°C (350°F) for aluminum structure and maximum temperatures of 316 and 482°C (600 and 900°F) for titanium structure. The aluminum structure was heavier and also exhibited greater weight sensitivity due to its lower operating temperature limit, as shown in Figure 68.

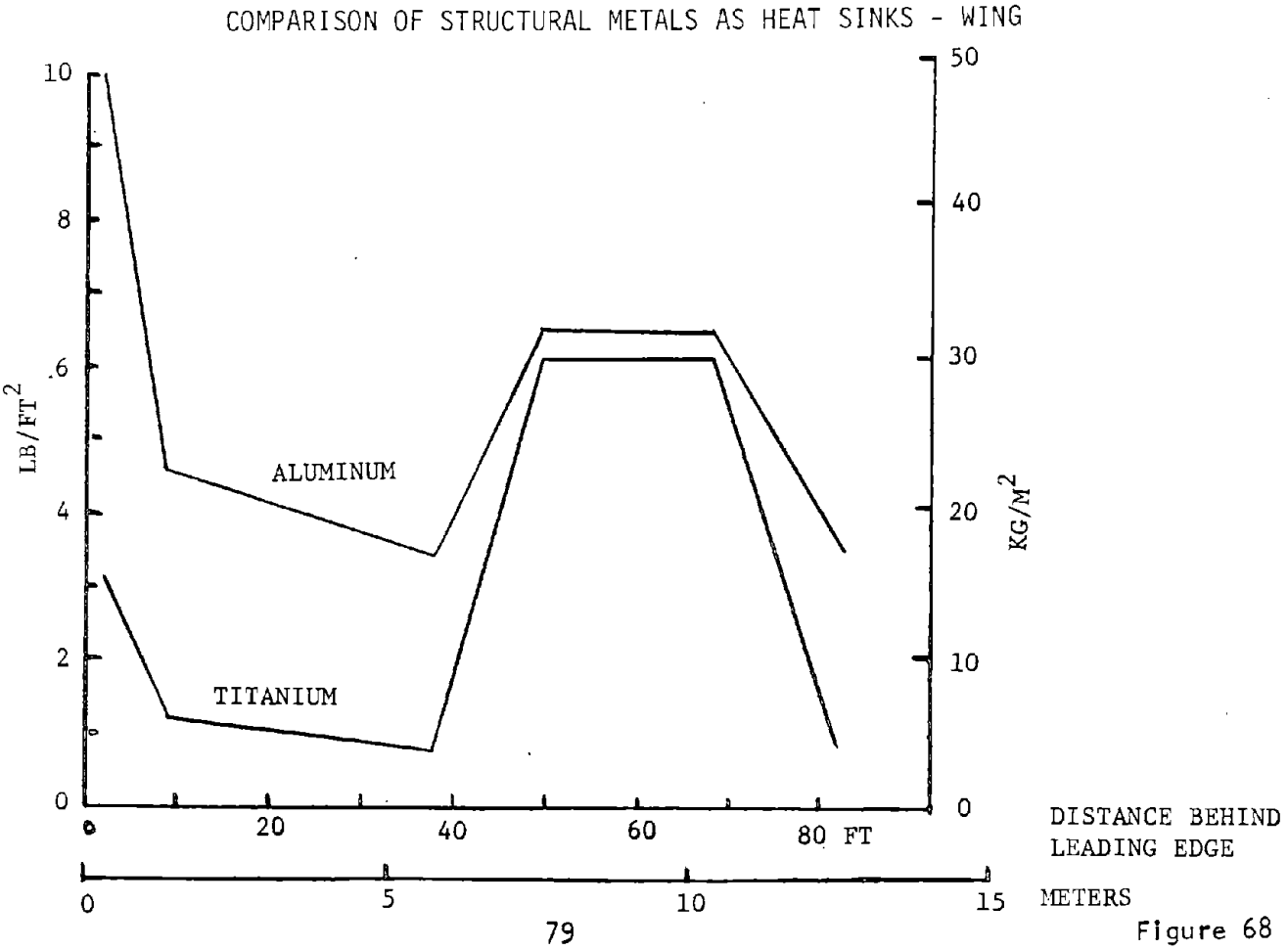

Figure 68

Both metals were also evaluated on a strength to weight basis for the upper wing covers. Titanium was again found to be superior. For the leading edge Inconel was found to be superior. The required thicknesses for each of these nonaluminum applications are given in Figure 69.

4.4 Alternate Heat Sink Approaches - Practically all the studies of the heat-sink concept have been concerned with the use of the structural material aluminum as the heat-sink material. Aluminum has both a high specific heat and a high strength-to-weight ratio; its high thermal conductivity would be important in maintaining acceptable temperature differences in stiffened structures. However, aluminum has a relatively low use-temperature limit.

4.4.1 Metals - A comparison of the thermal capacity of aluminum and other structural metals is given in Figure 70, illustrating the weight of material required to absorb a fixed quantity of heat as a function of temperature. An initial temperature of 300°K (80°F) was assumed. The higher use-temperatures of steel and titanium could provide a potential weight savings. These materials are limited in application to nontank areas of high heating rates and moderate structural loads.

Beryllium, because of its high heat capacity, is attractive when used for structure or as shim supplement with aluminum, either internally or externally. Although some difficulty might be encountered in providing the intimate contact of the shim necessary to give good thermal conduction, the potential weight reduction which could be obtained by attaching beryllium inside an aluminum skin is shown in Figure 71. An alternate approach using external beryllium shingles insulated from the aluminum could provide somewhat greater weight saving, but a considerably more complex design.

4.4.2 Nonmetals - The most promising alternates to thickened aluminum are high thermal capacity nonmetallic materials in contact with the aluminum structure. These materials could be attached either internally or externally.

1. Undercoats - For an internal application, the supplementary material must definitely have a higher specific heat than that of aluminum to provide any payoff since the shell achieves the maximum temperature of these systems. Kapton, a flexible polyimide coating, was investigated in this application. Figures 72 and 73 illustrate the relationship between existing aluminum gages and amounts of Kapton required to absorb nominal heat loads (bottom of fuselage). The example calculation in Figure 74 indicates a potential weight saving of 2.79 kg/m^2 (0.57 lb/ft^2)

COMPOSITE STRUCTURAL AND HEAT SINK COVER GAGES

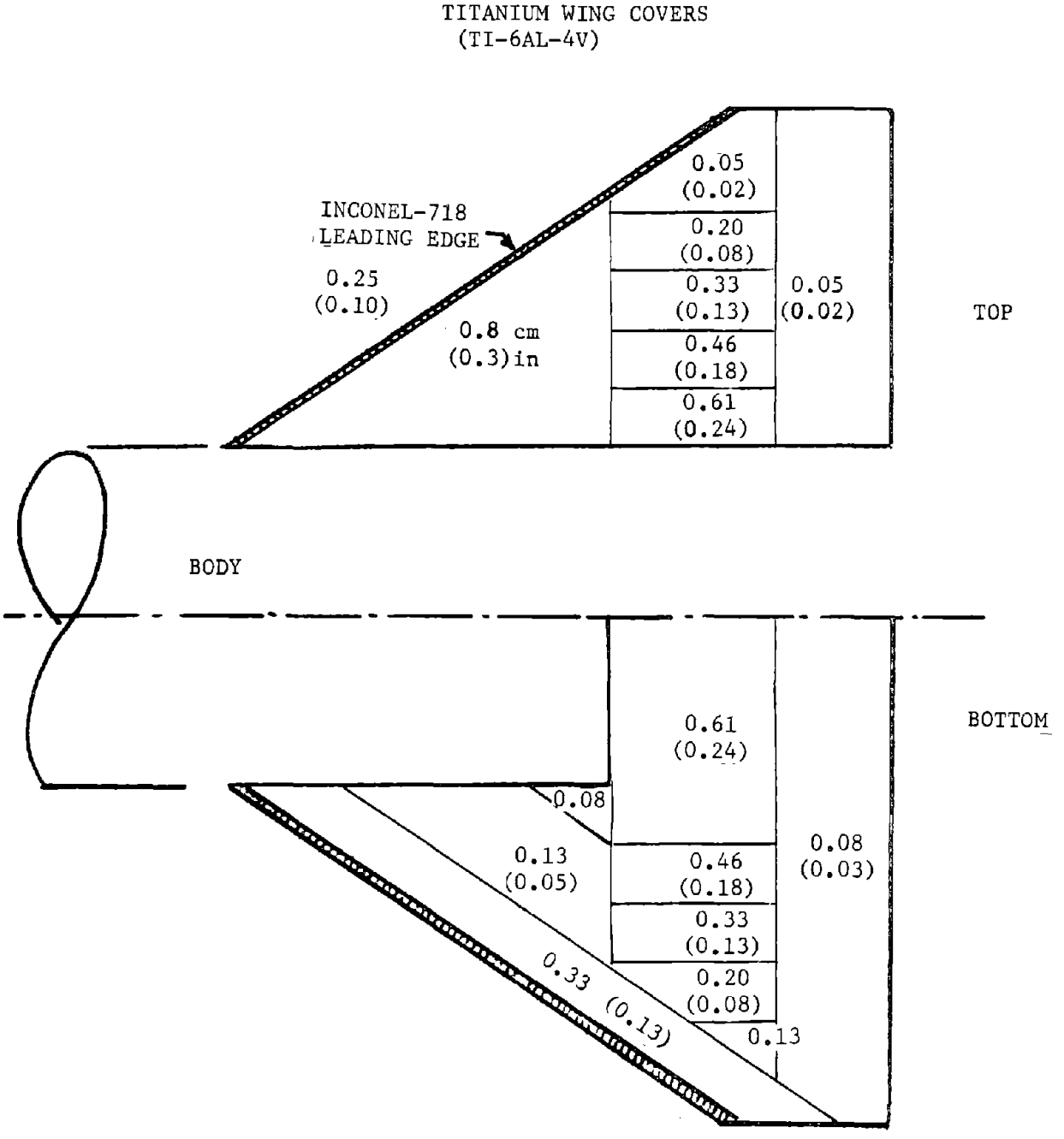

Figure 69

ALTERNATE HEAT SINKS - NON-ALUMINUM METALS

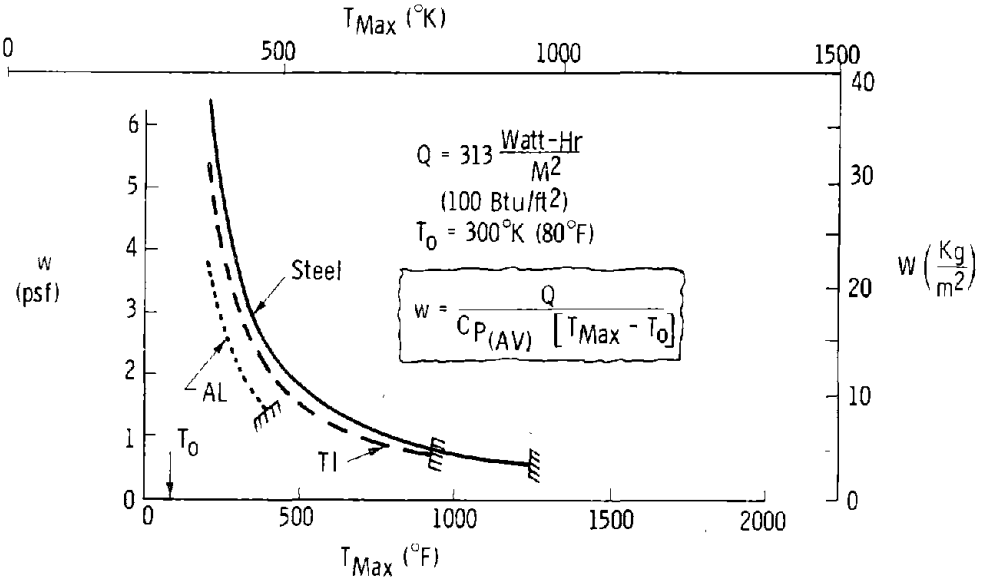

Not Included:

- Structural Requirement (s) & Associated Elevated Temperature Allowables

Figure 70

ALTERNATE HEAT SINK - BERYLLIUM SUPPLEMENT

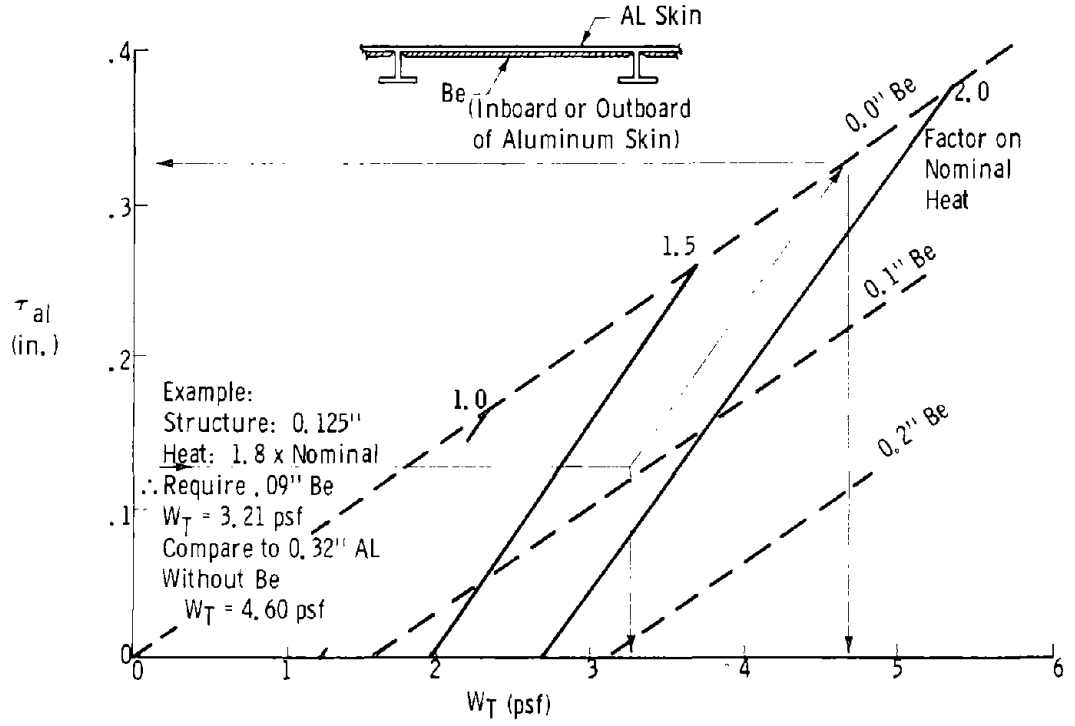

Figure 71

RELATIVE THICKNESSES, KAPTON

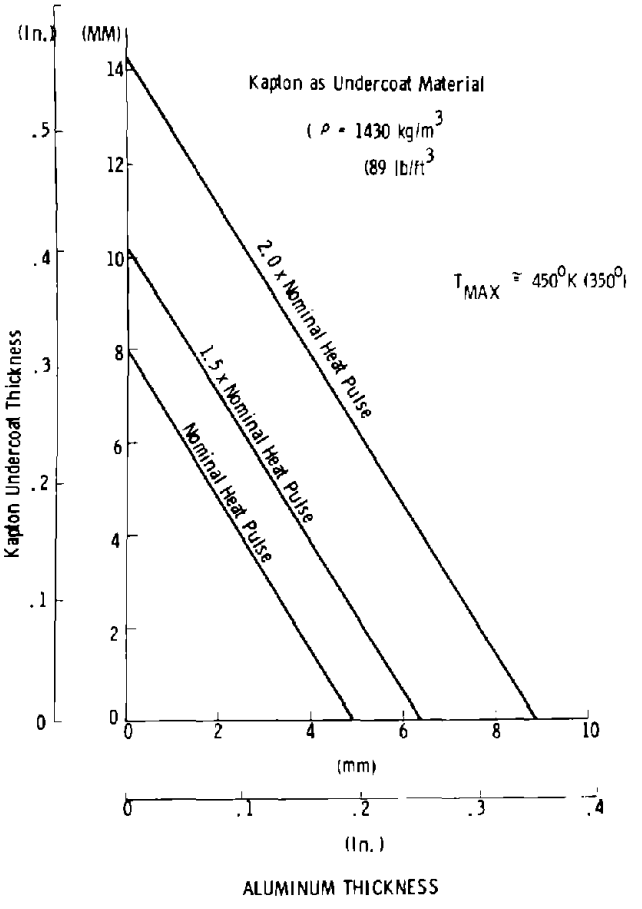

Figure 72

ALTERNATE HEAT SINK - KAPTON UNDERCOAT

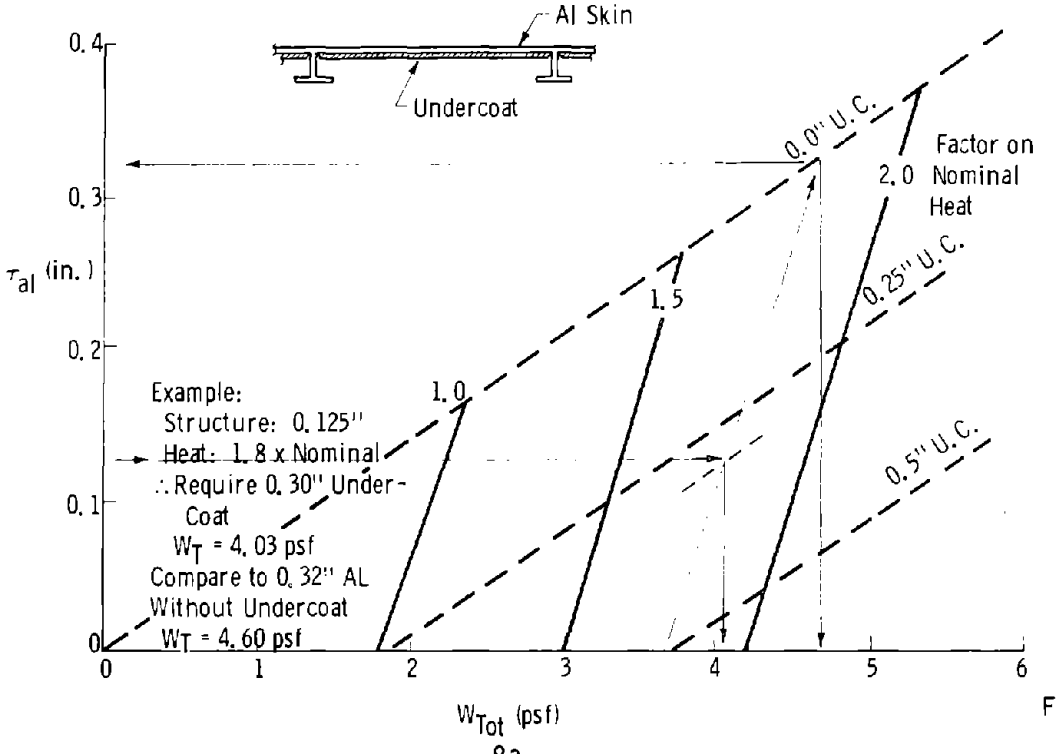

Figure 73

2. Overcoats - Analytical results have indicated that auxiliary nonmetallic heat sink materials, attached outside the structural skin, can produce significant unit weight reductions. Rather than thickening the basic (structurally-required) skin gages to maintain temperature limits, overcoats acting as combined insulation/heat sink can provide the protection. These supplementary materials, e.g. sprayable silicones, are characterized by high specific heats and higher (than aluminum) peak allowable temperatures. Therefore, they accomplish a total system weight lower than that of a thick aluminum skin approach. Since reuse was the paramount criterion, the auxiliary material must not degrade with temperature cycling.

In such a system, two temperatures were critical, that of the surface of the overcoat and that at the interface between the overcoat and the aluminum structure. For the most efficient system it was necessary to balance the temperature capability of the overcoat, its heat sink capability, and its thermal conductivity with that of the aluminum. Teflon and a variety of elastomeric silicone mixtures had favorable temperature, heat absorption, availability, and application characteristics for this approach.

A graphic comparison of the results obtained by using an overcoat is presented in Figure 74. Whereas a smeared thickness of aluminum heat sink of 0.89 cm (2.26 in) was required, a combination of 0.20 cm (0.51 in) overcoat and 0.46 cm (1.17 in) aluminum sufficed for the same heat pulse. The overcoat in this example was a silicone enriched with a high heat capacity salt.

Figure 75 presents parametric requirements for this heat sink concept in nontank regions. A silicone overcoat was considered baseline since off-the-shelf sprayable silicones are available.

Greater efficiency could be obtained by incorporating additives having greater specific heat than the silicone. Such additives, listed in order of decreasing specific heat, could include:

- o lithium
- o lithium oxide
- o lithium hydroxide
- o beryllium
- o hydrated aluminum sulfate
- o lithium carbonate

TYPICAL COMPARISON OF TRANSIENT TEMPERATURES

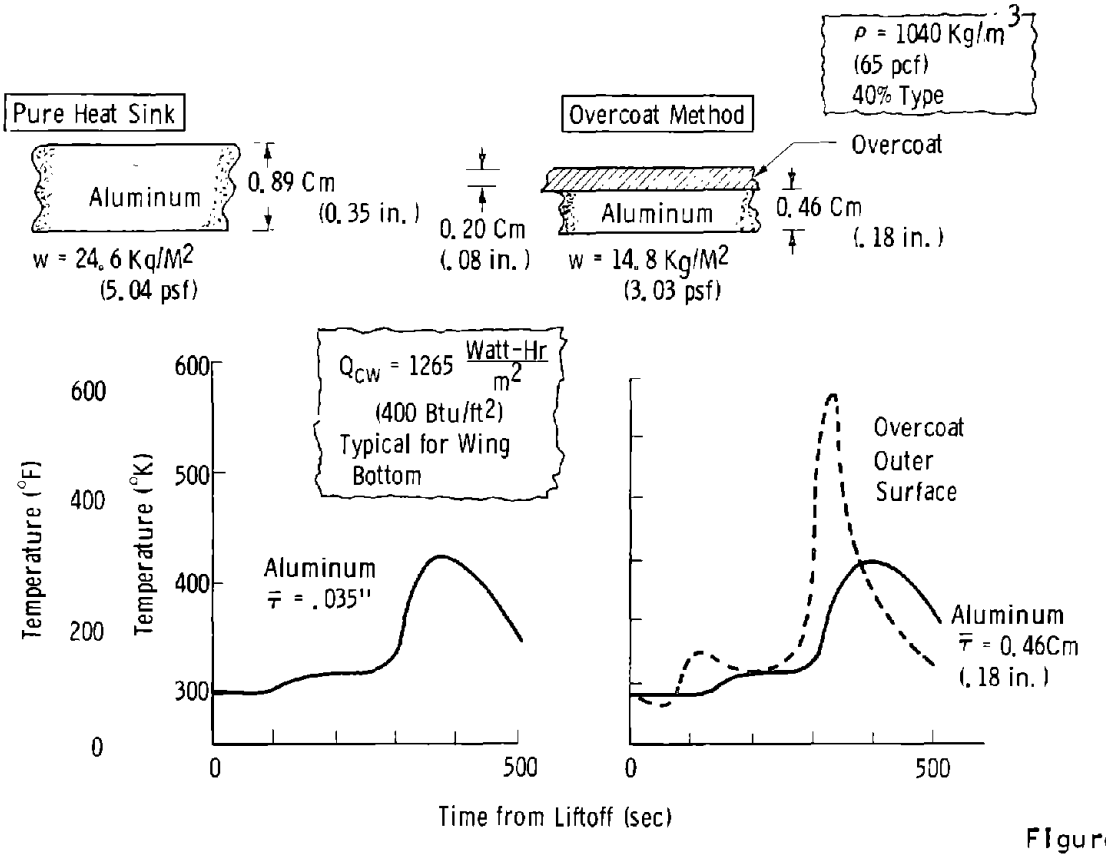

Figure 74

OVERCOAT DESIGN CURVE - NON TANK

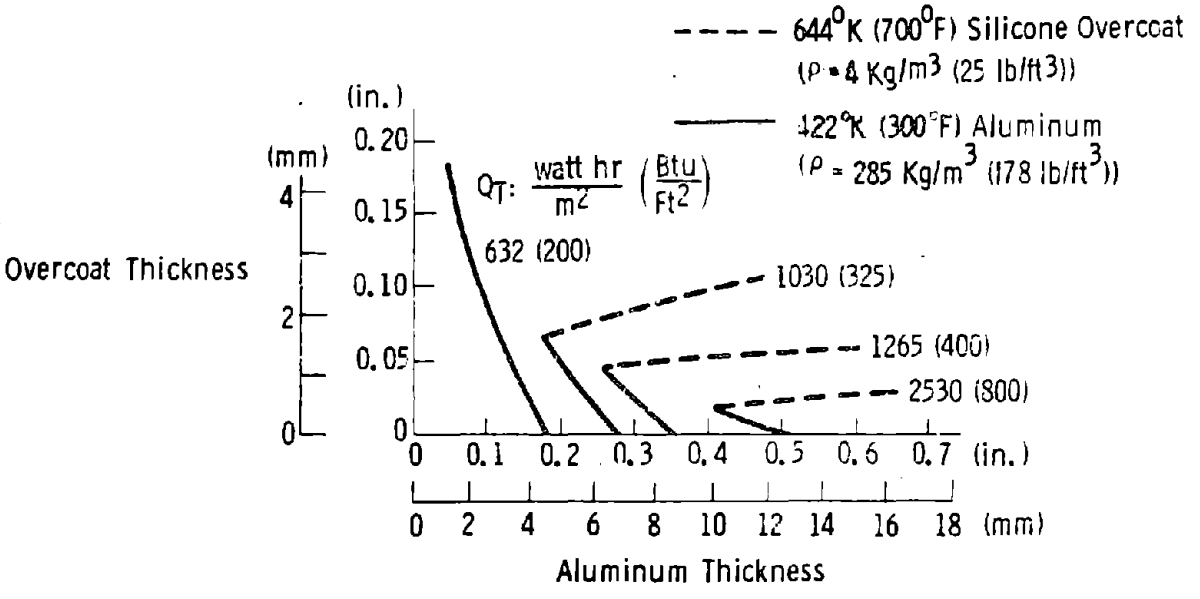

Figure 75

Since dehydration of the hydrated salts may be expected at the temperature to which the coating will be exposed, such materials were eliminated from consideration. (There are also a number of organic compounds having fairly high specific heat which could be included, but these either melt or decompose at relatively low temperatures). The high chemical reactivity of lithium would make it unsuitable. Thus, by a process of elimination, the best additives from the listed group are Beryllium and the lithium salts.

The effects of modifying the basic overcoat by adding 10 percent (by volume) of a high heat capacitance oxide (Li_{0_2}) on the overcoat efficiency was first investigated and compared with a system using unmodified silicone (Figure 76). The addition of the filler reduced the total system weight by 1.5 kg/m^2 (0.3 lb/ft^2), for a total heat load of 1020 watt hr/m^2 (325 BTU/ft^2). Interest in various percentages of enrichment added to the basic silicone mixture led to the construction of the weighted set of thermal properties shown in Figure 77. Using these properties, curves were generated to define heat sink weight as a function of total heat load heat, percent of LiO_2 additive, and aluminum thickness. The results are summarized in Figure 78.

TRENDS NOTED WITH HIGH C_p ADDITIVES TO COATING

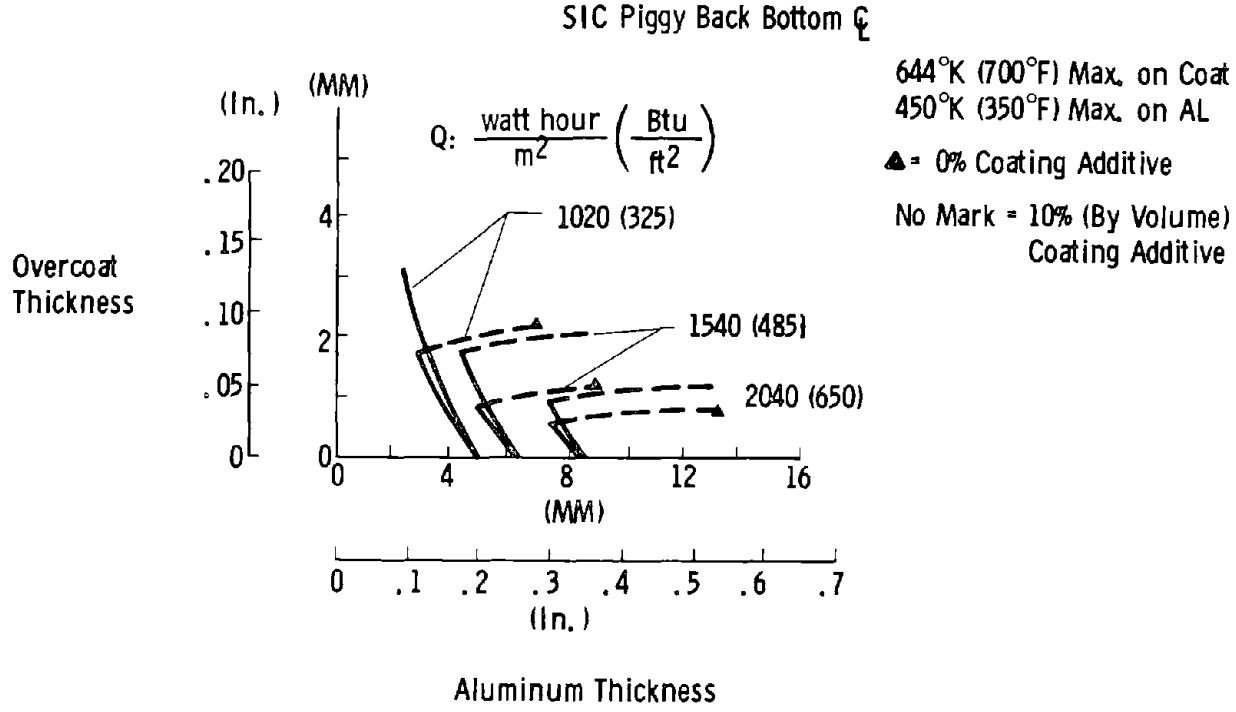

Figure 76

ESTIMATED THERMAL PROPERTIES OF OVERCOAT MIXTURES

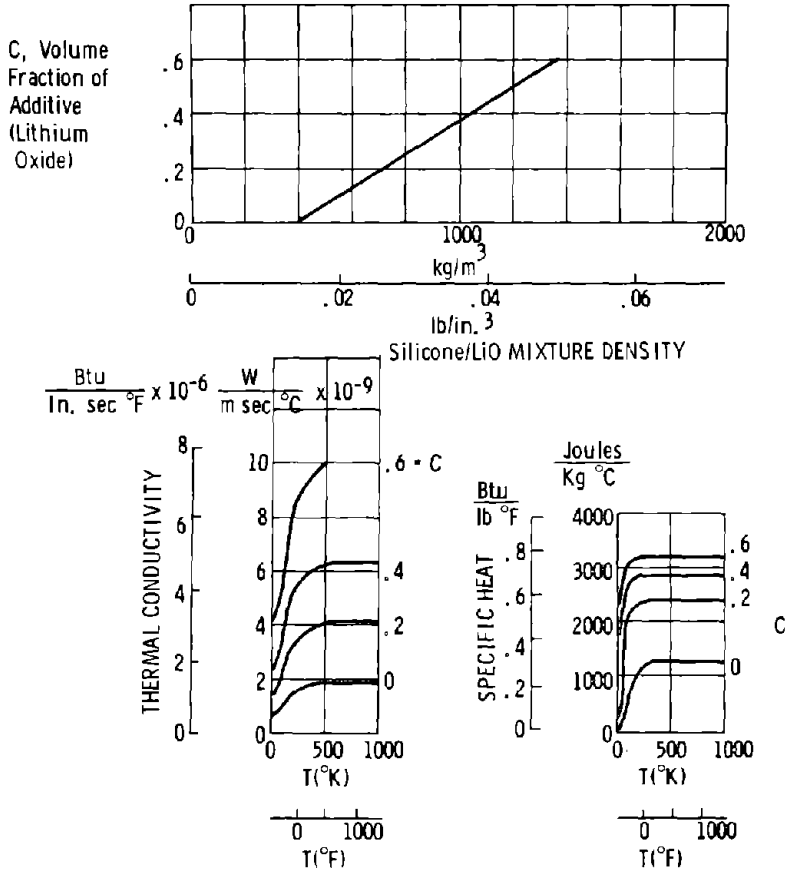

Figure 77

ALTERNATE HEAT SINK - SPRAYABLE OVERCOAT

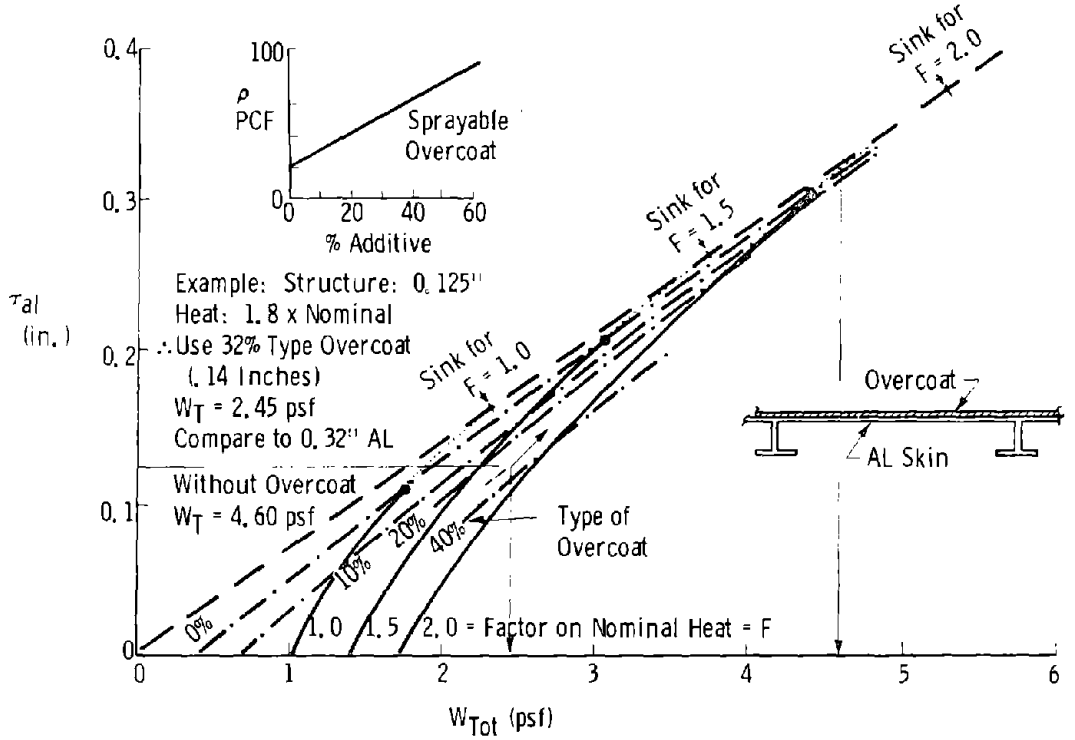

Figure 78

Although, on the basis of specific heat alone, lithium oxide is the most attractive additive, it reacts with water to form lithium hydroxide which, in the presence of water, corrodes aluminum.

Several approaches to reducing or eliminating the potential corrosiveness of a coating containing lithium hydroxide were postulated. The aluminum structure could be covered by a protective coating prior to the application of the main coating, to prevent any contact of the aluminum with lithium oxide or hydroxide. A moisture-proof external coating would prevent corrosion, since water is necessary for the reaction. Alternatives would be encapsulation of lithium oxide particles in an inert, waterproof material or the addition of a buffering material, such as lithium acetate. The use of other lithium compounds, e.g., lithium acetate, lithium formate, and lithium hydrogen aluminate would alleviate the corrosion problem, but information on the specific heats of these compounds is not readily available.

The potential for this concept was evaluated by MMC-D. A booster design extensively employing the overcoat approach was found to be 29,000 lb lighter than a booster which was basically a heat sink vehicle, augmented by rigidized surface insulation, as required. This weight increment included TPS savings plus associated reduced requirements for the fuselage structure, the hydraulic system, and the auxiliary power system.

4.5 Auxiliary Investigations - Three subjects of concern in heat sink booster analyses were also investigated. These include an assessment of potential error in assuming smeared thicknesses in heat storage computations, the booster skin temperatures at crew deplaning, and the effect of liftoff temperature assumptions.

4.5.1 Smeared Thickness Assumption - All of the thermal analyses previously described in this task were based on the assumption that the structure was composed of a uniform thick skin shell. The thickness used in each case represented a certain weight per unit area. In the actual case, the optimum structural design would consist of a relatively thin skin with local skin stiffners. Since such a configuration provides longer paths for heat conduction and larger temperature gradients than the simple uniform shell, analyses were conducted to determine the magnitude of the errors introduced by the smeared thickness assumption. The two structural concepts shown in Figure 79 were used in this study. A factor was determined which could be applied to the predicted heat transfer coefficients so that the desired maximum temperature could be obtained for a flat plate of given weight per unit area. Heating rate histories for which the smeared thickness requirements were 0.41 and 0.82 kg/m^2 (2 and 4 lb/ft^2) were applied to skin-and-stringer arrangements having components of different dimensions, but constrained to give the same weight per unit area. The results are shown in Figures 80 and 81. These results show that the smeared thickness assumption gives results which may be applied to actual configurations only over a narrow range of geometries, and even then some allowance will have to be made for the effect of the temperature distribution through the structure. This is shown in Figure 82 which is derived from Figure 81 using the values corresponding to a maximum temperature of 178°C (350°F) at Point A midway between stiffeners (see Figure 79). For a given span between stringers, any combination of web height and flange width on the curves of Figure 82 would give a peak temperature equal to 178°C (350°F). Combinations falling below and to the left of the curve would yield lower peak temperatures. Combinations of height and width on the other side of the line would result in excessive peak temperatures and so could not be used.

Further studies will be required to fully assess the implication of these results to actual design. Obviously, there will be no problem in those areas where the structural thickness is great enough so that the peak temperature is well below the allowable value. In those areas where considerable material must be added to keep the temperature down to the maximum value, the excess material should be added to the skin. Since less stiffening would be necessary, some of the material in the stiffening members could also be added to the skin. Therefore, the final configuration would tend to approximate a smeared thickness, with a small weight penalty for the nonuniformity of temperature. The most critical case is that in which the strucutral and thermal requirements more or less coincide. Furthermore, a geometry which is structurally nonoptimum may be required, due to the limitations depicted in Figure 82.

STRUCTURAL CONCEPTS

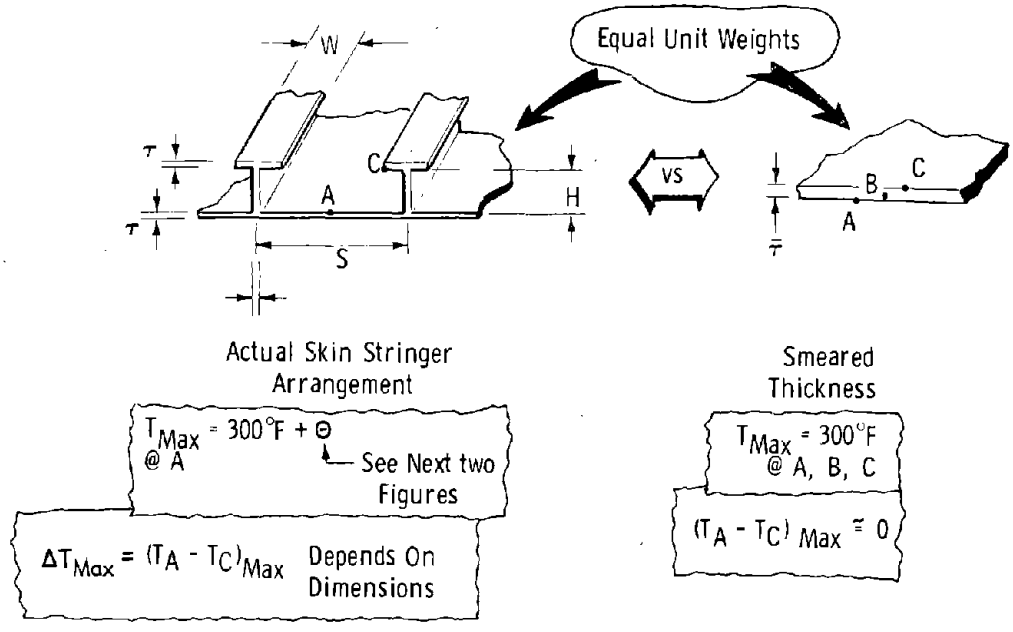

Figure 79

TEMPERATURE INCREMENTS FOR STIFFENED SKINS ALUMINUM AT 2 POUNDS PER SQUARE FOOT

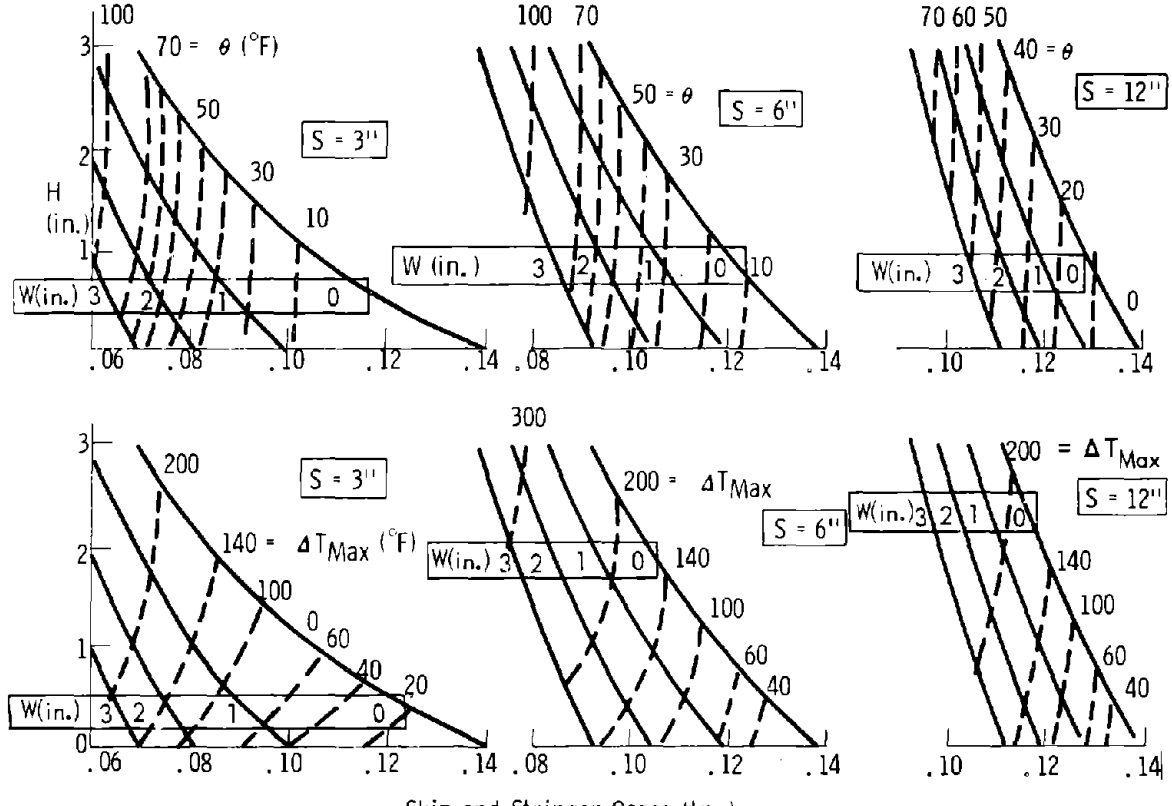

τ = Skin and Stringer Gages (In.)

Figure 80

TEMPERATURE INCREMENTS FOR STIFFENED SKINS
ALUMINUM AT 4 POUNDS PER SQUARE FOOT

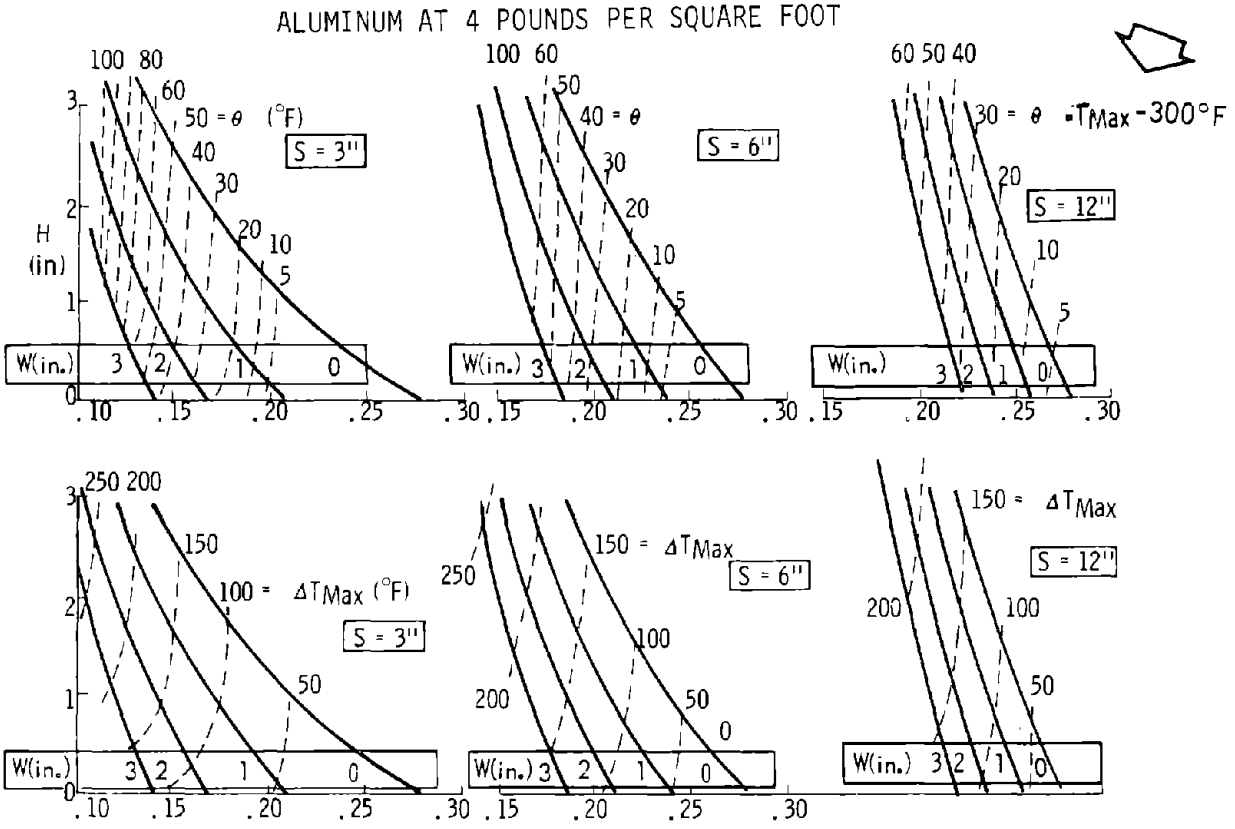

τ = Skin and Stringer Gages (in.)

Figure 81

ALLOWABLE STIFFENED GEOMETRIES -
ALUMINUM AT 4 POUNDS PER SQUARE FOOT

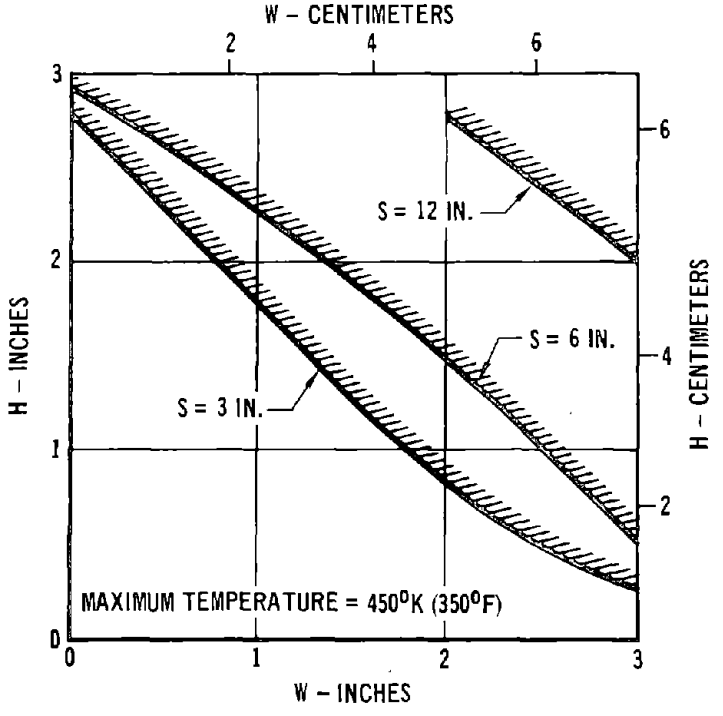

Figure 82

4.5.2 Crew Egress - The heat sink structure in the vicinity of the crew compartment, if sized to the full temperature potential of the basic metal, could peak in the neighborhood of 178°C (300 to 350°F) for aluminum and 316 to 482°C (600 to 900°F) for titanium. Egress of the crew and access to the compartment is possible at the 178°C (350°F) level with minimum personnel protection. The hazards at the titanium peak temperature could be significant, and, therefore, were analyzed further. The study extended past entry into the period of subsonic cruise, using approximate values of convective heat transfer coefficients and recovery temperatures. In two cases (Figure 83) the temperature of the titanium structure reached ambient temperature within 500 seconds after the time at which the peak temperature occurred, and well before landing. Therefore, the use of the structure as a heat sink should not cause any problem of crew egress after landing.

TEMPERATURE HISTORY OF TITANIUM NOSE CAP

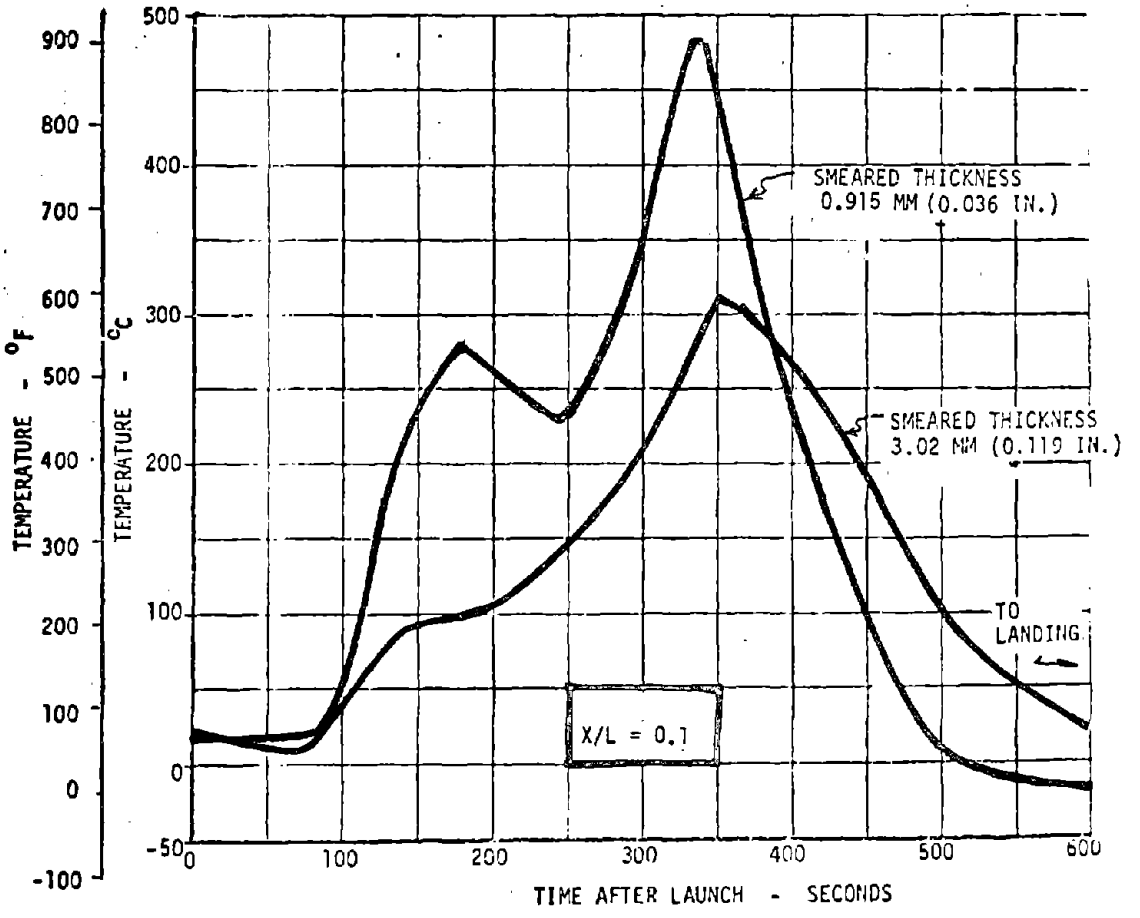

Figure 83

4.5.3 Effects of Initial Temperature Assumption - The liftoff temperatures of nontank areas may vary over a fairly wide range, due to weather conditions. This initial temperature will have an influence on the peak temperature reached during flight, as shown in Figure 84. However, for the two cases shown, the difference in maximum temperatures is only about 40 percent of the difference in liftoff temperature. This is caused by initial cooling which occurs as the vehicle enters cooler air during the low velocity phase of ascent flight. Since conservative design must be based on the use of the maximum likely initial temperature, this initial part of the ascent may have a pronounced effect on heat-sink thickness requirements. Therefore, boost phase aerodynamic heating uncertainties have greater effect on heat sink than on other thermal protection concepts. The effect of different initial liftoff temperatures on structural weight was further examined for aluminum and titanium. The results are summarized in Figure 85 and indicate that only aluminum exhibits much weight sensitivity, due to its low operating temperature limit.

EFFECT OF INITIAL TEMPERATURE ON PEAK TEMPERATURE

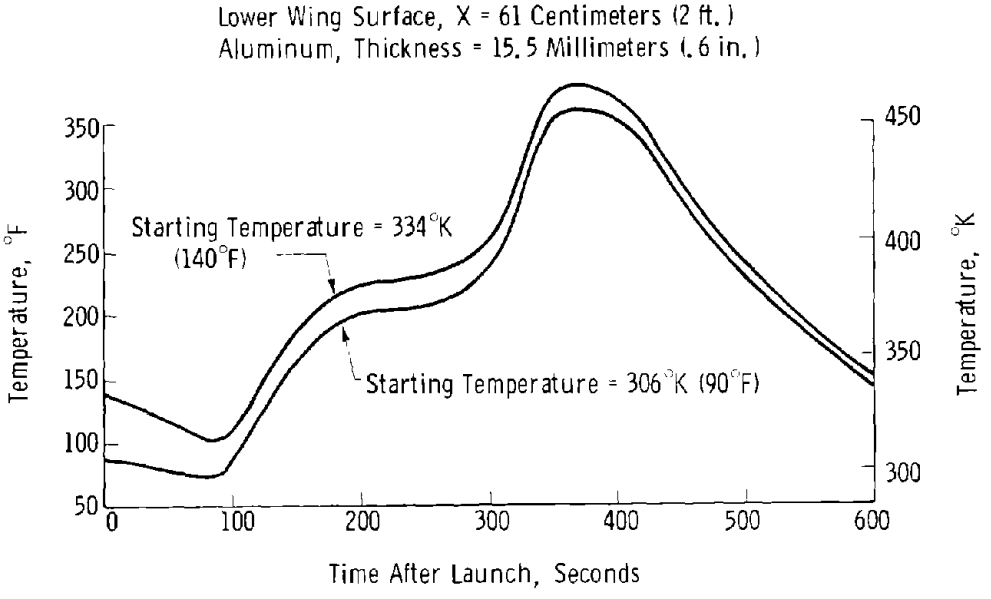

Figure 84

EFFECTS OF VARYING INITIAL TEMPERATURE

MATERIAL	MAXIMUM TEMPERATURE		INITIAL TEMPERATURE		REQUIRED UNIT WEIGHT	
	^{o}K	^{o}F	^{o}K	^{o}F	(Kg/m^2)	LB/FT^2
ALUMINUM	450	350	278	40	40.7	8.35
			306	90	44.0	9.03
			333	140	49.0	10.04
TITANIUM	589	600	278	40	31.9	6.54
			306	90	32.2	6.60
			333	140	32.8	6.69
TITANIUM	755	900	279	40	15.3	3.14
			306	90	15.4	3.15
			333	140	15.4	3.15

Figure 85

5. TASK 3: PHASE CHANGE MATERIAL (PCM) APPLICATION

The purpose of this task was to assess the feasibility of reducing the TPS weight by incorporating a phase change material (PCM) to provide structural cooling. The feasibility study included both analysis and testing. A test panel consisting of an aluminum honeycomb panel with graphite/epoxy face sheets containing the PCM, protected with waterproofed mullite fibers was constructed and tested. The analysis was conducted for the Phase B configuration using a NASA derived environment and extended to include an 040A type configuration for comparison. The results indicate that a weight reduction should be possible with the cooling provided by the PCM. With the material studied, the RSI with nominal density of 15 lb/ft^3, the weight reduction obtainable in the configurations with RSI directly bonded to the structural skin should be about 2 kg/m^2 (0.4 lb/ft^2). In the Phase B design, the weight reduction was greater; there was no weight penalty for a PCM container because the substructure served as the container. In this configuration, the weight reduction potential was found to be 4.5 kg/m^2 (0.92 lb/ft^2). The results of testing confirmed the analytically predicted weight reduction capability of the PCM approach.

5.1 Phase Change Material (PCM) Selection - Historically, the concept of temperature control with PCM has been directed primarily toward cooling electronic components or toward using PCM as a thermal capacitor to reduce the variation in a thermal control system heat load. These applications have been studied for some time by a number of investigators but few studies have been directed toward the entry TPS application. Therefore, a survey of available PCM was conducted to determine which would be most suitable for an inexpensive feasibility test article. Because of the relatively high temperature range involved in this application, many of the highly refined paraffins were precluded; they would liquify prior to entry. The survey, reported in Reference 16, narrowed the list of potential candidates to two families of materials for TPS application: high melting temperature waxes (paraffins and microparaffins); and hydrated inorganic salts. The characteristics of these materials are indicated in Figure 86. Some characteristics of the inorganic hydrates are superior to those of the wax. Heat storage capacity in fusion, for example, is higher, and while thermal conductivity data were not available, conductivity is expected to be adequate. The salts do have one drawback; they decompose at relatively low temperatures (104°C) and, therefore, their reuse characteristics are uncertain. Packaging these materials also presents some uncertainty, since material compatibility data are not available. In addition, the heat absorption advantage is not as great as first appears, since the available paraffins undergo solid/solid phase transitions that absorb about 25 percent as much heat as the latent heat of fusion. Additional heat can also be absorbed in the sensible temperature rise of the liquid paraffin which does not decompose and has a low vapor pressure. The paraffins are relatively inert, have a melting point high enough to ensure reversibility, and are readily available. These factors led to the selection of a high melting point paraffin for the feasibility test. A commercially available wax, Shellwax 700, was selected. This wax has a higher-than-average heat of fusion, 1.91 (10^5) J/kg (82 Btu/lb), solid-solid heats of transition of 0.5 (10^5) J/kg (25 Btu/lb), a high melting temperature of 84°C (183°F), and a higher heat absorption capacity than microparaffins with comparable melting points.

PHASE CHANGE MATERIAL (PCM) SELECTION

	CANDIDATE MATERIALS	
	WAXES (PARAFFINS AND MICROCRYSTALLINE)	INORGANIC HYDRATES
MATERIALS COMPATIBILITY	COMPATIBLE WITH MOST METALS AND PLASTICS, WAXES GENERALLY NON-REACTIVE AND STABLE	UNKNOWN, MATERIAL COMPOSITION PROPRIETARY
THERMAL PROPERTIES	HEAT OF FUSION ~1.67 (10^5) JOULE/KG SPECIFIC HEAT: SOLID 1886 – 2019 J/Kg ^{o}C LIQUID 2019 – 2837 J/Kg ^{o}C THERMAL CONDUCTIVITY ~ 0.0035 J/M–SEC ^{o}C EXPANSION ON LIQUEFACTION ~ 15–20%	HEAT OF FUSION ~ 2.6 (10^5) JOULE/KG SPECIFIC HEAT SOLID 1464–2092 J/Kg ^{o}C LIQUID 2092–3347 J Kg ^{o}C THERMAL CONDUCTIVITY – UNKNOWN EXPANSION ON LIQUEFACTION – UNKNOWN
MAXIMUM ALLOWABLE TEMPERATURE	200^{o}C (400^{o}F) (HIGHER WITH OXIDATION INHIBITOR)	104^{o}C (220^{o}F) (LIMITED BY DECOMPOSITION/ VAPOR GENERATION
PHASE CHANGE REVERSIBILITY	HIGH MELTING TEMPERATURE PARAFFINS SHOULD EXHIBIT MINIMAL SUPERCOOLING, BASED ON TESTS OF LOW MELTING PARAFFINS FOR MANY CYCLES. MICROCRYSTALLINES SHOULD HAVE SIMILAR BEHAVIOR	UNKNOWN, LIMITED TEST CONDUCTED, DATA INSUFFICIENT
FABRICABILITY	SMALL SAMPLE FABRICATED TO EXAMINE PCM BEHAVIOR, NO SPECIAL PROBLEMS	UNKNOWN, PROPRIETARY TO ROYAL INDUSTRIES
COST/AVAILABILITY	CHEAP, READILY AVAILABLE	UNCERTAIN

Figure 86

5.2 PCM System Trade Study - Subsequent to the selection of the PCM, the MDC Phase B orbiter metallic TPS was studied to determine whether a weight reduction could be effected by using the PCM for cooling. For this evaluation the PCM was assumed to be packaged in an aluminum honeycomb attached to the main propellant tank wall. Heat loads given in the Reference 2 trade study were used to determine the PCM quantity required with a PCM heat absorption capability of 464,800 j/kg (200 BTU/lb). The minimum unit weight was found to occur when the insulation thickness was large enough that no PCM was required. The analysis assumed the use of 56.5 kg/m^3 (3.5 lb/ft^3) Microquartz insulation. Should higher density insulation be required then a weight reduction would be likely. A prior study (Reference 7) determined that application of PCM results in a slight weight increase if 56.5 kg/m^3 (3.5 lb/ft^3) insulation was used, but concluded that PCM cooling should provide a weight reduction if moderately high density insulation was used. In particular the benefit from PCM was found to occur with an insulation density greater than 86 kg/m^3 (6 lb/ft^3). The highest density insulation contemplated for the MDC Phase B design was a composite of 172 kg/m^3 (12 lb/ft^3) Dynaflex against the hot shingle backed by 56.5 kg/m^3 (3.5 lb/ft^3) Microquartz. Even though this insulation has a composite density of 84 kg/m^3 (5.2 lb/ft^3), close to the breakeven density, the low density constituent would be traded against the PCM. Therefore, no payoff was apparent for the metallic system.

A Phase B TPS consisting of 215 kg/m^3 (15 lb/ft^3) mullite RSI had been considered in analysis prior to the contract award. This design consisted of RSI bonded to a honeycomb supporting panel. By placing the PCM in the honeycomb cells the bondline could be cooled directly and the PCM traded against the moderately high density external insulation. This prior analysis indicated that the use of PCM in the RSI system would provide a weight reduction in this configuration of the order of 1.46 kg/m^2 (0.3 lb/ft^2). The analytical and test effort to demonstrate feasibility was,therefore,concentrated on the TPS using RSI bonded to a honeycomb supporting panel.

5.3 Selected Concept Analyses

Thermal Analysis - A somewhat more severe heating environment than the Phase B environments used for Task 1 was applied in Task 3 design analyses. Environments supplied in Reference 17 were used to allow consistent comparisons with the RSI development work proceeding at MDAC-E under contract NAS 9-12082. The exposed surface heating rate, shown in Figure 87, was used in a two-dimensional model of the RSI/PCM system to determine the best RSI/PCM combination. The thermal model is illustrated in Figure 88. The quantity of PCM required to maintain a 149.8°C (300°F) bondline temperature, shown as a function of RSI thickness in Figure 89, was first determined. Using this curve, the optimized weight combination of RSI and PCM was determined, as illustrated in Figure 90. This figure indicates a potential weight saving of about 3.5 kg/m^2 (0.7 lb/ft^2) and a substantial RSI thickness reduction. Additional computations indicated that the potential weight saving was significantly affected by the bondline temperature. Figure 91 shows both PCM and non-PCM system weights for a Phase B type TPS. The potential weight reduction available with the PCM increases as the bondline temperature limit is lowered.

Fabrication Performance Studies - In addition to this analysis, a 15.2 by 15.2-cm (6 by 6-in.) honeycomb panel was constructed under IRAD funding to examine the behavior of the selected PCM under simulated heating, and to check on fabrication problems. Photographs in Figure 92 show the behavior of the material in the 4.8-mm (3.16 in.) aluminum honeycomb. When melted, the PCM wetted the honeycomb, forming a deep meniscus (indicated a high surface tension). Upon solidification, a relatively large contraction void formed, nearly in the center of the cell. Freezing occurred first near the aluminum honeycomb cell wall and the face sheet, and the subsequent contraction in the remainder caused the void. Thus, the PCM was positioned automatically after each cycle in position for excellent honeycomb/PCM heat transfer in subsequent heat pulses.

The face sheet on this assembly was bonded to the honeycomb after the honeycomb had been filled. The filling procedure consisted of partially immersing the honeycomb in melted PCM, chilling the wax to resolidify it, and removing excess wax. The bond was accomplished with a standard epoxy, using a room temperature cure.

The small, 15.2 by 15.2-cm (6 by 6-in.) honeycomb panel was tested to determine the behavior of the selected PCM and the temperature response under simulated heating. This mini-panel was constructed with a single face sheet so that the PCM behavior could be visually observed as the test progressed. The first few test

LOCAL HEATING RATE FOR ORBITER ENTRY

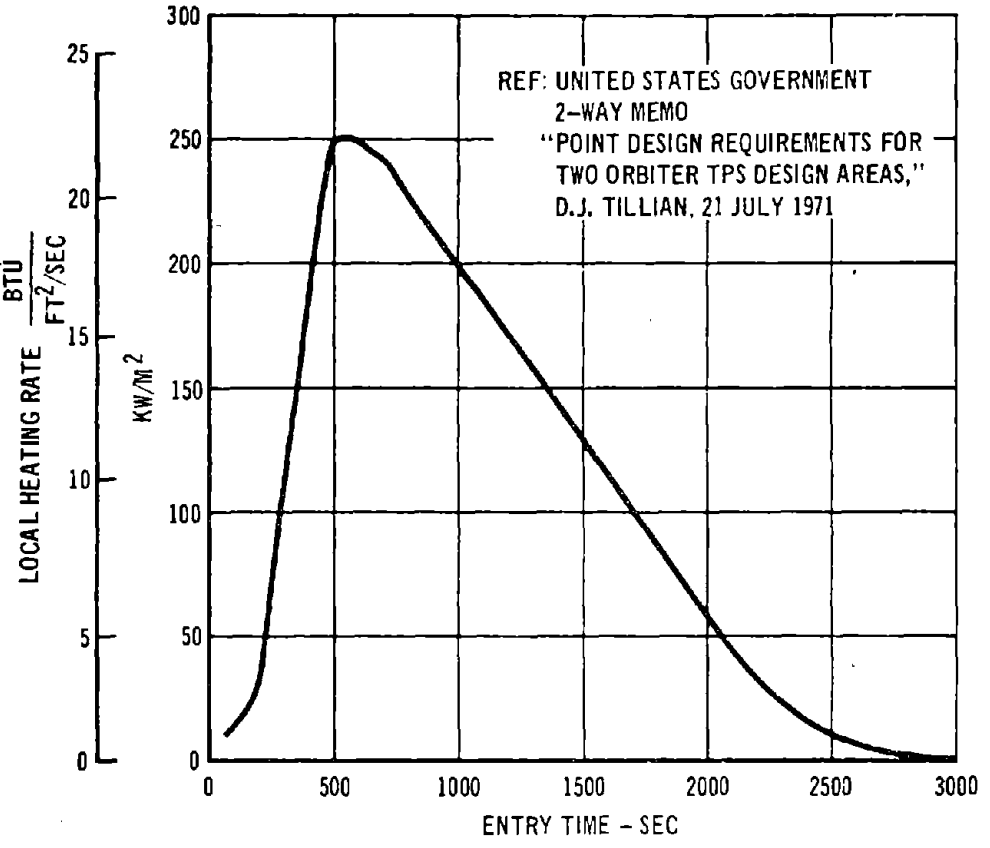

Figure 87

RSI - PCM TWO-DIMENSIONAL THERMAL MODEL

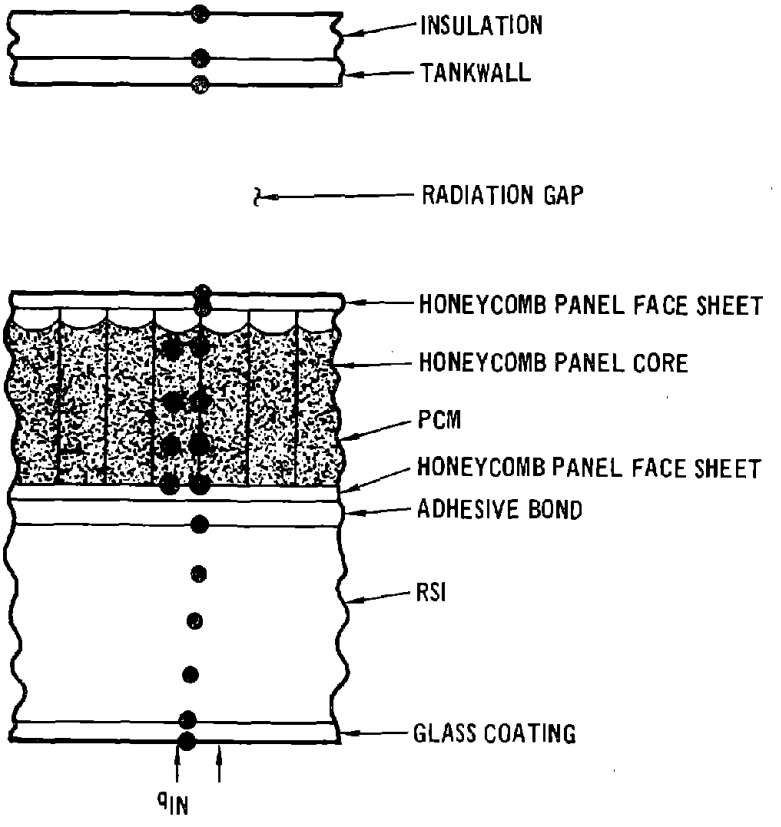

Figure 88

REUSABLE SURFACE INSULATION THICKNESS

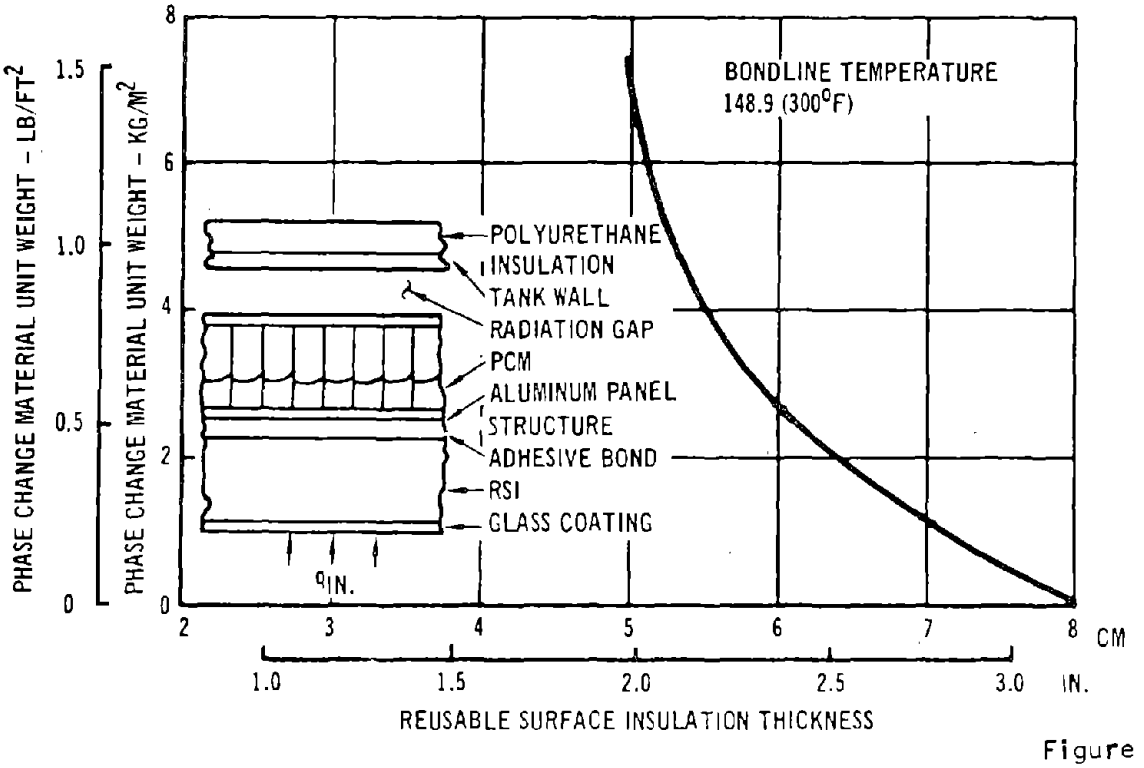

Figure 89

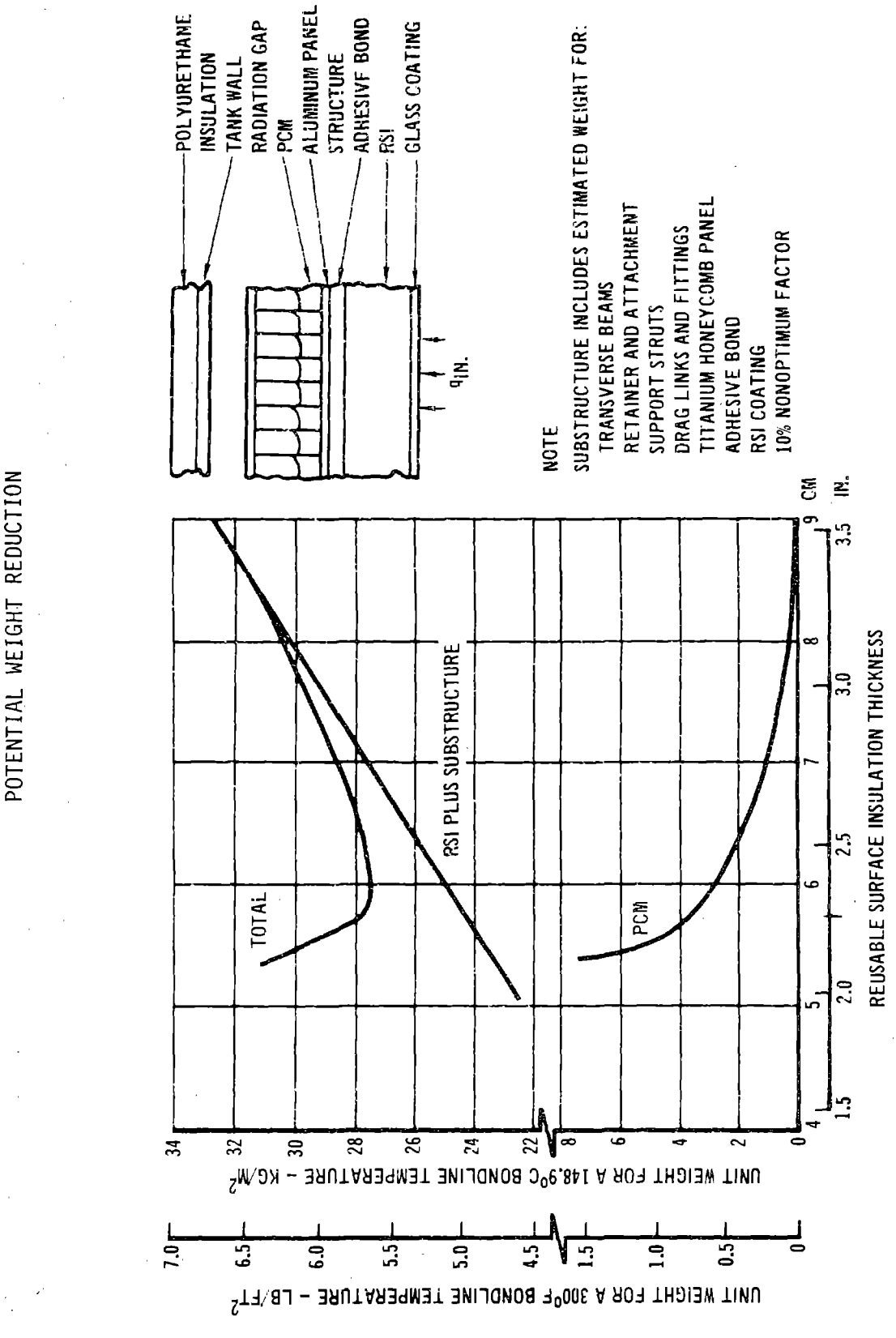
POLYURETHANE
INSULATION
TANK WALL
RADIATION GAP
PCM
ALUMINUM PANEL
STRUCTURE
ADHESIVF BOND
RSI
GLASS COATING
$q_{IN.}$
NOTE
SUBSTRUCTURE INCLUDES ESTIMATED WEIGHT FOR:
TRANSVERSE BEAMS
RETAINER AND ATTACHMENT
SUPPORT STRUTS
DRAG LINKS AND FITTINGS
TITANIUM HONEYCOMB PANEL
ADHESIVE BOND
RSI COATING
10% NONOPTIMUM FACTOR
POTENTIAL WEIGHT REDUCTION
TOTAL
RSI PLUS SUBSTRUCTURE
PCM
UNIT WEIGHT FOR A 300°F BONDLINE TEMPERATURE - LB/FT²
UNIT WEIGHT FOR A 148.9°C BONDLINE TEMPERATURE - KG/M²
REUSABLE SURFACE INSULATION THICKNESS
CM
IN.

Figure 90

LOWER BONDLINE TEMPERATURE MEANS HIGHER TPS WEIGHT

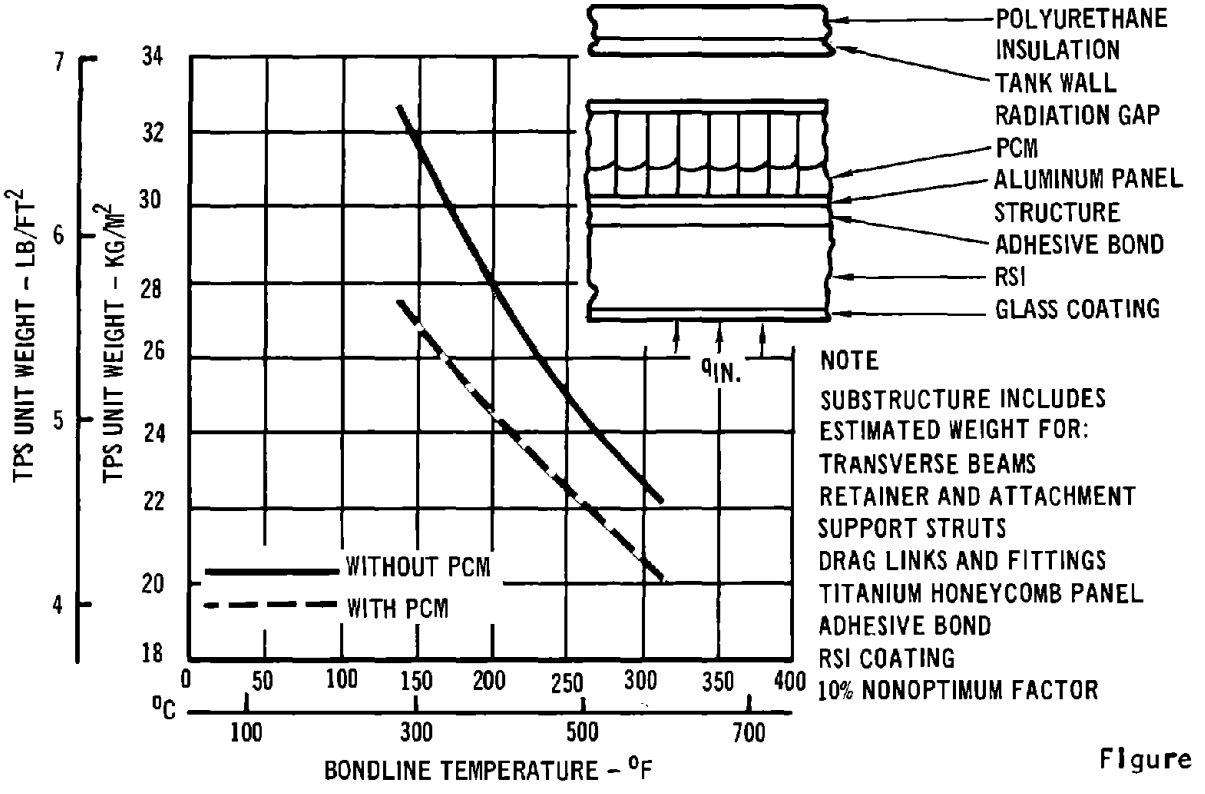

Figure 91

PHASE CHANGE MATERIAL (PCM) BEHAVIOR

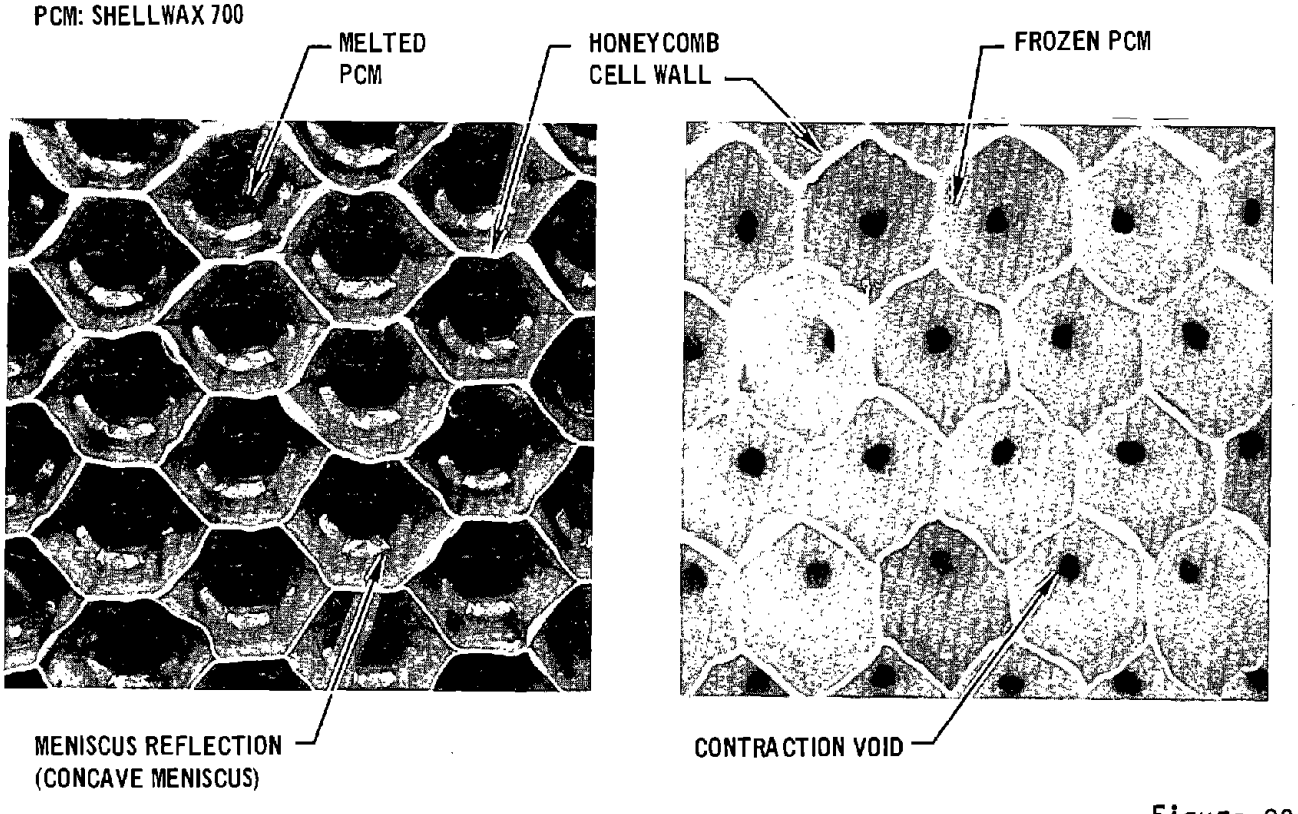

Figure 92

runs indicated fairly high heat losses from the open side of the honeycomb. To achieve a net heat input comparable with that expected for the full-scale test panel, a constant heat flux of 1.505 kw/m^2 (476 BTU/hr ft^2) was applied and the temperature response measured. Measurements of the heated surface, the PCM, and the honeycomb temperature response are shown in Figure 93. This test indicated that the conductance from the panel to the PCM was sufficient to provide adequate heat transfer into the PCM. This was evidenced by the relatively small temperature difference between the heated face sheet and the PCM. The temperature difference through the panel also remained relatively small,even though losses by radiation and convection from the unheated side were substantial, amounting to approximately 20 watts (68 BTU/hr) at 93°C (200°F). The rate of temperature change was consistent with the observed characteristics of the PCM, shown in Figure 94.

The Shellwax 700 PCM experienced solid phase changes beginning at approximately 43°C (110°F) and softened appreciably at 60°C (140°F). From 60 to 84°C (140 to 183°F) various constituents softened further and melted. At 84°C (183°F) all constituents were liquid. The observed temperature rate of change (Figure 93) reached a minimum at 77°C (170°F) peak effective C_p, and subsequently increased at higher temperatures. Because of increasing heat losses, the rate of increase remained somewhat lower at the higher temperatures.

Structural Analysis of Supporting Panel - Structural analysis of the supporting panel was conducted in parallel with the thermal analysis to arrive at a near-optimal weight solution. Eight different structural material combinations were evaluated to determine the minimum weight panel which would have a high probability of adequately supporting the RSI when subjected to the Reference 18 environments. The design criteria consisted of an allowable deflection of 4.35 mm(0.17 in) at the center of the panel. This was based on the design of a panel in the NASA 9-12082 contract that had successfully survived environmental testing and for which finite element analysis had predicted acceptable stress levels in the waterproof coating. The panel weights and corresponding TPS weights from the structural analysis are presented in Figure 95. The weights rank as normally expected, with the exception of the panel made up of titanium face sheets (which has a higher weight than expected). The titanium panel face sheets are somewhat thicker than required for strength alone, to prevent intercell buckling in the face sheets. This lower limit on the titanium face sheet thickness thus prevents optimal use of the material, since smaller cell size honeycomb is not available. Because the panels must also

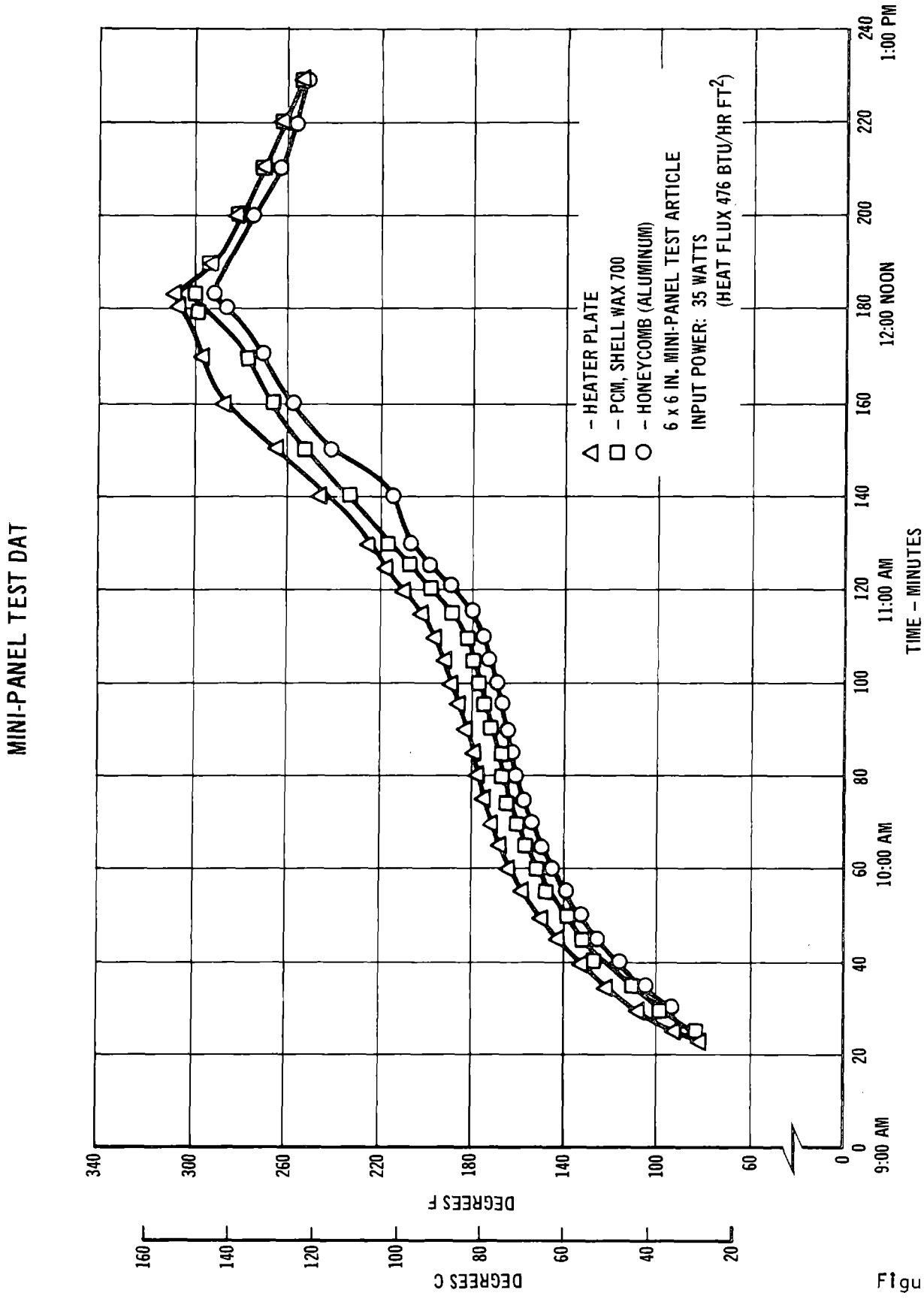
MINI-PANEL TEST DAT
△ - HEATER PLATE
□ - PCM, SHELL WAX 700
○ - HONEYCOMB (ALUMINUM)
6 x 6 IN. MINI-PANEL TEST ARTICLE
INPUT POWER: 35 WATTS
(HEAT FLUX 476 BTU/HR FT²)
TIME - MINUTES
9:00 AM
10:00 AM
11:00 AM
12:00 NOON
1:00 PM
0
20
40
60
80
100
120
140
160
180
200
220
240
DEGREES F
340
300
260
220
180
140
100
60
DEGREES C
160
140
120
100
80
60
40
20

Figure 93

COMPARISON OF MEASURED SPECIFIC HEAT WITH VALUES USED IN ANALYSIS

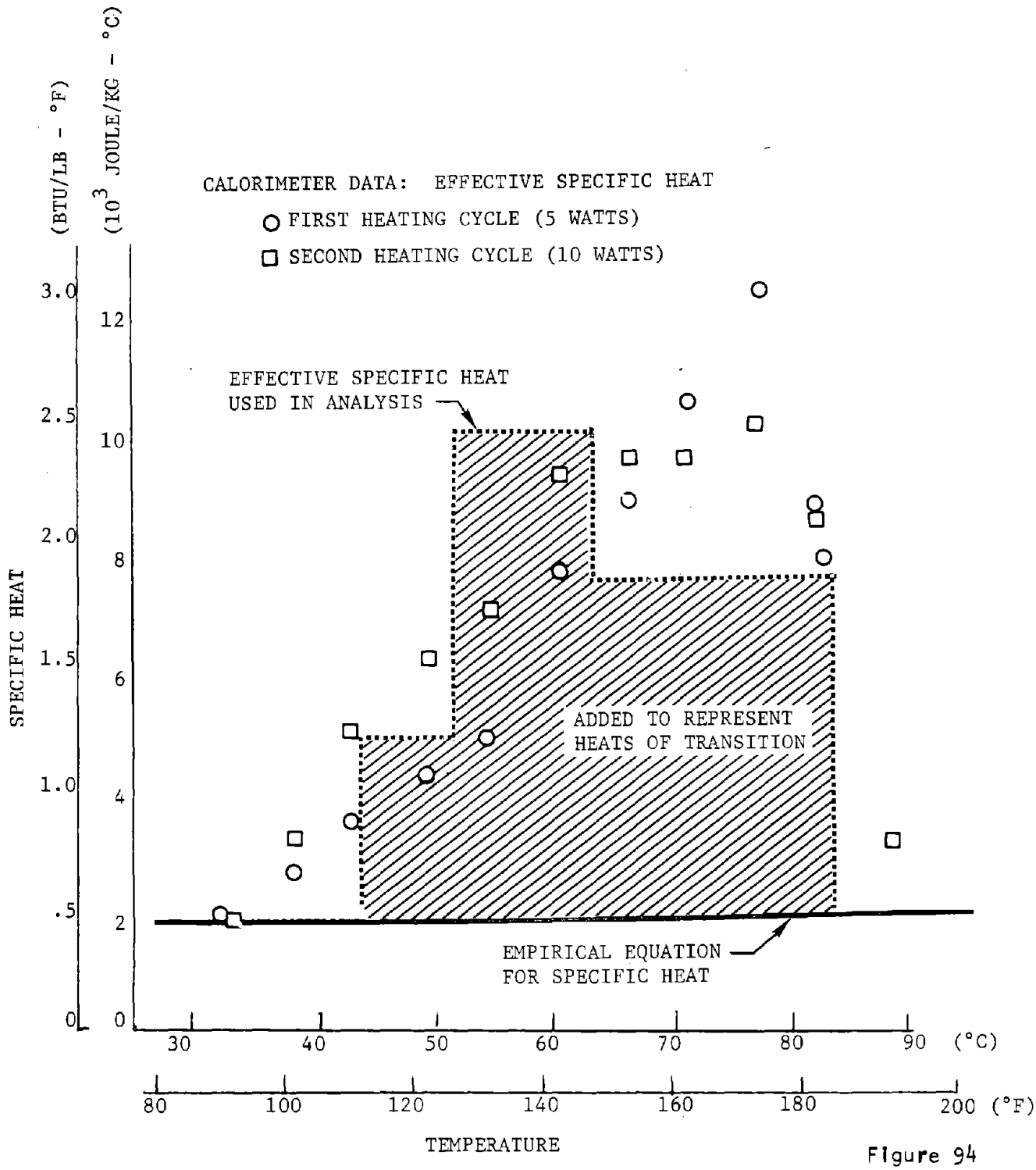

Figure 94

withstand an ultimate internal pressure of approximately 40 psia the face sheets were also checked to ensure they would adequately beam this load to the honeycomb cell wall. As indicated in Figure 95, the beryllium/aluminum and graphite polymide/aluminum are superior. Since there is no difference in the weights of the graphite and beryllium panels, graphite composite face sheets were selected for the feasibility test article.

It should be possible to vent the structure so that differential pressures on the panel would be much smaller than for the Phase B-type panel. Consequently, the panel would be designed primarily by PCM containment requirements and would, therefore, be lighter.

SUBSTRUCTURE TRADE STUDY SUMMARY

SUBSTRUCTURE MATERIAL FACE SHEET/ CORE	PANEL THICKNESS CM (IN.)	FACE SHEET THICKNESS CM (IN.)	FACE SHEET COEFFICIENT OF THERMAL EXPANSION CM/CM ^{o}C (IN./IN.^{o}F)	CORE SIZE/DENSITY CM/KG/M^3 (LB/FT^3)	PANEL WEIGHT KG (LB)	TOTAL TPS WEIGHT KG/M^2 (LB/FT^2)
ALUMINUM/ ALUMINUM	2.97 (1.17)	0.0177 (0.007)	24.5×10^{-6} (13.6×10^{-6})	0.477/49.7 (3/16 /3.1)	0.380 (0.66)	25.6 (5.26)
ALUMINUM/ TITANIUM	2.84 (1.04)	0.0228 (0.009)	23.8×10^{-6} (13.2×10^{-6})	0.635/66.2 (1/4 /3.5)	0.322 (0.71)	26.0 (5.32)
TITANIUM/ ALUMINUM	3.25 (1.28)	0.0144 (0.0057)	11.7×10^{-6} (6.5×10^{-6})	0.477/49.7 (3/16 /3.1)	0.336 (0.74)	26.1 (7.35)
TITANIUM/ TITANIUM	2.49 (0.98)	0.0190 (0.0075)	11.7×10^{-6} (6.5×10^{-6})	0.635/56.2 (1/4 /3.5)	0.354 (0.78)	26.4 (5.40)
BERYLLIUM/ ALUMINUM	2.16 (0.85)	0.0203 (0.008)	13.1×10^{-6} (7.3×10^{-6})	0.635/36.9 (1/4 /2.3)	0.213 (0.47)	24.5 (5.03)
BERYLLIUM/ TITANIUM	2.22 (0.876)	0.0198 (0.0078)	13.1×10^{-6} (7.3×10^{-6})	0.635/56.2 (1/4 /3.5)	0.249 (0.55)	25.0 (5.127)
GRAPHITE POLYIMIDE/ ALUMINUM	2.19 (0.863)	0.0228 (0.009)	2.3×10^{-6} (1.3×10^{-6})	0.635/36.9 (1/4 /2.3)	0.217 (0.47)	24.5 (5.03)
GRAPHITE POLYIMIDE/ ALUMINUM	2.19 (0.863)	0.0228 (0.009)	2.3×10^{-6} (1.3×10^{-6})	0.635/56.2 (1/4 /3.5)	0.254 (0.56)	26.0 (5.13)

LENGTH = 63.5 CM (25 IN.) P_{LIMIT} = 27,500 N/M^2 (4.0 LBF/IN.^{2}) P_{ULT} = 41,300 N/M^2 (6.0 LBF/IN.^{2})
DEFLECTION AT ENTRY LOAD IS 0.407 CM (0.17 IN.)

Figure 95

5.4 TPS Test Panel Design/Construction - The test panel was designed so that feasibility testing could be conducted in an available test facility at McDonnell Douglas in St. Louis, the graphite heater facility. This test hardware had been designed and used for testing TPS panels and insulation specimens for reuse characteristics. The holding fixture permitted a 30.5 by 61-cm (12 by 24-in.) test panel within an exposed surface area of 0.162 cm^2 (1.79 ft^2).

The test panel designed to demonstrate the feasibility of PCM cooling is shown in Figure 96. The design consisted of a 30.5 by 61-cm (12 by 24-in.) honeycomb panel (containing the PCM) protected from external heating by eight RSI tiles. The panel design utlized an aluminum honeycomb core sandwiched between graphite/epoxy composite skins. The honeycomb was constructed of 0.025-mm (0.001-in.) aluminum and had a cell size of 6.35 mm (0.25 in.). Shellwax 700 had been selected as the PCM. The graphite/epoxy composite skins were composed of three plies of tape material with the plies arranged so that the graphite fibers of two plies were aligned with the long axis of the panel,with the third ply at a right angle to the first two. This arrangement is shown in Figure 96. A two-ply configuration would have given adequate panel strength but the three-ply design was selected to give greater strength and ability to tolerate local unbonded areas. To assure a high integrity skin/core bond the panel was designed for installation of the PCM as individual pellets. The panel thickness was set at 2.21 cm (0.87 in.), consistent with the initial strength analysis.

Based on the thermal analyses,a thickness of 5.72 cm (2.25 in.) was selected for the RSI protecting the panel. A nominal 15.2 by 15.2-cm (6 by 6-in.) tile size was selected, with 8 tiles required. The tile edges were given an overlapping offset (see Figure 93) to prevent radiant heat transmission directly from the facility heat source to the supporting panel. The tiles on both ends of the panel were shortened to allow clamping the panel into the test fixture. Each tile was coated on five sides for waterproofing and bonded to the panel with a silicone adhesive. The components are shown prior to assembly ir Figure 97.

The panel was instrumented with 15 thermocouples. Of these, nine were located in the RSI/panel bond (beneath tile centers, between tiles to detect gap heating and at tile joint intersections). Three thermocouples were located in the PCM and the remaining three thermocouples were installed on the honeycomb skin opposite to the heated surface.

Prior to fabrication of the test hardware, a two-ply graphite/aluminum honeycomb panel was constructed to check out the fabrication procedures. This

STRUCTURAL ACTIVE COOLING

30 JUNE 1972

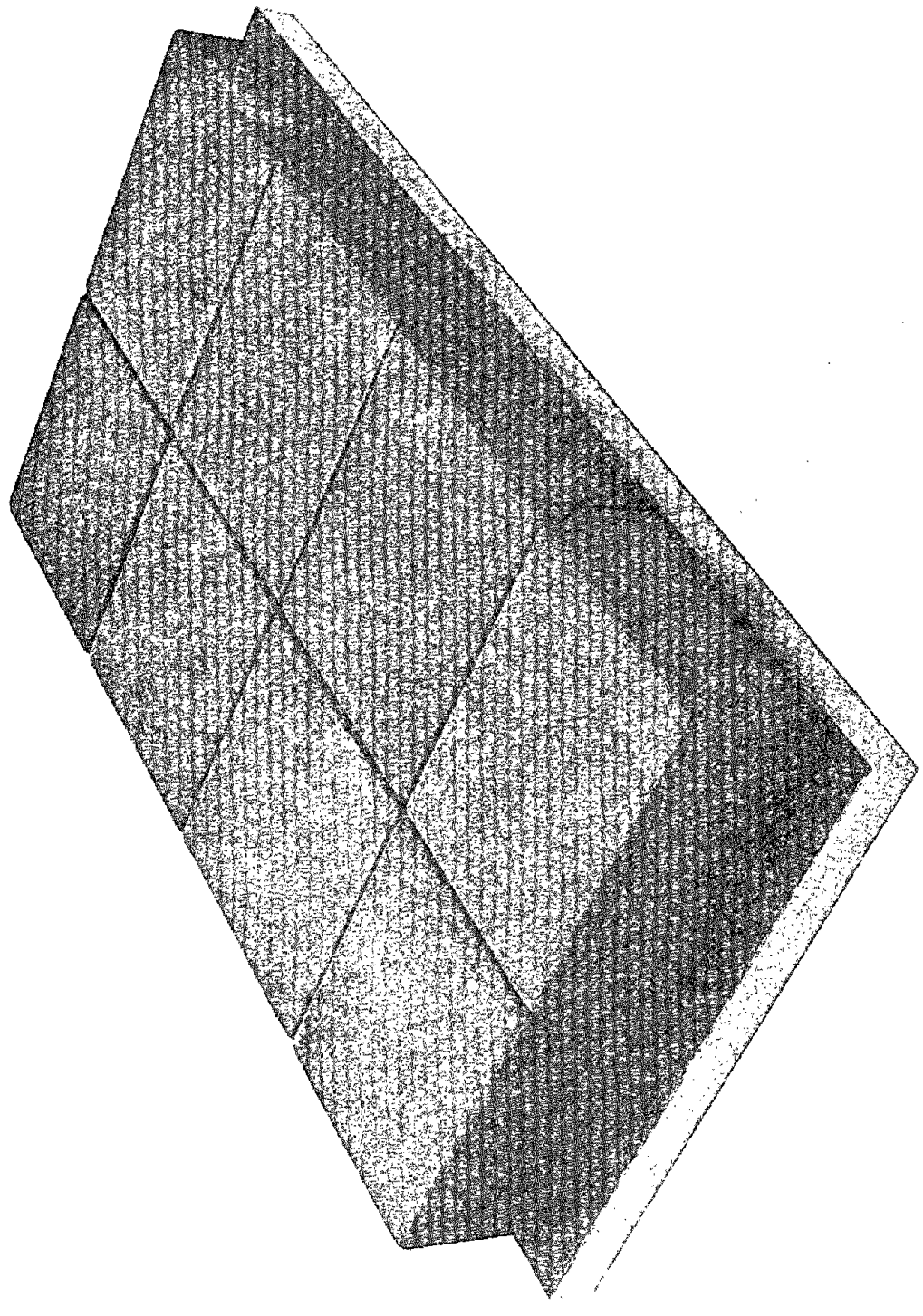

PCM FEASIBILITY TEST PANEL

Figure 96

STRUCTURAL ACTIVE COOLING

COMPONENTS PRIOR TO ASSEMBLY

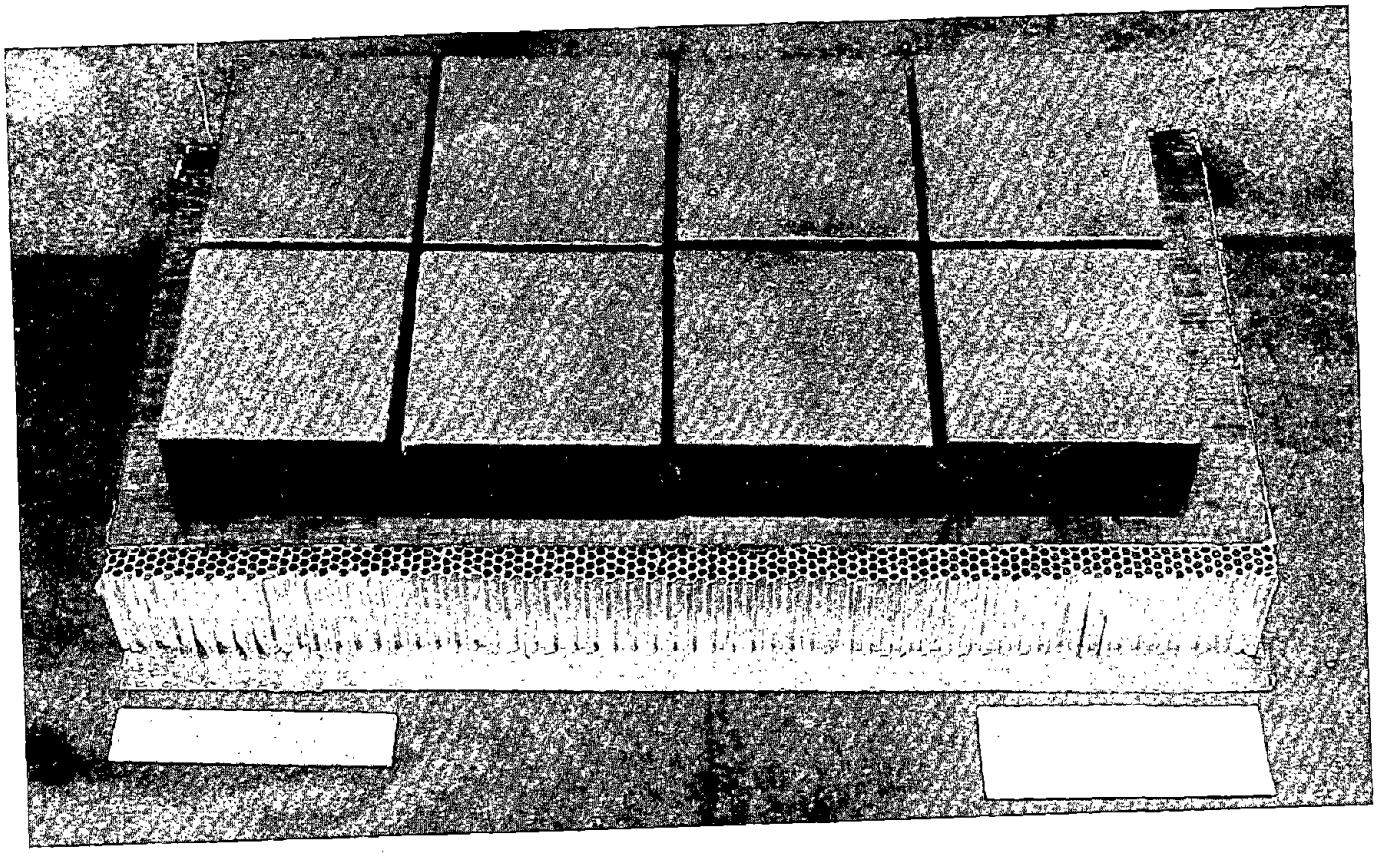

Figure 97

procedure required bonding the core to one skin in the absence of PCM, loading the PCM as individual pellets into the honeycomb cells, and then bonding the second skin on after the PCM was loaded. The cells in one region contained the wax PCM; the balance were empty. The panel was bonded in the autoclave in the same manner planned for the test hardware. Test samples were cut from the panel and subjected to a tensile pull test. The data are shown in Figure 98. All samples exhibited failure at force levels roughly an order of magnitude higher than the maximum forces expected from internal air pressure 1.85 by 10^5 n/m^2 (27 psid). Therefore, it was concluded that vaporization of volatile material from the PCM did not present a source of contamination that would jeopardize the integrity of the skin/core bond.

The wax pellets were made by casting the PCM into 4.75-mm (3/16-in.) cell size honeycomb of the correct depth. The honeycomb was peeled apart, yielding uniform pellets that could be easily loaded into the larger celled panel honeycomb. Sampling of the resulting pellets was then used to estimate weight variations. The sample histogram shown in Figure 99 indicates a 1 σ variation of about 4 percent.

The PCM pellets were placed in the honeycomb only where the RSI tiles would be attached for thermal protection. No PCM was placed in the two rows adjacent to the panel edge so that a good edge seal could be effected. Subsequent to bonding the panel face sheets to the honeycomb (in autoclave) the outer two rows of honeycomb cells were crushed back and the edge was sealed with a microballoon filled epoxy resin.

TENSILE PULL TEST SAMPLES

NO WAX IN CELLS			WAX PRESENT IN CELLS		
SAMPLE	TENSION		SAMPLE	TENSION	
	(N/M^2)	($LB/IN.^2$)		(N/M^2)	($LB/IN.^2$)
A1	1.89 (10^6)	274	B1	1.60 (10^3)	232
A2	2.14 (10^6)	310	B2*	1.19 (10^3)	173
A3	1.61 (10^6)	233	B3	1.67 (10^3)	242

*SAMPLE DAMAGED IN BONDING TO PULL TEST FIXTURE

Figure 98

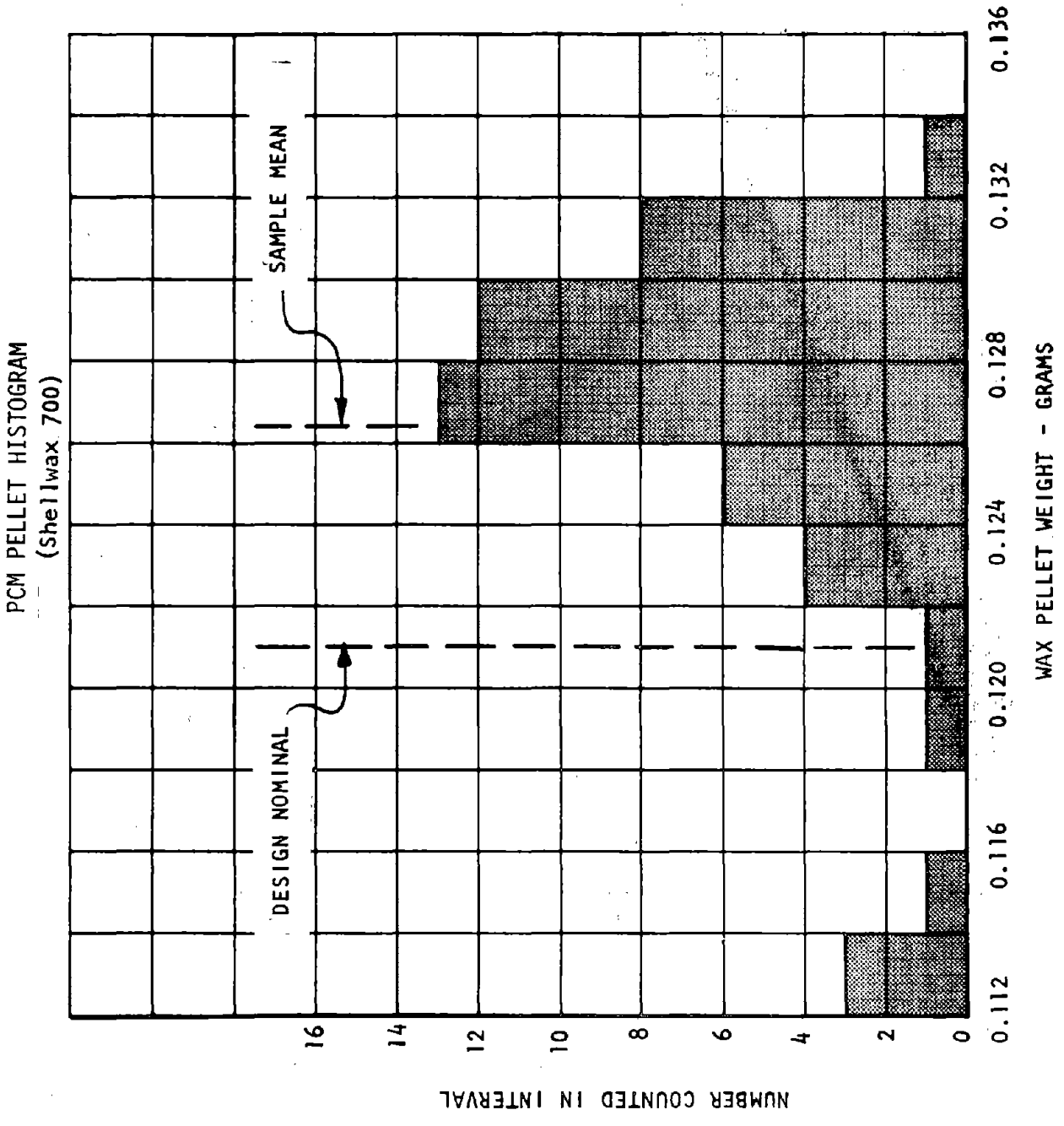
PCM PELLET HISTOGRAM
(Shellwax 700)
SAMPLE MEAN
DESIGN NOMINAL
NUMBER COUNTED IN INTERVAL
0
2
4
6
8
10
12
14
16
0.112
0.116
0.120
0.124
0.128
0.132
0.136
WAX PELLET WEIGHT - GRAMS

Figure 99

5.5 Feasibility Testing, Results, and Analysis - An initial series of three test cycles was run. The cycles were performed in order of increasing severity with peak temperatures of 427, 825, and 1205°C (800, 1600, and 2300°F) as shown in Figure 100. The 427°C and 825°C cycles were conducted at ambient pressure and the 1205°C pulse was conducted at reduced (10-25 torr) pressure. The 427°C peak temperature test truncated the cycle (Figure 87) with a 427°C "plateau". The data, acquired in this cycle, agreed well with pretest temperature predictions and the panel appeared undamaged. The 825°C maximum temperature run then was initiated. Again it was planned to use the same heating cycle, but with an 825°C "plateau".

During this test cycle,an attempt by the test conductor to prevent a temperature controller overshoot resulted in an excessive heatup rate. The peak rate was approximately double the planned rate. Then,shortly after 825°C was achieved, it was discovered that cooling water for the test fixture was not flowing. This was noted when an air spray bar bowed up, lifting guard insulation alongside the test panel. The fixture cooling water (used to vaporize purge LN_2 for the heater) had been frozen because the nitrogen purge had been left on between test cycles. When the cooling water flow could not be restored, the power to the graphite heater was shut off. The subsequent cool-down rate was much higher than planned, since power was required to follow the programmed cooling curve (Area 2P). Examination of the panel revealed extensive cracking of the RSI waterproof coating and the RSI appeared to have an in-depth crack on the side where the guard insulation had lifted. This cracking of HCF and coating was not anticipated at this relatively moderate temperature for the design heatup and cool-down rates, but may have been caused by the higher rates encountered in the test.

The coating was repaired and the test article readied for another test cycle. Because of the damage to the tiles, it was decided to proceed to the test cycle using the full 1250°C (2300°F) Area 2P profile at reduced pressure, rather than rerunning the 825°C case, since it appeared that the PCM-filled subpanel was behaving as predicted and a good test of the subpanel was desired before the HCF structural degradation from the aborted run became too great. The third test cycle was initiated and again the test was terminated prematurely. Several thermocouples were monitored and some exceeded pretest predictions, one by several hundred degrees. During the test the chamber pressure could not be controlled to 10 torr, and increased to 25 torr. It also appeared that some leakage of air or PCM from the panel occurred.

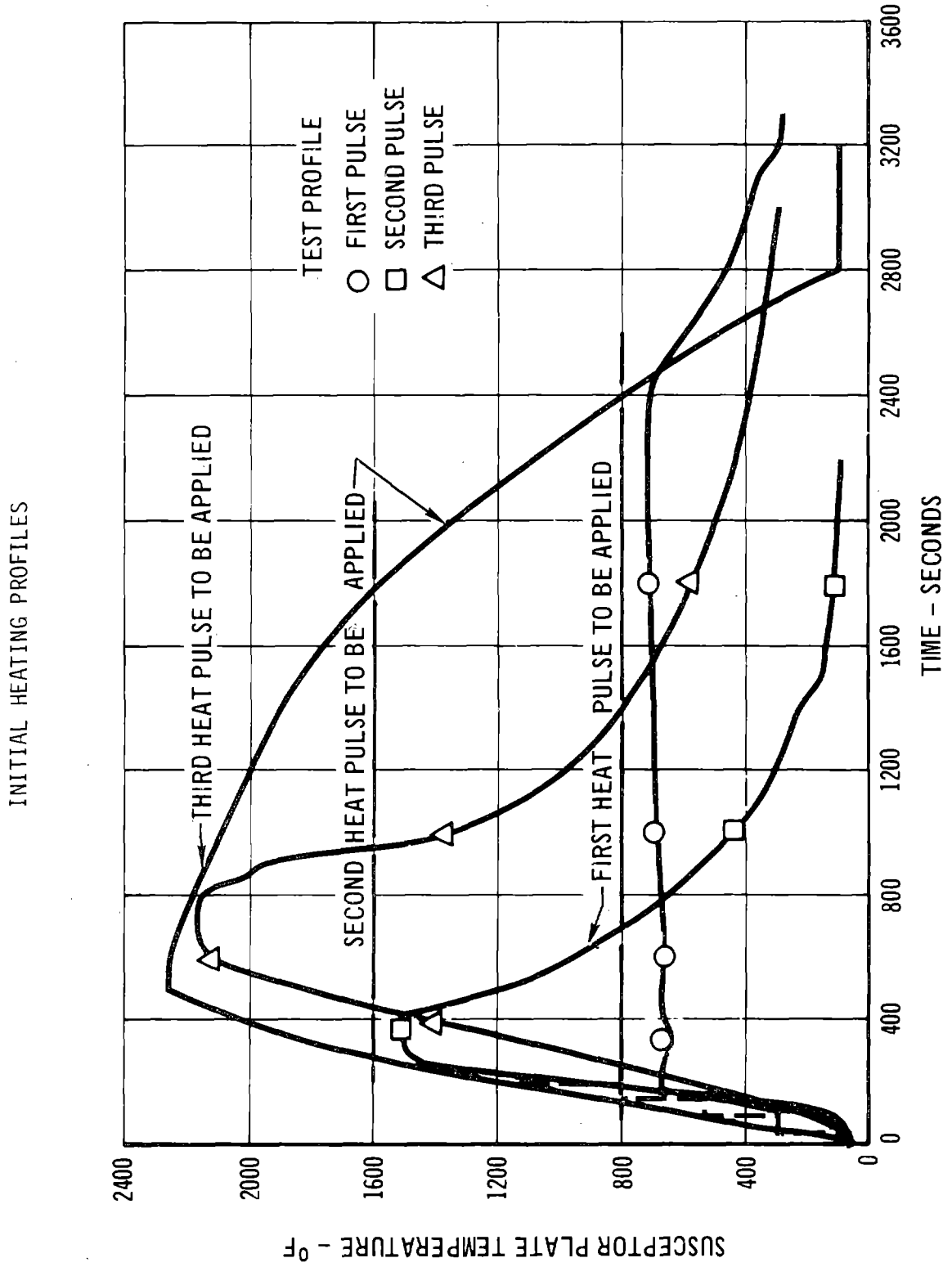
INITIAL HEATING PROFILES
TEST PROFILE
FIRST PULSE
SECOND PULSE
THIRD PULSE
THIRD HEAT PULSE TO BE APPLIED
SECOND HEAT PULSE TO BE APPLIED
FIRST HEAT PULSE TO BE APPLIED
SUSCEPTOR PLATE TEMPERATURE - °F
TIME - SECONDS
2400
2000
1600
1200
800
400
0
0
400
800
1200
1600
2000
2400
2800
3200
3600

Figure 100

Subsequent investigation disclosed that there was indeed leakage from the subpanel (apparently insignificant), and that new cracks had appeared in a number of the tiles.

The apparent excessive temperature read by one thermocouple appears to have been caused by mislocated instrumentation. Posttest x-rays shown in Figure 101 revealed that the thermocouple was 1-cm (0.4 in.) from the edge of the panel over an unfilled honeycomb cell, not in the center of the panel as shown in the drawings. The leakage of the PCM was caused by excessive temperatures experienced by the edge seal; which occurred because the panel edge guard insulation was not packed tightly and permitted direct heating of the edge seal producing the high thermocouple reading noted.

The first series of tests yielded anamalous results for which analytical correlation was good only for tests performed at ambient pressure. The prediction of the substructure temperature response matched the observed response well only for the initial two tests conducted at atmospheric pressure. The response in the third test was significantly underpredicted (Reference 18). Because of the poor correlation,additional testing was undertaken to verify the heat capacity of the PCM and the assembled subpanel.

A calorimeter test was conducted to determine experimentally the effective specific heat of the PCM. The effective specific heat was determined by measuring the transient thermal response of the PCM to two heating/cooling cycles. The PCM was heated at 5 and 10 watt rates and then allowed to cool. The effective specific heat then was determined from the temperature response. A determination of specific values for the transitional and fusion heat absorption was virtually impossible because the commercial wax selected was a mixture of components having different melting points. The data obtained were shown previously in Figure 94 with the analytical model employed to represent the PCM. The analytical model is based on empirical data for wax specific heat and heat of transition/fusion data obtained from Shell Petrochemicals Division. The calorimeter data verified the analytical model as a reasonable representation of the PCM heat storage properties.

Further tests were conducted to verify the heat capacity of the subpanel. Strip heaters were applied and a constant heat flux of (500 Btu/hr ft^2) was impressed on the uninsulated side of the panel. The test response was compared with the predicted response and shows good correspondence (Figure 102). Since the PCM and subpanel assembly thermal properties were nominally as expected the

STRUCTURAL ACTIVE COOLING

PANEL X-RAY

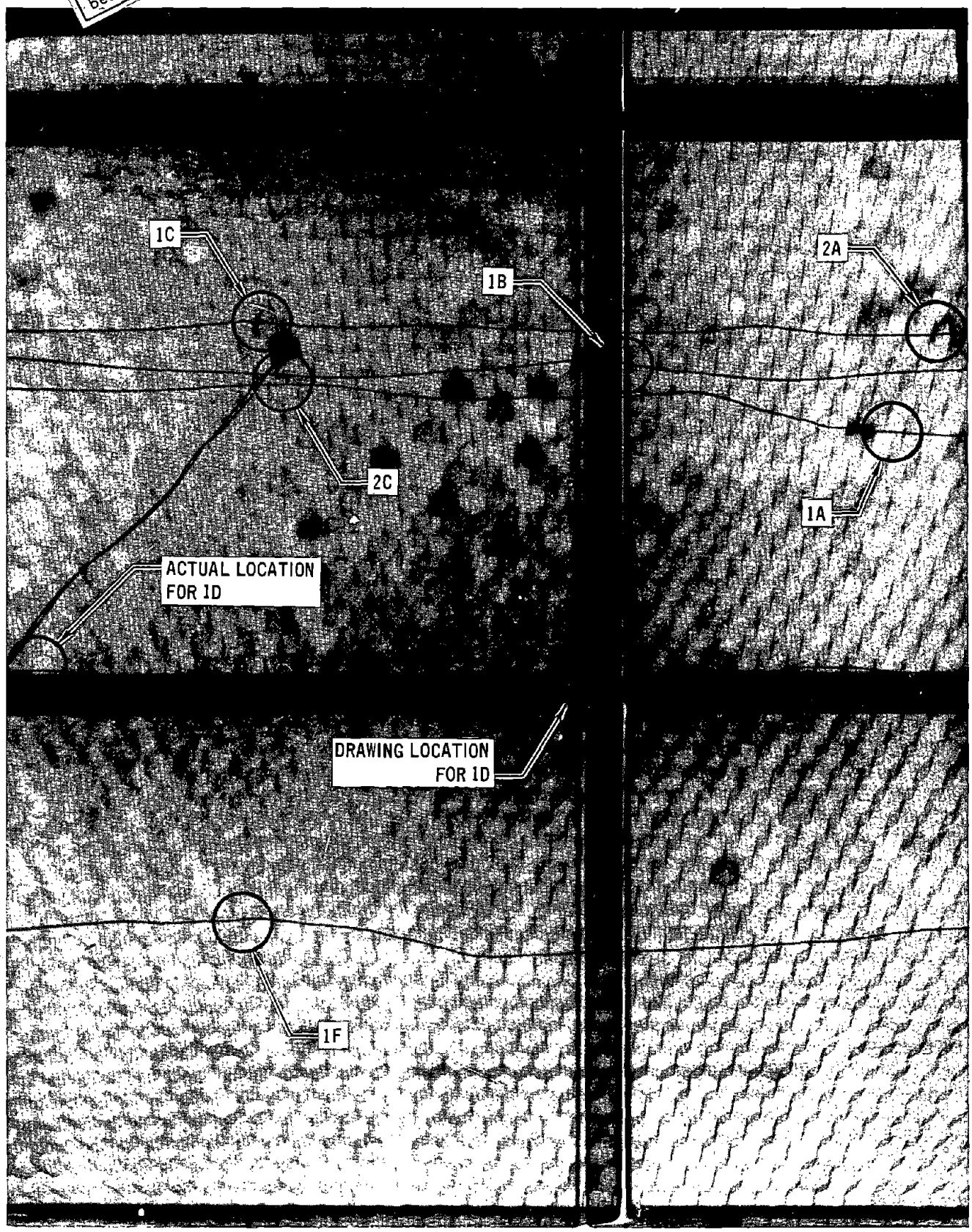

Figure 101

PANEL STRIP HEATER RESPONSE
PCM/TPS SUBPANEL INTEGRITY TEST RESULTS

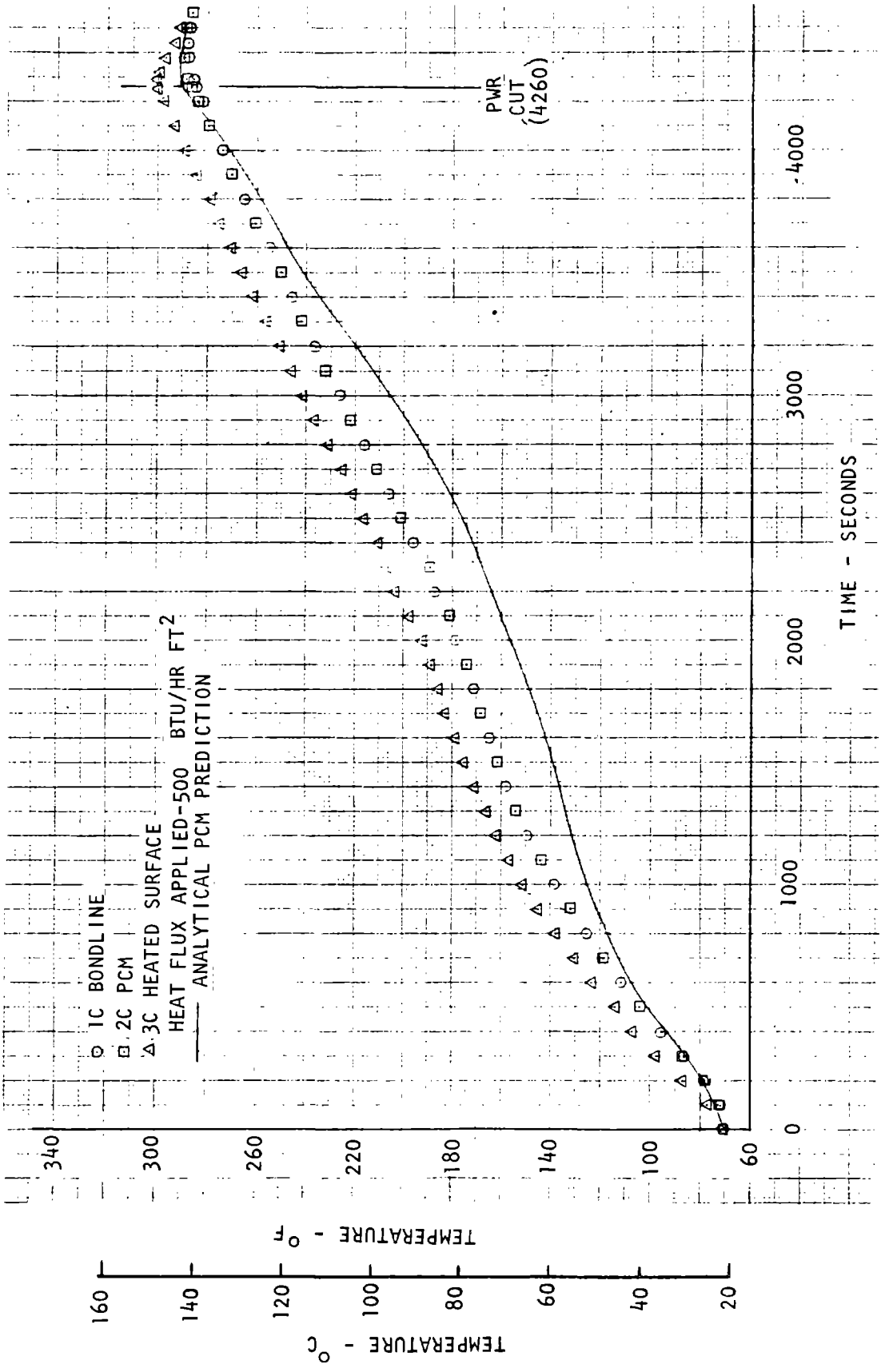

Figure 102

properties of RSI were assumed to be the source of the discrepancy, reported in Reference 18, between predicted temperatures and those measured in the test series.

Feasibility testing of the panel was concluded with a second sequence of profiles, shown in Figure 103, with the tests conducted at a pressure of 10 torr. The first two tests were analyzed with RSI conductivities derived from transient tests. Good correspondence was achieved and the analysis indicated that a test to the initially planned temperature profile would cause temperatures in excess of allowable values for the graphite epoxy honeycomb skin. Consequently an 040A environment with a lower integrated heat flux, but comparable peak heat flux was substituted for the initially proposed environment in the last test run. The results obtained in this run are given in Figure 104 with the analytical prediction. The correlation for all test runs was significantly improved and the data indicate that the effective conductivity of the early RSI material (designated MOD I) used in constructing the feasibility test article is somewhat higher than measured by guarded hot plate techniques. The panel survived the test series intact (Figure 96) and exhibited little additional damage in tests subsequent to the early abort that initially damaged the RSI.

Weight Reduction Potential - The potential weight savings to be realized for the 040A environments based on these data for this early version of the MDAC RSI (MOD I) are given in Figure 106. Current versions of this material should have improved properties and the weight savings would be less for the more thermally efficient versions. The potential weight savings would still be expected to be significant with current material (MOD III) design properties. A weight summary for this material that is based on analytical evaluation, also given in Figure 105, indicates a weight reduction potential of 1.95 kg/m^2 (0.4 lb/ft^2).

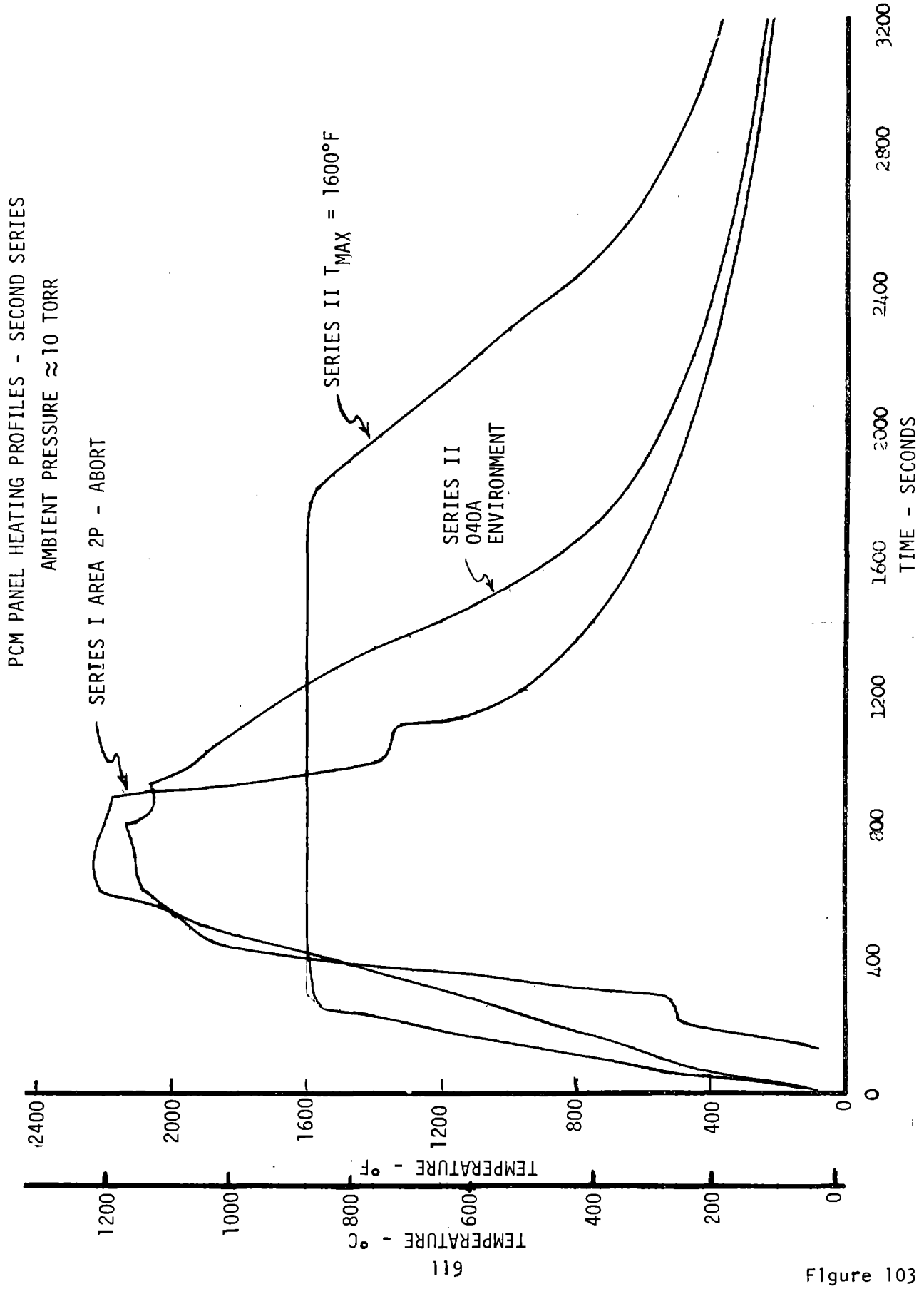
PCM PANEL HEATING PROFILES - SECOND SERIES
AMBIENT PRESSURE ≈10 TORR
SERIES I AREA 2P - ABORT
SERIES II T_{MAX} = 1600°F
SERIES II
040A
ENVIRONMENT
TIME - SECONDS
0
400
800
1200
1600
2000
2400
2800
3200
TEMPERATURE - °F
0
400
800
1200
1600
2000
2400
TEMPERATURE - °C
0
200
400
600
800
1000
1200

Figure 103

TEMPERATURE PREDICTION 040A PROFILE

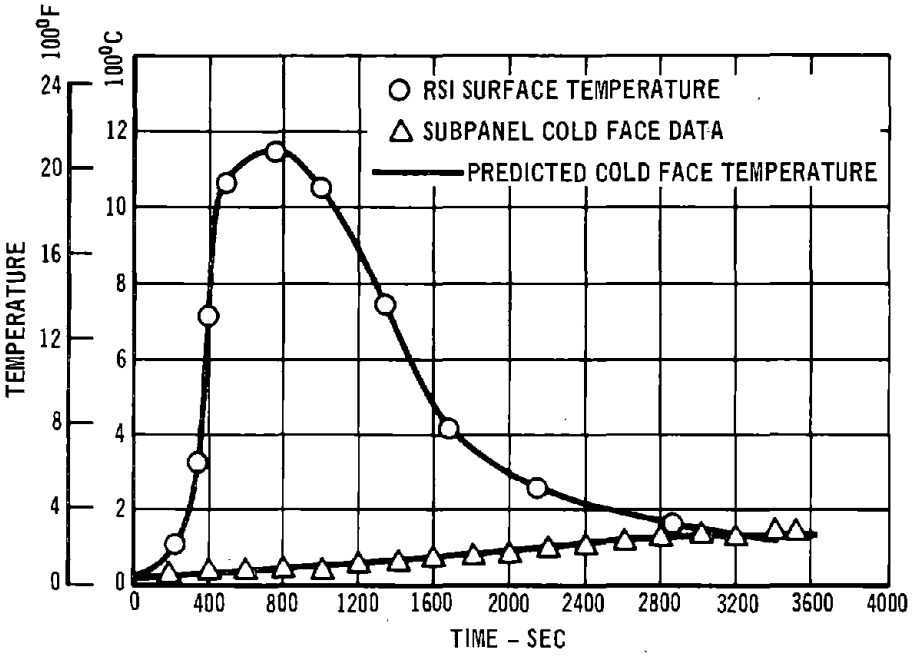

Figure 104

WEIGHT COMPARISON

(040A) Configuration and Trajectory.

MOD I MATERIAL

COMPONENT	NON PCM		PCM	
	KG/M^2	(LB/FT^2)	KG/M^2	(LB/FT^2)
RSI	21.37	(4.38)	12.20	(2.50)
COATING	2.54	(.52)	1.66	(.34)
BOND	.83	(.17)	.83	(.17)
HONEYCOMB	--	--	2.29	(.47)
PCM	--	--	3.51	(.72)
TPS TOTAL	24.74	(5.07)	20.49	(4.20)

ΔW_{SAVED} = 4.24 KG/M^2 (0.87 LB/FT^2)

MOD III MATERIAL (EXPECTED PERFORMANCE)

COMPONENT	NON PCM		PCM	
	KG/M^2	(LB/FT^2)	KG/M	(LB/FT^2)
RSI	18.0	(3.70)	11.9	(2.44)
COATING	2.4	(0.49)	1.0	(0.20)
BOND	1.8	(0.36)	0.8	(0.17)
HONEYCOMB	--	--	2.7	(0.55)
PCM	--	--	3.8	(0.77)
TPS TOTAL	22.2	(4.55)	20.1	(4.13)

ΔW_{SAVED} = 2.05 KG/M^2 (0.42 LB/FT^2)

Figure 105

6. TASK 4: HEAT PIPE APPLICATION TO LEADING EDGE AND STAGNATION POINTS

This study task was to examine the feasibility of using high temperature heat pipes for cooling nose and wing stagnation regions to permit fully reusable TPS. The study included both the orbiter and the booster of the fully reusable Phase B configuration.

The initial analysis indicated that the booster applications showed little promise. With a staging velocity of about 2.35 km/sec (7000 ft/sec) a reusable metallic leading edge was found adequate. At higher staging velocities, approximately 5.7 km/sec (15,000 ft/sec) the high heating rates coincided with high axial acceleration. The acceleration produced an adverse pressure which reduced the pumping capability of the heat pipe wick. Consequently operation of the heat pipe was marginal and the design would be much heavier than other available TPS. Because the booster application showed little potential the study effort concentrated on orbiter applications.

The orbiter applications were found initially to be feasible with respect to the heating and acceleration environments. Subsequent design work revealed, however, that the nose cap application was unlikely to prove successful. The three dimensional shape of the nose cap yielded a small highly heated region which would require intersecting heat pipes. In addition the nose cap heating rates were sufficiently high that cascaded heat pipes would be required. This dual complexity yielded a required configuration virtually impossible to construct and service with working fluid. The wing leading edge segment was found to be amenable to a much simpler design. Cascading was not required and the shape was essentially two-dimensional, permitting an assembly of conventional high temperature heat pipes. The leading edge design was developed in detail and is presented in this report. In addition several alternate TPS (ablative, carbon-carbon, columbium) designs were explored for comparison with the heat pipe leading edge. The heat pipe version was found to be somewhat heavier than the alternate candidates but much less expensive than the baseline ablative version on the basis of total program costs.

6.1 Configuration/Environment - Complete sets of ascent and entry trajectory data were developed for both the orbiter and booster and documented in Reference 3. Only orbiter related data is presented in this report, however, since recent redirection of the Shuttle Program has redefined the booster design and requirements and because the study results indicated little potential for the booster applications.

The orbiter ascent and entry stagnation heating rates and the resultant radiation equilibrium temperatures are given in Figures 106 through 109. These curves correspond with Phase B baseline trajectories but the entry heating rates include a heating rate multiplier of 1.37. Although MDAC-E Phase B analyses indicate temperatures below 1650°K (2500°F) for the wing leading edge, designs by Grumman (Reference 20) and North American Rockwell (Reference 21) indicate higher temperatures, above the columbium reuse temperature limit. Therefore, the heating multiplier was applied to yield a peak temperature in excess of the columbium reuse temperature limit. Both heating rates (with and without the multiplier) were used in performing the analysis for the orbiter applications, resulting in two designs corresponding to the different heating rates. The final results from the Shuttle Program Phase B study indicated that the lower rate better represented expected flight conditions. Load factors for orbiter launch and reentry are given in Figures 110 and 111. The relationship between g-loads and heating rates is important in the design of the system and is discussed further in Sections 6.2 and 6.3. In Figures 112, 113, and 114, heating profiles are shown for the nose cap and a representative section of the wing leading edge. Figures 112 and 113 were determined with the methods of References 22 and 23. The nonzero angle-of-attack curves of Figure 115 are based on test data used in the Phase B TPS analtyical effort; the zero angle-of-attack curve was determined by analytical methods.

These figures provide all the data required to specify thermal performance requirements for the heat pipes. To perform the structural analysis, additional trajectory data are required,in particular, pressure distribution and the relationship between temperature and pressure as a function of time. The values used in this program are given in Figures 115 through 118, and are based on the Phase B Study results.

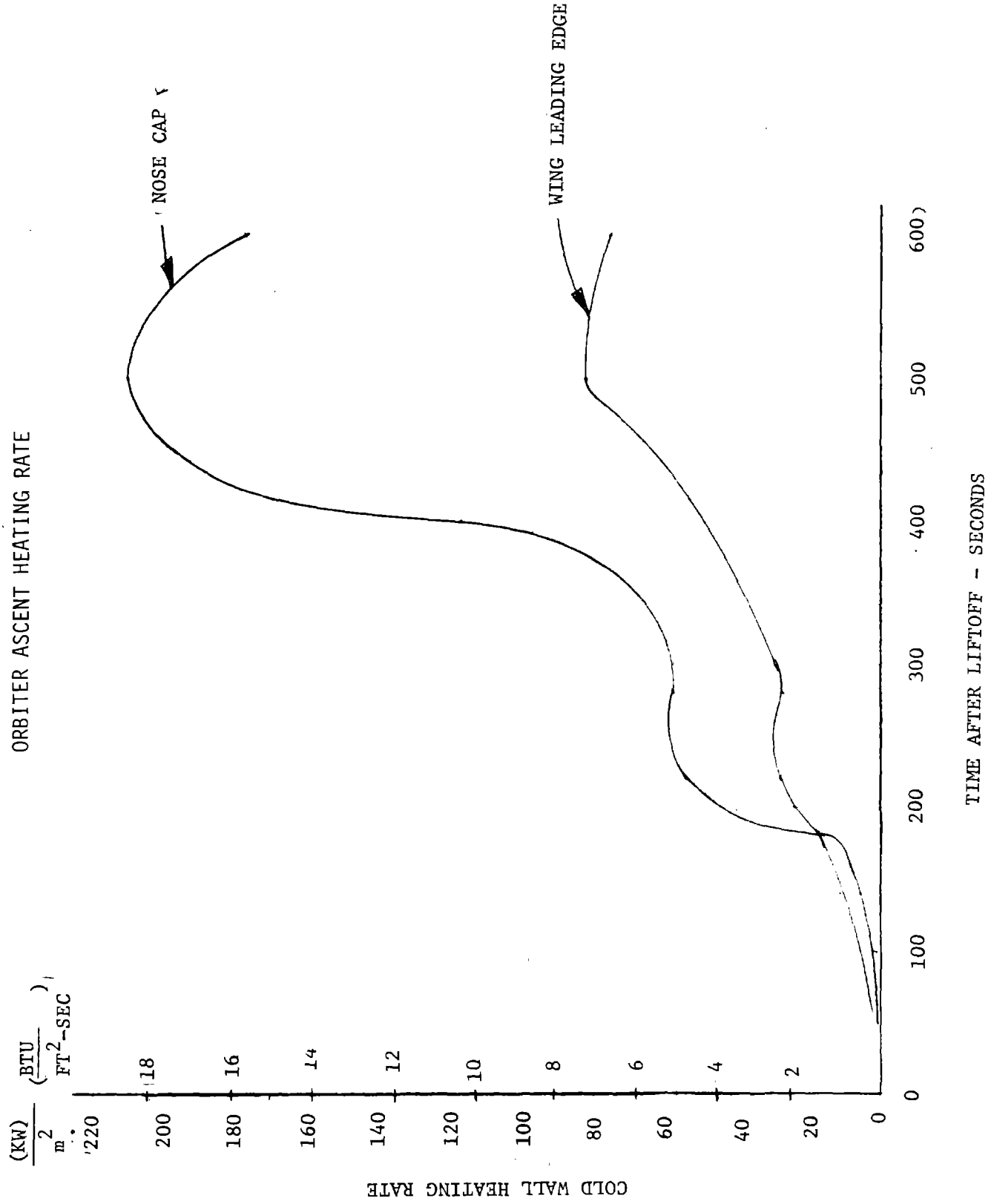
ORBITER ASCENT HEATING RATE
COLD WALL HEATING RATE
(KW)/m² (BTU/FT²-SEC)
220
200
180
160
140
120
100
80
60
40
20
0
18
16
14
12
10
8
6
4
2
0
100
200
300
400
500
600
TIME AFTER LIFTOFF - SECONDS
NOSE CAP
WING LEADING EDGE

Figure 106

ORBITER ASCENT TEMPERATURES

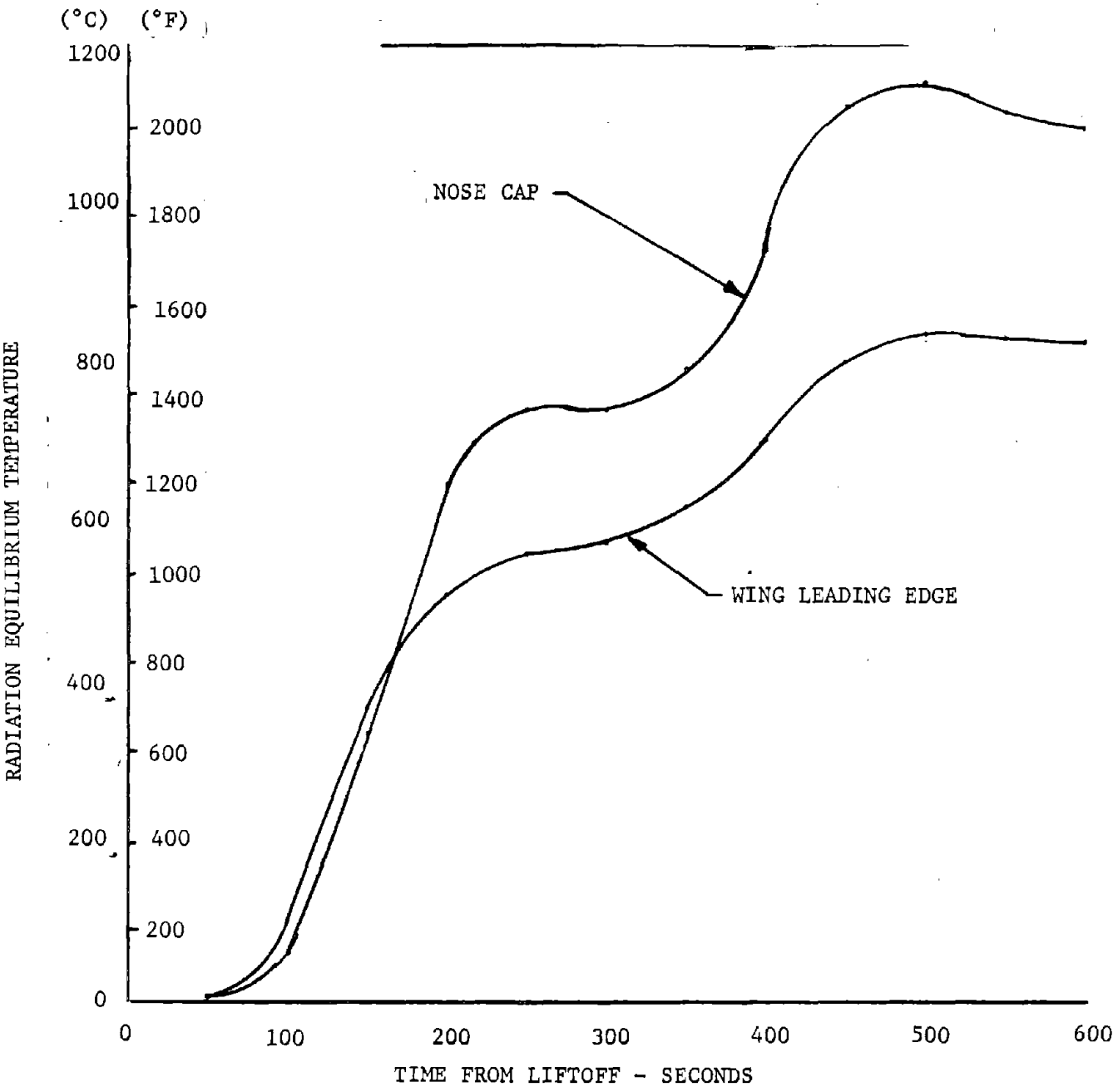

Figure 107

ORBITER ENTRY HEATING RATE

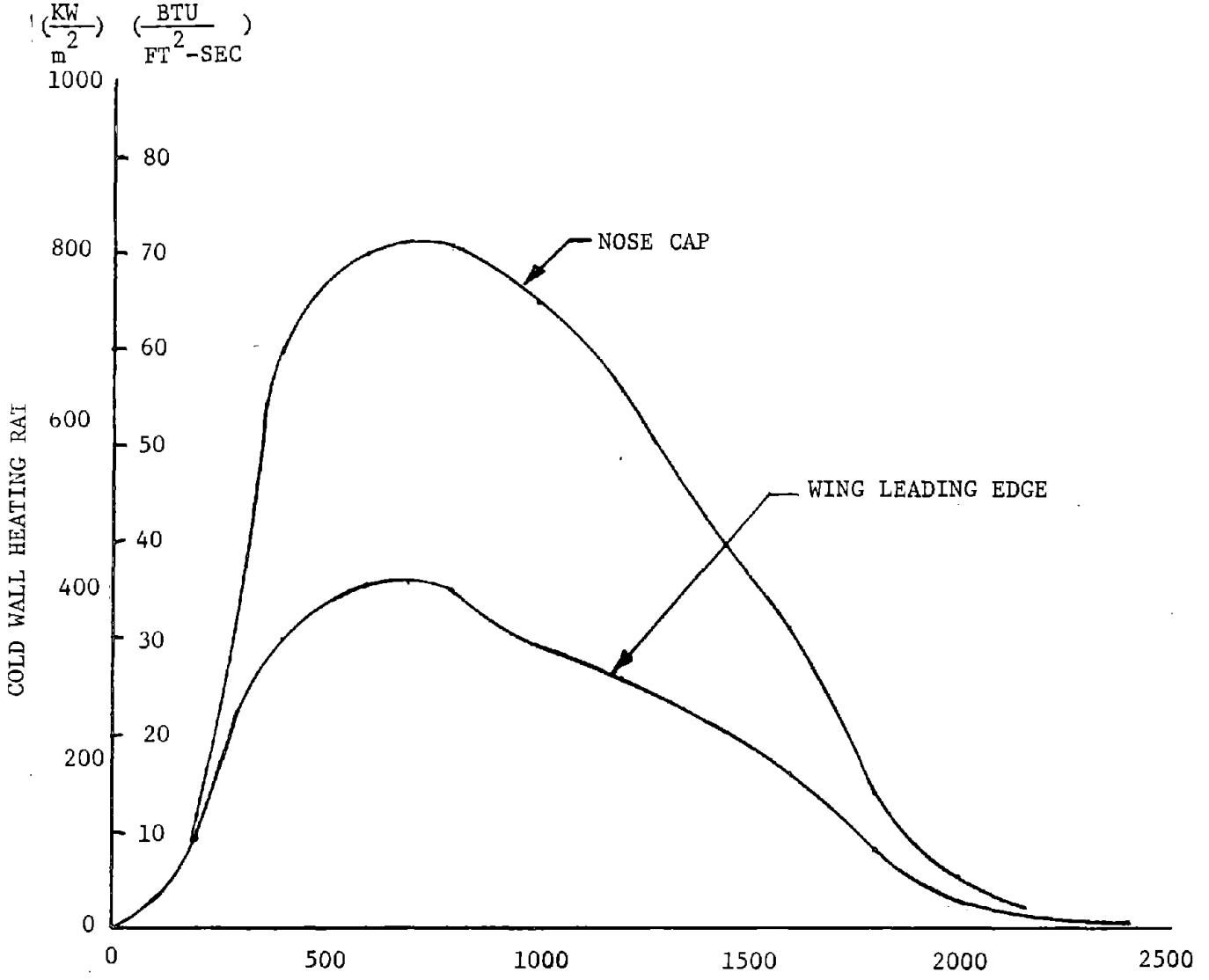

Figure 108

ORBITER ENTRY TEMPERATURES

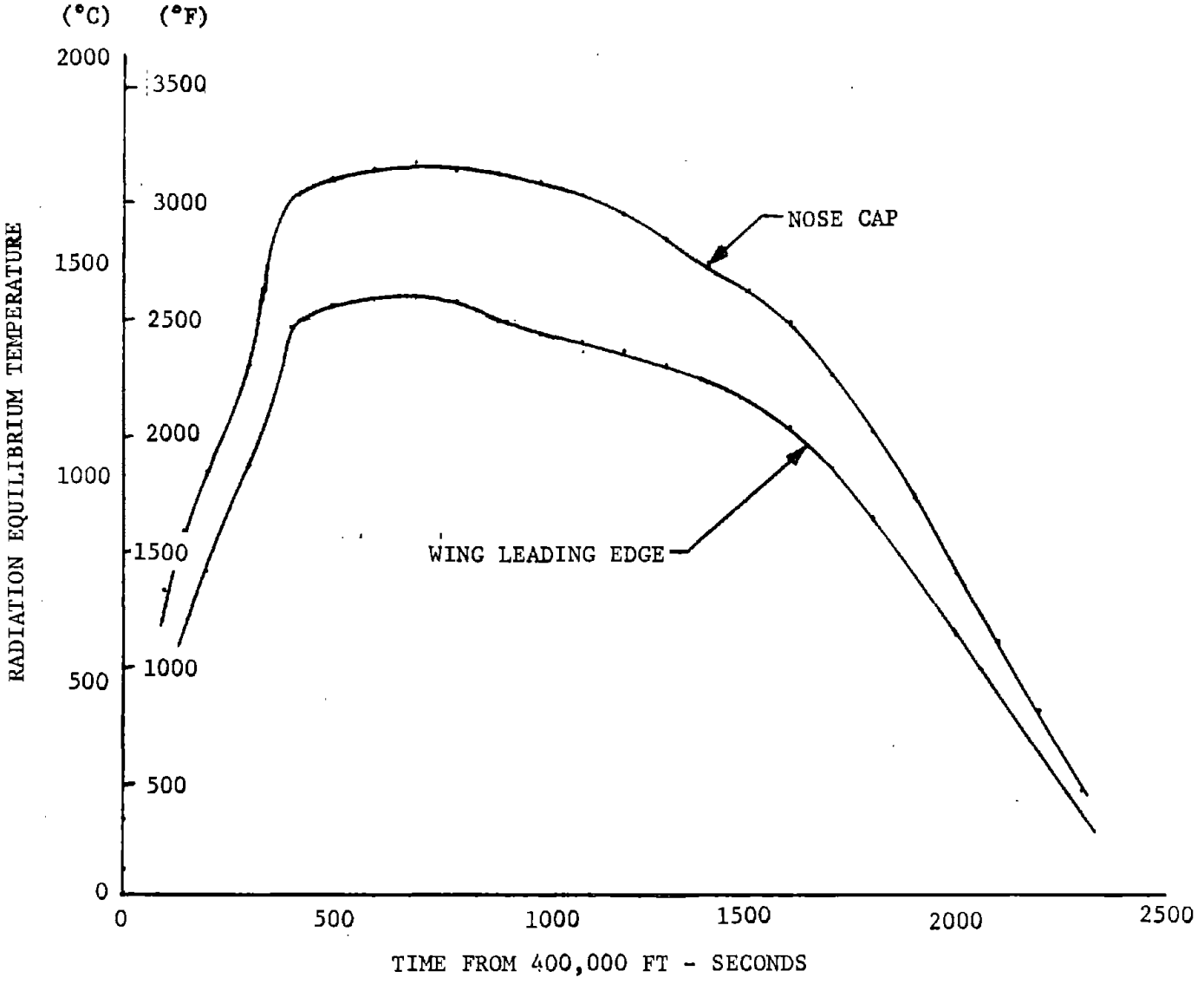

Figure 109

BOOSTER AND ORBITER ASCENT AXIAL LOAD FACTOR

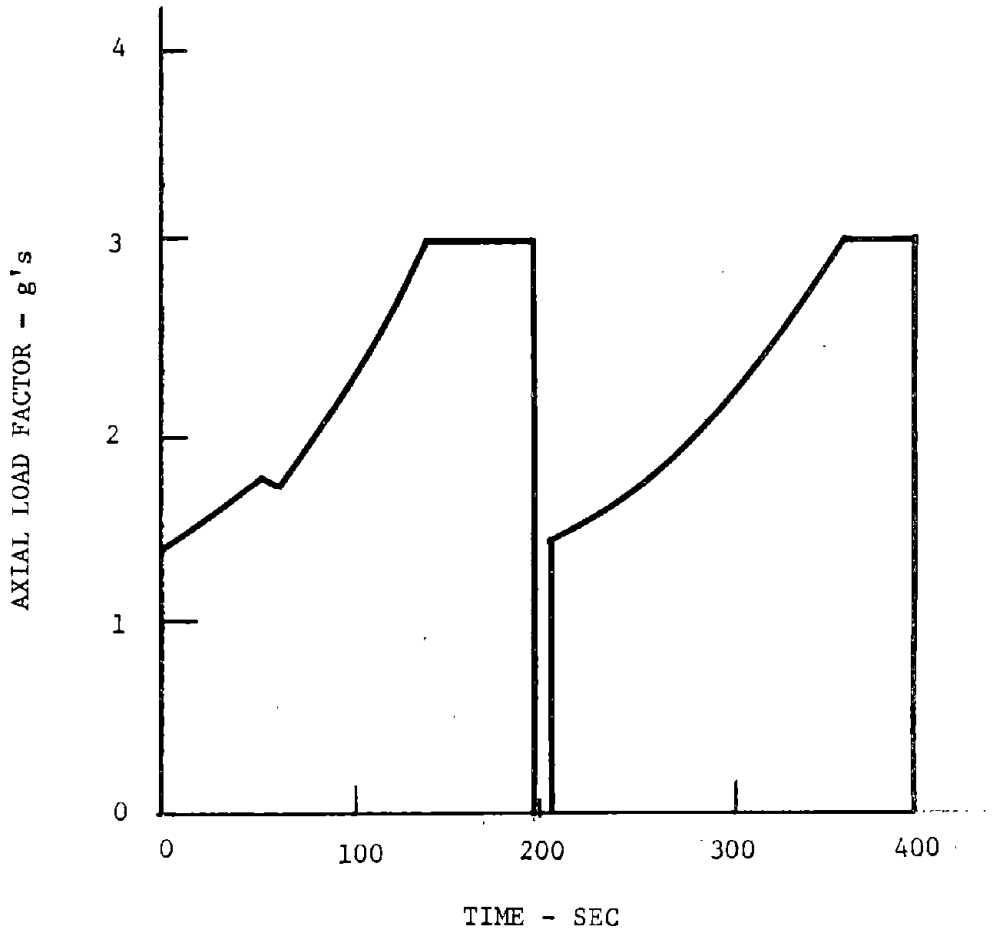

Figure 110

ORBITER ENTRY LOAD FACTOR

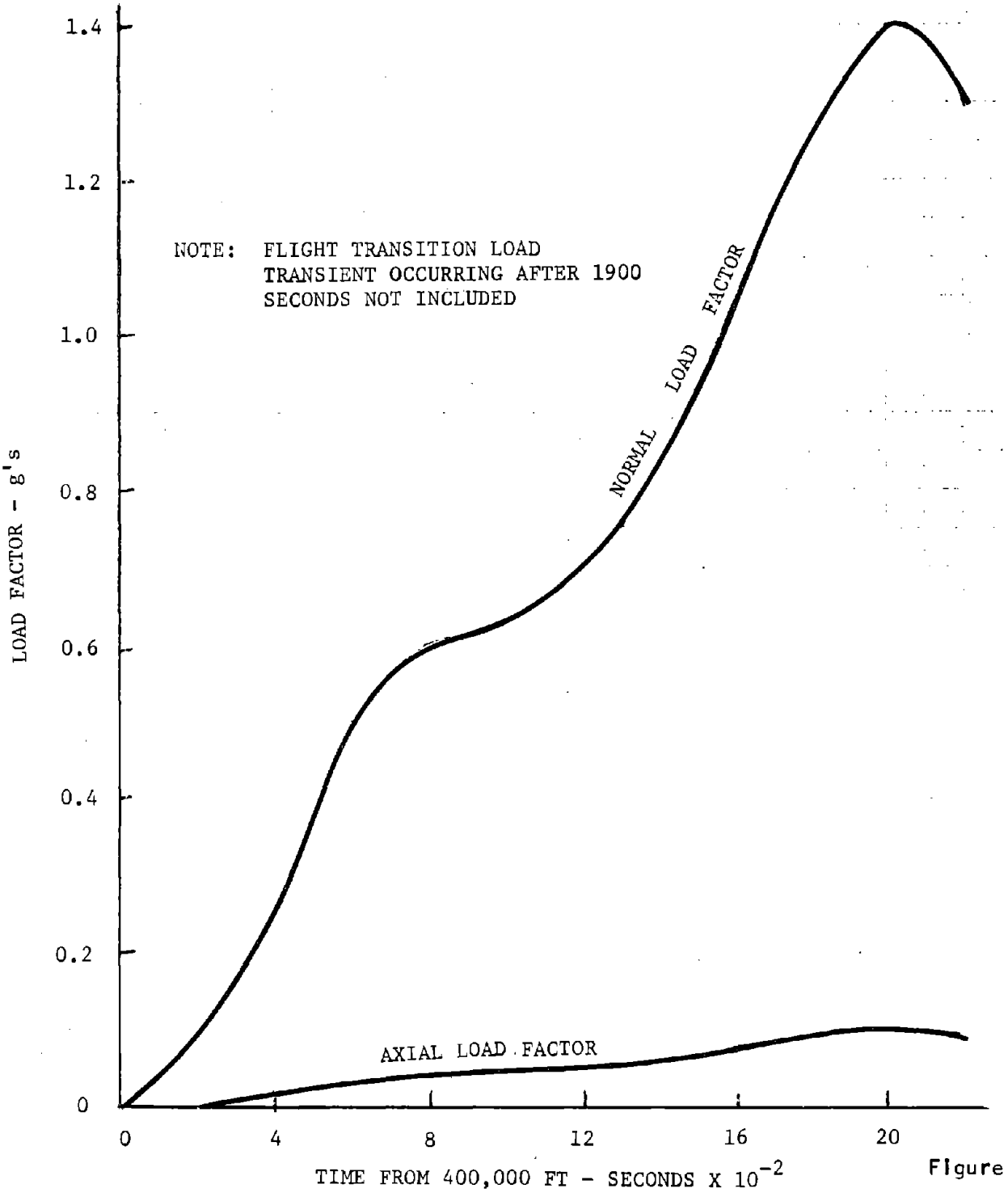

Figure 111

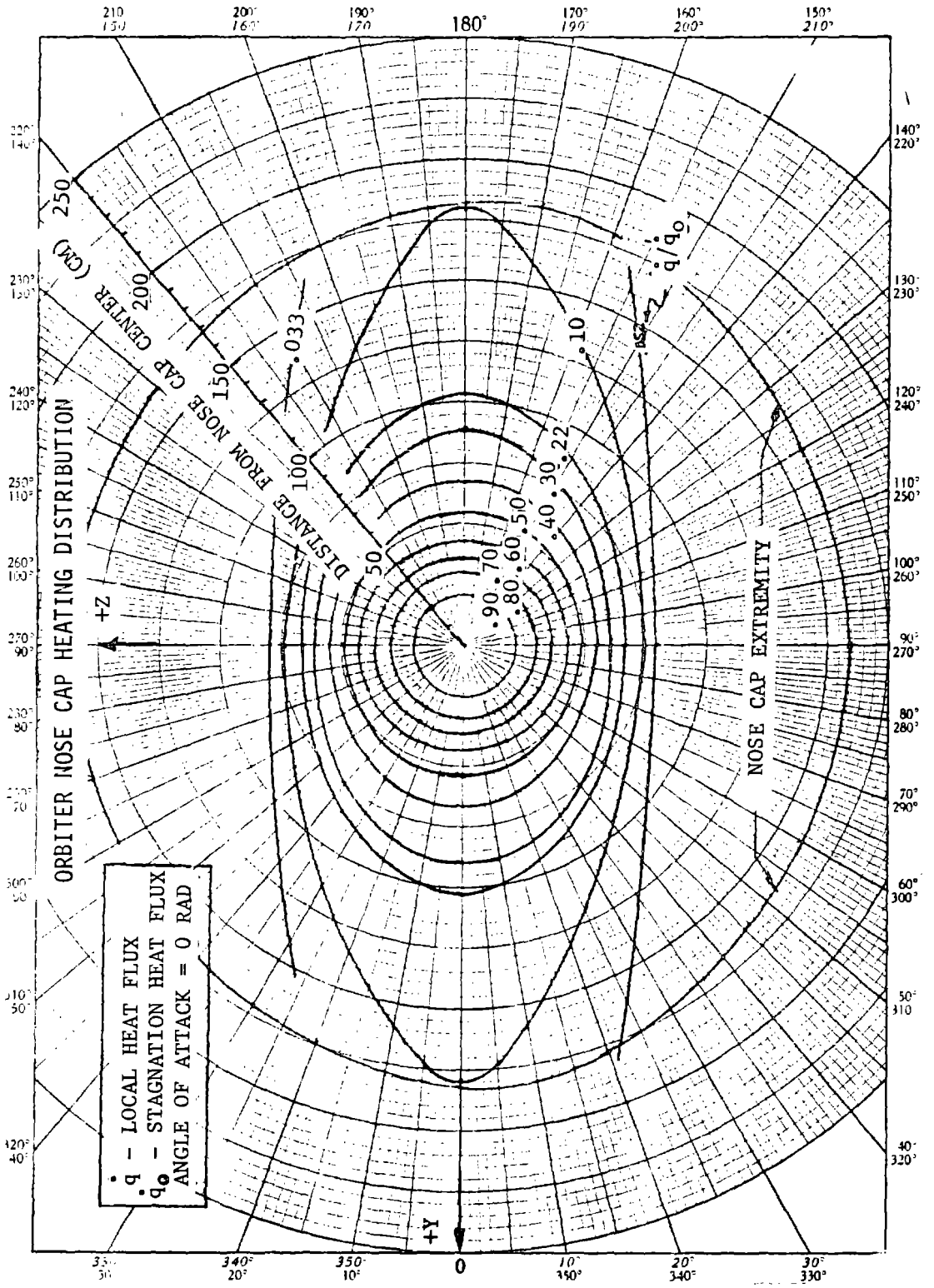
ORBITER NOSE CAP HEATING DISTRIBUTION
DISTANCE FROM NOSE CAP CENTER (CM)
250
200
150
100
50
.033
.10
.22
.30
.40
.50
.60
.70
.80
.90
$\dot{q}/\dot{q}_o$
NOSE CAP EXTREMITY
+Z
+Y
0
180°
$\dot{q}$ - LOCAL HEAT FLUX
$\dot{q}_o$ - STAGNATION HEAT FLUX
ANGLE OF ATTACK = 0 RAD

Figure 112

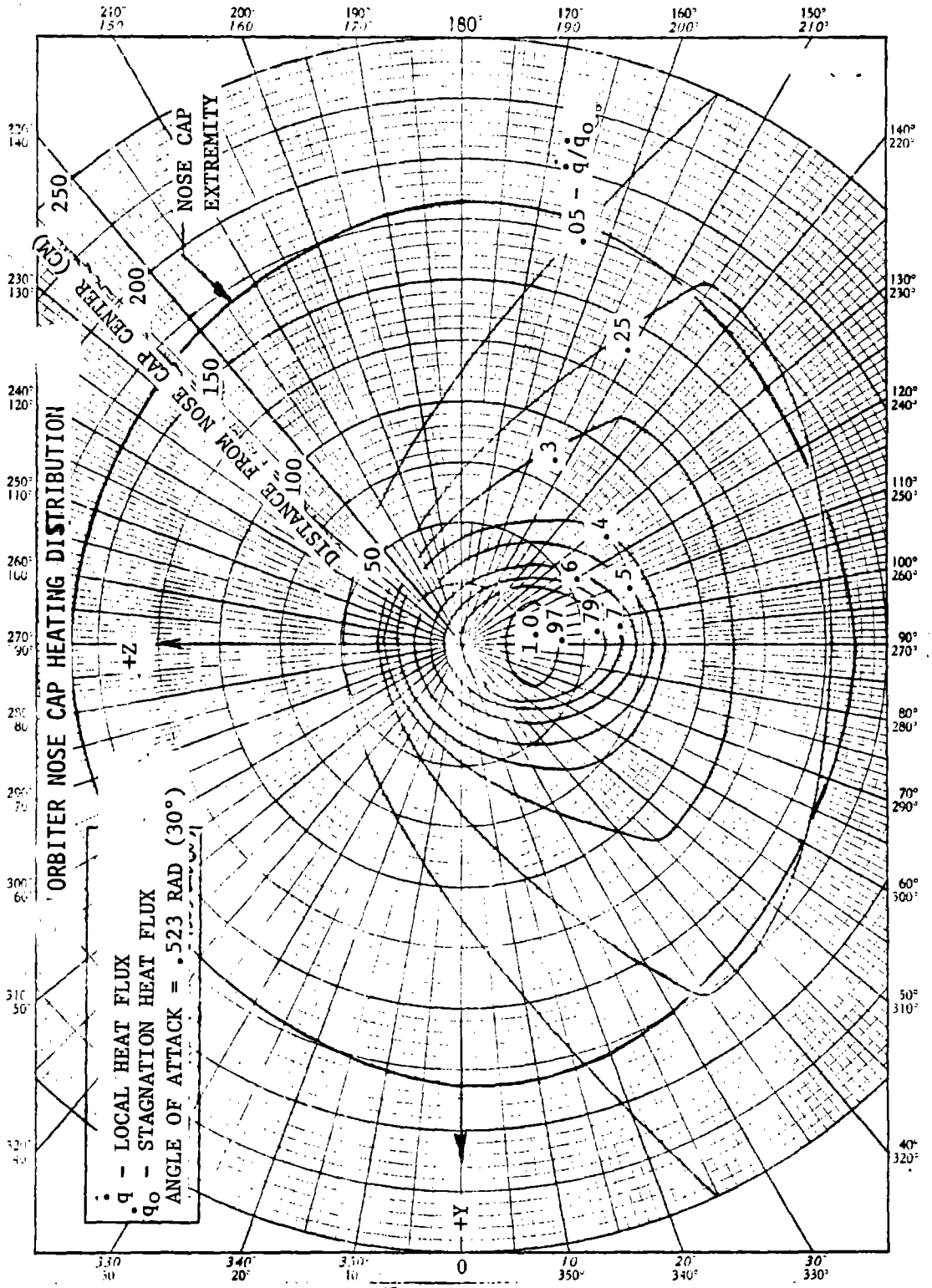
ORBITER NOSE CAP HEATING DISTRIBUTION
$\dot{q}$ - LOCAL HEAT FLUX
$\dot{q}_o$ - STAGNATION HEAT FLUX
ANGLE OF ATTACK = .523 RAD (30°)
DISTANCE FROM NOSE CAP CENTER (CM)
250
200
150
100
50
NOSE CAP EXTREMITY
$\dot{q}/\dot{q}_o$ = .05
.25
.3
.4
.6
.79
.97
1.0
.7
.5
+Z
+Y
0
180°

Figure 113

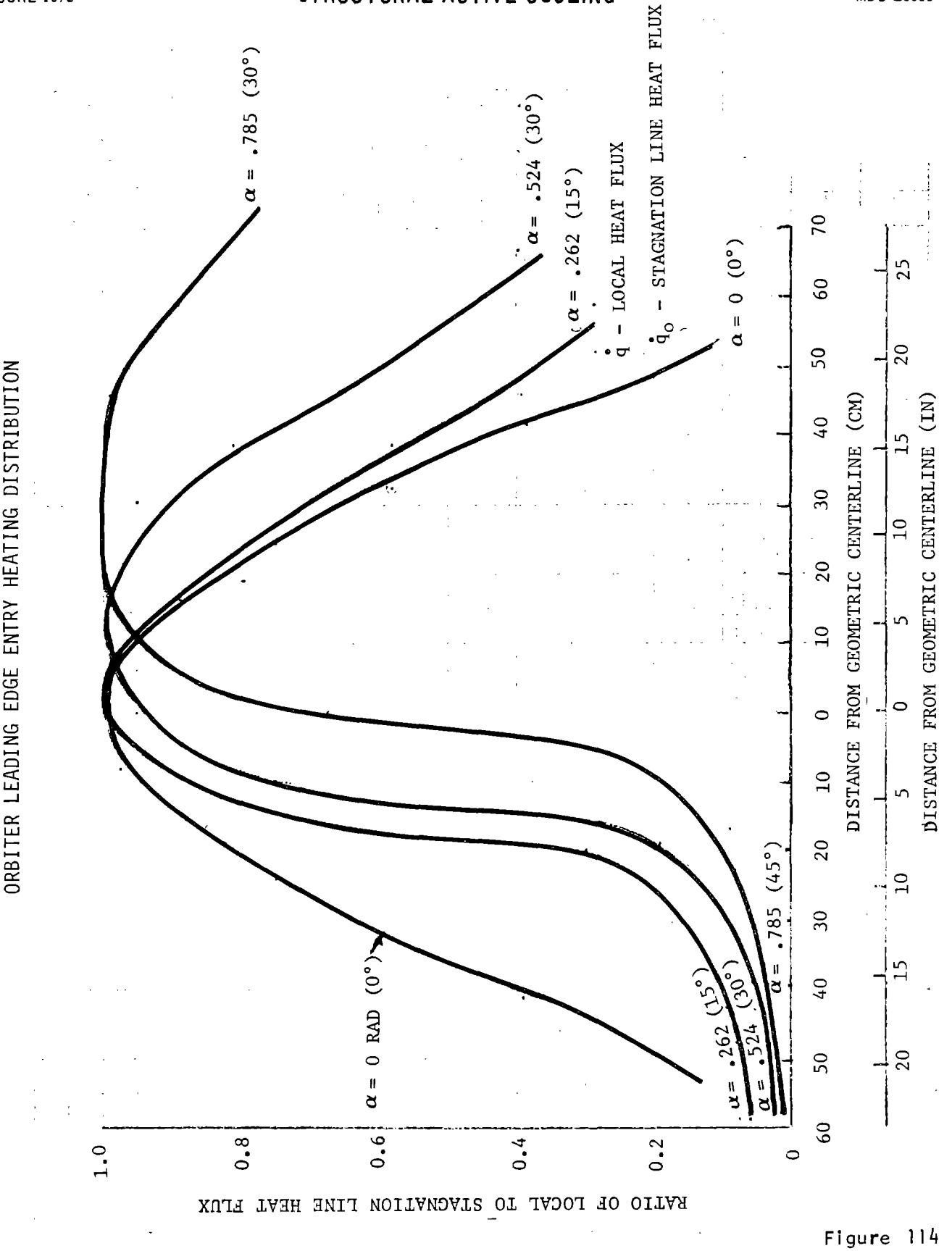
ORBITER LEADING EDGE ENTRY HEATING DISTRIBUTION
$\dot{q}$ - LOCAL HEAT FLUX
$\dot{q}_o$ - STAGNATION LINE HEAT FLUX
RATIO OF LOCAL TO STAGNATION LINE HEAT FLUX
1.0
0.8
0.6
0.4
0.2
0
α = .785 (30°)
α = .524 (30°)
α = .262 (15°)
α = 0 (0°)
α = 0 RAD (0°)
α = .262 (15°)
α = .524 (30°)
α = .785 (45°)
60 50 40 30 20 10 0 10 20 30 40 50 60 70
DISTANCE FROM GEOMETRIC CENTERLINE (CM)
20 15 10 5 0 5 10 15 20 25
DISTANCE FROM GEOMETRIC CENTERLINE (IN)

Figure 114

LEADING EDGE PRESSURE DISTRIBUTION

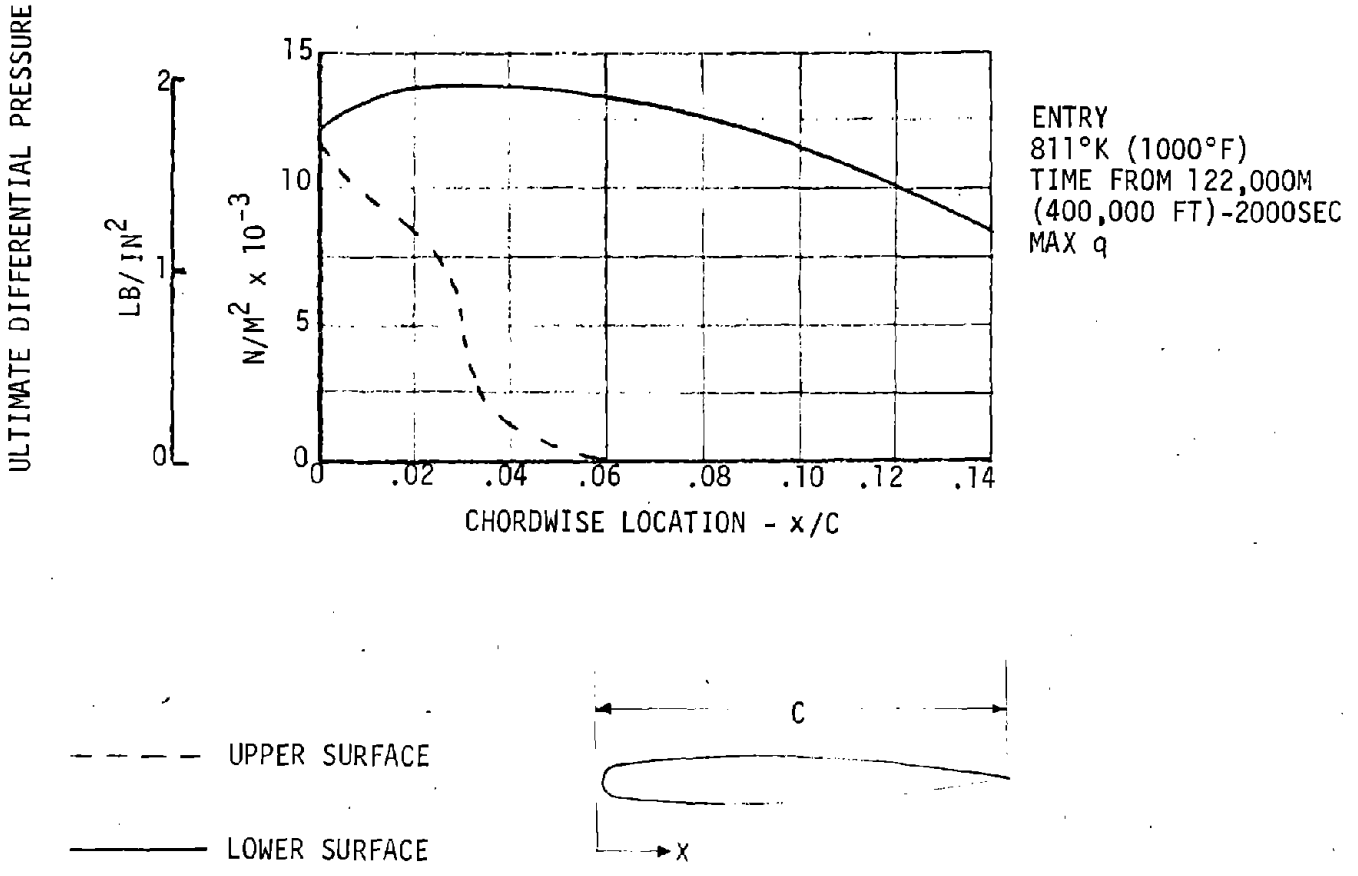

NOTE: POSITIVE PRESSURES ARE COLLAPSING
NEGATIVE PRESSURES ARE BURSTING

Figure 115

LEADING EDGE PRESSURE DISTRIBUTION

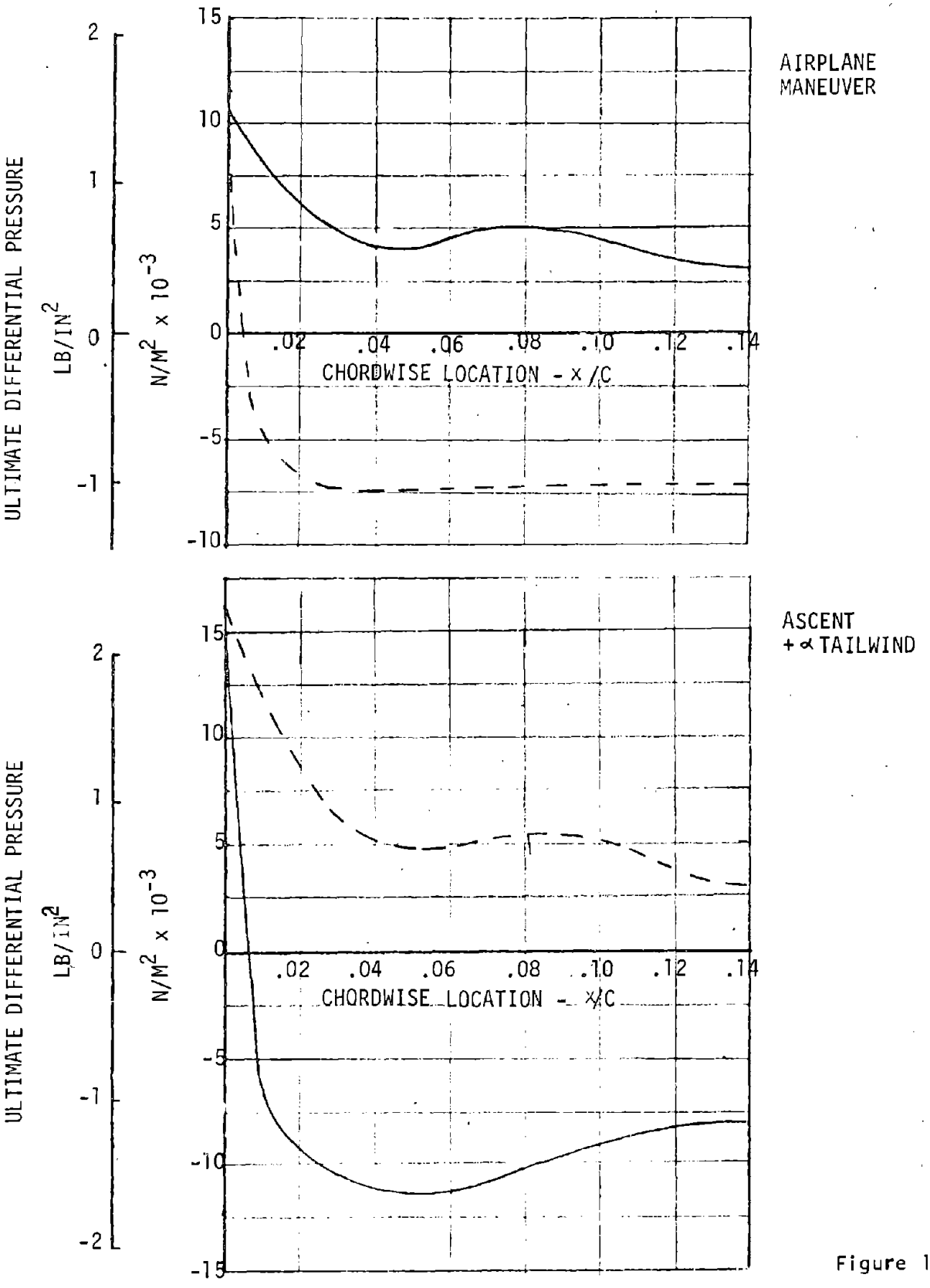

Figure 116

LEADING EDGE PRESSURE DISTRIBUTION

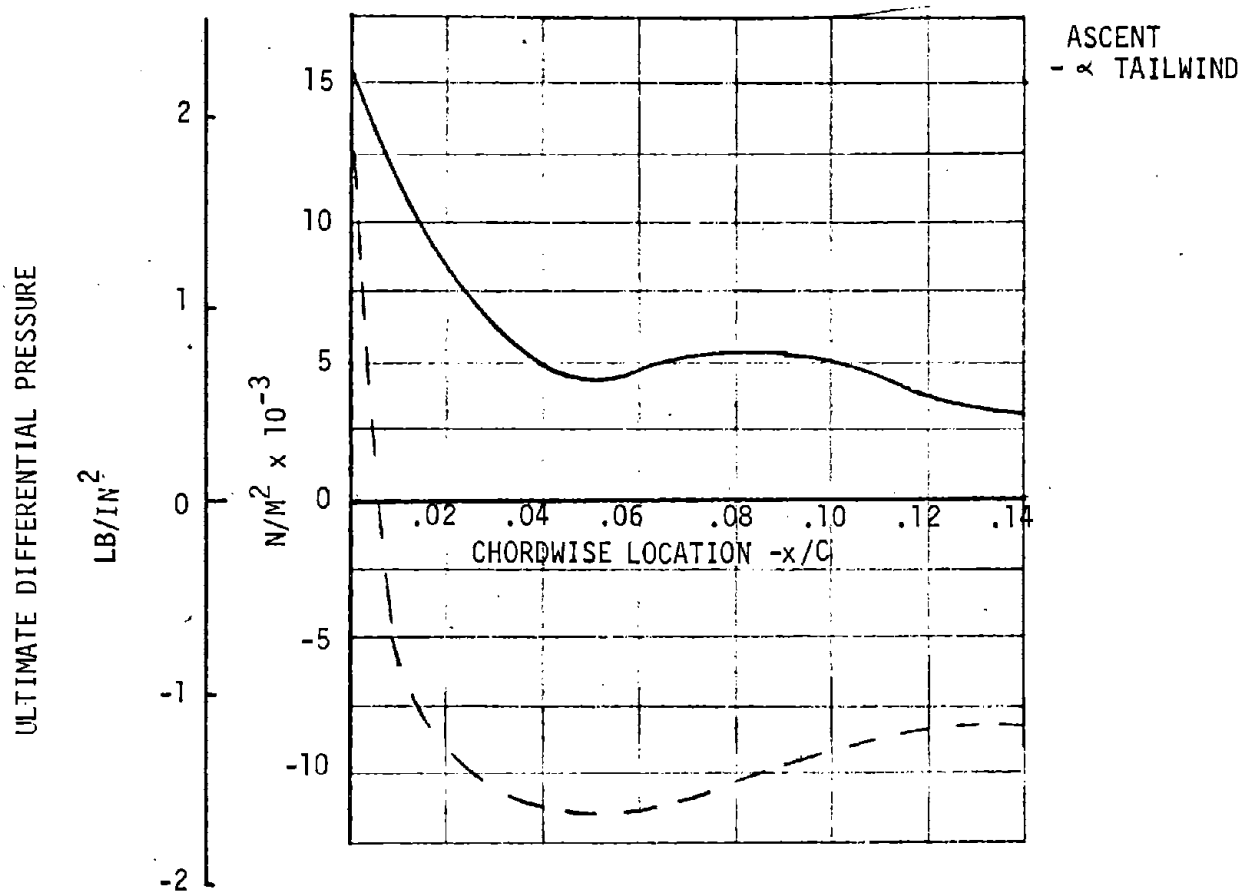

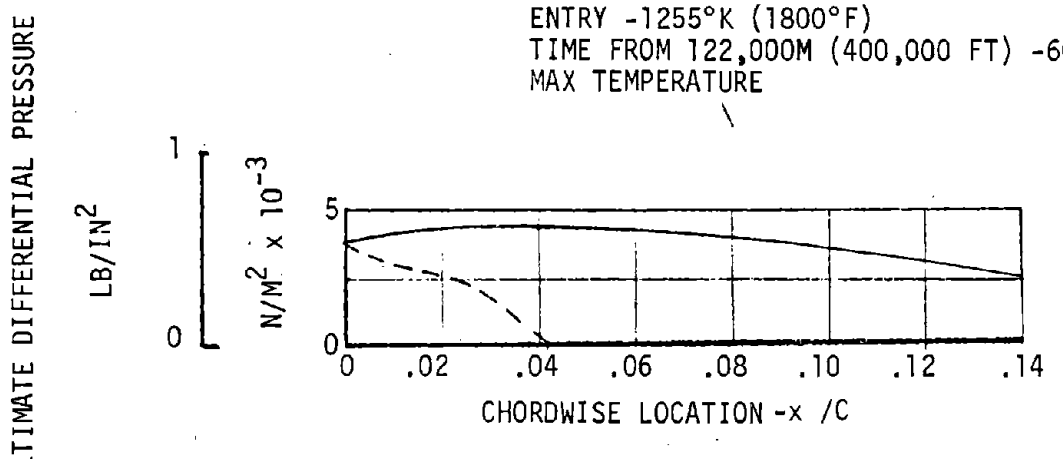

Figure 117

DESIGN ENTRY DYNAMIC PRESSURE AND SURFACE TEMPERATURE

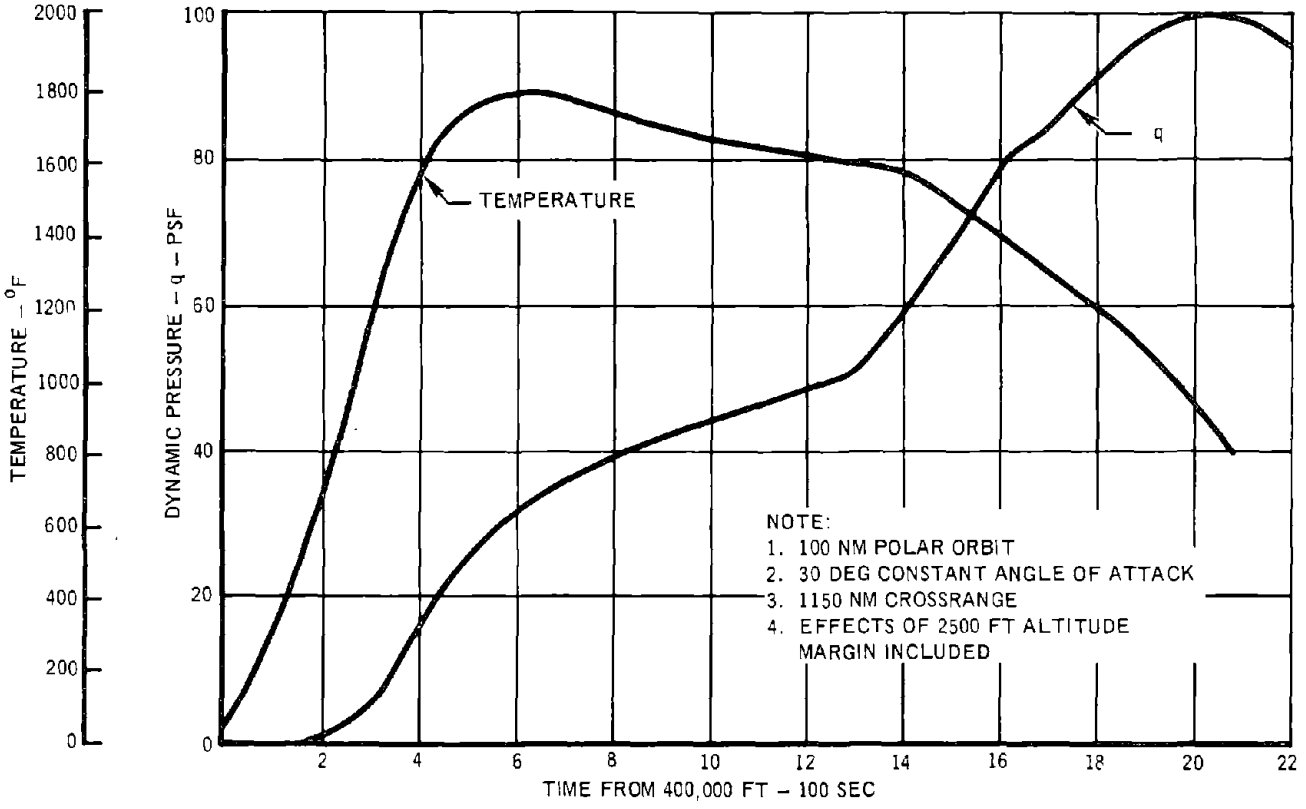

Figure 118

6.2 Heat Pipe Design

6.2.1 Fluid Dynamic Model/Analysis - Basic elements and operational characteristics of a heat pipe are shown in Figure 119. Heat is absorbed in the evaporator region of the heat pipe causing a phase change in the working fluid from liquid to vapor. Vapor flows from the evaporator to the cooler condenser regions where the process is reversed. Return of the liquid from the condenser to the evaporator by a capillary pumping medium completes the cycle. The system consists of three elements, (1) a tube or container, (2) a working fluid, and (3) a liquid return mechanism. Design of each element is discussed in the following sections.

Performance of the system is governed by the phenomenon which limit the liquid and vapor flow within the systems. Four limiting conditions on maximum heat flux are shown in Figure 120. At low temperatures, vapor flow considerations tend to limit performance. Vapor density is low and with the high velocities required to transfer large quantities of heat, choking of the flow could occur, and to a lesser degree, stripping of the liquid from the wall (entrainment) could limit performance.

The equations used to predict sonic and entrainment limits for this model are as follows:

Sonic Limit $$\dot{m}_{MAX} = A_v \rho_v \sqrt{\frac{RTg_c \gamma}{2M(\gamma + 1)}} \quad (1)$$

Entrainment Limit $$\dot{m}_{MAX} = A_v \sqrt{\frac{\rho_v \sigma g_c}{2r_c}} \quad (2)$$

At low temperatures, the sonic limit may be reached without causing a failure, only an increase in temperature. Burnout will not occur, providing startup conditions are such that the operating points move to the right of the sonic limit curve prior to intersection of one of the other limiting curves.

Entrainment of the liquid in the vapor flow is, in general, only a problem when open groove type wicking systems are employed and the operating conditions result in high vapor velocities. Entrainment was not a factor in this application.

At higher temperatures, wicking limits govern performance. Equations used here are based on Cotter's theory.

$$\Delta P_L + \Delta P_v + \Delta P_g \leq \Delta P_c \quad (3)$$

$$\Delta P_L = \frac{1}{K_\rho A_w} \frac{\mu_L}{\rho_L} \int \dot{m}\,(x)\, dx \quad (4)$$

BASIC HEAT PIPE OPERATION

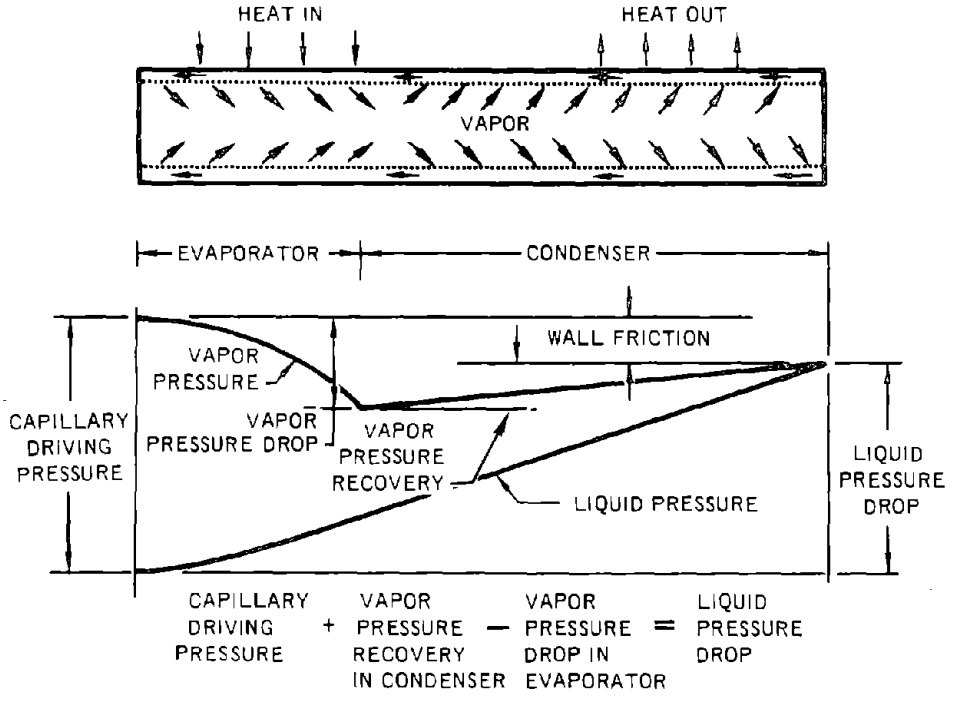

Figure 119

HEAT PIPE LIMITATIONS

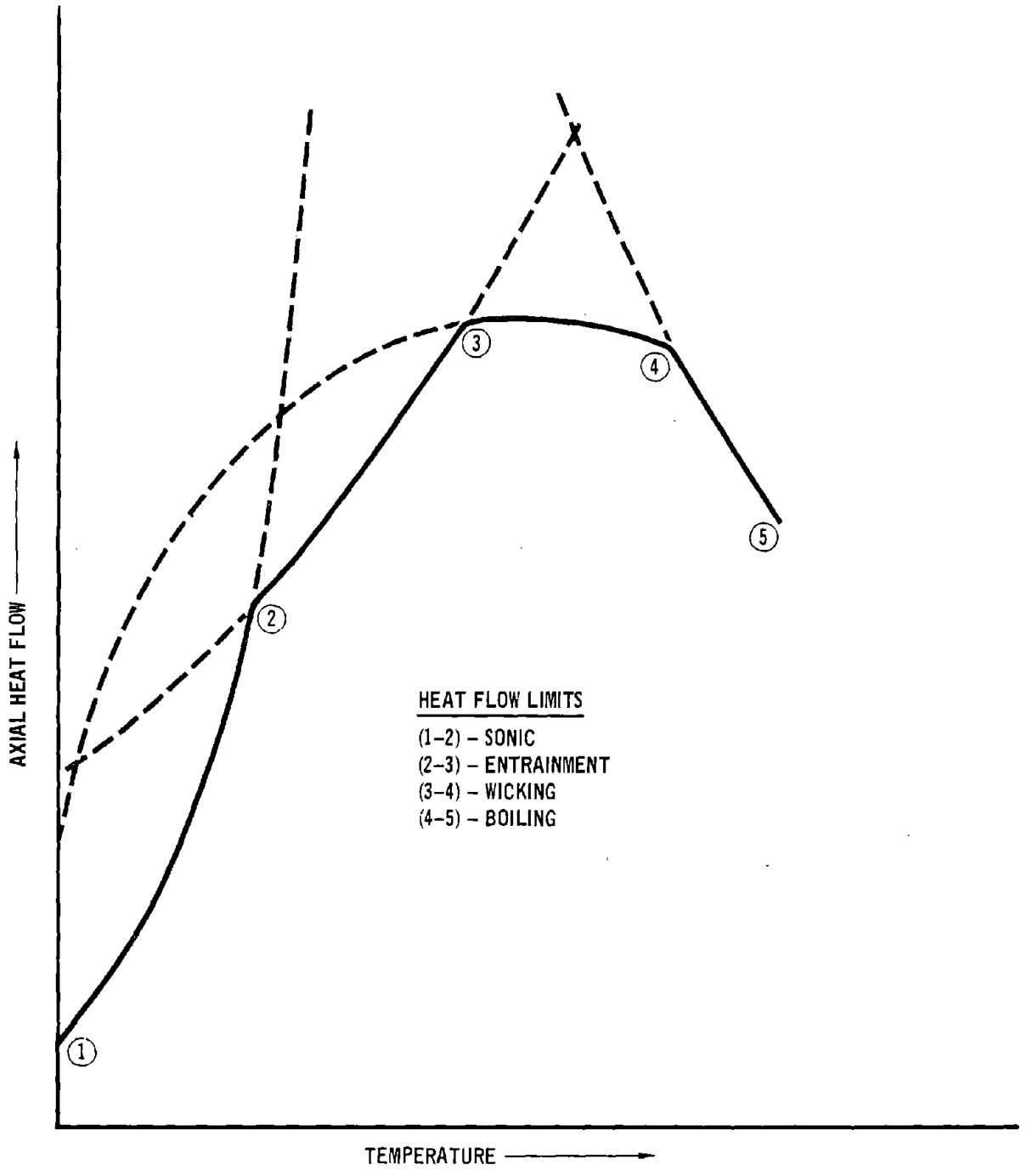

Figure 120

$$\Delta P_v = \frac{8}{A_v r_v^2} \frac{\mu_v}{\rho_v} \int \dot{m}(x)dx \quad (5)$$

$$\Delta P_g = \frac{\rho_L}{g_c} \int g(x)dx \quad (6)$$

$$\Delta P_c = \frac{2\sigma}{r_c} \quad (7)$$

Very high local fluxes can cause nucleate boiling in the system. To predict this limit, the following equation was used:

$$\left(\frac{Q}{A}\right)_{MAX} = \frac{2RK_{eff}\sigma T^2}{t_w Y_B \rho_v M h_{fg}} \quad (8)$$

The procedure used in analyzing the data involved the following steps.

1. Calculate operating temperature, T_1, from

$$\left(T_1\right)^4 = \left[\frac{q_o}{\tau\varepsilon}\left(\frac{\bar{q}}{q_o}\right)\right] \quad (9)$$

where $\frac{\bar{q}}{q_o}$ is obtained by integrating q/q_o, Figure 122 , and dividing by the length over which the integration is performed.

2. Calculate

$$\dot{m}(x) = \frac{\ell q_o}{h_{fg}} \int \frac{q(x)}{q_o} dx \quad (10)$$

and check to see that $\dot{m}(x) \leq \dot{m}_{MAX}$ calculated from equations (1) and (2).

3. Calculate

$$\int \dot{m}(x)dx = \frac{\ell q_o}{h_{fg}} \iint \frac{q(x)}{q_o} dxdx \quad (11)$$

and use along with g-loads (Figures 111 and 112) in equations (3) through (7) for wick design.

4. Check to insure that local values of $q_o\left(\frac{q(x)}{q_o}\right)$ are less than $(Q/A)_{MAX}$ from equation (8).

Operation of the system must be checked from launch to landing to insure acceptable performance through the entire trajectory.

The temperature response of the orbiter heat pipe leading edge to the Phase B launch, coast and entry heating environment is shown in Figure 122. The results

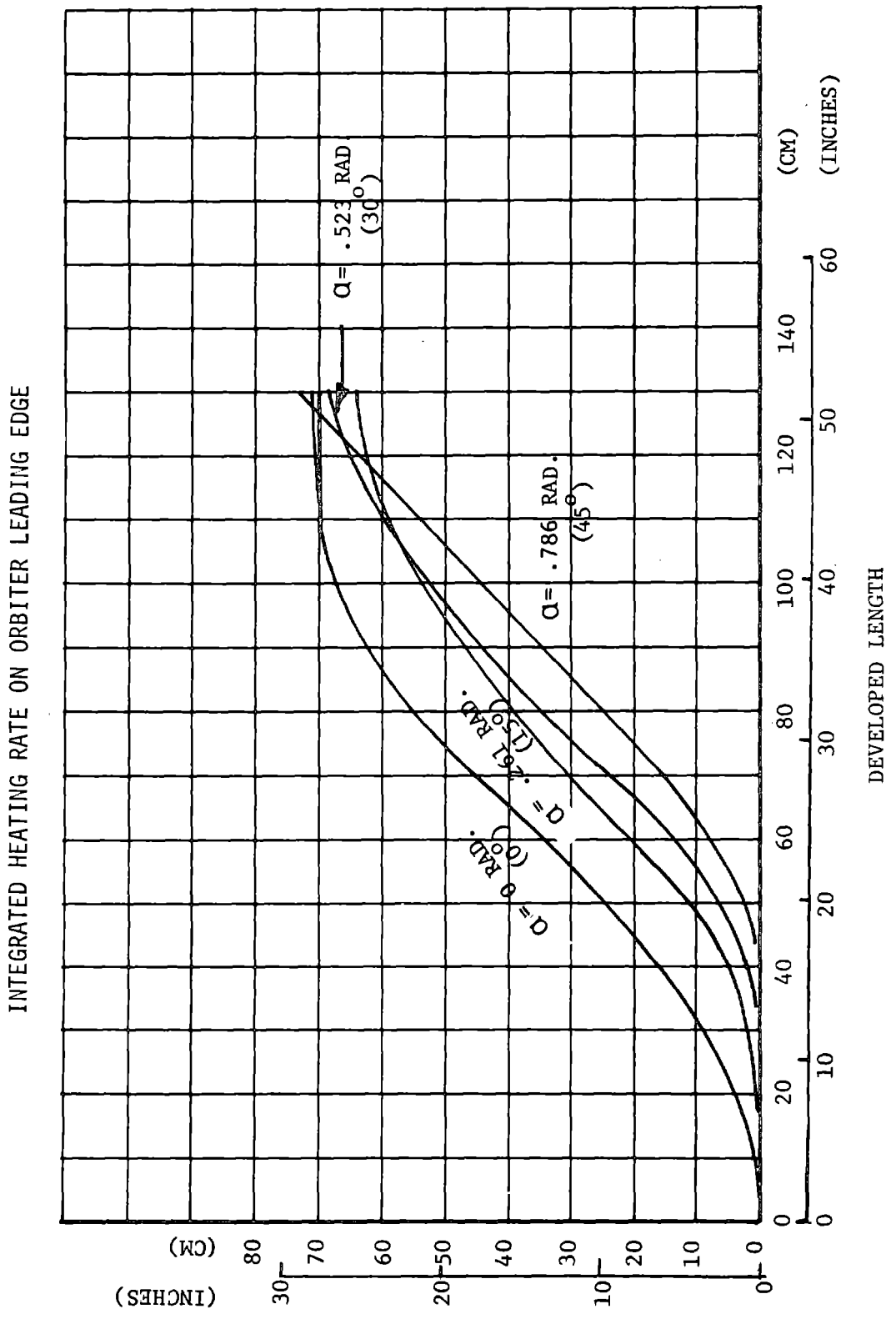
INTEGRATED HEATING RATE ON ORBITER LEADING EDGE
$\int q/q_{xp}$
(INCHES)
(CM)
0
10
20
30
40
50
60
70
80
0
20
10
40
20
60
30
80
40
100
120
140
50
60
DEVELOPED LENGTH
(INCHES)
(CM)
Q = .523 RAD (30°)
Q = .786 RAD. (45°)
Q = 0 RAD. (0°)
Q = .785 RAD. (45°)

Figure 121

HEAT PIPE LEADING EDGE TEMPERATURE

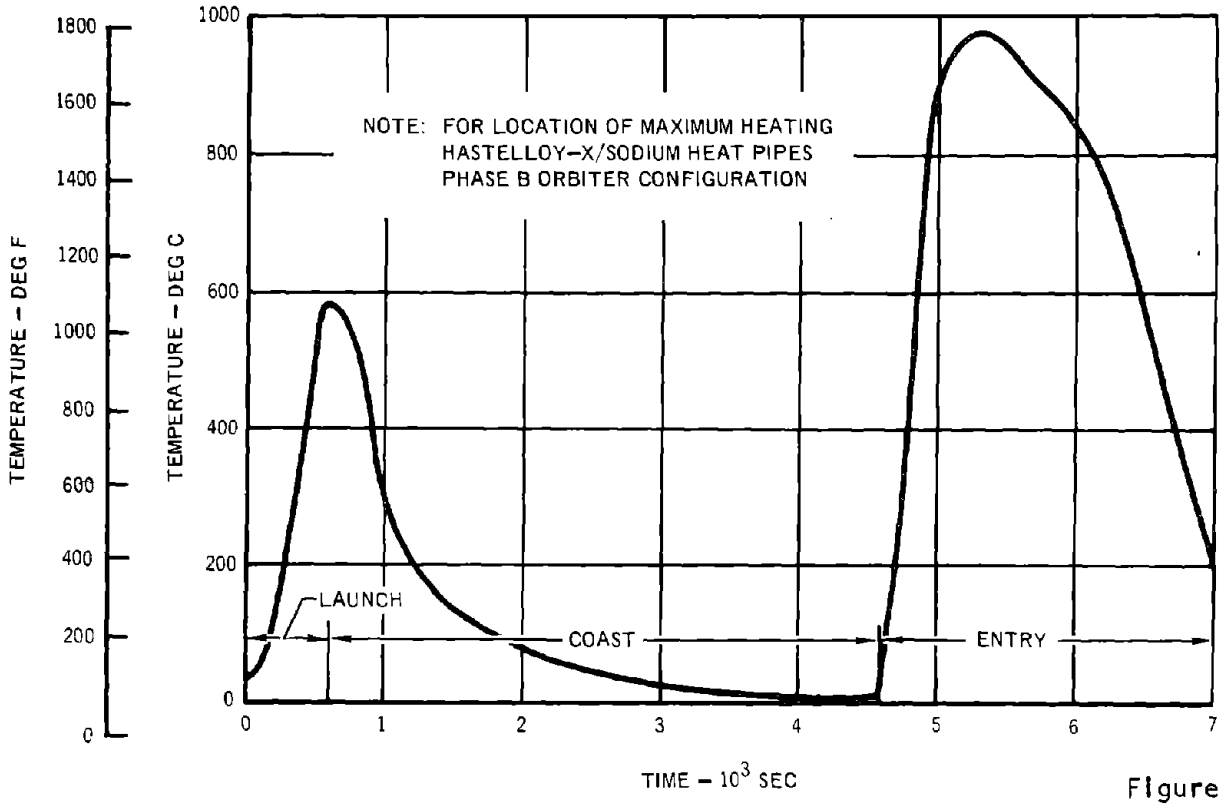

Figure 122

show the temperature history of a point on the leading edge experiencing maximum temperature of the entire heat pipe leading edge. This local maximum temperature occurs along the stagnation line on the skin midway between adjacent pipe centers. The analysis was conducted simulating a single orbit abort from a polar orbit. The launch heating was extended to include free molecular heating during the coast to high altitude after orbital injection. An approximate coast trajectory was used as the basis for the free molecular heating calculations. The resulting heating profile constructed for these conditions was shown previously in Reference 5.

A description of the performance characteristics of the heat pipe for all flight phases is shown schematically in Figure 123. During launch, the heat pipe operates in degraded mode due to adverse launch "g". During coast to apogee, the heat pipe continues to operate and repositions the working fluid. Working fluid freezes as cooldown continues. Maximum heat flux conditions for the entire mission occur during reentry and a maximum temperature of 1000°C (1830°F) is attained; although the temperature of most of the heat pipe structure is isothermal at approximately 927°C (1700°F).

SHUTTLE ORBITER MISSION PROFILE/HEAT PIPE LEADING EDGE OPERATION

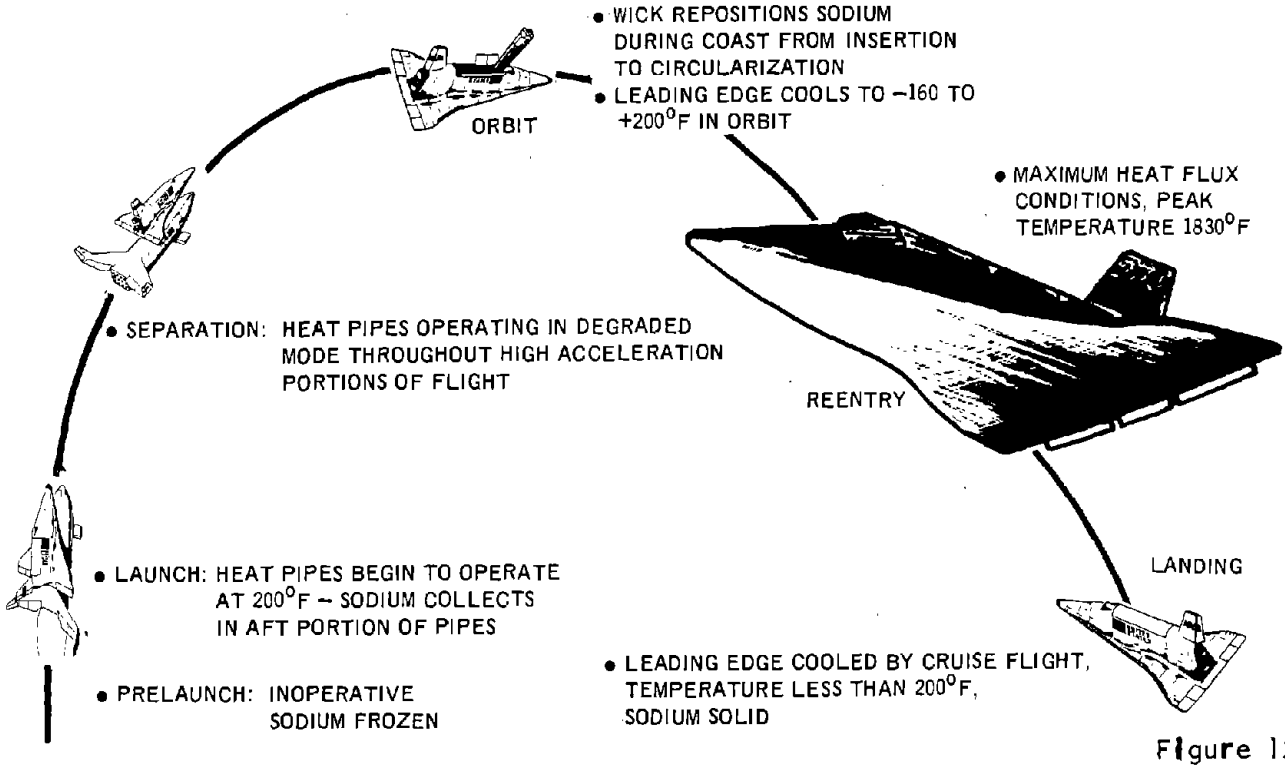

Figure 123

6.2.2 Heat Pipe Fluid Dynamics/Startup - In addition to steady state performance requirements, startup or transient behavior must be considered in the design of the system. Since radiation equilibrium temperatures do not exceed the allowable limits for the material during launch, startup during reentry is the principle concern. The launch environment could affect the distribution of fluid in the pipe prior to reentry, however, and heating rates and g-loads during launch were examined. The principal concern was that the axial g-loads during launch force the fluid to the aft end of the heat pipes. If the liquid were to freeze in this region, leaving the wick in the forward portion void of fluid, problems could occur during reentry. The highest heating rates during ascent, however, occurred after the axial g-loads had diminished. During cooldown the working fluid would be distributed throughout the wick prior to freezing.

As the orbiter reenters the atmosphere, melting of the working fluid occurs first at the stagnation point where heating rates are highest. Very rapid startup conditions could evaporate all the fluid in this region. If it froze in the cooler condenser regions, this could cause burnout. Two approaches have been identified to avoid this problem, (1) a fluid with a low melting point (such as sodium) can be used so that the fluid throughout the pipe is liquid before the heating in the stagnation region causes burnout, and (2) a small amount of inert gas can be added

to control startup. This latter approach has been used successfully in both high and low temperature systems to control and facilitate startup.

In the previous section, sonic limit was mentioned as one of the conditions which affect performance. Unlike the other limits defined, reaching the sonic limit does not, by itself, cause failure. Most high temperature systems operate in a choked flow condition during startup. When a choked flow condition occurs in a heat pipe, the evaporator temperature rises and pressure increases. Assuming that none of the other limiting conditions are reached during the process, the increase in pressure will cause the flow to become subsonic and the pipe will operate normally.

6.2.3 Compatibility/Fluid Selection - Selection of working fluid is heavily dependent on the temperature range of interest. Two temperature ranges were considered, 1000°C (1830°F) and 1300°C (2372°F), which correspond to the maximum reuse levels for superalloys and refractory metals, respectively. The lower range is applicable to the booster, as originally defined, and to one version of the orbiter. .. higher temperatures apply to an orbiter with higher heating rates than the MDC Phase B configurations.

Selection of the working fluid involves:

1. an evaluation of the thermophysical properties of candidate fluids and their relationship with the operational limits of the system
2. compatibility considerations
3. effect of fluid selected on the design of the other system elements, such as the wick and container
4. overall system considerations such as weight, cost, safety, startup, etc.

In liquid metal systems with high thermal conductivity fluids, boiling has seldom been a limiting condition and the design heat fluxes were well below maximum obtainable values. Entrainment was not a limiting condition for this system if an isotropic wick was used to accommodate the high accelerations. The performance of the working fluids, therefore, was based on pumping and sonic limit considerations.

Absolute pumping limit performance cannot be calculated without specifying the other elements of the system; namely, the wick and container design. Relative performance, however, is measured in terms of zero- and 1-g figure of merit (FOM) curves (Figures 124 and 125). The zero-g FOM curve relates maximum performance when frictional losses dominate. If vapor losses and gravity effects are neglected, equation(3)(Section 6.2a) can be written as follows:

$$\Delta P_L = \Delta P_c \tag{12}$$

$$\text{or} \quad q_o \iint \frac{q(x)}{q_o} dxdx = \left(\frac{\sigma \rho_L h_{fg}}{\mu L}\right)\left[\frac{2K_p A_w}{r_c \ell}\right] \tag{13}$$

The term in the parenthesis contains only physical properties of the working fluid and the term in the bracket contains terms relating only to the geometry of the heat pipe. Thus, for a given heat pipe design the term in the bracket is a constant and the only variables are the physical properties of the working fluid. The term in the parenthesis is commonly called the Figure of Merit (FOM) for 0-g, thus

$$(FOM)_{og} = \frac{\sigma \rho_L h_{fg}}{\mu_L} \tag{14}$$

From this expression it can be seen that the highest heat transport capability will be obtained with the fluid possessing the highest value of the FOM. Figure 124 shows the 0-g FOM for 10 potential working fluids as a function of temperature.

If the heat pipe must operate against a gravity field such that both the liquid and vapor pressure drops are insignificant compared to the gravity head, ΔP_L and $\Delta P_v << \Delta P_g$, a different FOM must be used. This FOM for gravity fields is given as

$$(FOM)_{lg} = \frac{\sigma}{\rho_L} \tag{15}$$

Figure 125 shows this FOM as a function of temperature for the same fluids used in Figure 124. On the basis of either FOM, lithium presented the best choice as a high temperature working fluid.

The most appropriate working fluid was not, however, selected solely on the basis of a FOM. Selecting the fluid with the highest FOM only guarantees that the performance predicted by an equation such as equation(3)will be the highest for that fluid. Such other factors as vapor pressure of the working fluid and corrosion behavior can significantly affect the choice of fluid.

ZERO -g
FIGURE OF MERIT

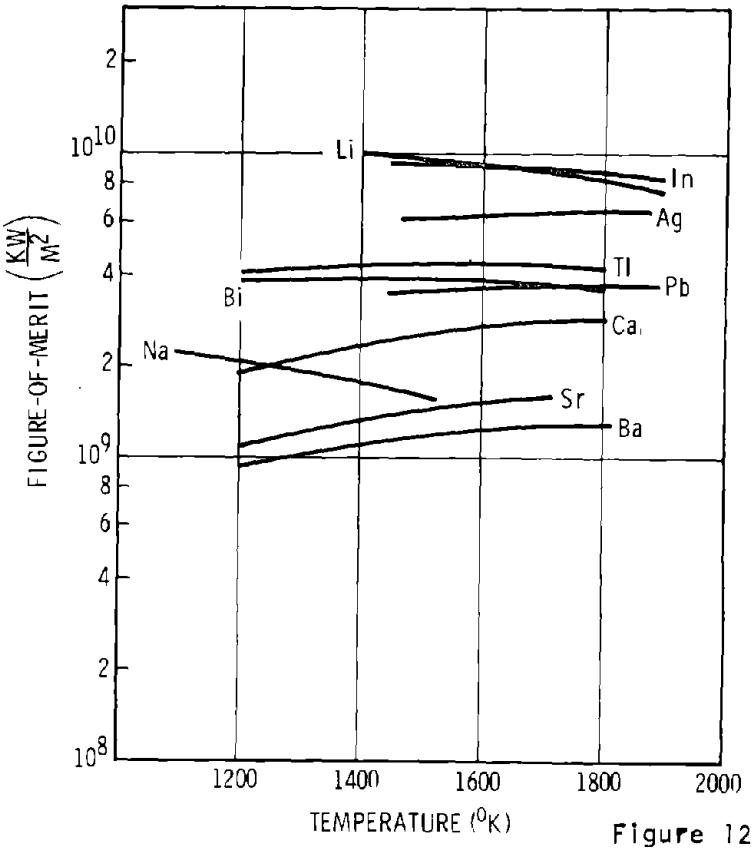

Figure 124

ONE-g
FIGURE OF MERIT

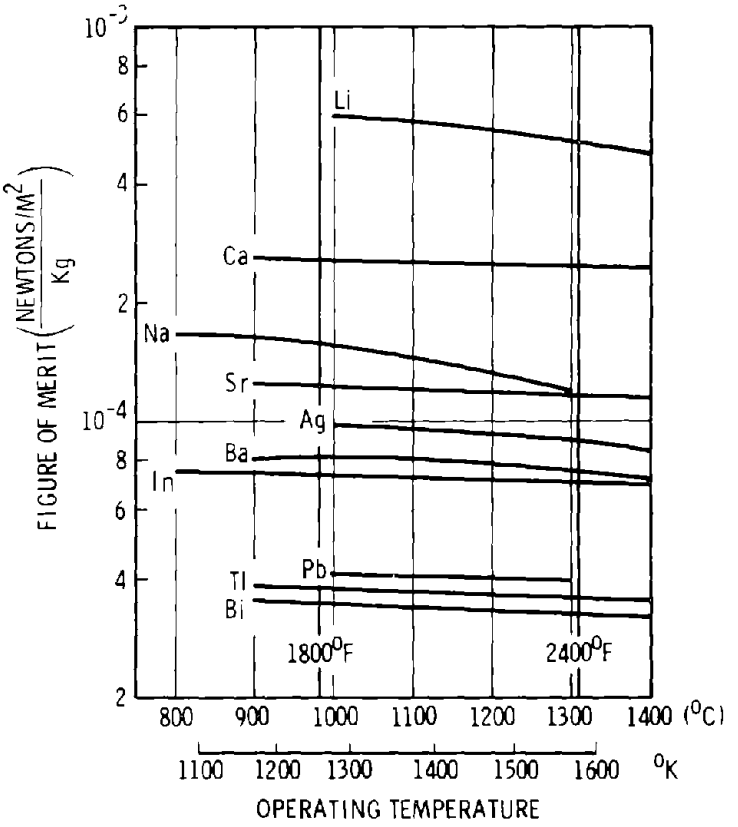

Figure 125

The vapor pressure plays a very important role in two ways. First, pressure vessel limitations will determine the maximum allowable vapor pressure. Second, startup conditions of the heat pipe are affected by the vapor pressure of the working fluid. A so-called sonic limit may be encountered during startup of a heat pipe. This limit is usually encountered in heat pipes designed for high temperature operation when the heating of working fluid is initiated from room temperature. The vapor velocity reaches a sonic limit due to low pressure and low vapor density in the pipe. This process has been well documented in the literature by Cotter, Deverall, et. al, and Levy in References 24 through 26. While sonic operation is acceptable at the beginning of startup, steady state operation near the sonic limit is not acceptable.

When a heat pipe is operating with low vapor densities and high vapor velocities near the sonic limit, isothermal operation is not possible. The sonic limit has been calculated for several high temperature working fluids and the results are shown in Figure 126. It should be noted that indium showed a high value of (FOM) O-g but from Figure 126, one could expect operational problems with indium, since the sonic heat flux values are quite low.

Even though a particular fluid may have the ideal combination of physical properties, it must be chemically compatible with the wick and container to ensure a reasonable lifetime. The most obvious information to examine first is that of solubility data. If one element dissolves another one, it would be a poor choice as a heat pipe fluid. Basic solubility information on compound formation, and phase equilibria is given in References 27, 28, and 29, and is summarized in Figure 127. The working fluids listed are those discussed earlier and the structural material elements are those which would be the major element present in a refractory alloy (Cb, Ta, M_o, W) or an iron or nickel base superalloy (Co, Cr, Fe, Ni). Although the information presented in Figure 128 is incomplete, it does provide some information pointing to possible combinations and also some totally incompatible systems. For example, Bi and Pb will not work with Co, Cr, Fe, or Ni, while Na would probably be a good choice with most of them. Likewise, it appears that the refractory metals, Cb, Ta, Mo, and W are better choices than Cu, Cr, Fe, and Ni. About half of the working fluids appear to be compatible with any of the refractory metals but information was lacking on the others.

The most conclusive evidence for corrosion behavior comes from actual corrosion tests conducted in a loop, reflux capsule, or actual heat pipe. A considerable

SONIC LIMITS

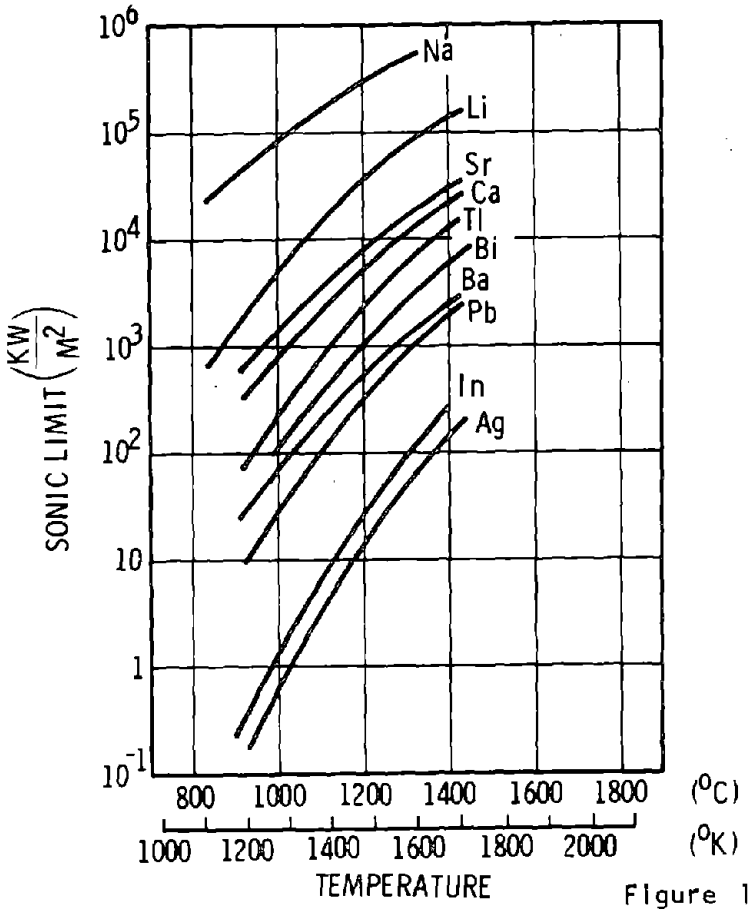

Figure 126

COMPATIBILITY BASED ON PHASE DIAGRAM INFORMATION

	Structural Material Element							
Working Fluid	Co	Cr	Fe	Ni	Cb	Ta	Mo	W
Ag	2	1	2	1	3	3	1	3
Ba	4	4	3	1	4	4	4	4
Bi	1	1	1	1	1	4	2	4
Ca	1	4	4	2	3	4	4	3
In	3	4	4	1	4	4	2	4
Li	2	2	2	1	3	3	3	3
Na	2	4	3	3	3	3	4	4
Pb	1	1	1	1	3	4	3	3
Sr	4	4	4	4	4	4	4	4
Tl	1	4	3	2	4	4	4	4

1 Definitely not compatible

2 Probably not compatible

3 Possible combination for heat pipe

4 Unknown due to inconclusive data or lack of data

Figure 127

amount of corrosion information has been generated on sodium or lithium, mainly because of interest in using them as coolants for nuclear reactors. An excellent summary for Na and Li is given in Reference 30. Pertinent results from this extensive survey are listed below:

1. Use of sodium with austenitic stainless steels should not exceed 1000°F for long term operation and 1500°F for short term operation.
2. Cr-alloy steels can be used with Na up to 1200°F.
3. Below 1300°F nickel base alloys suffer very little attack by sodium.
4. Sodium has been used with Hastelloy-X at 1500°F for 1000 hours with no attack. Similar data for Hastelloy B and W.
5. Sodium has been used with Cb-1Zr at 2200-3000°F for periods up to 8000 hours. Attack was very slight when oxygen levels in the sodium were low.
6. Lithium produces severe corrosion with iron and nickel base alloys in the temperature range 1200-1800°F.
7. Cb-1Zr has been operated with lithium at 2000°F for up to 5000 hours.
8. Attack of columbium base alloys by lithium is extremely dependent upon the oxygen content of the lithium.
9. Tantalum, molybdenum, and tungsten base alloys in contact with lithium exhibit behavior similar to that of columbium base alloys.

A more recent review in Reference 31 has substantiated the findings on lithium with refractory alloys. As along as the oxygen content is kept low, corrosion rates are quite low. Much work with sodium and lithium has been conducted at ORNL. Work reported recently in Reference 32 shows that Na and various refractory metals were compatible at 2192°F.

All the work on reactor systems has been confined to the alkali metals. Corrosion data on the other possible working fluids were obtained from the literature on heat pipes. Operational data on liquid metal heat pipes are summarized in Figure 128,which shows that the longest lifetimes have been obtained with sodium and lithium. The reported failures with lithium were due to excessive oxygen in the system. Use of lithium with refractory metals requires a very low oxygen content (a few ppm) in both the lithium and the container material. Use of other fluids such as Pb, Bi, In, Ba, Ag, and Tl resulted in corrosive attack except for the following combinations: Ag/W and Ph/W. Reference 33 reported Tl/Ta as a good combination, but later examination (Reference 34) revealed that corrosion had occurred.

HEAT PIPE OPERATIONAL DATA

Fluid	Container	Temp. (°F)	Time of Operation (hours)	Remarks	Reference
Pb	Cb	2912	3	Corrosion observed	10
Pb	Cb-1Zr	2912	10	Corrosion observed	10
Pb	Ta	2912	280	No attack	10
Li	Cb-1Zr	2912	132	Leak in container	10
Bi	Cb-1Zr	2912	1	Corrosion observed	11
Pb	Cb-1Zr	2912	19	Corrosion observed	11
Tl	Cb-1Zr	2912	40	Corrosion observed	11
Li	Cb-1Zr	2912	132	Corrosion observed	11
Ba	Cb-1Zr	2912	287	Corrosion observed	11
Bi	Ta	2912	39	Corrosion attack	11
Pb	Ta	2912	1000	Corrosion attack	11
Tl	Ta	2912	248	No attack	11
Li	Ta	2912	17	Corrosion	11
Ba	Ta	2912	340	Corrosion	11
Tl	Ta	2912	2000		11
Bi	W	2912	118	Corrosion attack	11
Pb	W	2912	1000	Low corrosion	11
Tl	W	2912	75	Corrosion attack	11
Li	W	2912	1000	Low corrosion	11
Ba	W	2912	358	Corrosion attack	11
Na	Cb-1Zr	2012	1000	No attack	11
Li	Cb-1Zr	1832	2444	Some attack	11
Li	Cb-1Zr	2732	1000	Some attack	12
Li	Ta	2912	1000	Almost no attack	12
Tl	Ta	2912	2600	Attack	13
Li	Cb-1Zr	2012	4300	No attack	14
Ag	Ta	3452	100	Strong attack	14
In	W	3452	75	Strong attack	14
In	Re	3542	1000	Strong attack	15
Ag	Re	3632	373	Possible attack	15
Ag	W	3452	1000	No attack	15
Na	Hastelloy X	1320	20000	Still operating	16
Na	Ni	1472	4000	Still operating	16
Na	304SS	1472	8000	Still operating	16
Li	TZM	2732	10400	Weld failure	16
Li	TZM	2732	9800	Weld failure	16
Ca	Ta-10W	2732	300	No failure	17

Figure 128

Additional data on heat pipe systems have been determined in a series of reflux capsule tests conducted at 1832°F to 3272°F, References 35 and 36. Systems tested were Ba, Ca, In, Pb and Tl with Ta-10W; Ba, Ca, and Pb with Cb-1Zr, and In with TZM. Test times were generally 1000 hours. Virtually no corrosion was found in the Ca/Ta-10W system, and only slight attach was measured with Ca/Cb-1Zr. Short term operation with In/Ta-10W should be possible at temperatures less than 2500°F.

After examining physical property data, startup dynamics, and corrosion behavior, it was possible to determine a best choice for a fluid in contact with a given material over a specified temperature range. For the temperature of 1000°C (1830°F) where the use of nickel base superalloys was being considered for the booster and orbiter leading edge applications, the best fluid would be sodium. This choice was based principally on corrosion data, heat pipe operation, good FOM for gravity operation, and good startup capability. The corrosion data and heat pipe data were based mainly upon the use of Hastelloy-X as the container, which should be entirely suitable for the orbiter application.

At the higher temperatures, where refractory metals such as Cb-1Zr must be used, the best choice would be calcium. The selection again was based mainly on corrosion data. Lithium was superior based on startup and Figure of Merits, but was rejected because of short lifetimes reported for lithium. This has always been attributed to the oxygen level in the components, and since this is difficult to control to low levels, calcium presents a better choice. Oxygen problems are minimized with the use of calcium since it effectively ties up the oxygen and prevents it from interacting with the container and/or wick.

All of the other fluids considered in the FOM charts do not present good choices mainly because of corrosion problems. It should be noted that strontium appears to be a good choice based on Figures 124 and 125, but there has not been any corrosion data generated on it, thus it can not be recommended for use in a heat pipe.

Safety - The safety of the proposed heat pipe working fluid must be assured in the ground handling, launch, and reentry environments. Potential causes of hazardous exposure to heat pipe working fluids were examined and are discussed below. The conclusion was that a heat pipe leading edge should present a minimal safety hazard.

In the unlikely event of puncture or rupture of a sodium heat pipe, the sodium would burn in air or react with water. The critical water reaction is $Na + H_2O \rightarrow NaOH + \frac{1}{2} H_2 + 33.67$ kcal at 25°C.

A single heat pipe would contain 15 gm of sodium. The heat released in the reaction of this amount of sodium with 12 gm of water is 22 kcal. If there is an insufficient supply of water (<12 gm), the reaction will proceed to Na_2O instead of NaOH as the reaction product with a lower release of heat. For excess water (>12 gm), the water will provide a heat sink to reduce temperatures. Therefore, the worst case would occur when exactly 12 gm (12 cm^3 at ambient temperature) of water reacts with the entire mass of sodium in a heat pipe at a concentrated location. For a 1/2 in. OD heat pipe, the combined liquid reactants would fill a length of 25 cm (10 in.) at low initial temperature. Assuming a worst-case adiabatic reaction, the temperature of the mixture plus pipe section would rise rapidly to a maximum of 870°C (1565°F) over the initial temperature, well below the melting point of Hastelloy-X. This assumes all heat released by the critical mixture raises the heat content in the reaction zone. The water has, by far, the greatest portion of the total heat capacity and is the principal constituent. Thus, the initial temperature of the sodium reacting with cold water would have only a small effect on the final temperature.

Only reactions of sodium with a critical mass of pressurized hot water (above approximately 427°C (800°F) or steam (heat release of sodium-steam reactions is about 40 percent higher) in one heat pipe could initiate a chain reaction involving adjacent pipes. The chain of unlikely events and conservative assumptions leading to this condition seemed outside the realm of possibility for a controlled mission. Consider that one needs:

1. a concentration of sodium at one location
2. a pipe rupture at that location
3. a critical mass of water
4. water temperatures above about 427°C (800°F)
5. an adiabatic reaction and heat transfer to adjacent pipes
6. similar conditions in each successive ruptured pipe

The fifth condition is especially unrealistic. In the actual case, there is a finite time span (estimated to be seconds) for the temperature rise. Although reaction rates are nearly instantaneous, the rate of mixing is not. In addition, the reacted NaOH provides a partial barrier between the sodium and water which further slows the temperature rise. The time span, plus the separation between pipes, should allow considerable heat loss along the support plate and ruptured pipe.

Shock wave energy is characteristically low for sodium-water reactions, generally less than 1 percent of the total energy release. No shock wave damage to adjacent pipes would be expected from rupture of one or several tubes.

Rupture of a heat pipe at high altitudes would not lead to a sodium fire or reaction due to the low oxygen and water availability. Crash landing of the vehicle could lead to multiple pipe rupture and a sodium fire. Flame temperatures of sodium fires are characteristically around 927°C (1700°F) and below the Hastelloy-X melting point. Thus, a fire would not necessarily spread to all heat pipes. Launch abort fireball temperatures, on the other hand, range up to 5000°F (for short times) for chemical boosters. Shock energies of the launch explosion could also rupture the pipes. All sodium will likely burn in such a severe environment, but this represents an infinitesimal addition to the fireball energy.

Hazards from the standpoint of personnel protection are relatively small. During fabrication of the heat pipe assembly, standard industry safety precautions for sodium (Liquid Metals Handbook, Sodium-NaK Supplement) or other working fluids are maintained. The assembled system in the prelaunch phase has a substantially low safety risk because the sodium (or other working fluid) is contained in solid form and in small, modular containers of high strength and corrosion resistance.

The most common hazard of the assembled system is accidental mechanical rupture (by an outside force) of one or several heat pipes and reaction of the sodium metal with the skin and eyes, causing alkali burns. The possibility of a reaction between sodium and the throat and lungs is generally limited to contact of oxide smoke from a fire or caustic mist from sodium-water reaction. Control and precautions can limit probabilities of mechanical rupture, contact with water, and fire to acceptable levels. Also, use of Hastelloy-X heat pipe tubes will provide excellent oxidation resistance even up to building fire temperatures.

The preceding discussion indicates that the heat pipe leading edges present some safety hazard. It should be noted, however, that the hazard is essentially exposure of personnel to the working fluid. The working fluid is contained in an extremely strong container and should be at or near ambient temperature when the orbiter is on the ground. No transfer of hazardous fluids is required, as with hypergolic or cryogenic propellants and the total quantity of working fluid is small. Even crash damage would be effectively localized. Consequently, the heat pipe leading edge presents a minimal safety hazard.

6.3 Stagnation TPS Designs

6.3.1 Wick Design - Four wick configurations, which were evaluated for this system, are depicted in Figure 129. Close packed composite grooves, covered grooves and open grooves give comparable performance, all better than a homogeneous screen. Small longitudinal grooves, however, would be very difficult to fabricate in a thin wall superalloy tube. The close packed composite and homogeneous screen have both been used successfully,but the homogeneous screen has an advantage in simplicity of manufacture. In general, the differences in weight between the various wick concepts will not be excessive,and homogeneous screen wicks will be used because of their structural simplicity.

Wick Requirements - The general operating condition common to both the orbiter and booster which have an effect on the wick design are as follows:

1. Heat pipe operation is not required during ascent since heating rates are not high enough to raise temperatures above the maximum allowable.

2. Heating rates during ascent, however, are high enough to melt the working fluids. Gravity forces tend to force the fluid to the condenser regions. Refilling of the evaporator region by capillary or gravity action must be ensured prior to onset of high reentry heating rates.

3. During reentry, the wicking structure must provide an adequate supply of working fluid to the heated regions.

The heat pipes for all of the systems will have a thin layer of wick on all heated surfaces. This is to promote uniform fluid distribution and prevent thermocapillary or nucleate boiling dryout. A thermocapillary dryout occurs because of the variation in thickness of a liquid film on a heated surface. This film thickness variation causes temperature gradients that produce gradients in the surface tension of the working fluid. These surface tension gradients tend to cause locally thin spots to thin even more until a localized dryout occurs. Even a thin wick layer can significantly reduce the chance of such a localized dryout occurring. A certain portion of the wing or nose cap must have a wicking system which can supply heat in an adverse gravity field. The amount of the surface which requires such wicking is a function of the angle of attack.

In the case of the orbiter leading edge, analysis was performed with two fluids, calcium and sodium, corresponding to operation at 1300°C (2372°F) and 1000°C (1832°F), respectively. Figure 130 defines the area where wicking is required based on liquid pumping requirements and not including that which is required in

WICK CONFIGURATIONS

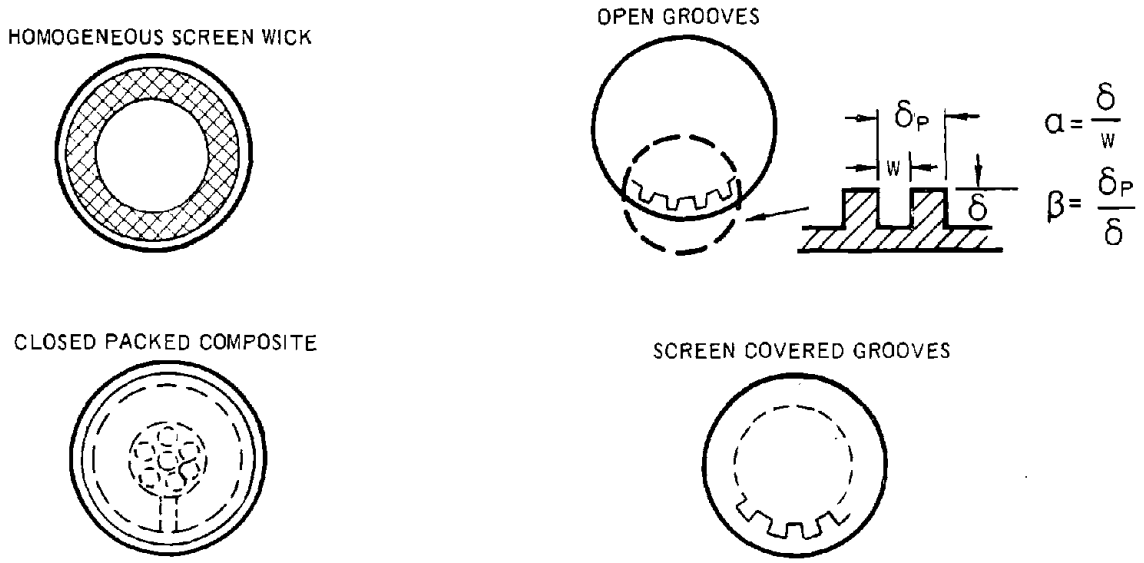

Figure 129

WICKING LENGTH REQUIREMENT

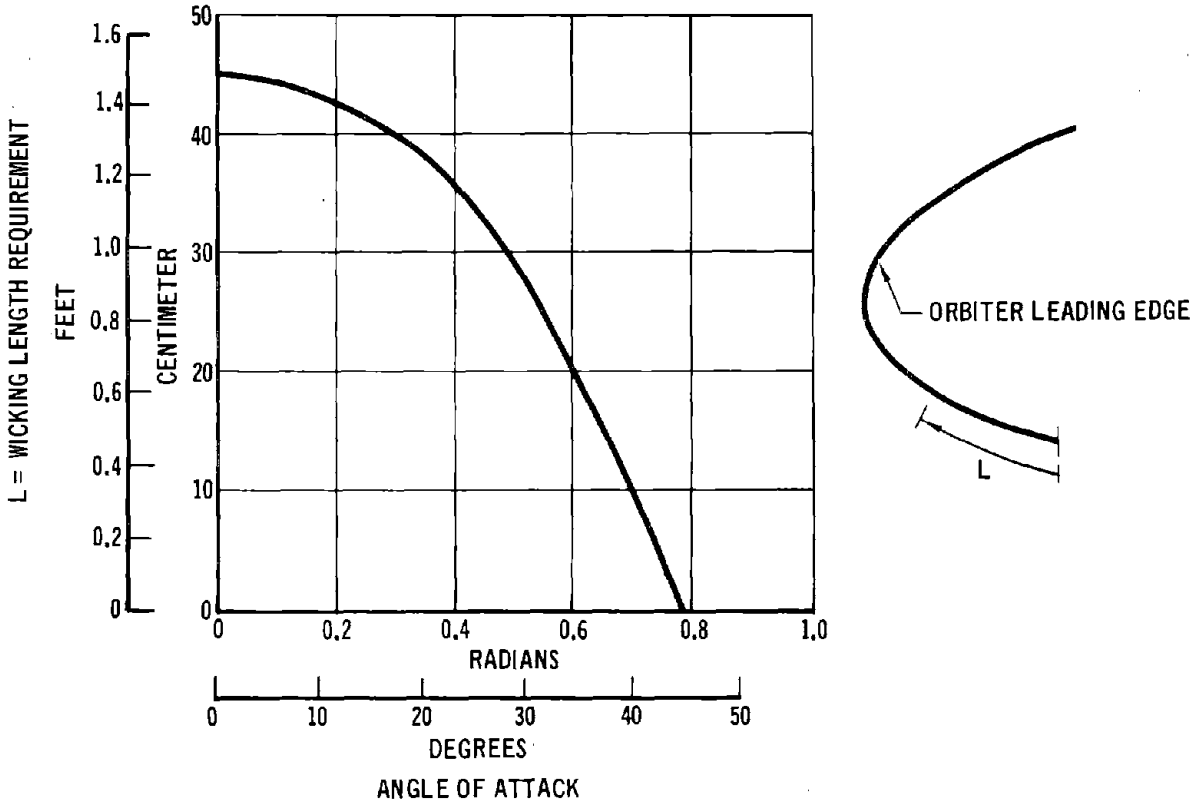

Figure 130

heated regions to prevent thermocapillary dryout. For angles of attack above 0.785 rad (45°), wicking is not required for pumping. For the angle of attack of 0.523 rad (30°) during high reentry heating, 27.4 cm (10.8 in.) of wicking length are required along the windward surface.

Required values of $K_p \left(\frac{A_w}{w}\right)$ for calcium and sodium leading edge designs are presented as a function of angle of attack in Figure 131. Curves for two commonly used mesh sizes, 100 and 200, are shown. With 200 mesh screen, the required value of $K_p \left(\frac{A_w}{w}\right)$ is less than 0.1×10^{-12} m^4/m at 0.523 rad (30°) angle of attack for either calcium or sodium. Figure 132 illustrates that this characteristic, which is independent of the working fluid, can be used to translate this requirement into wick thickness. Two tube sizes are shown, 1.27 cm (1/2 in.) and 2.54 cm (1 in.). However, for values of $K_p \left(\frac{A_w}{w}\right)$, less than 0.15×10^{-12} m^4/m, the curves coincide. For any selected tube size between 1.27 cm (0.5 in.) and 2.54 cm (1.0 in.), therefore, a wick thickness of 0.0381 cm (0.015 in.) is required. As indicated on the figure, a factor of 2 has been included to provide a margin of safety.

Wicking requirements in the nose cap region have also been evaluated. For a reentry angle of 0.523 rad (30°) during peak heating rates, no portion of the windward edge acts as a condenser. Therefore, no wicking is required for the pumping purposes, and only a thin layer is required in the heated regions to prevent thermocapillary dryout.

In addition to pumping requirements during reentry, the wick must be designed to ensure that adequate fluid is located in the evaporator region prior to the onset of high reentry heating rates. During launch, heating rates are sufficient to melt sodium and cause localized melting of calcium. The high gravity forces tend to force the liquid to the aft portions of the heat pipe. Fortunately, in the case of the orbiter, the highest heating rates occur during the low-g portion of the trajectory. Ample time for redistribution, which takes less than 100 sec for either calcium or sodium, is available and the wick in the evaporator will be saturated prior to reentry. These considerations, therefore, impose no additional constraint on wick design. The wick designs for the orbiter are summarized in Figure 133.

ORBITER LEADING EDGE WICK PERFORMANCE REQUIREMENTS

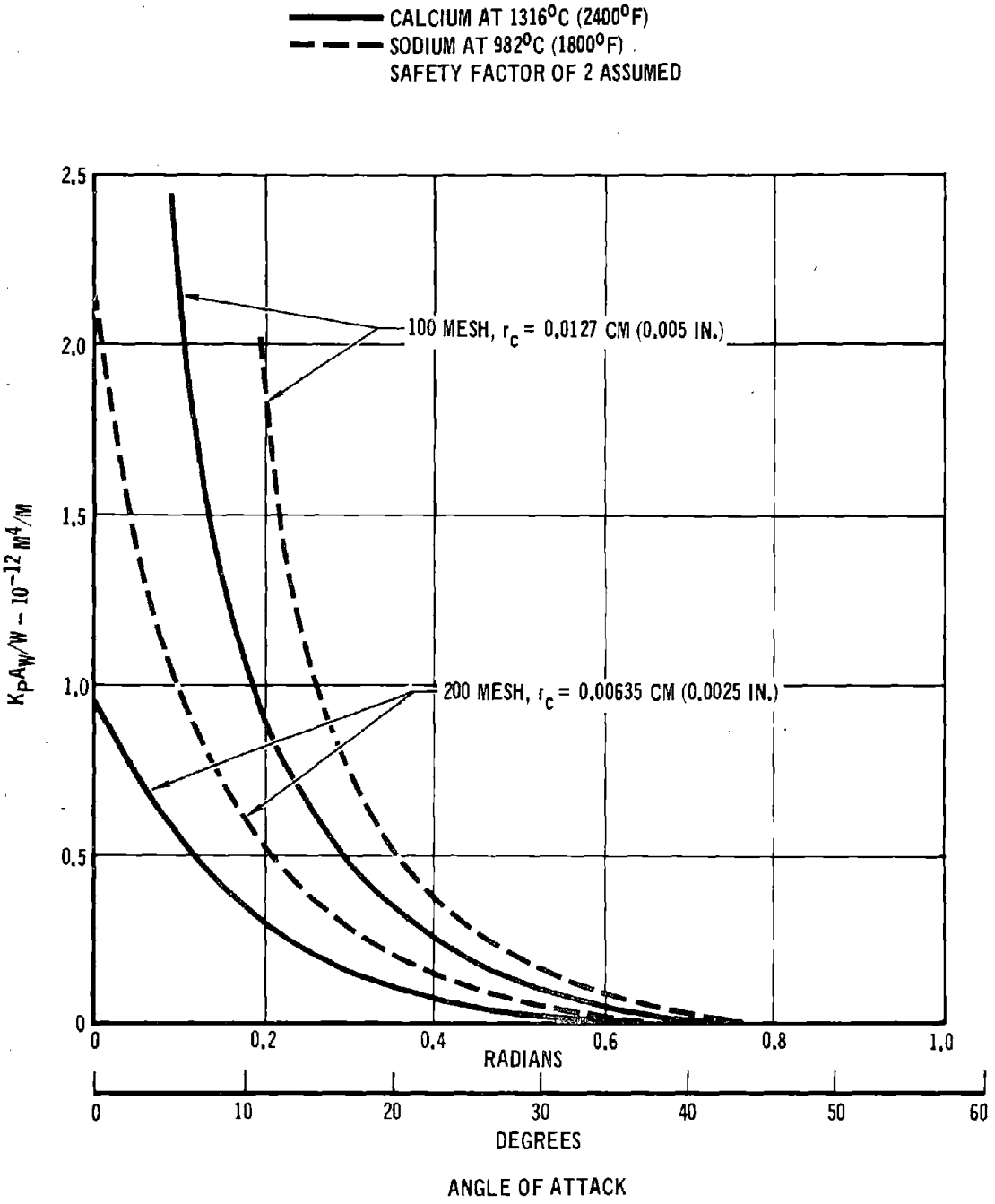

Figure 131

THICKNESS FOR ORBITER LEADING EDGE

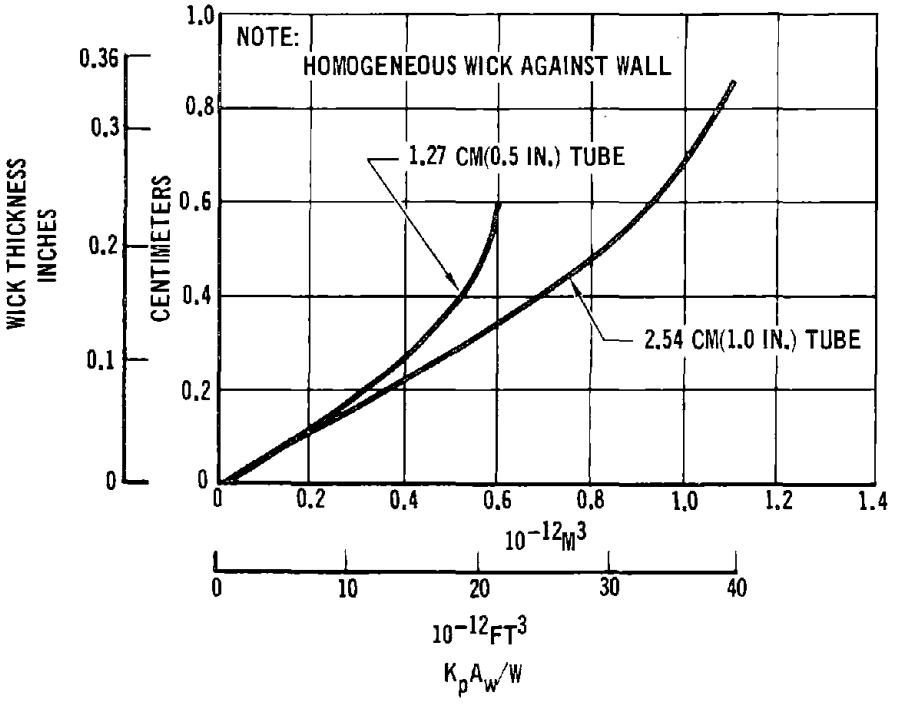

Figure 132

ORBITER WICK SPECIFICATION

• LEADING EDGE	
TYPE:	HOMOGENEOUS SCREEN WICK
MESH SIZE:	200 MESH AT HEATED SURFACE PLUS 100 MESH OVERLAY
DIMENSIONS:	0.0381 CM (0.015 IN.) FOR 45.7 CM (1.5 FT) AND SINGLE LAYER 100 MESH THROUGHOUT HEATED REGIONS
• NOSE CAP	
TYPE:	HOMOGENEOUS SCREEN WICK
MESH SIZE:	100 MESH
DIMENSIONS:	SINGLE LAYER 100 MESH THROUGHOUT HEATED REGION

Figure 133

6.3.2 Container Optimization - Various container configurations were evaluated based on thermal and structural requirements with weight as the principle criterion for comparison. In order to compare candidate leading edge configurations, a planar finite element model of the heat pipe leading edge configuration was constructed. The model was used to determine internal loads resulting from aerodynamic and thermal loading. The model, consisting of the leading edge and its truss support, is shown schematically in Figure 134. The truss supports were assumed every 50.8 cm (20 in.) along the span and the planar model representation of the heat pipe consisted of an effective 50.8 cm (20 in.) width.

Seven loading conditions, shown below, were analyzed with Phase B pressure distributions given in Figures 116 through 118.

Condition	Description
1	Max + α Tailwind + vent lag
2	Max + α Tailwind - vent lag
3	Max - α Tailwind + vent lag
4	Max - α Tailwind - vent lag
5	Entry (pressure + thermal)
6	+ vent lag
7	- vent lag

Condition 3 provided the maximum moment 410 nm/m (92 in.-lb/in.) on the heat pipe section. This value was then used as input to the optimization of the heat pipe cross section.

The cross section optimization compared relative weights of tubular and corrugated heat pipe configurations for various internal vapor pressure levels. The results are shown in Figure 135. The tubular concept was found to be lighter at all pressure levels. This resulted from internal pressure effects that limited the minimum weight of corrugated configurations, making the corrugated section less efficient for reacting aerodynamic bending loads. The tubular configuration was designed by the aerodynamic bending loads and therefore showed no weight variation with internal vapor pressure level.

The tubular concept was evaluated on the basis of thermal and structural optimizations. Effects of design parameters such as tube diameter, tube spacing, skin thickness, fillet size, and tube thickness on temperature gradients and weight were evaluated using a computer heat transfer model specifically designed for this application. Fillet size was found to be very important based both on weight and

FINITE ELEMENT MODEL OF LEADING EDGE HEAT PIPE CONFIGURATION

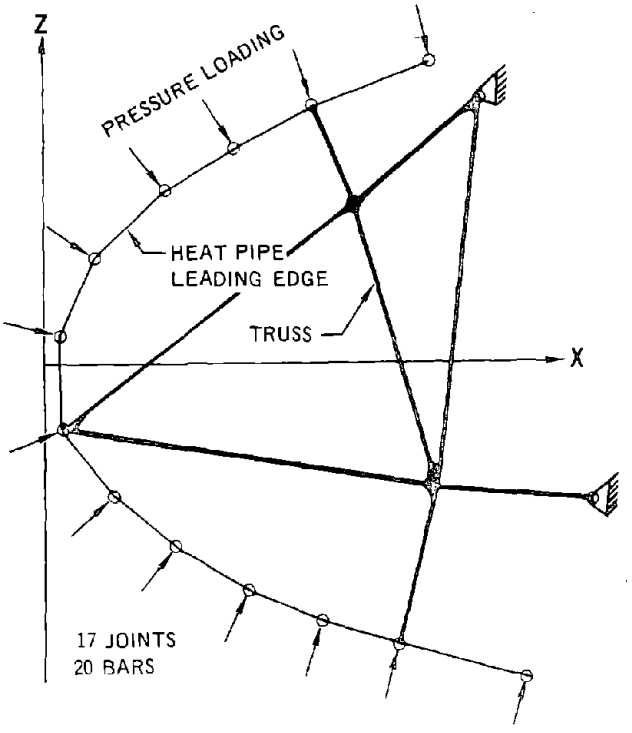

Figure 134

HEAT PIPE CROSS SECTION OPTIMIZATION

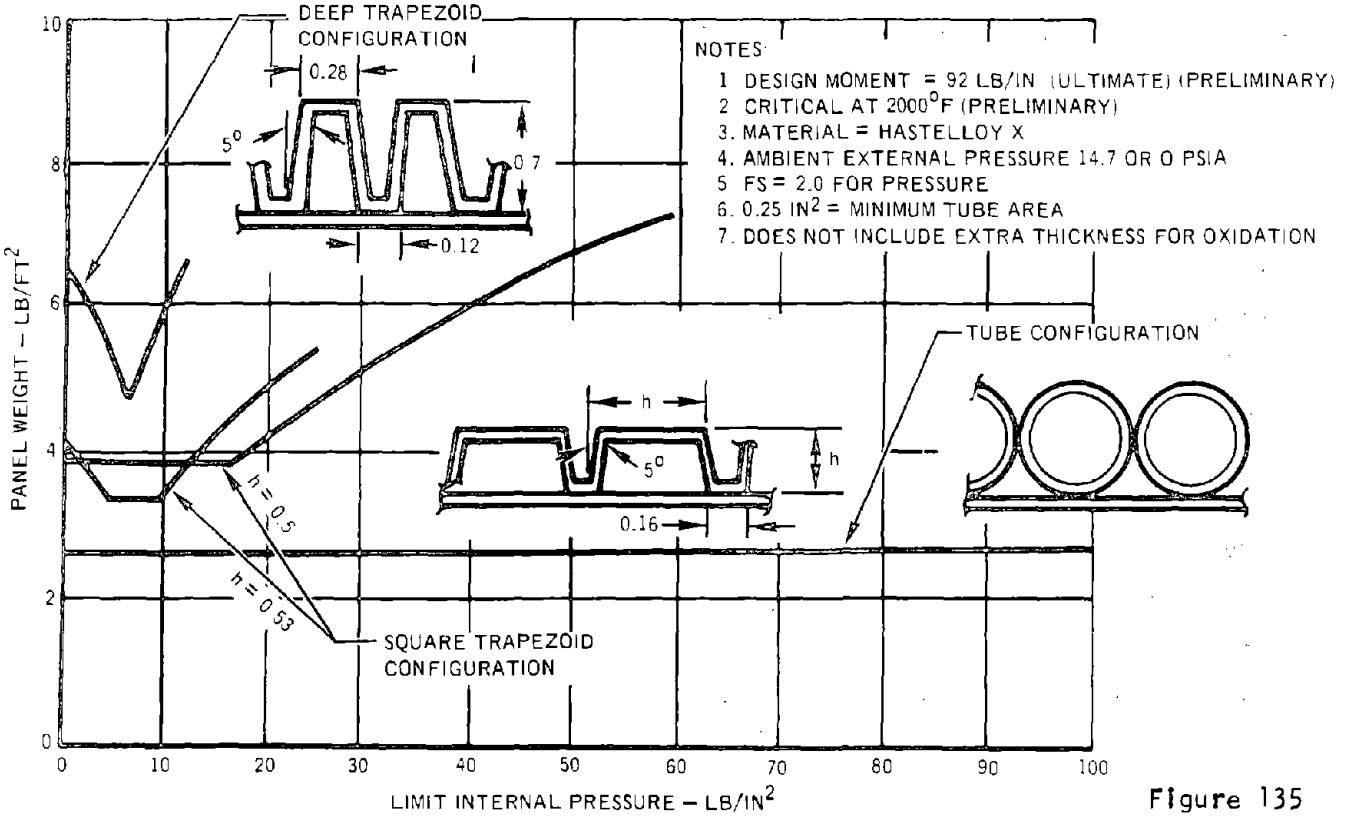

Figure 135

temperature gradient considerations. Figure 136 presents weight variation as a function of fillet angle required to achieve a specific temperature difference under the off-nominal condition of one heat pipe nonoperational. Optimum fillet angle depends on the acceptable ΔT; however, values between 1.0 and 1.2 rad (60 to 70°)are close to optimum in most cases. Manufacturing constraints may also effect fillet angle.

Each nickel base brazing alloy has a characteristic fillet shape based on its surface tension at the brazing temperature. The size and shape of the fillet can be varied somewhat by the geometry of the mating parts and, in particular, by adjusting the brazing temperature within the flow limits of the brazing alloy. Fillet size can be reduced to essentially no fillet by controlling the quantity of brazing alloy per unit length of braze interface. A natural upper limit is established by the joint configuration and the surface tension of the brazing alloy. Any excess brazing alloy which cannot be supported by surface tension runs across the adjacent metal surfaces or collects in low areas of the brazed assembly and,in the process, tends to erode the parts. If unnaturally large fillets are needed for heat transfer, it is necessary to add a powdered base metal to the braze alloy to act as a sponge and keep the brazing alloy from draining away, a technique called "wide-gapping." Studies at DWDL (Figure 137) indicate that fillet widths between 0.38 and 1.04 cm (0.15 and 0.41 in.), which correspond to included angles of 0.7 to $\pi/2$ rad (40 to 90°) in nominal 0.76 cm (0.3 in.) OD tubes brazed to flat sheets, can be held to a tolerance within $\pm$ 0.1 rad ($\pm$5°) for weight control.

A trade study was performed for the heat pipe cooled leading edge to determine the optimum tube diameter based on a 1.22 rad (70°) braze fillet angle. This study indicated that approximately a 1.9 cm (0.75 in.) diameter tube results in the lightest weight system, as shown in Figure 138. Also shown in Figure 138 is the normal maximum temperature and maximum temperature with one heat pipe nonoperational, assuming heat pipe operation at 982°C (1800°F). Maximum temperature increases with tube diameter. Since the weight curve is very flat near the optimum, smaller tube diameters than 1.9 cm (0.73 in.) may be optimum.

The unit weights shown in Figure 138 are based on preliminary designs and are somewhat less than finally derived, but the optimum diameters remained unchanged. Only a vertical shift in the curves was involved.

WEIGHT AND FILLET ANGLE COMPARISON

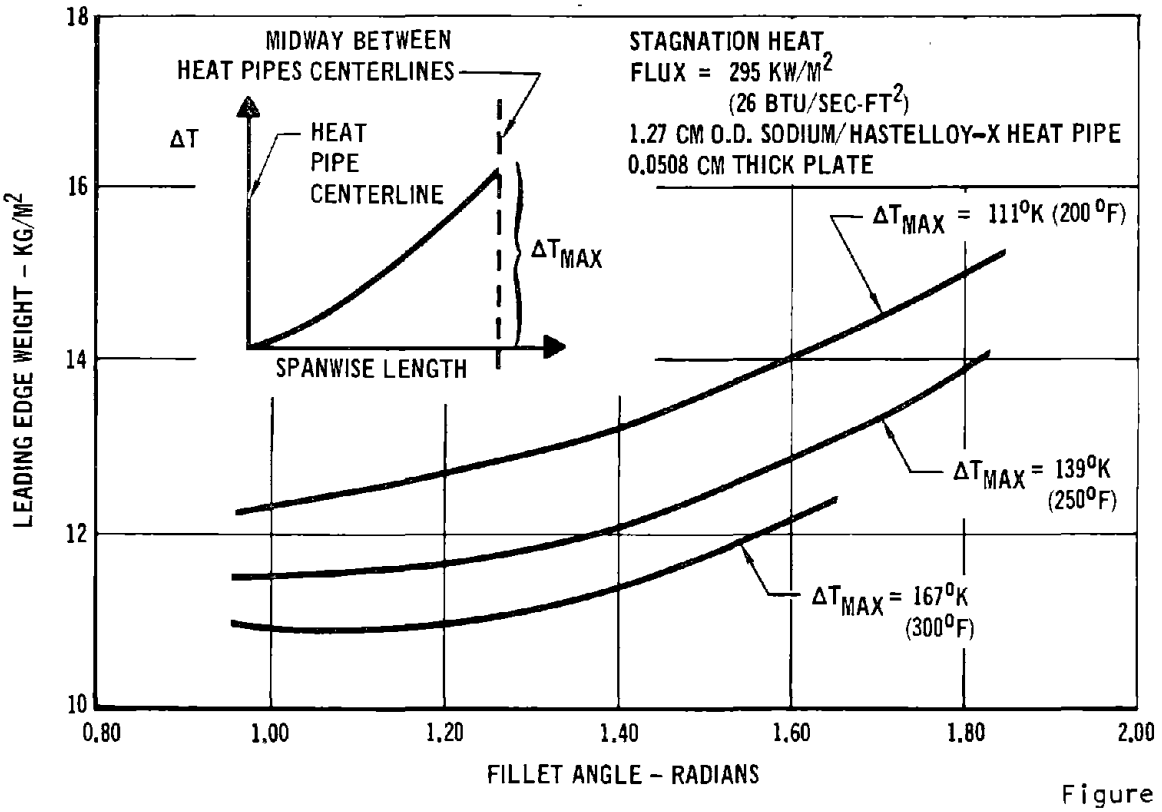

Figure 136

FILLET EVALUATION STUDIES

BRAZING ALLOY	SPEC	TEMPERATURE		TIME MINUTES	AVERAGE FILLET WIDTH 12.7 MM (0.5 IN.) TUBE ON PLATE		AVERAGE INCLUDED ANGLE OF JOINT	REMARKS
		DEG C	DEG F		MM	IN.	DEG	
NICROBRAZ 30	AMS 4782	1149	2100	30	4.2	0.165	38	JOINTS STARVED OF ALLOY FOR MIN FILLETS
NICROBRAZ 30	AMS 4782	1149	2100	30	5.92	0.235	54	NEAR OPTIMUM AMOUNT OF BRAZING ALLOY
NICROBRAZ 30	AMS 4782	1121	2050	30	7.62	0.300	69	EXCESS ALLOY FLOWED OUT OF JOINT
NICROBRAZ 160	–	1163	2125	30	8.39	0.330	76	GOOD FILLETS NEAR OPTIMUM ALLOY QUANTITY
NICROBRAZ 160	–	1136	2075	30	8.65	0.340	79	GOOD FILLETS NEAR OPTIMUM ALLOY QUANTITY
NICROBRAZ 160	–	1136	2075	30	10.02	0.395	91	EXCESS ALLOY ADDED FOR MAXIMUM FILLET SIZE
AMDRY 914	BTS 1025	1136	2075	30	8.14	0.320	74	GOOD FILLETS NEAR OPTIMUM ALLOY QUANTITY
NICROBRAZ 170		1177	2150	30	7.62	0.300	69	FILLETS SOMEWHAT ROUGH – NEAR OPTIMUM QUANTITY
NICROBRAZ 200		1121	2050	30	8.5	0.335	77	GOOD FILLETS, NEAR OPTIMUM ALLOY QUANTITY

Figure 137

HEAT PIPE PANEL

Thermal and Weight Performance

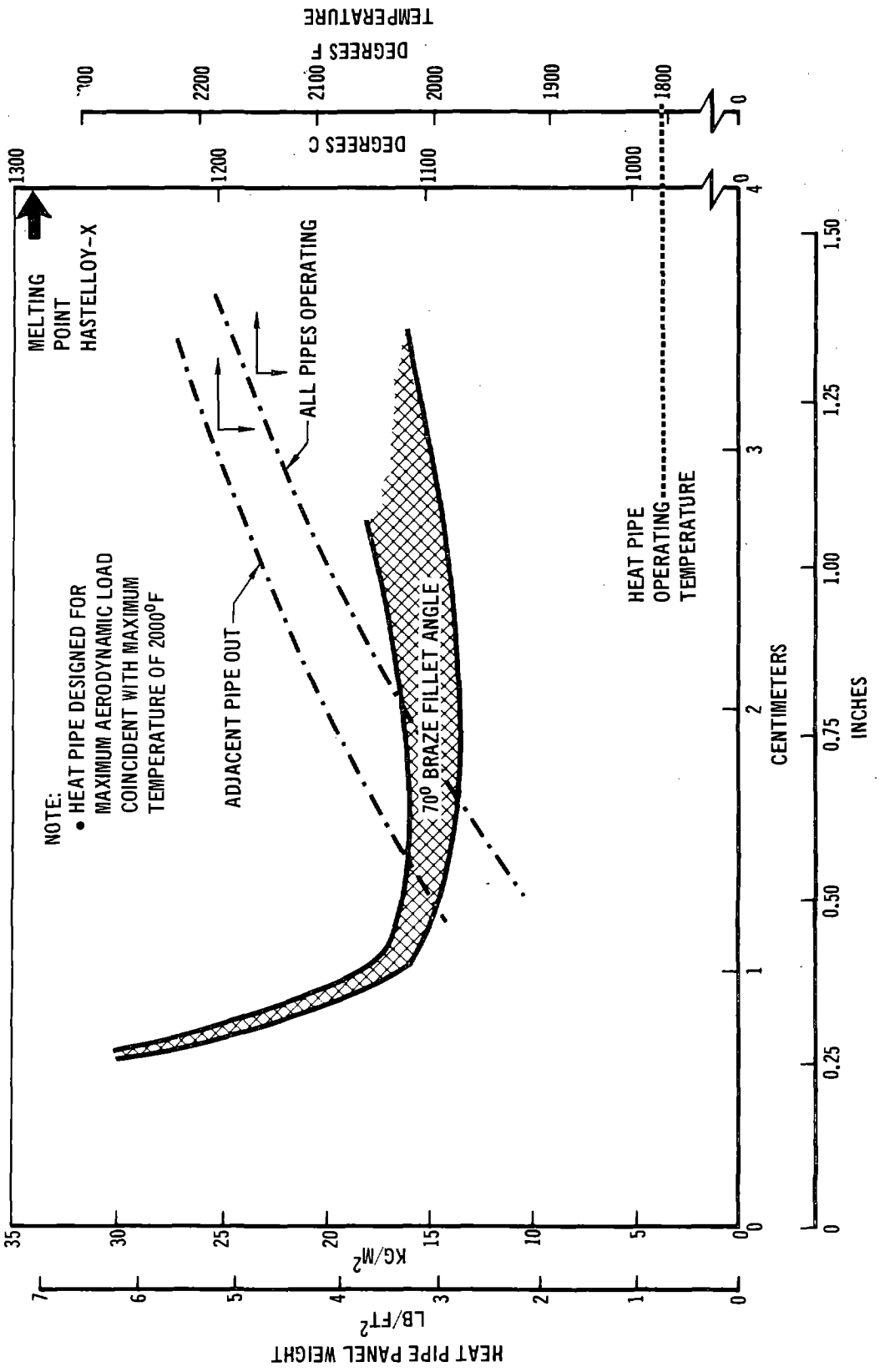

Figure 138

6.3.3 Orbiter Heat Pipe Leading Edge Design - The orbiter heat pipe leading edge design, illustrated in Figure 139,consisted of a heat pipe cooled Hastelloy-X panel with Hastelloy-X channel member edge frames and hat section spanwise stiffeners. The panel formed the entire leading edge cap and was supported from the wing forward spar with a Hastelloy-X truss. The titanium forward spar was insulated from the hotter leading edge assembly with a packaged fibrous insulation blanket, and the long conduction paths of the truss assembly.

The heat pipe cooled panel utilized heat pipes constructed from 0.5 mm (0.02 in.) wall thickness seamless Hastelloy-X tubing with an outside diameter of 1.27 cm (0.5 in.). The heat pipes would be formed in the wing chord airfoil cross-section after installation of the wick (Hastelloy-X screen). Subsequent to forming, the end fitting for servicing with the working fluid would be welded in place. The heat pipes then would be assembled into a panel using a covering Hastelloy skin, and hydrogen brazed with an alloy (Nicrobraze) having a remelt temperature of 1290°C (2350°F). The individual heat pipes would be serviced with 15 gm (.033 lb) of sodium and operated at 316°C (600°F) for 72 hours to deoxidize the pipes and thoroughly wet the wick.

The truss assembly consists of 10 element planar trusses normal to the leading edge spar linked with diagonal members to provide lateral stability. The leading edge panel is attached with a pin connection near the stagnation line. The remaining connectors utilize a slotted hole with expansion bearing washers to allow thermal expansion of the panel.

The forward spar was protected with a 7.62-cm (3-in.)thick insulation blanket. Microquartz insulation with a density of 56.5 kg/m^3 (3.5 lb/ft^3) packaged in Inconel foil was selected because it provided the lowest weight thermal protection.

STRUCTURAL ACTIVE COOLING

VEHICLE LEADING EDGE DESIGN

FOLDOUT FRAME 1

MDC E0638

FOLDOUT FRAME 2

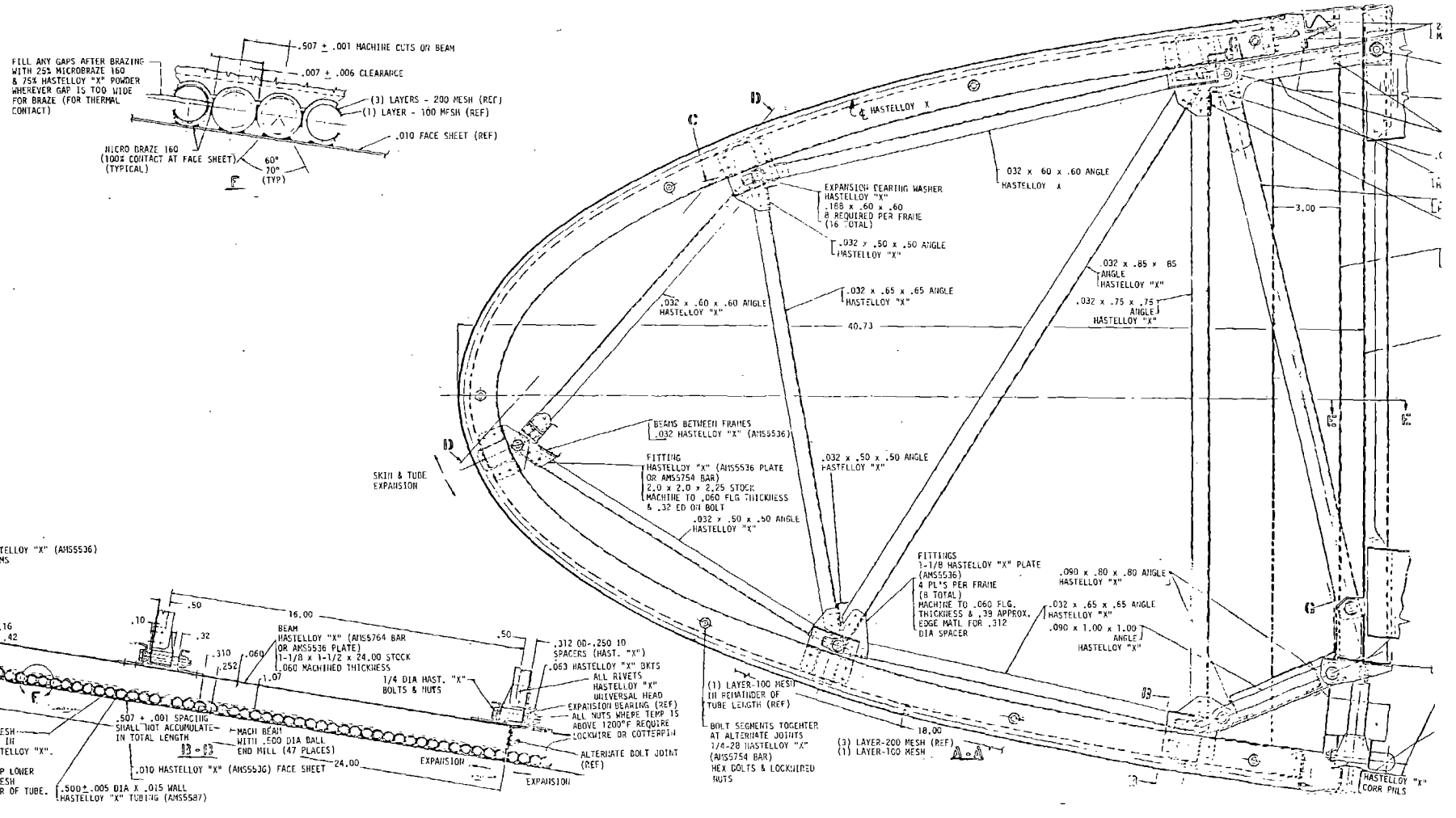

Figure 139

FOLDOUT FRAME 1

FOLDOUT FRAME 2

FOLDOUT FRAME 3

ILING

SIGN

MDC E0638

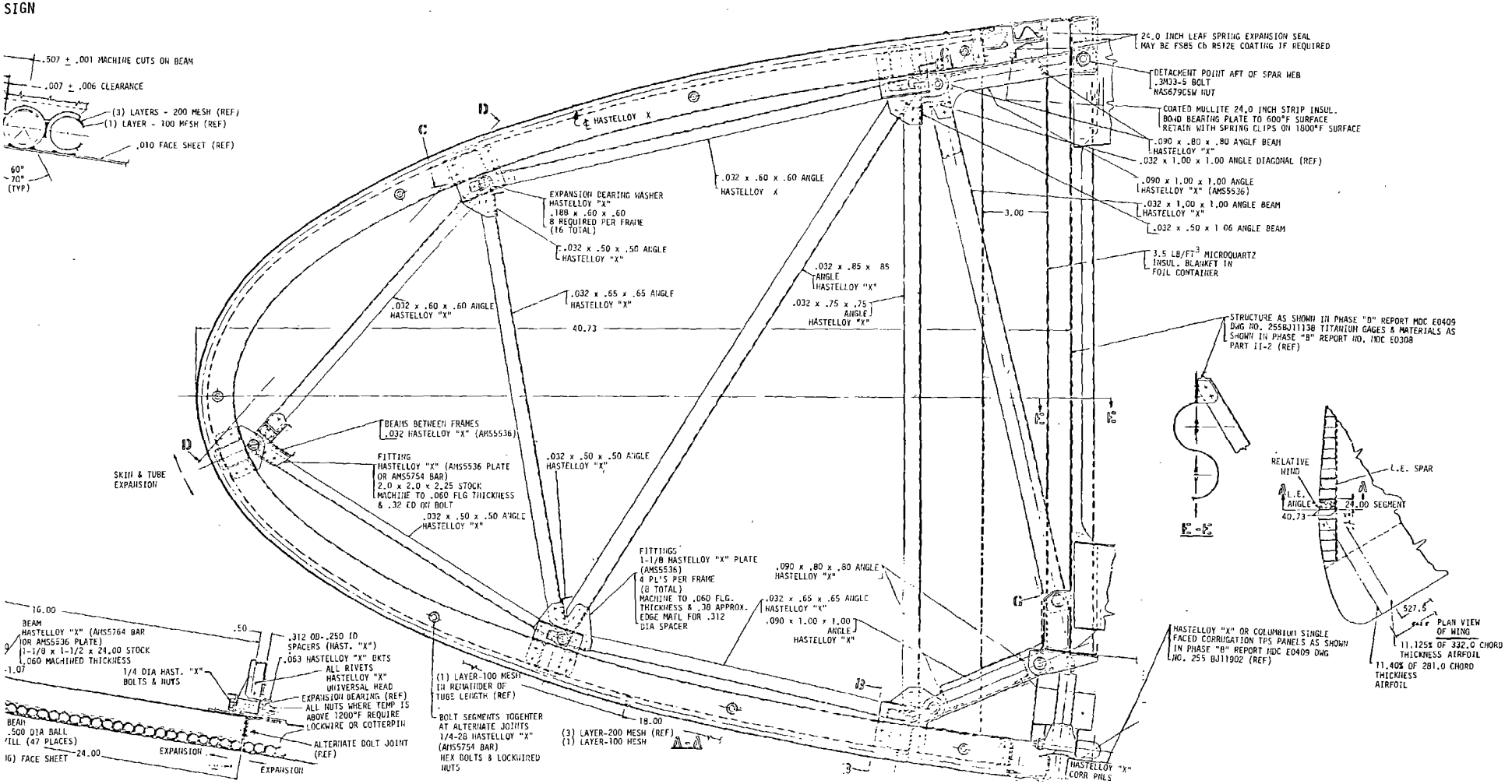

Figure 139

6.3.4 Feasibility Test Model Design - A preliminary design of a feasibility test model, similar to the flight version, is illustrated in Figure 140. The test article assembly would consist of a segment having the same airfoil cross-section as the carbon-carbon assembly constructed under contract NAS 8-26016. The panels will consist of 1.27-cm (0.5-in.) OD Hastelloy tubes brazed to a 0.5-mm (0.02-in.) thick facesheet. The heat pipes, as in the flight model, would contain sodium as the working fluid. The test article was designed to reduce the peak temperature from 1315°C (2400°F) to a maximum of 1010°C (1850°F). The design contained the fail-safe provision of structural integrity should a pipe fail, since the two adjacent pipes could absorb the additional heat and prevent the failed pipe from exceeding 1093°C (2000°F). Because of the small size of the test segment, no supporting truss work was required. The tube ends would be brazed directly into two fittings, one at the upper and one at the lower aft end of assembly. The fittings would be mounted on trunnions on a box cantilevered from the test facility sting. Structural analysis of the configuration indicated that the upper bracket should be pinned, but the lower connection should be slotted to allow expansion to relieve thermal stresses. A brief study of materials indicated the best material for construction would be Hastelloy-X for the purpose of demonstrating feasibility. For flight configurations, TD-NiCr could give a lighter weight unit but seemed an inappropriate selection for an inexpensive feasibility test.

TEST MODEL DESIGN

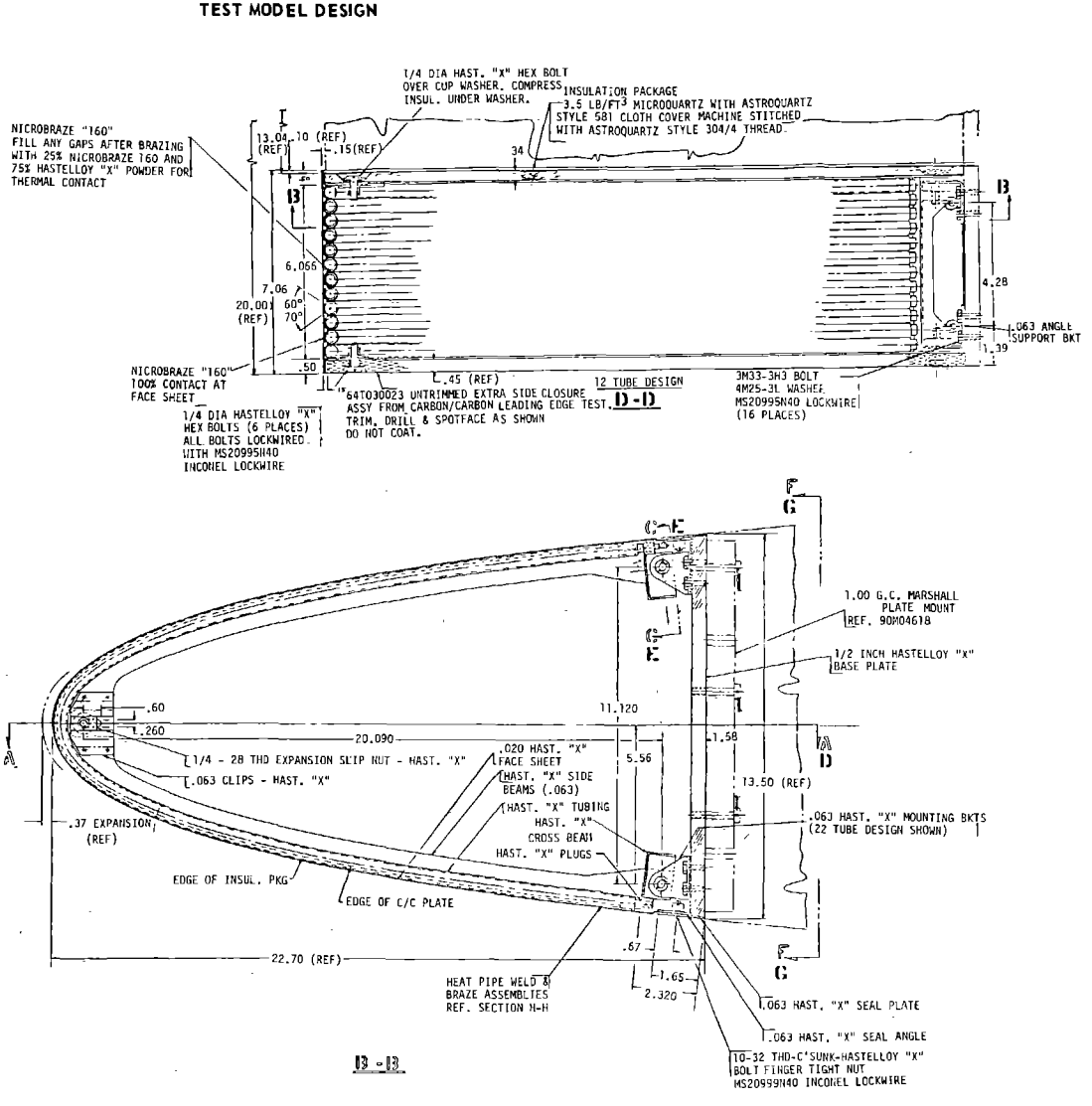

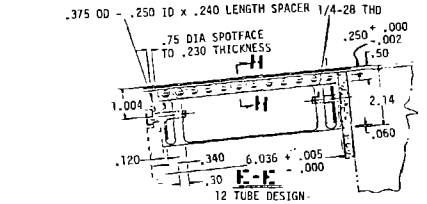

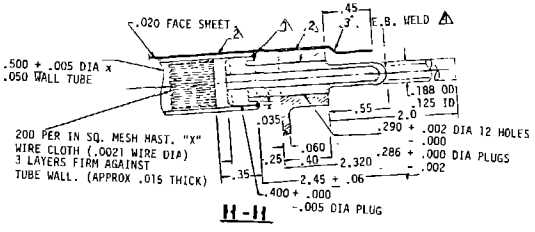

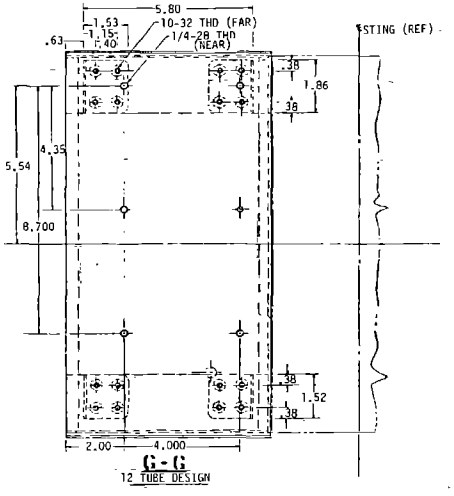

Figure 140

6.4 Operational Performance/Trade Studies - Four types of leading edge TPS designs were analyzed in depth to enable a high-confidence trade study. With the exception of one preliminary study, previous studies have considered these designs but the design environments have been different for each case and no direct independent comparison has been made. The candidate leading edge designs included a heat pipe system using Hastelloy-X tubing brazed to a Hastelloy-X face sheet, an ablator system using an MDAC-E ablative material (designated S-3) bonded to titanium honeycomb substructure, a carbon/carbon structure and a columbium structure. For this study all leading edges were assumed to be exposed to the same environment, including heating and pressure profiles, and were assumed to be located at the same wing station on the final design version of the Phase B delta wing orbiter. To provide valid trade study results the design approach was to minimize the use of exotic or expensive mat rials. The designs utilized metallic TPS panels where emperatures permitted but were compared on the basis of the entire leading edge cap TPS, including internal supports, insulation, and the candidate materials. The design environment was given in Paragraph 6.1.

The ablative leading edge design evolved from IRAD studies at MDAC-E. These included preliminary design analysis and construction of a scale model leading edge which demonstrated the feasibility of a proposed refurbishment concept.

A carbon-carbon leading edge was designed and manufactured as part of the Space Shuttle Supplementary Structural Test Program, Contract NAS 8-26016. This SSTP leading edge was reported in Reference 37. The manufacture of the SSTP carbon-carbon leading edge demonstrated manufacturing feasibility and established material allowables for complex shapes. This leading edge was a section of a straight wing orbiter and, therefore, the shape was dissimilar to that used for final Phase B designs. In addition, the design pressures were appreciably higher. The SSTP carbon-carbon leading edge weight, therefore, should not be compared with the weight for the Phase B heat pipe leading edge design. The Vought Missile and Space Company designed and manufactured a carbon-carbon wing leading edge under Contract NAS 9-11224, Reference 38. This leading edge was similar in shape (delta wing) and the design environment was similar to that which would be applicable for our Phase B configuration. The carbon-carbon leading edge concept studied is similar to the Vought concept, but the mechanical properties determined in the Reference 37 program were used for structural sizing.

Extensive work was done on columbium single-face corrugated TPS panel design by the MDC Space Shuttle Phase B Study. The project sized, manufactured, and tested columbium panels and substructure. This technology, reported in References 39 and 40 was utilized when designing the columbium leading edge for the trade study.

A preliminary trade study, Reference 41, considering leading edges using ablators, carbon-carbon, ceramic, heat pipe,and water transpiration systems was performed during Phase B by MDAC-E. The study assumed that entry temperatures would be too high to permit the use of columbium. The study results provided screening criteria that eliminated ceramic and water transpiration systems from further consideration.

Leading Edge Design Environments - The leading edges were designed to withstand the MDC Phase B environment, with the ultimate load defined as 1.4 times limit load. Each leading edge assembly was designed to withstand the ultimate load at operating temperature without failure. To prevent undesirable deformation of the leading edge structure due to creep, the structures were designed to restrict creep strains to less than 0.5 percent in 100 mission cycles. As a safety feature, a "fail-safe" requirement was imposed on the heat pipe design. The requirement was that no structural failure would result if one heat pipe was inoperative. Heat pipe tubes were designed to withstand a proof pressure equal to two times operating pressure without yielding,and a burst pressure equal to four times operating pressure without failing.

The orbiter configuration and environment selected for this study was the final MDC Phase B Baseline for 1100 nmi cross range entry. The seven loading conditions, Section 6.3.2, were included in the design analysis. The maximum entry temperatures for the columbium and carbon-carbon leading edges was 1290°C(2350°F), and the temperature distribution at the time of maximum temperature is given in Figure 141. Design factors of safety of 1.4 for metallic parts (based on minimum guaranteed properties) and 2.0 for carbon-carbon based on typical properties were applied in determining strength requirements. The wing was the Phase B modified NASA 0012 air foil. The cross section selected for this study was normal to the forward spar at the point of maximum chord length of the leading edge cap. The forwardmost edge of the cross section was at wing stations Y562.5 and the aft edge of the cross section terminated at the forward spar at wing station Y527.5,as shown in Figure 139.

The heat pipe system, described in detail in Paragraph 6.3.3, consisted of round tubing, a thin face sheet, support frame,and truss work with the tubes

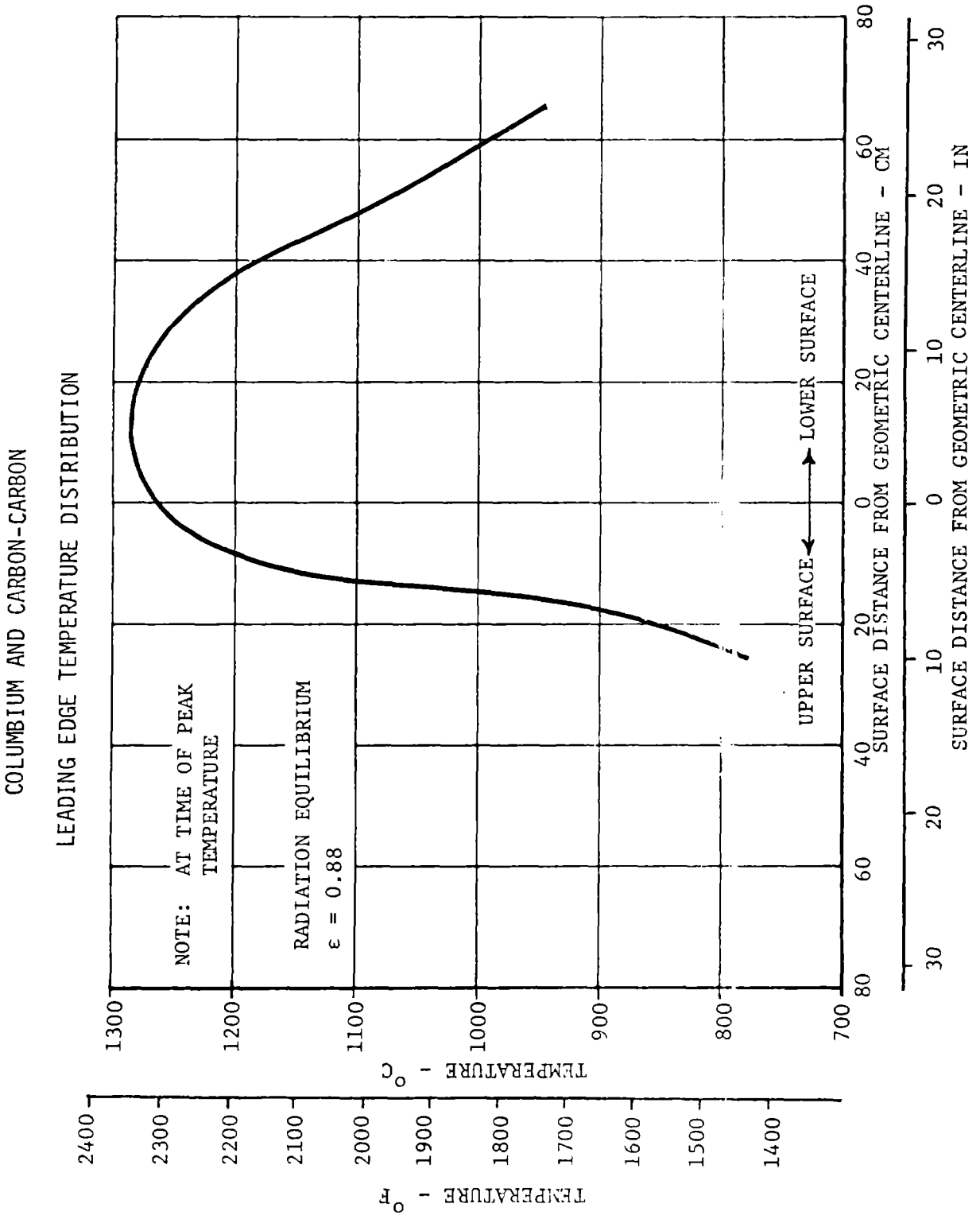
COLUMBIUM AND CARBON-CARBON
LEADING EDGE TEMPERATURE DISTRIBUTION
NOTE: AT TIME OF PEAK TEMPERATURE
RADIATION EQUILIBRIUM
ε = 0.88
UPPER SURFACE
LOWER SURFACE
TEMPERATURE - °F
TEMPERATURE - °C
SURFACE DISTANCE FROM GEOMETRIC CENTERLINE - CM
SURFACE DISTANCE FROM GEOMETRIC CENTERLINE - IN

Figure 141

brazed together and to the face sheet. Circular tubing was used because of the internal pressure. Plugs welded to each end of the tubes provided end seals and a filler port. A planar truss work, located spanwise at 16-in. intervals, supported the leading edge. Each truss assembly was aligned with wing stringers to form a forward extension of the wing structure. The tube/face sheet assembly was pinned to the truss at the forward edge and attached at other points with slotted fittings to minimize axial thermal stresses.

The weight of heat pipe cooled leading edge assemblies made from Hastelloy-X and Td-Ni-Cr and a preliminary check of a Haynes 188 system was made. Haynes 188 was dismissed because the relatively high modulus of elasticity at 982°C (1800°F) induced high thermal stresses and resulted in a heavier design. In each case the truss material was specified to be the same as the heat pipe material.

A finite element model of the heat pipe leading edge was constructed and analyzed using the STRUDL-II computer program. The model was used to determine displacements, reactions, and internal loads resulting from the aerodynamic and thermal loading conditions of Paragraph 6.1. The model, consisting of the leading edge and its truss support is shown schematically in Figure 142. Each set of truss members carried aerodynamic and thermal loads acting on 41.6 cm (16-in.) of leading edge span. Modifications of this model were used in the analysis of the other candidates leading edges. Each truss member was designed to carry critical combinations of compression loads and bending moments using beam-comumn analysis. All truss members have positive margins of safety under the most critical leading (ascent) conditions.

The heat pipes (skin and tubes) were sized using internal loads obtained from the computer model. The 982°C (1800°F) thermal and pressure loading (Condition 8) was most critical for Hastelloy-X and Haynes 188 due to the creep criteria. The Td-Ni-Cr tubes and face sheet were not creep critical and the minimum gage considered practical for manufacturing was specified.

A fail-safe analysis was performed by comparing applied ultimate loads resulting from Condition 8 to allowable ultimate loads at 1093°C (2000°F). (If one pipe should fail to operate the temperature of that pipe would be 2000°F). Heat pipe margins of safety for fail-safe designs were 2.06 for Hastelloy-X and 4.7 for Haynes 188. The Td-Ni-Cr alloy would be less critical. Creep was not restricted for the fail-Safe requirement.

Heat pipe leading edge total weights and component weights based on the structural analysis are shown with weights of other candidates leading edges

FINITE ELEMENT MODEL OF LEADING EDGE HEAT PIPE CONFIGURATION

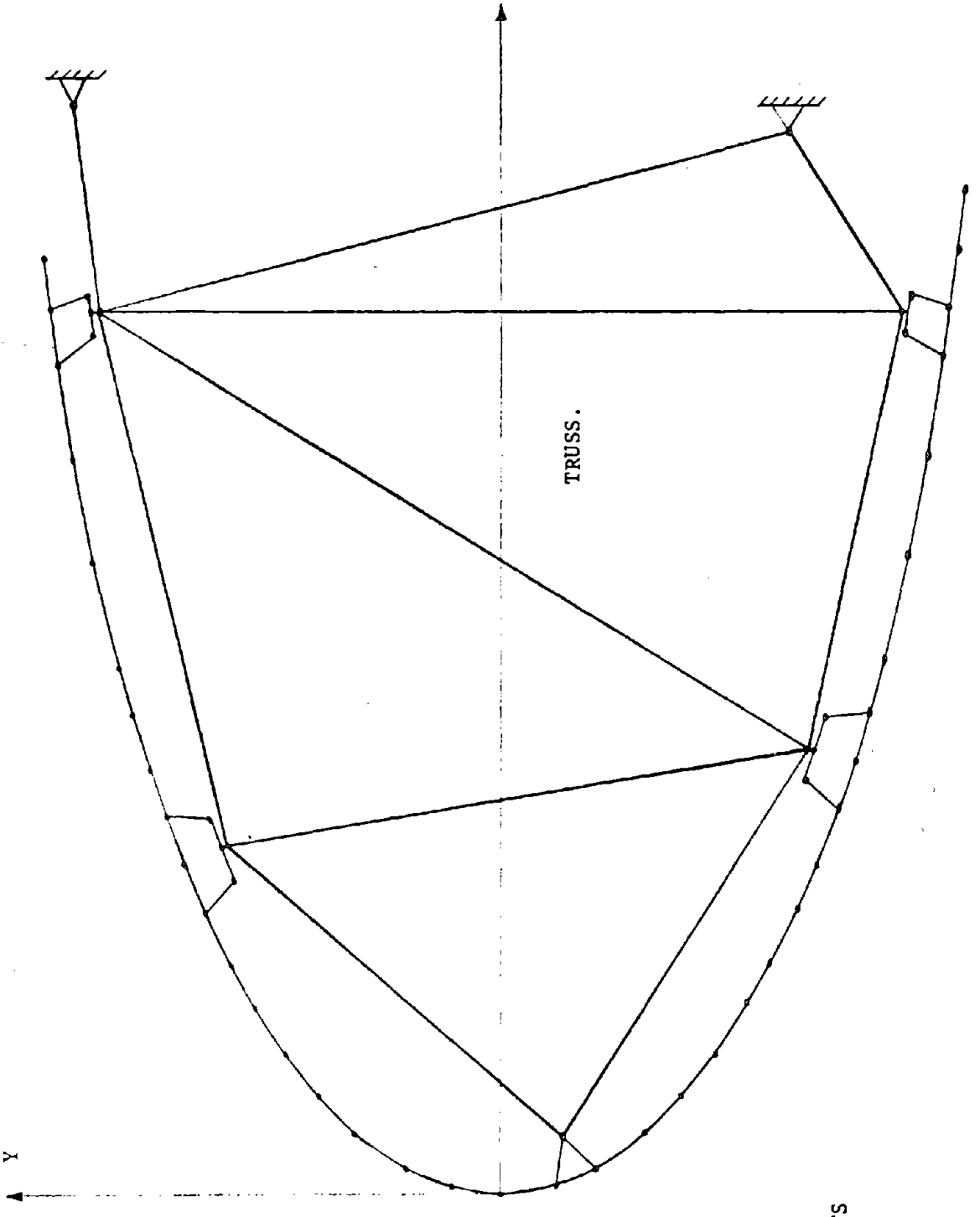

Figure 142

in Figure 143. The Hastelloy-X leading edge is heavier than the other concepts because the allowable stress level at elevated temperature is limited by the creep criteria. The alternate version of this leading edge concept utilizing the Td-Ni-Cr alloy is lighter and weight competitive with the other alternates.

Ablative Leading Edge - The ablative leading edge, illustrated in Figure 144, consisted of ablative material bonded to metal substructure. A high density (896 kg/m^3,, 56 lb/ft^3) MDC ablator, designated S-3, was selected to provide good resistance to aerodynamic shear. The ablator thickness was sized to prevent the bond line temperature from exceeding 316°C (600°F).

The forward section of this leading edge was a readily removable panel consisting of ablator bonded to a titanium honeycomb. The titanium honeycomb was 40.6 cm (16 in.) wide and was framed with titanium channels. The sections are attached with quick release fasteners as shown in Figure 144. After each flight the ablative segment is removed and taken to a refurbishment area where the ablator would be stripped off and replaced.

Aft of the ablative section, in regions of lower heating, the leading edge skins consisted of Hastelloy-X panels. The panels were corrugation stiffened in a configuration derived from similar panels designed in Phase B by MDAC-E. The panels are backed with insulation blankets of 56-kg/m^3 (3.5 lb/ft^3) density insulation packaged in Inconel foil.

Internal loads, shears, bending moments, and axial loads and displacements were determined using load conditions of Section 4, the math model shown in Figure 145, and the STRUDL-II computer program. It was assumed that the minimum practical gage honeycomb face sheet would be 0.010 in. and that the minimum thickness core would be 0.23 in. These dimensions were used for the titanium panel, and subsequent analysis indicated that the panel would have a substantial strength margin. Weight estimates for the ablative leading edge design are shown in Figure 143.

Carbon/Carbon Leading Edge - The carbon-carbon leading edge is illustrated in Figure 146. The carbon/carbon extended over the same portion of the leading edge design as the ablative in the previously described design. The remainder was Hastelloy-X single face corrugated panels. The same type of truss work used for the ablative leading edge supported the Hastelloy-X panels. Stiffening ribs were provided around the perimeter of the carbon-carbon panel. In contrast, the SSTP carbon-carbon panel, which was designed for a straight wing orbiter, had a relatively longer flat lower surface and higher air loads, so that intermediate

LEADING EDGE WEIGHT BREAKDOWN

	HEAT PIPES			ABLATIVE
	HASTELLOY-X LB/FT^2	TD-Ni-CR LB/FT^2		LB/FT^2
FACESHEET & TUBING	2.40	1.82	ABLATOR	1.95
BRAZE FILLETS	0.59	0.60	HONEYCOMB	0.42
WICK	0.38	0.40	HASTELLOY-X PANELS	0.43
WORKING FLUID	0.07	0.10	SUPPORT STRUCTURE	0.33
SUPPORT STRUCTURE	0.80	0.80	INSULATION	0.44
INSULATION	0.50	0.50		3.57
	4.94	4.22		

	CARBON/CARBON LB/FT^2		COLUMBIUM LB/FT^2
CARBON/CARBON	1.30	COLUMBIUM PANELS	0.77
HASTELLOY-X PANELS	0.53	HASTELLOY-X PANELS	0.60
SUPPORT STRUCTURE	0.60	RETAINER STRAPS	0.35
INSULATION	0.90	SUPPORT STRUCTURE	0.90
	3.33	INSULATION	0.50
			3.12

Figure 143

SUPPORT STRUCTURE MODEL FOR CARBON/CARBON AND ABLATIVE LEADING EDGES

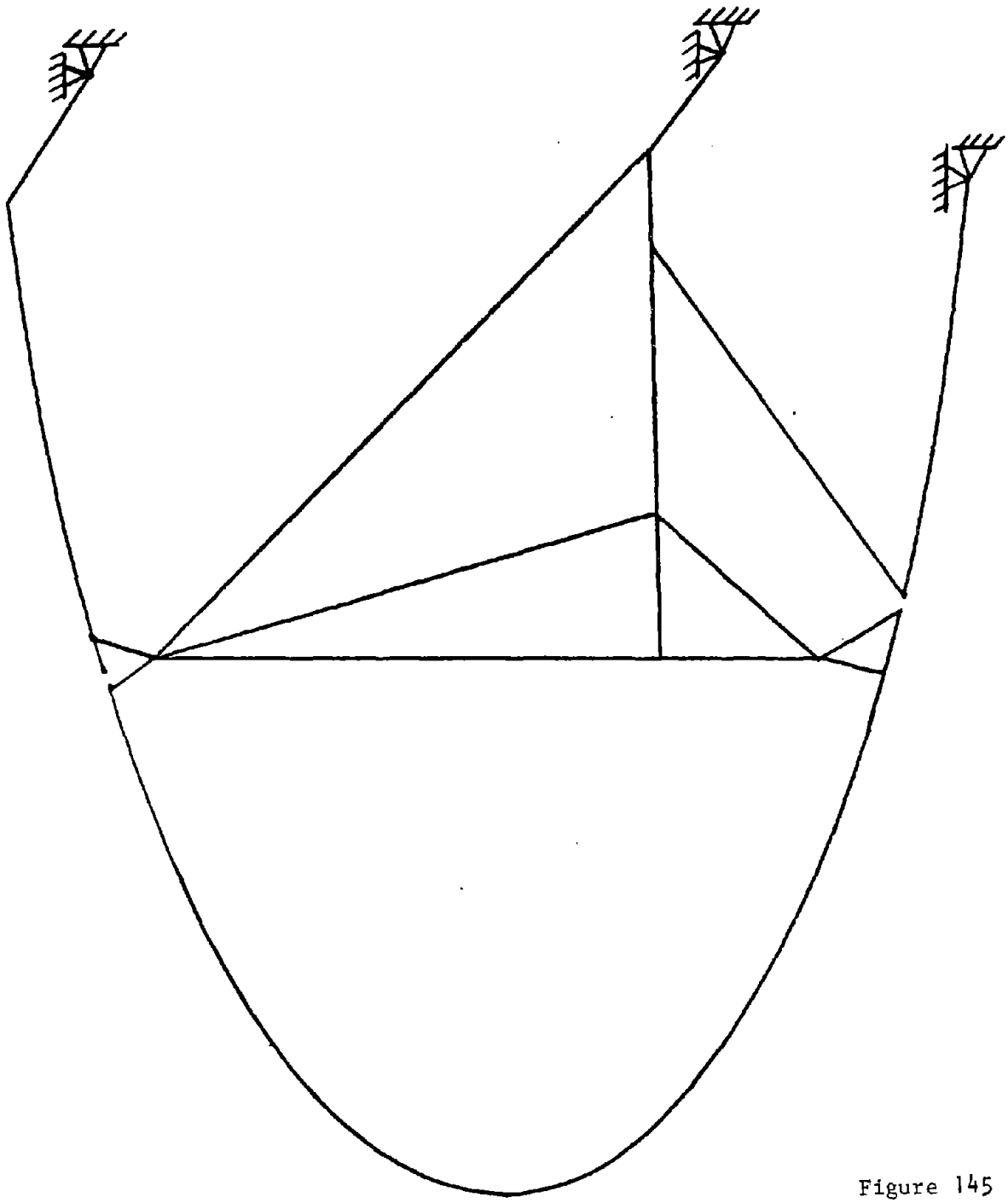

47 JOINTS
51 BARS

Figure 145

FOLDOUT FRAME 1

FOLDOUT FRAME 2

ABLATIVE LEADING EDGE

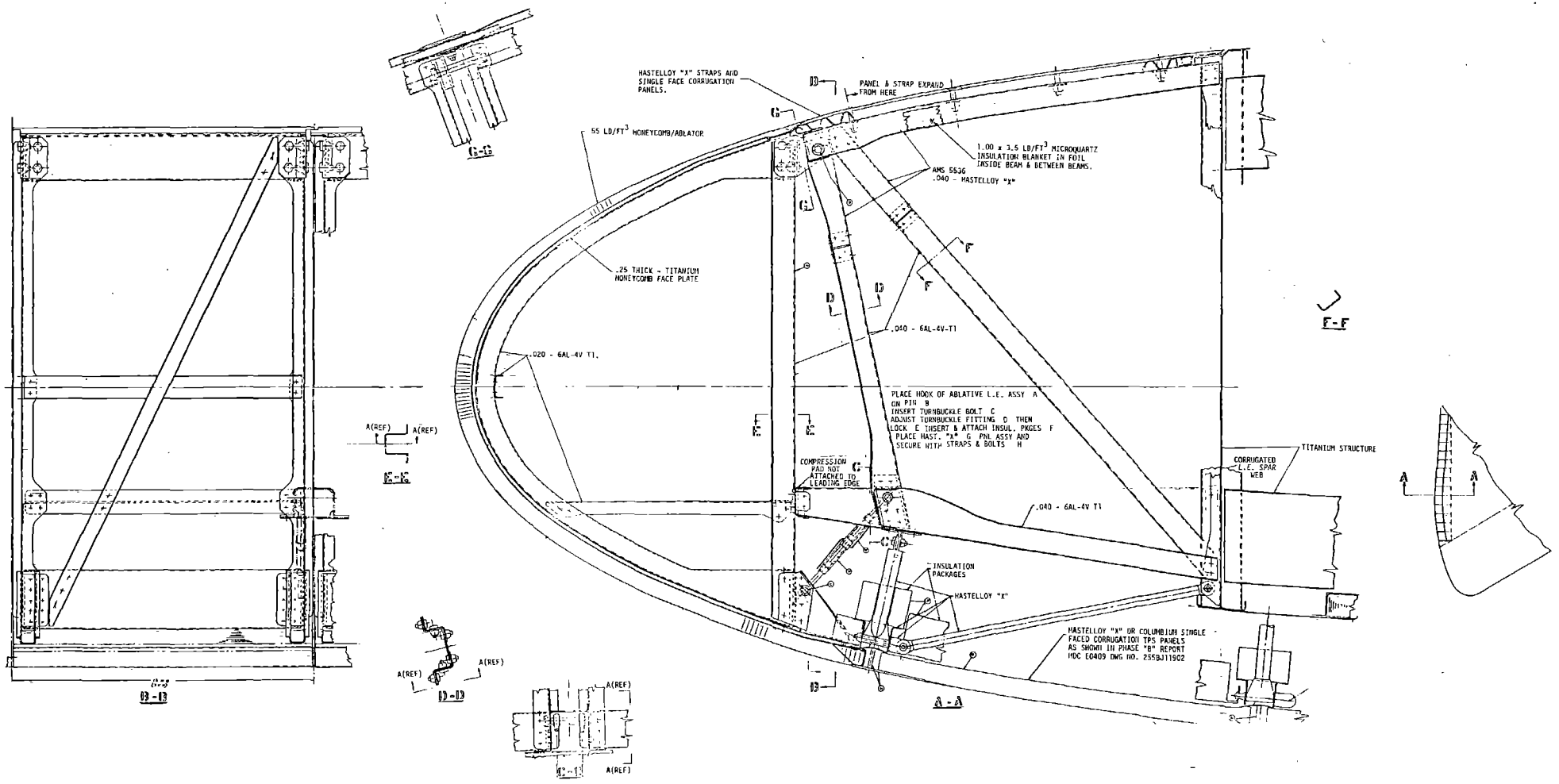

Figure 144

FOLDOUT FRAME 2

FOLDOUT FRAME 1

CARBON/CARBON LEADING EDGE

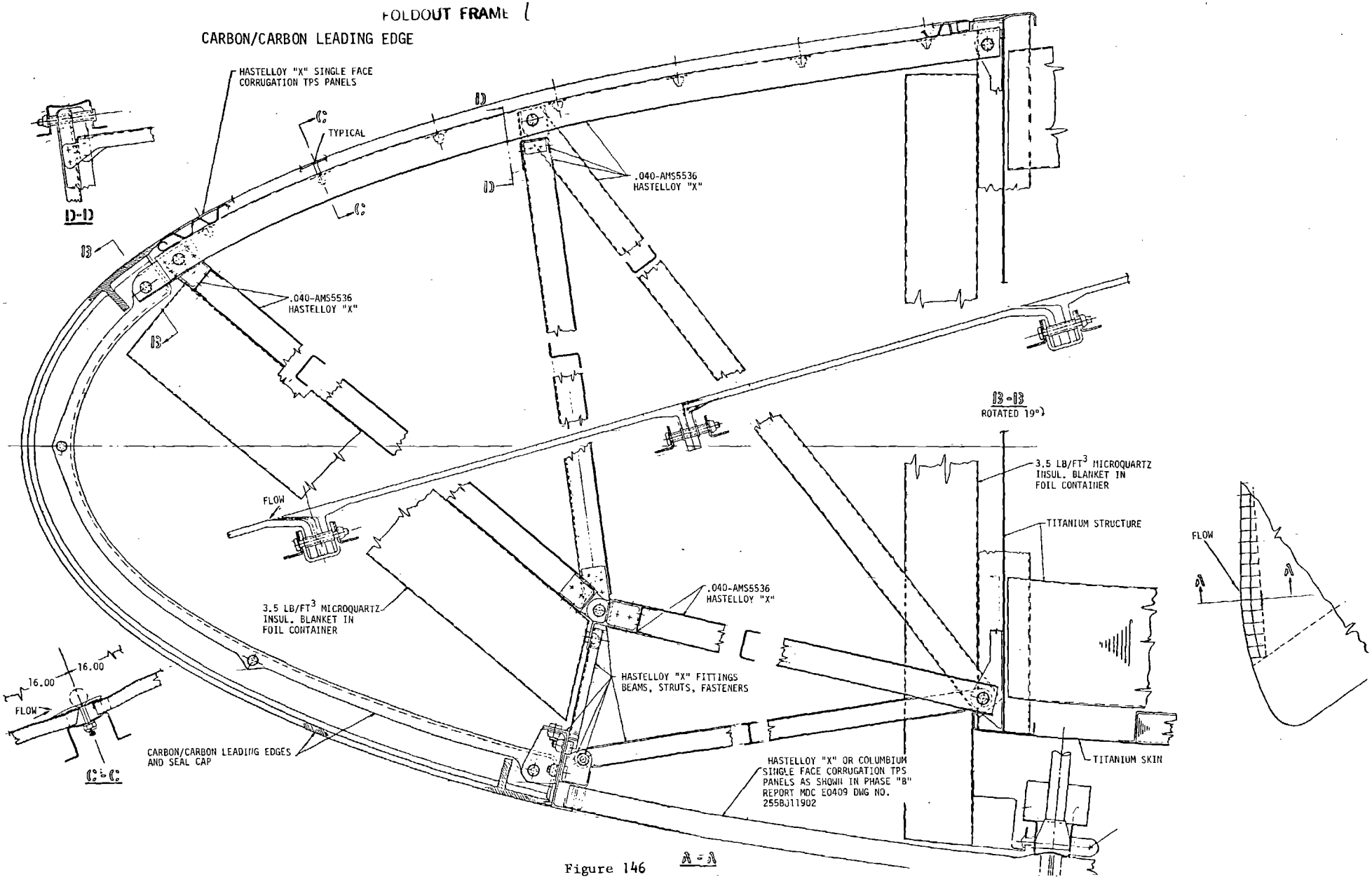

Figure 146

177

ribs were required (References 37 and 38). Integral lugs at the four corners of the carbon-carbon assembly provide for attachment to the truss work with Hastelloy-X bolts.

To provide oxidation resistance, the carbon-carbon would be impregnated with silicon carbide and zirconium diboride powders and coated with a compound of silicon (pure) and silicon carbide. The impregnated materials act as a backup for oxidation inhibition in case of a coating failure. Further details of fabrication of carbon-carbon are discussed in Reference 37.

The carbon-carbon element of the leading edge assembly was first modeled separately and analyzed using the CASD computer program. This element was idealized as a grid work of beams interconnected with shear panels as depicted in Figure 147. Bending moments calculated for the beams by the CASD program were then converted to bending moments per inch of width and used to establish the required carbon-carbon thicknesses. No allowance was made for fail safe (oxidation of coating fails) in these sizing studies.

The single face corrugated panel construction shown again was based on the studies made by the Space Shuttle project, and loads on the supporting truss work were calculated using the STRUDL II computer program. Weight estimates for the carbon-carbon leading edge based on these computations are given in Figure 143.

Columbium Leading Edge - The columbium leading edge, Figure 148, consisted of single face corrugated panels supported on columbium ribs attached to the wing forward spar. A study performed to determine the possibility of saving weight by supporting the columbium ribs at intermediate points with a truss support indicated that no appreciable weight saving was possible. Therefore, the simple rib support was adopted. Simple tubular struts support side loads. Panel retainer straps are the same as those used on the Phase B final design.

The panel and rib weights were determined using the design curves of Reference 40(Appendix B-1) although the cross section geometry was not explicitly determined. Rib bending moments required for this approach were calculated using the STRUDL II computer program.

Leading Edge Costs - The leading edge cost estimates were developed using the Space Shuttle Cost Model. This cost model was based on cost estimating relationships (CERs) derived from a broad mix of data sources. These included Gemini, Mercury, F-4, ASSET, BGRV, S-IVB,commercial aircraft and various vendor data. The thermal protection CERs were developed as functions of wetted area, type of construction, type of material, panel size, and panel shape. These same techniques were used throughout the Space Shuttle Phase A and B studies.

CARBON/CARBON LEADING EDGE MODEL

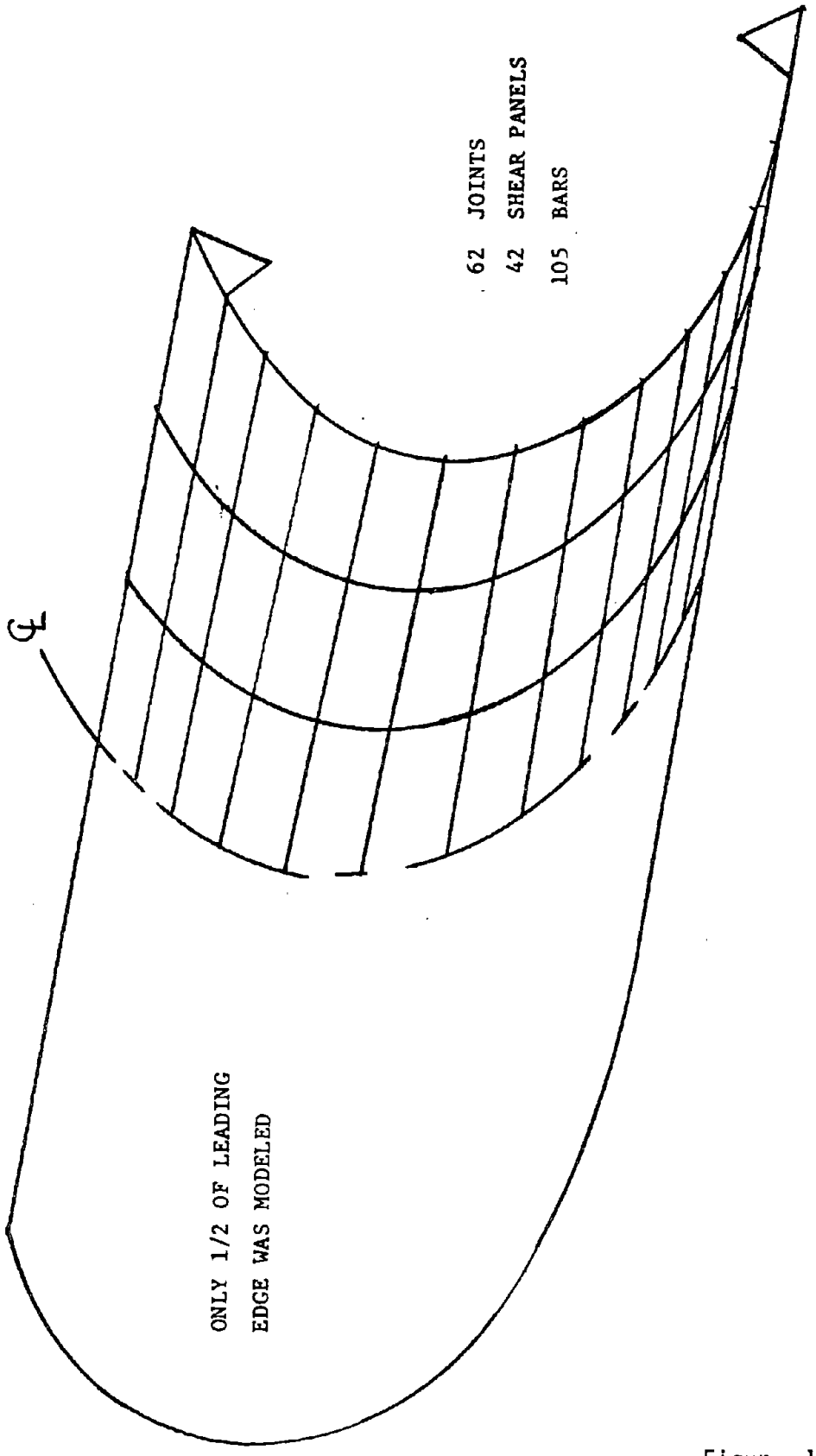

Figure 147

COLUMBIUM LEADING EDGE

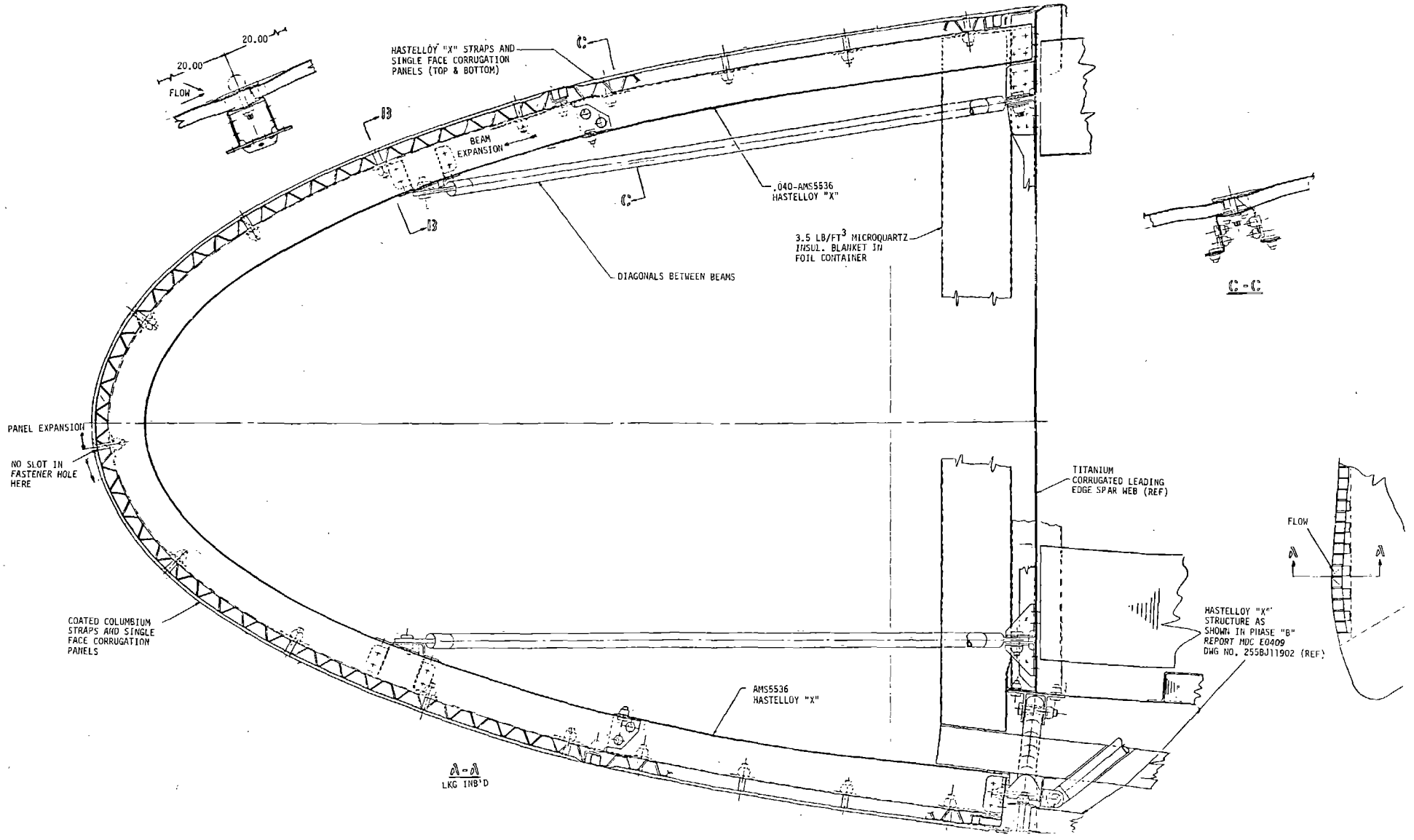

Figure 148

The groundrules used for these estimates were the same as those identified for Phases C and D. The more significant groundrules were: 5 flight vehicles, 2 flight test and 3 production; 6 development flights, and 471 operational flights; 6-year development schedule, and 10 years of operation.

The results of the leading edge cost analysis are summarized in Figure 149. The ablative system was the most expensive by a large margin, at $108 million, with the costs of the reusable candidates in the $30 to $40 million range. The carbon-carbon and columbium segments of the leading edges were substantially more expensive per unit of surface than the heat pipe designs,as shown in Figure 150. However, the use of the high temperature materials was required only in the small cap area (as was the ablative). In contrast, the heat pipe versions required the entire leading edge surface to accomplish the temperature reduction necessary to allow the use of less expensive materials. This area increase offset the lightly lower unit area cost.

Leading Edge Trade Study Considerations - The weight and cost assessments previously shown constituted the two readily quantifiable trade study considerations. In addition to these two, a number of less readily quantified but nonetheless important considerations affect the trade study outcome. These include material availability, fabricability, prior experience with the material, and material property characteristics. Some of these considerations are summarized in Figure 151 which also includes the estimated weight and cost.

The heat pipe designs, both Hastelloy-X and TD-NiCr, would use materials that are readily fabricated. The TD-NiCr availability would be less certain than for Hastelloy-X but would provide a lighter design, although, a slightly more expensive one. The Hastelloy-X design would tend to oxidize, but the rate would be so low that the metal loss would be insignificant. Both designs would require inspection and verification of pipe operation and this would be a more complex task than with the carbon-carbon design. The Hastelloy-X design, because it was designed to creep criteria, would be very strong at low temperatures when it would be exposed to handling or impact damage. This design thus should not be very susceptible to

LEADING EDGE THERMAL PROTECTION ALTERNATES
COSTS IN MILLIONS OF 1971 DOLLARS

	ABLATIVE	CARBON-CARBON	COLUMBIUM	HASTELLOY-X HEAT PIPE	TD-NiCr HEAT PIPE
RDT&E	10.40	12.61	12.19	13.87	14.32
PRODUCTION (3 VEHICLES)	3.40	4.91	4.89	5.75	6.26
*OPERATIONAL SPARES	94.16	15.77	15.74	17.32	18.56
TOTALS	107.96	33.29	32.82	36.94	39.14

* REPLACEMENT ASSUMPTIONS
ABLATOR - 100%/FLIGHT
OTHER - 3%/FLIGHT

Figure 149

THERMAL PROTECTION PANELS
TOTAL PROGRAM COST/SQUARE FOOT

MATERIAL	$/FT^2
ABLATOR	358,560
CARBON/CARBON	59,880
COLUMBIUM	58,000
HASTELLOY HEAT PIPE	51,950
TD NICKEL HEAT PIPE	55,050

Figure 150

SUMMARY

LEADING EDGE TRADE STUDY

Consideration	Heat Pipe Hastelloy-X	Heat Pipe Td-Ni-Cr	Ablative	Carbon/ Carbon	Columbium
Cost, Millions of Dollars, Total Program	36.94	39.14	107.96	33.29	32.82
Weight - PSF	4.94	4.22	3.57	3.33	3.12
Relative Availability of Material	2	3	1	2	1
Relative Fabricability	2	2	1	3	2
Compatibility (Working Fluid)	Acceptable	Acceptable	N. A.	N. A.	N. A.
Relative Fabrication Experience	1	2	1	3	1
Relative Inspectability	2	2	1	1	3
Oxidation (100 HR - 2000°F)	0.0003 IN	< 0.0003 IN	N. A.	Coating Required	Coating Required
Primary Disadvantage	Weight	Weight	Cost	Fabrication Experience	Coating

Relative Scale: 1 = Highest ranking, i.e., is best candidate.

Figure 151

damage in operation, the principal hazard being meteoroid damage. The probability of a meteoroid penetration was not computed but should be low because the surface area of an individual heat pipe (1.27 cm-0.5 in.) was small in the optimum design. Failure of the heat pipe leading edge would be very unlikely, because the design permits safe operation subsequent to the failure of any heat pipe. The current design of the heat pipe is competitive with the ablative approach on a weight basis and, for the total program, should prove less expensive. Extended study of the structure should provide some additional weight reduction in this first-generation design.

The ablative leading edge design was clearly the design candidate with the least uncertainty for successful development. The ablative materials would be available from prior programs, the structural materials selected were readily available, easily fabricated, and had wide prior application that accumulated considerable manufacturing experience. The ablative design would accommodate an overshoot in the entry heating rate if the total heat were not significantly increased. Should a large total heat increase occur, serious structural damage would be unlikely,but replacement or recertification of the leading edge structure would be required. The ablative leading edge would be very strong prior to entry, but more susceptible to damage in installation and ground servicing. Subsequent to entry the charred ablator would be very rough in comparison with the other concepts and susceptible to rain erosion. The roughness would yield a higher wing drag,as would rain erosion of the char. The ablative design would be subject to a much greater probability of a meteoroid impact than the heat pipe design but probably would not suffer catastrophic damage. Inspection of the ablative TPS would be superior because the leading edge cap region would be removed after each flight and replaced with refurbished assembly. The inspection would be carried out in a manufacturing area; a bench inspection would be possible. The design that evolved was somewhat heavier than the carbon-carbon and columbium versions, but not decisively so. Because of very large refurbishment costs,the ablative version would be much more expensive than any of the other leading edge concepts.

The carbon-carbon design utilized the material with the most uncertain development status. Carbon-carbon structures have been produced only in limited prototype quantities and, although feasible, present the greatest TPS development risk of the candidate approaches. The strength of carbon-carbon is

approximately the same from room temperature to 1650°C (3000°F). Consequently, the structure as designed for flight may be more susceptible to damage after flights than the ablative and heat pipe designs which are much stronger at low temperatures. Testing at MDAC-E has revealed a potential inflight rain erosion problem. The test condition was more severe than the expected flight conditions and the erosion was inhibited by a heavier than usual oxidation resistant coating. The phenomenon represented an additional uncertainty, however, in the evaluation of this high-potential material. The inspection of carbon-carbon would be only slightly more difficult than with an ablator because the design could provide for quick access. Inspection would not require removal of the carbon-carbon segment and none of the oxidation resistant surface coating would be hidden from view. The replacement rate should be low and,even though carbon-carbon was the most expensive on a unit basis,the limited area requirement resulted in approximately the same cost as the other reusable designs. The carbon-carbon approach resulted in essentially the same weight as the columbium design and was significantly lighter than either the ablative or heat pipe designs.

The columbium design resulted in estimated costs and weight approximately the same as the carbon-carbon. Columbium has been more widely used and, consequently,fabrication experience and material availability are better than for carbon-carbon, indicating lower risk development. The columbium leading edge would be rather difficult to inspect in place on the wing. Columbium would require an oxidation protection coating even inside the corrugations. Here inspection would be very difficult, and the coating would be subject to damage in ground handling and also to damage from meteoroid impact. The probability of coating damage from a meteoroid impact would be far greater than the probability of the penetration of a heat pipe in that TPS design. Coating damage would probably not result in a catastrophic failure. Minor damage observed in the ASSET program indicated "healing" fusion of small cracks and localization of burnthroughs to small holes. Fabrication experience has shown columbium to be difficult to weld in the SSTP program in which corrugated panels were constructed. Production tooling would somewhat alleviate this problem.

One usual advantage of carbon-carbon and ablative designs was not achieved in the trade study configurations; temperature overshoot. To minimize costs in the trade study designs the high unit cost component (e.g. carbon-carbon) use was minimized to a small case and metallic panels completed the cross section. A heating rate increase on the cap region would be accompanied by a proportional

increase on the metallic panel. The temperature increase would be more than proportional. Thus, the inherent temperature overshoot capability of ablators and carbon-carbon could not be realized in these designs, since it would have required increased cap area and a much higher cost. The heat pipe design does have some inherent overshoot capability because of fail-safe design approach. The fail-safe feature of the heat pipe design was not obtainable in the columbium version. Failure of the oxidation resistant coating of the carbon-carbon design would allow a significant loss of material. Thus a thicker (and heavier) section would be required to provide a fail-safe carbon-carbon leading edge.

In summary, the reusable designs all cost roughly the same and were found to be much less expensive than the nonreusable ablative TPS. Of the reusable designs the columbium and carbon-carbon designs seems most susceptible to operational damage. The process/manufacturing development risk of the carbon-carbon and columbium design seemed comparable with heat pipe development risk. The heat pipe design should be less susceptible to catastrophic failure in flight. The heat pipe was somewhat heavier than the other reusable candidates, but as a first-generation design may be subject to weight reduction.

7. CONCLUSIONS

The major general conclusions from each task of this study are:

Task 1 - Active cooling of the Space Shuttle orbiter structure is feasible and has the potential for reducing TPS weight and Shuttle system cost. The decision to incorporate active cooling into the Shuttle must be made early in Phase C if these cost savings are to accrue. The payoff for active cooling is substantial if operational criteria/mission requirements preclude preconditioning the TPS prior to reentry from "hot" orbital inclinations ($20 million for T_i = 114°C (200°F)). However, active cooling is not recommended if pre-entry temperatures are below 38°C (100°F).

Task 2 - A reusable heat sink booster poses no insurmountable thermostructural problems. A significant weight savings is possible if thickened aluminum heat sink is replaced with a nonmetallic heat sink concept for the wing. The nonmetallic heat sink consists of a sprayable silicone filled with high heat capacity filler.

Task 3 - The successful test demonstration of the use of PCM for temperature control of the RSI/structure bondline has shown that this TPS concept can be used to reduce orbiter TPS weight.

Task 4 - Integrating heat pipes into the orbiter leading edge structure allows use of Hastelloy-X or Td-Ni-Cr superalloys in place of coated columbium with small weight and cost penalties. Hastelloy-X tubes of 1.27 cm (0.5 in.) diameter brazed to a thin face sheet provided the optimum structural configuration. Sodium, the working fluid, prevented temperatures of the assembly from exceeding 1000°C (1832°F) when all heat pipes were functioning and 1093°C (2000°F) if two pipes surrounding a failed pipe were still functioning.

A number of specific conclusions were also derived from this study program. These are summarized for each task in the following paragraphs.

7.1 Task 1: Orbiter Structural Active Cooling - The principal conclusion drawn from this task was that the incorporation of an active subsystem could provide both a weight and cost reduction for the Space Shuttle orbiter, but only under certain conditions. An orbiter weight reduction should be possible by employing an active subsystem for structural cooling that permits substantial RSI thickness reduction. This large RSI thickness and weight reduction was found to be attainable only in designs where the RSI was bonded to a surface to which cooling passages could be readily attached. The lightweight insulation possible with metallic TPS precluded a significant weight reduction.

The potential cost reduction would occur only if the actual subsystem were included in the orbiter before the design of the SRM and expendable tank were fixed. The active subsystem would increase the cost of the orbiter but the lowest TPS weight could result in a lower total program cost for the Space Shuttle. These conclusions are further dependent upon the temperature of the structure just prior to entry. For this study a design value of 38°C (100°F) was selected. If operational criteria permit, preconditioning of the lower surface may allow a much lower design temperature. In this case, the projected weight and cost reductions shown in this study would not be achieved. If, on the other hand, operational criteria permit no constraints on attitude control during orbital flight, the temperature of the structure could substantially exceed the design value. With the surface characteristics of RSI (α_s = 0.72, ϵ = 0.80) the structural temperature would approach 121°C (250°F) with direct solar heating (normal incidence).

Cooling may be provided by the evaporation of either hydrogen or water with essentially the same active subsystem weight. The use of hydrogen would, however, increase the active subsystem cost $2.5 million because the hydrogen supply tanks are much more expensive than water supply tanks. Of the fluids studied for application as the circulating coolant, Coolanol 15 resulted in the lightest weight active system. The total TPS weight was not sensitive to cooling passage spacing. Therefore, the passage spacing could be compatible with the optimal spacing for stiffeners, readily allowing structural integration.

7.2 Task 2: Heat Sink Concepts for the Booster - The analyses demonstrated that thermal stresses due to peripheral heating distributions significantly impact the skin thickness requirements of cryogenic tankages used as integral structure. Nonmetallic reusable overcoats for an aluminum structure can serve to protect it for moderate heating rates and effect a weight reduction, neglecting thermal stress considerations. A synergistic benefit seems likely if thermal stress effects are considered. The aluminum heat sink designs displayed the greatest sensitivity to liftoff temperature assumptions because of aluminums low peak allowable temperature. The higher temperature allowable for the nonmetallic coating should reduce this sensitivity.

The investigation of the smeared thickness assumption showed that caution must be exercised when using this approximation because of the transient nature of the booster heat pulse. The nontank regions allow the use of titanium to high temperatures, e.g., 316°C (600°F). Under these conditions,titanium is a more efficient heat sink material than aluminum.

Crew egress was not affected by the structural temperature rise, even with the use of the titanium heat sink design. Cooling during cruise would reduce the surface temperatures to approximately sea level ambient conditions.

7.3 Task 3: Phase Change Material (PCM) Applications - The implementation of structural cooling with a fusible PCM can provide an orbiter TPS weight reduction, affected by the design conditions postulated. A lower pre-entry design temperature for the structure (study based on 38°C/100°F) would tend to reduce the weight saving potential, although not as rapidly as for a TPS with an active subsystem. The heat storage capacity of the PCM would increase as the pre-entry temperature decreased, in effect increasing the efficiency of the PCM and the trade of PCM for RSI. Generally reduced requirements for RSI should, however, tend to override the increased PCM efficiency so that the weight reduction possible would decrease with lower design pre-entry temperatures. Increased pre-entry design temperatures might require selection of other PCM and yield either greater or smaller weight reduction benefits. Efficient packaging of the PCM would be essential in achieving a weight reduction. A structure which could act also as the PCM container would enhance the ability of the PCM to reduce the TPS weight.

7.4 Task 4: Heat Pipe Application to Leading Edge and Stagnation Points - The application of heat pipes to the reusable boosters was not found feasible. The coincidence of maximum heating and acceleration produced adverse design conditions precluding heat pipe designs competitive with simple metallic TPS. The orbiter application yielded feasible approaches weight and cost competitive with alternate approaches. The heat pipe leading edge, in the Phase B configuration and environment would weigh approximately the same as an ablative TPS. Being reusable, however, would have a much lower ($70 million) total program cost. Alternate reusable TPS have approximately the same cost as the heat pipe approach,but are somewhat lighter in the Phase B configuration. The heat pipe technique provides reduction of temperatures that allows the use of Hastelloy-X for the heat pipes, with an attendant reduction in process/manufacturing risk. The design criteria (creep limited) produced a heat pipe design highly resistant to ground handling damage. Consequently the heat pipe appears to be a lower risk design than alternate reusable TPS studied.

8. RECOMMENDATIONS FOR FOLLOW-ON

This study program has shown the desirability of additional analyses and tests (1) to complete feasibility demonstration of the postulated TPS concepts, (2) to extend the work to current Shuttle configurations or (3) to initiate development of key elements of the TPS. The resulting recommendations for follow-on are summarized by task and given priority ranking in the following subsections.

8.1 Task 1: Structural Active Cooling

1. As indicated in Section 7, the payoff for active structural cooling is conditional. The decision to pursue this task in further depth must be made by program management since the trade is essentially mission flexibility versus development of an active system. To assist management in this decision making process it is recommended that comprehensive analysis be conducted to define mission constraints, i.e., limits in orbital inclination/time in orbit corresponding to peak reentry temperatures of 38°C (100°F). These analyses should be performed for the appropriate RSI passive TPS. Supplementing this work should be an evaluation of abort missions, e.g. abort to orbital flight with once-around to landing. This should be given high priority,since the penalty to the passive system may not be tolerable.

2. Since any cost savings can only be expected if the decision to use active cooling is made prior to design freeze of the booster, and is due to system weight reduction, the predicted weight reduction should be verified through comparative tests of actively cooled and passive TPS designs. This task is of secondary priority since the results of the previous task may establish that active cooling is not required.

3. Detailed design and prototype construction of key components in the active system should be initiated. In particular, coolant pumps of size required for the active system have not been developed and could be pacing items in the development of the system. This task also has secondary priority and should not be initiated prior to the completion of the first task.

8.2 Task 2: Heat Sink Concepts for the Booster - Shuttle program decisions which have replaced the fully reusable Shuttle system with the orbiter mounted piggyback on throw-away drop tanks and refurbishable solid rocket motors (SRMs) for boost, have caused a modification to the preliminary assessment of recommendations for follow-on.

1. First priority should be given to performance requirements and capabilities of a low cost insulation system for the drop tank. Primary emphasis should be on

reducing the fabrication cost of the tanks and insulation system. Reuse is not required and expendable (ablative) insulation systems merit careful consideration. Because of the low heat load and shear at high altitude, inexpensive foam insulation systems may be adequate to prevent both air condensation and to provide boost phase heating protection. This work should include assessment of SRM plume heating and its impact on TPS design.

2. The nonmetallic heat sink concept using filled silicone should be reviewed for applicability to the shielded surfaces of the orbiter, e.g., upper wing covers. The analyses reported in Reference 42 have shown that nominal heating is low enough that aluminum or titanium heat sink concepts are lighter in weight than the baseline RSI concept, but heavier for off-nominal heating. Small thicknesses of filled silicone may be lighter than the RSI system,since the minimum thicknesses limitations attendant to RSI application, 6.3 cm (0.25 in.), are not present for the sprayable ablative. Evaluation of this concept, at least analytically, should be given high priority.

3. The dependency of the silicone heat sink system on a high heat capacity filler suggest that materials development be initiated to define viable combination of sprayable silicone and filler. This task should include experimental demonstration of concept feasibility. Pursuit of this development task should be initiated only after the second task has identified potential for orbiter application.

8.3 Task 3: Phase Change Material Applications

1. This task has demonstrated the feasibility of the PCM concept for reducing orbiter TPS weight. Incorporating such a system and/or further evaluations are contingent upon the results of Item 1 of Section 8.1. The key remaining questions are packaging design constraints and integration/attachment of the packaged material to the cooled structure. It is recommended that these questions be addressed for the current orbiter design.

2. The selected PCM must have its melting temperature above the temperature experienced at initiation of the reentry sequence or the performance advantage of the system over the passive concept could be nullified. The PCM used in the feasibility test had more than 80 percent of its total heat capacity between 38°C (100°F) and 94°C (200°F), the region in which Shellwax 700 undergoes the solid-solid transition and melting. If preconditioning is shown to be impractical an alternate PCM is required. Therefore, it is recommended that alternate PCMs having melting temperatues above 94°C (200°F) be evaluated for this application.

8.4 Heat Pipe Applications to Leading Edge and Stagnation Points

1. Early feasibility demonstration tests of the heat-pipe-cooled system should be given first priority. The objective of the tests should be to prove the ability of the pipes to start up properly and reduce the temperature in the stagnation areas to acceptable values for superalloy designs. This demonstration test would also demonstrate the cost and fabricability of such a system which utilizes high temperature heat pipes. This task is currently being conducted for NASA MSFC under contract NAS 8-28656.

2. Trade study results derived in this task should be extended to include the current Shuttle concept. The trades in this program assumed an all-metallic TPS for the orbiter. The problems of integrating the design with RSI attached to aluminum substructure were not addressed. Additional insulation will be required to isolate the leading edge from the aluminum structure, and differential thermal expansion of the leading edge and RSI may produce unacceptable geometric discontinuities and hot spots. This work should be given a high priority.

3. Should the feasibility tests (Item 1) provide positive results, operational problems should be identified and solved. These include detailed checkout approaches and fixture design, demonstration of performance with a failed heat pipe, and definition of handling and safety procedures.

9. REFERENCES

1. MDC Report No. E0308, "Space Shuttle System Study Phase B Final Report," Technical Summary, 30 June 1971.

2. Kavanaugh, B. and Bauer, P. E., "Active vs. Passive Trade Study of Thermal Protection System on Delta and Straight Wing Orbiter," Space Shutttle Program TPS Design Note O-EAST-TPS-4.

3. Contract NAS8-27708 "Study of Structural Active Cooling and Heat Sink Systems for Space Shuttle," Monthly Progress Report No. 2, 31 August 1971.

4. Masek, R. V., and Niblock, G. A., "Study of Structural Active Cooling and Heat Sink Systems for Space Shuttle," Progress Report for the Period 28 September - 28 October 1971, 8 November 1971 McDonnell Douglas Astronautics Co.

5. Masek, R. V., and Niblock, G. A., "Study of Structural Active Cooling and Heat Sink Systems for Space Shuttle," Progress Report for the Period 28 October - 28 November 1971, 8 December 1971, McDonnell Douglas Astronautics Co.

Schultz, H. D., and Guard, F. L., "Comparison of Active and Passive Thermal Protection System Weights for a Delta-body Orbiter," NASA Space Shuttle Technology Conference, 2-4 March 1971.

7. Anthony, F. M., Monthly Progress Report 8629-900108. Contract NAS8-26347, "Reusable Space Shuttle Vehicle Thermal Protection," Bell Aerospace Co.

8. Masek, R. V. and Niblock, G. A., "Study of Structural Active Cooling and Heat Sink Systems for Space Shuttle," Progress Report for the period 29 January 1972 through 28 February 1972, 8 March 1972, McDonnell Douglas Astronautics Co.

9. Fessenden, R. D., "Computer Aided Weight/Sizing Program for Entry Spacecraft," SAWE Paper No. 797, 28th Annual Conference of the Society of Aeronautical Weight Engineers, 5-8 May 1969.

10. Hower, K. L., "Mars Landing and Reconnaissance Mission Environmental Control and Life Support System Study," Report SLS 404, Hamilton Standard Division, United Aircraft Corp. (Contract NAS 9-1701), Section 6.0.

11. "Manned Orbiting Space Station Environmental Control and Life Support System Study," Hamilton Standard Division, United Aircraft Corp., Mid-Term Report SLS 331 (Contract NAS 9-1498).

12. "Manned Orbiting Space Station Environmental Control and Life Support System Study," Hamilton Standard Division, United Aircraft Corp., Final Report SLS 410-3, May 1964 (Contract NAS 9-1498).

13. Knights, A. F., "Choice of Fluids for Cooling Electronic Equipment," Electro-Technology, June 1963, pp. 57-63.

14. Armstrong, R. C., "Life Support System for Space Flights of Extended Time Periods," NASA CR-614, November 1966 (Contract NAS 1-2934), Section 3.1.3.2.

9. REFERENCES (Continued)

15. Stenzel, W. W., "Methodology for Determining Optimum GLOW, Thrust, and Staging Velocity Values on the Basis of Program Cost," Space Shuttle Program Design Note I-East-CA-4, McDonnell Douglas Astronautics Company, 16 November 1970.

16. Contract NAS 8-27708, "Study of Structural Active Cooling and Heat Sink Systems for Space Shuttle," Monthly Progress Report No. 1, 31 July 1971.

17. MDC Report No. E0348, "Structural Active Cooling and Heat Sink Systems for Space Shuttle," Volume 1 - Technical Proposal.

18. Tillian, D. J., "Point Design Requirements for Two Orbiter TPS Design Areas - Reusable Surface Insulation TPS Development," Phase B, 21 July 1971.

19. Masek, R. V. and Niblock, G. A., "Study of Structural Active Cooling and Heat Sink Systems for Space Shuttle," Progress Report for the Period 30 December 1971 through 28 January 1972, 8 February 1972.

20. Alternate Space Shuttle Concepts Study, Final Report, Report No. MSC 03809, Part 1 Executive Summary, Grumman Aerospace, July 1971.

21. Phase B Final Report, Volume II Technical Summary Orbiter Vehicle Definition, North American Rockwell, 25 June 1971.

22. Hankey, W. L. Jr., Neumann, R. D., Flinn, E. H., Design Procedures for Computing Aerodynamic Heating at Hypersonic Speeds, WADC TR 59-610, June 1960.

23. Thomas, A. C., Perlbachs, A., and Nagel, A. L., Advanced Re-entry Systems Heat-transfer Manual for Hypersonic Flight, AFFDL-TR-65-195, October 1966.

24. T. P. Cotter, Heat Pipe Startup Dynamics, presented at 1967 Thermionic Conversion Specialist Conference, November 1967, Palo Alto, Calif.

25. J. E. Deverall, J. E. Kemme, and L. W. Florshuetz, Sonic Limitations and Startup Problems of Heat Pipes, LA-4518, Nov. 1970.

26. E. K. Levy, Theoretical Investigation of Heat Pipes Operating at Low Vapor Pressures, presented at the ASME Aviation and Space Conference, Beverly Hills, Calif. 1968.

27. M. Hansen, Constitution of Binary Alloys, McGraw-Hill Book Co., Inc. New York, 1958.

28. R. P. Elliott, Constitution of Binary Alloys-First Supplement, McGraw-Hill, New York, 1965.

29. F. A. Shunk, Constitution of Binary Alloys-Second Supplement, McGraw-Hill, New York, 1969.

30. J. H. Stang, et al., Compatibility of Liquid and Vapor Alkali Metals with Construction Materials, DMIC Report 227, 1966.

9. REFERENCES (Continued)

31. J. Cowles and A. D. Pasternak, Lithium Properties Related to Use as a Nuclear Reactor Coolant, UCRL-50647, 1969.

32. J. R. DiStefano, Refluxing Experiments with Refractory Metals in Boiling Alkali Metals, ORNL-4323, 1969.

33. C. A. Busse, et. al., Heat Pipe Life Tests at 1600°C and 1000°C, Thermionic Conversion Specialist Conference, Houston, Texas, 1966.

34. C. A. Busse, et. al., High Temperature Lithium Heat Pipes, Second International Conference on Thermionic Electrical Power Generation, Stresa, Italy, 1968.

35. G. D. Johnson, Liquid Metal Heat Pipe for 1000° to 1800°C, MDC G1669, June 1970.

36. G. D. Johnson, Corrosion Studies of Liquid Metal Heat Pipe Systems at 1000°C to 1800°C, pages 321-337 of Corrosion by Liquid Metals, Plenum Press, New York, 1970.

37. McDonnell Douglas Report E0561 "Final Report Carbon/Carbon Leading Edge," dated 30 March 1972.

38. Vaught Missiles and Space Company Report T143-5R-00124 "Development of a Thermal Protection System for the Wing of A Space Shuttle Vehicle," dated 30 April 1972.

39. McDonnell Douglas Report E0375 "Space Shuttle Data, Part II Orbiter, Airframe Appendices" dated 30 June 1971.

40. McDonnell Douglas Report E0562 "Final Report Large TPS Panels", dated 30 March 1972.

41. McDonnell Douglas Space Shuttle Program Design Note O-East-TPS-6 "Leading Edge Trade Study of Thermal Protection System Unit Weight and Cost for Delta and Straight Wing Orbiters", dated March 1971.

42. McDonnell Douglas Report E0639 "Study of Uncertainties of Predicting Space Shuttle Thermal Environment", dated 30 June 1972.

10. NOMENCLATURE

AL	Aluminum
A_v	Cross sectional area of vapor passage
A_w	Cross sectional area of wick
BS	Body station
C_p	Specific heat
FS	Factor of safety
g	Acceleration
g_c	Gravitational constant
h_{fg}	Heat of vaporization
K_p	Permeability constant
$K_p A_w/W$	Wick design parameter
LH_2	Liquid hydrogen
LOX	Liquid oxygen
$\dot{m}$	Mass flow rate
$\dot{m}_{max}$	Maximum mass flow rate
M	Molecular weight
n_z	Normalized acceleration in z axis
PM	Stress due to bending moment
P_{limit}	Limit panel differential pressure load
P_{Ult}	Ultimate panel differential pressure load
psid	Differential pressure in lb/in^2
P_{axial}	Axial stress due to end loading
P_{ullage}	Tank pressure due to ullage
Q	Heat flow
q	Local heat flux
$q\alpha$	Product of aerodynamic pressure and angle of attack
q/qo	Ratio of local to stagnation heat flux
q_o	Stagnation heat flux

q/q_{ref}	Ratio of local heating to heating on a 1 ft radius reference sphere
Q_T	Time-integral of external heat flux
R	Universal gas constant
RP-1	Rocket Propellant (Hydrocarbon)
r_c	Capillary radius
r_v	Radius of vapor passage
RSI	Reusable surface insulation
Sta	Body station
T_{max}	Maximum temperature
t	Thickness
$\bar{t}$	Smeared (average) thickness
TPS	Thermal protection system
W	Width of stringer (Beam Cap) or unit length along the leading edge
WBL	Wing butt line
WT	Total unit weight
X/L	Dimensionless length ratio
v_s	Sonic velocity
x/C	Dimensionless chordwise length

α	Angle of attack
α_s	Solar absorbtance
ΔP	Pressure drop
ΔP_L	Liquid Pressure Drop

ΔP_c	Available capillary pumping pressure rise
ΔP_v	Vapor pressure drop
ϵ	Emissivity
μ_L	Liquid viscosity
ρ_v	Vapor density
ρ_L	Liquid density
σ	Surface tension
γ	Ratio of specific heats
μ	Vapor viscosity
T	Stefan-Boltzman constant
ΔT	Temperature difference